Single-cell Imaging and Mathematical Modelling of the Hypoxia-Inducible Factor Signalling Network

Thesis submitted in accordance with the requirements of the
University of Liverpool
For the degree of Doctor in Philosophy by

James Steven Bagnall

September 2011

Abstract

Hypoxia-inducible Factor (HIF) is an oxygen-sensitive transcription factor present in all multicellular life, including humans. It is responsible for mediating the cellular response to hypoxia, a situation in which oxygen supply falls below adequate levels. In the presence of oxygen HIF is constitutively degraded and inactivated. In the absence or reduction of oxygen, HIF escapes degradation and accumulates. Once accumulated, HIF elicits an adaptive response by inducing a diverse array of genes affecting the processes of cell fate, vascularisation and red blood cell production. However, there are many instances of the pathological activation of this pathway, which is known to cause serious and maladaptive issues, as found in cancer.

HIF is functional as a heterodimer comprised of an O_2-sensitive alpha subunit (HIF-α), of which there are two isoforms (-1α and -2α), and an O_2-insensitive beta subunit (HIF-β). The O_2-dependent destabilisation of HIF-α is carried out by the prolyl hydroxylase domain proteins (PHDs). Importantly, several of the PHDs are themselves HIF target genes, thereby forming a delayed negative feedback loop. Delayed negative feedback loops are a common signalling motif able to confer dynamic properties to the signalling network. The resulting kinetics may have the capacity to encode additional information into the system and alter the course of downstream gene expression. The dissection and understanding of this requires a high-degree of characterisation of the temporal profile of response. Live-cell imaging offers an experimental system ideally suited to this approach. To date, the dynamics of HIF-1 accumulation have not been investigated in this detail and so it was a main aim of this study to depict the temporal properties of the HIF signalling system.

The dynamic response of HIF-α protein to hypoxia and re-oxygenation was imaged by live-cell time-lapse confocal microscopy. Interestingly, it was observed that the hypoxic accumulation of HIF-α was heterogeneous and transient. The duration of HIF-α accumulation was found to be a distinctive and robust temporal feature of the response. This assorted data was used in building a mathematical model depicting the HIF-PHD feedback motif. Subsequently, the model was utilised to accurately predict the consequence of loss of the PHD feedback. Additionally the model provided predictions on how HIF-α dynamics are differentially responsive to varied hypoxic and re-oxygenation conditions.

Live-cell imaging of the HIF-α response also provided insight into the novel subcellular localisation pattern of the HIF-2α protein, which differs distinctly from HIF-1α. HIF-2α was found to reside in several types of subcellular bodies. The dynamic interplay and flux of protein in and out of these bodies was investigated. Evidence gathered supports the involvement of HIF-2α in aggresomes and PML bodies and also the involvement of the subcellular landscape in the HIF regulatory network.

Overall, research arising from this thesis offers new insights into the intracellular spatial and temporal dynamics of the HIF signalling system.

List of Abbreviations

2C	2-component mathematical model
4C	4-component mathematical model
AA	Amino Acid
ATP	Adenosine Triphosphate
BSA	Bovine Serum Albumin
CBP	CREB Binding Protein
CFP	Cyan Fluorescent Protein
CMV	Cytomegalo Virus
DMOG	Dimethyloxalylglycine
DNA	Deoxyribose Nucleic Acid
dNTP	Deoxribonucleotide Triphosphate
DsRedxp	DsRed-Express
EGFP	Enhanced Green Fluorescent Protein
FCS	Fetal Calf Serum
FIH	Factor Inhibiting Hypoxia-Inducible Factor
FP	Fluorescent Protein
HIF	Hypoxia-Inducible Factor
HIF-α	HIF-1α and/or HIF-2α
HIF-β	HIF-1β and/or HIF-2β
HIF-1	HIF-1α:HIF-β dimer
HIF-2	HIF-2α:HIF-β dimer
HRE	Hypoxia Response Element
Hrs	Hours
IκBα	Inihibitory κB α
IKKβ	IκB Kinase β
LMB	Leptomycin B
Luc	Luciferase
MDM2	Murine Double Minute
MEM	Modified Eagle's Medium
Min	Minutes
mRNA	Messenger Ribose Nucleic Acid
N:C	Nuclear : Cytoplasmic Ratio
NES	Nuclear Export Sequence
NF-κB	Nuclear Factor κB
NLS	Nuclear Import Sequence
ODE	Ordinary Differential Equation
PBS	Phosphate Buffered Saline
PCR	Polymerase Chain Reaction
PHD	Prolyl Hydroxylase Domain
RLU	Relative Light Units

PML	Promycrocytic Leukemia factor
ROI	Region of Interest
ROS	Reactive Oxygen Species
RNApol	RNA polymerase
Sec	Seconds
SEM	Standard Error of the Mean
ShPHD2	Short Hairpin Silenced PHD2 Hela Cells
SIAH	Seven in absentia homolog
Tris	Tris(hydroxymethyl)aminomethane
pVHL	Von Hippel-Lindau protein
V/V	Volume per Volume
WT	Wild-type
W/V	Weight per Volume
YFP	Yellow Fluorescent Protein

Contents

List of Figures

List of Tables

Chapter 1: Introduction

1.1 Cell signalling

The maintenance of highly ordered organisms requires cells to be able to sense and respond to various environmental and chemical cues. This is further complicated in multicellular organisms, whereby the maintenance of the whole organism requires cells in different local environments (e.g. across tissues) to communicate with one another, and for the survival of the whole organism to be prioritised over the constituent cells. Individual cells are able to communicate extracellular and intracellular signals through transduction pathways, often leading to changes in gene expression which in turn leads to changes in the cellular protein make up, eliciting an appropriate response. There is a vast array of biological complexity underlying this simple notion, due to the wide range of stimuli and arrangements of signal transduction. Often stimuli are considered simply as biologically produced cytokines or hormones, though cells can also sense environmental cues such as pH, temperature and shear-stress etc. Additionally, eukaryotic cells are also able to detect the availability of molecular oxygen (O_2) and it is the transduction pathway underlying the ability of cells to sense and respond to O_2 with which this study is principally interested.

1.2 Oxygen biology

Life began in a strongly anoxic environment 3.7 billion years ago and this environment remained anoxic until the arrival of the first photosynthetic organism, cyanobacteria, approximately 2.4-3.2 billion years ago (Taylor and Pouyssegur 2007; Saker, Moreira et al. 2009). These early organisms were capable of utilising water as an electron donor and this process released molecular oxygen as a by-product, which alongside other geological factors led eventually to the significant rise in available atmospheric oxygen (Falkowski 2006; Thannickal 2009) (**Fig 1.1**). The emergence of oxygen has had a profound effect upon life and is linked with a dramatic increase in the complexity of living things (Raymond and Segre 2006; Berner, Vandenbrooks et al. 2007). The effect that molecular oxygen has had on the development of life can be broadly separated into three categories; (i) oxidative-metabolism, (ii) oxygen-toxicity and (iii) oxygenic biosynthesis.

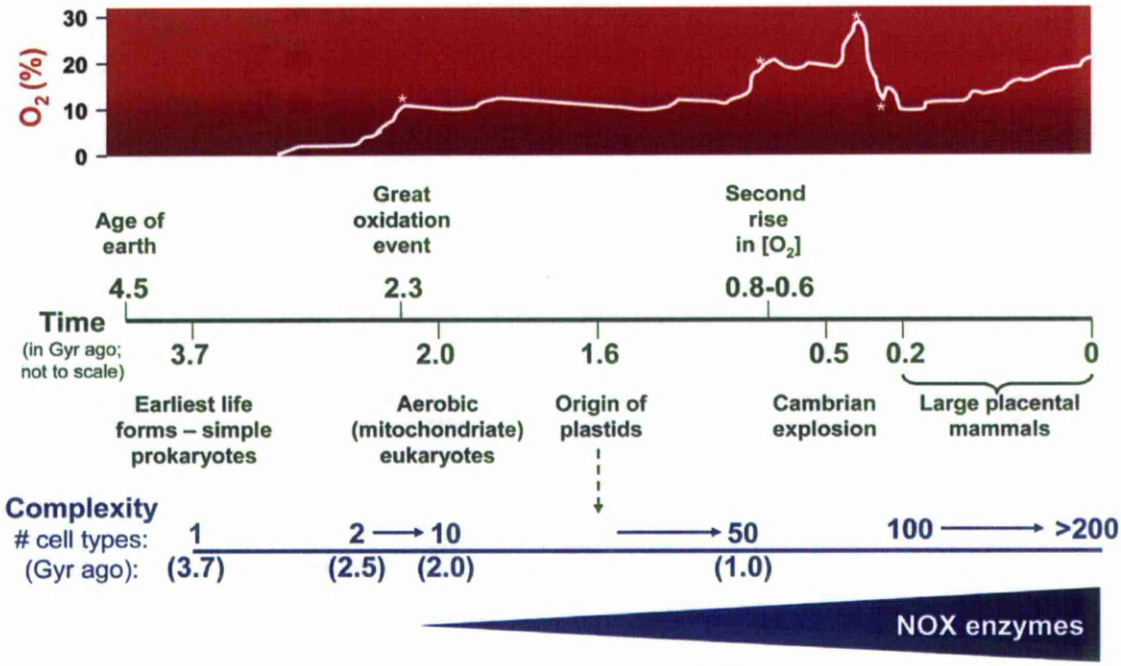

Fig 1.1. Timeline showing the relationship between atmospheric O_2 concentrations, evolutionary diversification and biological complexity. Also indicated is the increasing number of NADPH oxidase (NOX) homologs, specialised O_2-reducing enzymes dedicated to reactive oxygen species production. Figure taken from Thannickal *et al.* (2009).

1.3 Aerobic respiration

A critical step in the evolution of life occurred when certain microbes adapted to the increasing availability of oxygen and developed aerobic respiration, oxidising organic matter to water. Aerobic respiration offers a very prolific form of energy production, in which oxygen is used as a terminal electron acceptor. This process of energy production is now carried out by mitochondria in virtually all eukaryotic cells, thus providing enough energy for the diversification of high-order life. Nevertheless the initial advantage of aerobic respiration was balanced against the toxicity of oxidative metabolism.

1.3.1 Oxygen Toxicity

Oxygen toxicity arises from the partial reduction of oxygen resulting in the formation of reactive oxygen species (ROS), which are defined as highly reactive oxygen radicals (Wiseman and Halliwell 1996). ROS are capable of damaging DNA/RNA, oxidising lipids and oxidising proteins (Stadtman 2006; Adibhatla and Hatcher 2010). Aerobically respiring organisms have therefore developed strategies to minimise ROS damage, including restricted oxygen exposure, repair mechanisms and anti-oxidant defences (Hetz and Bradley 2005; Buonocore, Perrone et al. 2010). In addition, aerobically respiring organisms have also developed ways in which to usefully utilise ROS, as found in the processes of sperm-egg fertilisation, the immune response against invading

microbes and several intracellular & extracellular signalling systems (Thannickal and Fanburg 2000). It is also possible that one of the driving forces of multicellular life was the arrival of oxygen, and that increased size and multicellularity evolved in part to reduce the dangers of oxygen toxicity by reducing the exposure of cells/mitochondria to oxygen (Henry and Harrison 2004; Zhao, Zhou et al. 2010).

1.3.2 Oxygen-derived biosynthesis

Together with energy production and toxicity, the arrival of usable atmospheric molecular oxygen led also to the generation of new metabolites and secondary gene products, such as indoles, penicillin and sterols (Falkowski 2006). The emergence of these new biologically active compounds enabled new biochemical reaction networks, further increasing the potential for biological complexity. This is illustrated with the connection between sterols and molecular oxygen availability, in which molecular oxygen is an absolute necessity for sterol biosynthesis. Sterols are classified as a subgroup of steroids; the best known example being cholesterol, an organic compound that is often considered a defining feature of eukaryotes (Espenshade and Hughes 2007). In mammalian biology, cholesterol is an integral component of cell membranes as well as a key precursor molecule for the formation of bile, vitamin D, cortisol, aldosterone, progesterone, estrogen and testosterone (Galea and Brown 2009). Ultimately it has now been estimated that oxygen plays a role in 10^3 reactions in the metabalome, making it one of the most used compounds in various biosynthetic pathways (Raymond and Segre 2006).

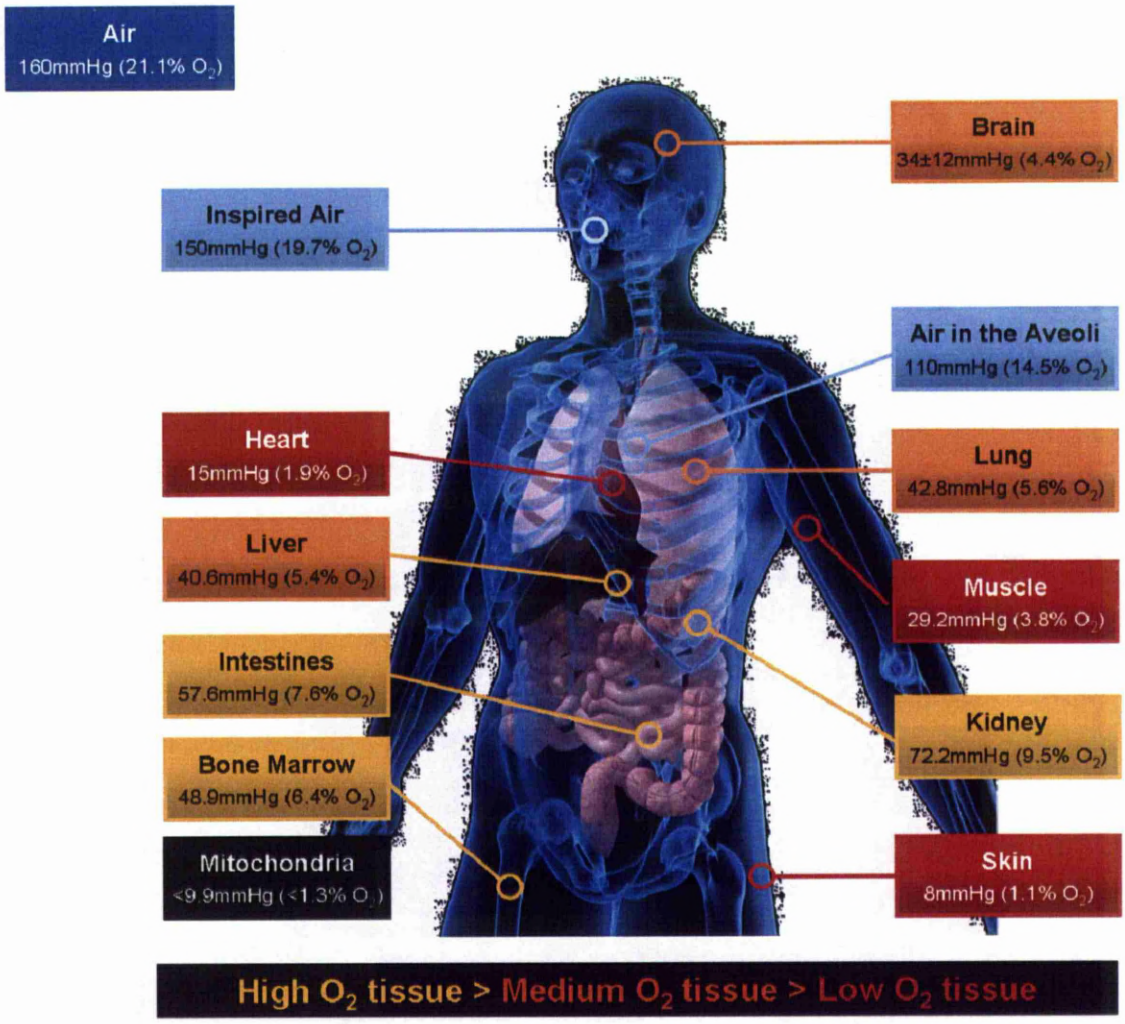

Fig 1.2. Anatomy of the human body with measured O_2 values of several tissues indicated. Values used were from Carreau *et al.*and Wiener *et al.* (Wiener, Feola et al. 1976; Carreau, El Hafny-Rahbi et al. 2011) Many of these values are of a specific tissue and so conflicting information exists in the literature for a definitive oxygen tension for an organ. Specifically there are several citations reporting low kidney oxygen tensions.

1.4 Sensing oxygen and maintaining homeostasis

In the context of modern biology, a wide-array of organisms have evolved a dependency on the availability of oxygen and die in anoxic or hypoxic conditions. For unicellular life this dependency extends to simply finding and living in the optimal environment. However complex multicellular life needs to maintain oxygen homeostasis over many cells and tissues, regulating the needs of both the whole organism and individual cells. Across a multicellular organism, such as *Homo sapiens*, different tissues and organs have varying degrees of oxygenation (**Fig 1.2**) (Birol, Wang et al. 2007; Evans, Gardiner et al. 2008; Carreau, El Hafny-Rahbi et al. 2011). This variability is attributable in part to the differing vasculature, metabolic demands and cellular functions, best

illustrated by the O_2 requirements of the brain; an organ accounting for 2% of human body mass but 20% of total body-wide O_2 consumption (Nilsson 1996). Oxygen homeostasis can be disrupted at a number of levels and in a number of ways. So though dysregulated, disrupted or altered oxygen homeostasis is a common feature of many processes, the precise manifestation of these changes can be complex. Normoxia is a term used to describe the *ordinary* resting oxygen tension, whether describing atmospheric or tissue oxygenation status. As the cellular make-up of the body experiences different physiological oxygen tensions, so to is there a great range of normoxic tensions. In the atmosphere, 21% O_2 is considered normoxia, whereas in the upper airways 12% is said to be the norm and in the retina as low as ~1% are normal (Wangsa-Wirawan and Linsenmeier 2003; Taylor and McElwain 2010). Alteration to normoxia occurs in two ways, either oxygen levels are increased or decreased. Most research focuses on the decrease from normoxia, known as hypoxia. The opposite situation is hyperoxia. Hyperoxia is often used to describe O_2 tensions above atmospheric levels, but could be correctly used to describe cells exposed to levels above physiological norms, such as found in most cell culture conditions. Changes from normoxia can therefore occur at various levels: atmospheric, body-wide or tissue-specific. The mode of alteration is also said to have a consequence. The hypoxic or hyperoxic episode can be described as acute, chronic, transient, prolonged, intermittent or as a combination. Acute episodes are characterised as rapidly occurring changes (seconds-hours), as discussed for stroke and myocardial infarction and also in the case of wounding, in which oxygen is introduced to tissues not normally exposed to the atmosphere. Chronic insults are opposite to acute, in which changes from normoxia are gradual (days-weeks) as is the case for atherosclerosis and often cancer. Transient and prolonged situations also skew the nature of the insult as pre-insult conditions are either reached rapidly, or slowly; acute and prolonged will often have severe-to-fatal consequences in the context of stroke. Intermittent insults place a different stress upon the tissue, occurring as a cycle of alterations. This is known to occur in the prevalent disorder of sleep apnoea, in which patients experience pauses or periods of abnormally slow breathing (Belaidi, Joyeux-Faure et al. 2009). On the cellular level, intermittent hypoxia can often be a feature within solid tumours due to transient changes in blood flow (Toffoli and Michiels 2008). Finally the last complication in the

manifestation of altered oxygen homeostasis is re-oxygenation. Re-oxygenation is a cycled feature of intermittent disorders, as well as a common event following many hypoxic episodes characterised by reduced/obstructed blood flow. Resolving of the blood flow issues results in reperfusion, the rapid return of oxygenated blood to the affected area. As mentioned earlier, re-oxygenation brings a host of problems and is not a simple reset to normoxia (Shi 2009). A principal requisite of oxygen homeostasis is the ability to sense oxygen availability and mediate the appropriate response. As previously discussed, oxygen has impacted a number of biological processes, including bioenergetic status, ROS production and biosynthetic pathways. There are therefore numerous postulated biological events capable of relaying information concerning the availability of molecular oxygen (Chimploy, Tassotto et al. 2000; Giaccia, Simon et al. 2004; Agbor and Taylor 2008; Malthankar-Phatak, Patel et al. 2008). Despite this, mammalian oxygen sensing can be broadly considered in two categories (i) organism level regulation and (ii) cellular level regulation.

1.4.1 Molecular mechanisms behind regulated breathing

In human physiology, oxygen homeostasis is maintained at the level of the whole organism *via* breathing and the circulatory system. Underpinning this system is the oxygen sensitive organ, the carotid body, which is found in the neck at the carotid bifurcation (Lopez-Barneo, Ortega-Saenz et al. 2009). The carotid artery is well-irrigated by blood, screening continuously and rapidly detecting chemical changes, such as pH, CO_2, glucose and O_2. On the molecular level, the O_2 responsiveness of the carotid body is mediated through the O_2-sensitive K^+ channels, which are inhibited by the absence or reduction of O_2. The hypoxic stimulation of these channels then leads to the sending of afferent projections onto brainstem respiratory nuclei and serves to provoke hyperventilation, thereby increasing blood O_2 levels. (Joseph and Pequignot 2009). The breathing response to insufficient oxygen is rapid occurring within seconds. This is indicative of the body's absolute reliance on available O_2, as even brief periods of restricted breathing (hypoxemic hypoxia) can have severe if not fatal consequences within minutes. The reason for this is the reliance of neuronal cells on aerobic respiration to maintain sufficient ATP levels, which when sufficiently hindered leads to disruption of ATP-sensitive K^+ channels. The disruption of these channels results in 'irreversible ionic derangements' resulting in Na^+ and Ca^{2+} overload (Yamada and Inagaki 2002).

1.4.2 The ubiquitous cellular response to altered oxygen levels

As well as the carotid body's ability to govern the body-wide hypoxic response, all cells of the body are able to elicit their own response to O_2 availability. This can be considered to be the generic cellular response to O_2 and this is chiefly governed by the transcription factor, Hypoxia-Inducible Factor (HIF). The role of the HIF-driven cellular response to hypoxia is to mediate an appropriate change in gene expression and therefore these adaptive changes occur in the order of hours. The mode of cellular adaptation is broad and this is evident in the sheer range of processes governed or affected by HIF activity (Semenza 2003; Lee, Bae et al. 2004). A primary purpose of the adaptive response is to drive the formation of new vasculature in a process known as angiogenesis. Cells secrete the cytokine VEGF which serves to stimulate blood vessel formation, enriching the blood supply for nearby tissues and therefore increasing the oxygen delivery to nearby cells. The production of VEGF is regulated by the activity of HIF and the activity of HIF is dependent on O_2 availability. This mode of action confers a functional feedback system for tissue level oxygen homeostasis. Angiogenesis is an important adaptive process to overcome hypoxic microenvironments but this is not the only adaptive physiological response mediated by HIF signalling. HIF is also known to drive erythropoiesis via the transcription of erythropoietin (EPO), a cytokine that signals bone marrow to produce erythrocytes which are red blood cell precursors. The increase in red blood cell production increases the capacity of the blood to carry and deliver oxygen and thus reduces tissue hypoxia. These two processes alone have garnered much research interest in hypoxia. Aside from its medical importance, there is sufficient interest in hypoxia for the potential benefits to professional sports training or high-altitude activities. For the purpose of this thesis, this facet of hypoxia research represents more of a curiosity than a driving force. However, interesting insights are often made from this avenue of research, including the active measurement of body-produced free radicals during exercise, the bizarre ability of some individuals to hold their breath underwater for over 15 minutes, genetic dispositions to altitude sickness and the effectiveness of hypoxic training regimes etc (Hendriksen and Meeuwsen 2003; Bailey, Young et al. 2004; Lindholm and Lundgren 2009; Sahlin, Shabalina et al. ; Ding, Liu et al.). Outside of these interests, HIF has still far-reaching implications.

HIF is found in all multicellular life and has evolved alongside the geological changes in atmospheric conditions, as well as the biological changes apparent from the increasing complexity of life (Rytkonen and Storz 2010). There has been a growing interest in the HIF system, due to its role in many physiological and pathological processes, including metabolism, vascularisation, erythropoiesis, autophagy, atherosclerosis, ageing, wound-healing, embryogenesis, inflammation, transplantation, sleep apnoea, ischaemic insult and perhaps the most researched aspect, the role of the HIF signalling system in cancer and tumour progression (Lee, Bae et al. 2004; Murdoch, Muthana et al. 2005; Katschinski 2006; Belaidi, Joyeux-Faure et al. 2009; Bellot, Garcia-Medina et al. 2009; Lau, Henriksnas et al. 2009; Zhang, Shao et al. 2009; Brigati, Banelli et al. 2010; Cassavaugh and Lounsbury 2011).

Ischaemia describes a situation in which blood supply to a tissue becomes restricted, with the flow falling below normal tissue tolerance. The decrease in blood flow precedes a decrease in blood-borne supplies, importantly including oxygen. An ischemic insult therefore leads to a subsequent period of hypoxia. There are a number of medical conditions that cause ischaemia and therefore hypoxia occurs as a secondary event in a number of pathological contexts. A widely known setting for ischaemic insult can be found in strokes, in which a haemorrhage or embolism leads to rapid loss of blood flow to the brain. Another well known source of ischaemic insult is in the occurrence of ischaemic heart disease, a prevalent cause of cardiac arrest often arising from atherosclerosis. As well as decreased oxygen delivery to the heart, the loss of heart function and therefore system wide blood flow can lead to hypoxic events occurring throughout the body. As indicated earlier, different tissues have varying oxygenation statuses and differing metabolic demands and this further transpires into differing sensitivities and responses to hypoxia (**Fig 1.2**). Two of the most consequential and sensitive areas to oxygen deprivation are the heart and the brain due to their high metabolic demands and importance. The effects of hypoxia on these tissues can be quite immediate, occurring within minutes. However, the time-scale of the initial damage arising from ischaemia occurs faster than a plausible transcription factor-mediated response and so the role of HIF in ischaemic pathologies is largely in prevention or treatment of secondary events that come about hours after the initial insult. Several references have suggested the pre-conditioning activation of the HIF system to have a

neuroprotective affect against ischaemic stroke, investigated both *in vitro* and *in vivo* (Shi 2009). However, there is evidence to suggest a double-edged sword mechanism, in that activation of HIF-1 can promote apoptosis in cortical neurons. A significant portion of damage after an ischaemic insult (as found in cerebral ischaemia or myocardial infarction) occurs hours after the initial damage and is characterised by a large degree of apoptosis (Krijnen, Nijmeijer et al. 2002; Broughton, Reutens et al. 2009). It is thought that HIF may have a role to play in this wave of apoptosis, either preventitive or conducive (Helton, Cui et al. 2005; Li, Qu et al. 2007; Malhotra, Tyson et al. 2008). Prevention of the damage could positively affect the recovery, predisposition to further complications and/or quality of life of the patient.

A further pathological instance of dysregulated HIF can be found in cancer and tumour progression. Mutations within the HIF system are known to be partially responsible for the development of cancer, such as in the case of von Hippel-Lindau disease. Furthermore, numerous factors of cancer often lead to the pathological activation of the pathway and this often has maladaptive repercussions (Maxwell, Pugh et al. 2001). For example, as tumours develop they often outgrow their blood supplies, hypoxic regions begin to form and this in turn leads to HIF activation (**Fig 1.3**). Activation of the HIF pathway in cancerous cells has been shown to increase malignancy and is associated with poor prognosis for some cancers (Zhou, Schmid et al. 2006). In light of the current understanding of downstream HIF regulation, it is now known that HIF can encourage almost every aspect of metastasis (Lu and Kang 2010). As well as increasing the invasive ability of cancer, the pathological activation of HIF can also confer resistance to chemotherapy (Liu, Ning et al. 2008; Nardinocchi, Puca et al. 2009). In spite of the many oncogenic properties of HIF-1, there are several instances of the reverse. There has been debate whether HIF-1 plays a pro- or anti-apoptotic role. There is considerable evidence for both arguments and it is now well-established that HIF may act in either capacities (Piret, Mottet et al. 2002). The pro-apoptotic role of HIF-1 has been surmised to contribute to significantly longer survival times in patients diagnosed with lung carcinoma (Volm and Koomagi 2000). However, it is also appreciated that the hypoxic tumour environment acts as a selection pressure, encouraging the emergence of the more aggressive phenotypic traits. Nevertheless it appears

HIF activation has a greater role to play in the detrimental effects in cancer than the anti-tumourigenic effects (Semenza 2003).

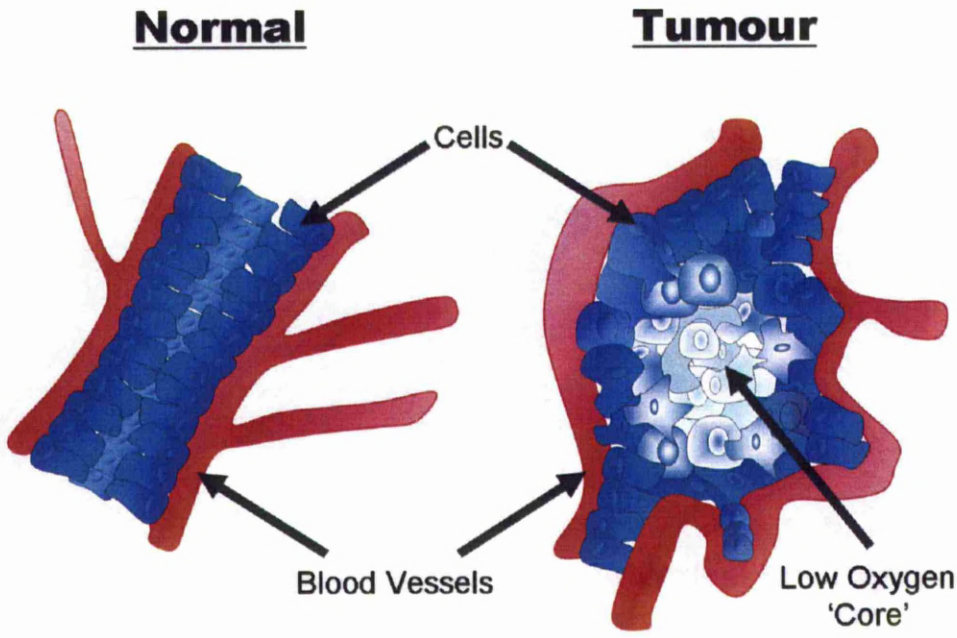

Fig 1.3. Graphic depiction of dysregulated oxygen homeostasis arising from tumour growth and abnormal vasculature, as occurs in many solid tumours.

In summary, a controlled oxygen microenvironment is a hallmark feature in many physiological events, critical throughout embryogenesis and development, an important factor in stem cell biology, a cue in the immune response and relevant to spermatogenesis amongst other well-documented events (Yun, Maecker et al. 2002; Wenger and Katschinski 2005; Novak and Tyson ; Eliasson and Jonsson ; Gale and Maxwell ; Patterson and Zhang 2010). It is very difficult to overemphasise the pervasive importance of oxygen to a multicellular organism such as humans. This importance extends to the HIF signalling network which has evolved and intertwined with the cellular oxygen microenvironment creating an interdependence between the two. The involvement of HIF in the critical physiological events listed, as well as roles in the pathological events discussed has made the molecular HIF network an increasingly desirable pharmaceutical target. It is therefore an important goal to better understand the regulatory motifs governing HIF activity with a view towards the stronger rationale behind the development of future therapeutics (Nangaku, Kojima et al. 2006; Niatsetskaya, Basso et al. ; Smith and Talbot).

1.5 Canonical oxygen-dependent HIF signalling

The transcription factor HIF has emerged as a central element involved in the cellular response to altered oxygen availability. HIF-1 was initially discovered by Greg Semenza's group in 1993 and shown to be the transcription factor that confers the hypoxia-inducibility of the EPO gene, the hormone controlling red blood cell production (Semenza and Wang 1992). Since then, it has been found that HIF can mediate wide changes in gene expression and is implicated in regulating over 400 genes (Elvidge, Glenny et al. 2006) influencing such diverse functions as apoptosis, cell-cycle, differentiation, immune response, energy metabolism, cell migration and angiogenesis (**Table 1.1**) (Piret, Mottet et al. 2002; Lee, Bae et al. 2004; Semenza 2011). Furthermore, in a study by Glenny *et al.* (2006), it was shown that HIF was responsible for up-regulating 53% of all hypoxia-inducible genes in the MCF7 cell line (Elvidge, Glenny et al. 2006).

HIF is functional as a heterodimeric transcription factor compromised of an O_2 regulated α-subunit and a constitutively available β-subunit. Both the protein stability and the transcriptional activity of HIF are governed by the availability of molecular oxygen. In the presence of oxygen, HIF-α is hydroxylated at two proline residues found within the oxygen-dependent degradation domain (ODD) (**Fig 1.4**). The hydroxylation is catalysed by the intracellular prolyl hydroxylases 1-3 (PHDs) and requires molecular oxygen as well as iron, 2-oxoglutarate and ascorbate. The tumour suppressor protein von Hippel Lindau protein (pVHL) is then able to interact with the hydroxylated HIF-α subunit, leading to ubiquitination and subsequent degradation by the 26S proteasome (Maxwell, Wiesener et al. 1999). This mechanism therefore confers an oxygen-sensitive control of HIF-α protein levels. The transcriptional activity of HIF is regulated by a further hydroxylase, known as Factor Inhibiting HIF-1α (FIH). FIH is able to hydroxylate an asparagine in the C-terminal of HIF-α in a manner similar to the PHDs. This modification prevents HIF from recruiting CBP/p300, a necessary co-activator for the transcriptional activity of HIF (**Fig 1.4**) (Lee, Bae et al. 2004; Taylor and Pouyssegur 2007).

In sufficiently hypoxic conditions, HIF-α escapes the hydroxylation events and is able to accumulate in the nucleus and bind with HIF-β. The complete heterodimer, HIF, is then able to activate genes containing a hypoxic response element (HRE) consensus sequence (-RCTTG-) in their promoter or enhancer regions (**Fig 1.4**). As well as acting as an transcriptional inducer, HIF has also

been shown to act as a repressor, reducing the expression of several notable genes, such as; p53, FADD and ENT1 among others (Lee, Lee et al. 2001; Eltzschig, Abdulla et al. 2005; Hindryckx, De Vos et al. 2010) The mechanisms for this activity remain poorly understood, though it appears it is not mediated through direct-interaction but possibly through co-operative action with other proteins.

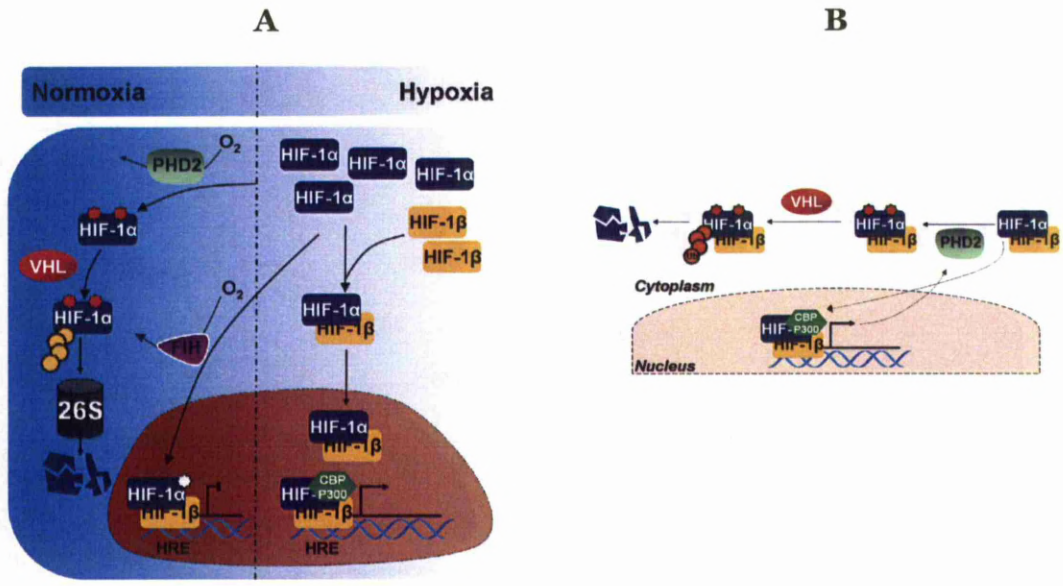

Fig 1.4 A representation of (**A**) the canonical HIF oxygen sensing pathway and (**B**) the featured negative feedback loop within the canonical HIF signalling pathway.

An additional regulatory aspect to HIF signalling, which is of interest to this study, is the presence of an auto-regulatory negative feedback loop within the core HIF signalling motif (Epstein, Gleadle et al. 2001; Stiehl, Wirthner et al. 2006). Both PHD2 and PHD3 themselves are target genes for HIF and therefore upon the hypoxic activation of HIF are subject to up-regulation. This signalling motif is commonly referred to as a delayed negative feedback loop, with the delayed aspect arising from the time needed for transcription and translation of the PHDs. Delayed negative feedback loops are a common signalling motif in dynamic systems (and necessary in oscillatory systems) (Yeger-Lotem, Sattath et al. 2004; Novak and Tyson 2008). Typically this motif is commonly viewed as a standard mechanism for homeostasis, though it also offers the potential for encoding additional complexity within the HIF transduction pathway; a concept paramount to this thesis which will be discussed in greater depth later.

Function	Effect Mediated by
Angiogenesis	↑**MRNA;** VEGF, ENG, LEP, LRP1, TGF-β3
Apoptosis	↑**MRNA;** NIP3, NIX, RTP801
Autophagy	↑**MRNA;** BNIP3, BNIP3L (Bellot, Garcia-Medina et al. 2009)
Cell Adhesion	↑**MRNA;** MIC2
Cell Migration	↑**MRNA;** ANF/GPI, c-MET, LRP1, TGF-α
Cell Proliferation	↑**MRNA;** Cyclin G2, IGF2, IGF-BP1-3, WAF-1, TGF-α, TGF-β3 VEGF, HGF, & FGF (Tamama, Kawasaki et al. 2011)
Cell Survival	↑**MRNA;** ADM, EPO, IGF-BP1-3, NOS2, TGF-α, VEGF
Circadian Clock	Synergistic relationship with CLOCK to ↑**MRNA** of Vasopressin (Ghorbel, Coulson et al. 2003)
Cytoskeletal Structure	↑**MRNA;** KRT14, KRT18, KRT19, VIM
Differentiation	Inhibits differentiation *via* synergistic relationship with NOTCH to ↑**MRNA;** at least PGK1 (Sainson and Harris 2006). Promoting of adipogenesis *via* ↑**MRNA;** GLUt1, GLU4, IRS3 (Shimba, Wada et al. 2004)
DNA repair	↑**MRNA;** Twist(Sun, Ning et al. 2009) Inhibitory relationship with myc leads to ↓**MRNA & Protein;** NBS1 (To, Sedelnikova et al. 2006)
Drug Resistance	↑**MRNA;** MDR (Comerford, Wallace et al. 2002)
Erythropoiesis	↑**MRNA;** EPO
Glucose Metabolism	↑**MRNA;** HK1, HK2, AMF/GPI/ ENO1, GLUT1, GADPH, LDHA, PFKBF3, PFKL, PGK1, PKM, TPI, ALDA, ALDC
HIF-1 Response	↑**MRNA;** EGLN1, EGLN3
Immune Function	HIF regulates a myriad of genes associated with Macrophage, Monocyte and Neutrophil function (Murdoch, Muthana et al. 2005)
Iron Metabolism	↑**MRNA;** Ceruloplasmin, Transferrin, Transferrin receptor
pH Regulation	↑**MRNA;** Carbonic anhydrase 9
Stem Cell Maintenance	↑**MRNA;** Oct-4 (Covello, Kehler et al. 2006), pref-1 (Lin, Lee et al. 2006), DEC1 (Yun, Maecker et al. 2002)
Transcriptional Regulation	↑**MRNA;** DEC1, DEC2, ETS-1, NUR77
Vascular Tone	↑**MRNA;** α1B-adrenergic receptor, ADM, ET1, NOS-2, Haemoxygenase-1

Table 1.1. A non-exhaustive table of HIF-mediated biological processes and the mode of regulation. This table is heavily adapted from Lee *et al.* 2004 with additional contributions referenced (Lee, Bae et al. 2004)

1.6 Alternative O_2-dependent HIF pathway

For simplicity, convenience and effect, the mechanisms of HIF regulation detailed below have been divided into O_2-dependent and O_2-independent modes of action. A degree of caution must be taken in this segregation, as there is significant possibility of crossover e.g. NF-κB, HuR and ROS may contribute both to the O_2-dependent and O_2-independent regulation of HIF.

The canonical oxygen-dependent HIF signalling pathway is well established, however there are alternative modes of HIF regulation that are directly or indirectly dependent on the availability of molecular oxygen. The regulatory mechanisms discussed below outline the complexity of molecular oxygen as an environmental cue/stimulus and how some of this complexity is integrated within the HIF pathway. However, the mechanisms discussed below are far from an exhaustive overview of all non-canonical interactions. Major transcriptional hubs, such as HIF, are often exposed to a staggering amount of crosstalk and modulation and therefore only the most salient crosstalk events are discussed, both for the alternative O_2-dependent HIF pathway and the following section detailing O_2-independent regulation of HIF. Notable crosstalk events not discussed in the text are listed in **Table 1.2** (found at the end of the section).

1.6.1 Mitochondria & reactive oxygen species

Perhaps the best researched and most controversial alternative HIF regulatory mechanism is the involvement of ROS in mediating the HIF hypoxic response. Essentially the proposed mechanism can be separated into two aspects, (1) the hypoxia driven production of ROS and (2) the integration of ROS into the canonical oxygen sensing pathway. Biological ROS has been shown to be primarily produced by mitochondria as a result of an active electron transport chain (Murphy 2009). The electron transport chain is composed of a uni-directional sequence of four complexes functioning as electron acceptors/donors. These complexes are termed Complex I, II, III and IV, in which IV acts as the terminal acceptor complex donating the electrons to reduce O_2 to H_2O. Complex I,II and III leak a portion of the electrons transferred causing the partial reduction of O_2 and formation of the superoxide anion $O_2^{-\bullet}$ (Turrens 2003). The superoxide anion is then converted to other forms of cellular ROS, such as H_2O_2 or the highly reactive hydroxyl radical when in the presence of transition metals (Thannickal and Fanburg 2000). The availability of cellular molecular oxygen affects the activity of the electron transport chain and therefore the production of ROS. Classical physics suggests increasing O_2 should increase ROS production. However the opposite effect has also been several times reported, in which hypoxia leads to an increase in ROS (Hamanaka and Chandel 2009). The hypothesised molecular mechanisms

controlling hypoxia-mediated ROS production centre on Complex III as the source (Hamanaka and Chandel 2009). The other side of the involvement of ROS in O_2-sensing is how the hypoxia-produced ROS translates into a physiological hypoxic response. ROS has been shown to function in a number of signal transduction pathways, particularly redox-sensitive pathways such as NRF2 and NF-κB (Bowie and O'Neill 2000). It is therefore possible that some hypoxic sensitivity is conferred through these separate signalling systems and these may have downstream implications on the activity of the HIF signalling system (Malec, Gottschald et al. 2010). However, it has also been suggested that ROS may have a more direct affect on the HIF signalling system and is capable of stabilising HIF protein by modulating PHD hydroxylation activity. This effect is proposed to occur *via* the ROS-driven conversion of Fe^{2+} to Fe^{3+}, where Fe^{2+} is a necessary cofactor of the PHDs (Gerald, Berra et al. 2004; Patten, Lafleur et al. 2010). This mechanism is suggested to work within a range of hypoxic tensions and is abated at near-anoxia at which point the PHD hydroxylation rates become overwhelmingly diminished (Guzy, Hoyos et al. 2005).

1.6.2 NF-κB crosstalk

NF-κB is a dimeric transcription factor that affects a wide and diverse array of cellular activities, representing a major transcriptional hub (Pahl 1999). It is principally known as a stress response factor involved in inflammation and the immune response, and is activated by a plethora of stimuli, such as cytokines, oxidative stress, bacterial toxins and DNA damage etc (Bowie and O'Neill 2000; Janssens and Tschopp 2006; Culver, Sundqvist et al. 2010). Amongst these activating stimuli, hypoxia has been shown to also stimulate NF-κB and there are several molecular mechanisms proposed to explain this (Culver, Sundqvist et al. 2010). (i) The first potential mechanism relates to the previously discussed production of ROS in hypoxia and the subsequent activation of NF-κB *via* the ROS-induced post-translational modification of Inhibitor of κBα (IκBα), a negative-regulator of NF-κB (Imbert, Rupec et al. 1996). (ii) Another hypothesised mechanism is the potential hydroxylation of the Inhibitory Kinase Kinase (IKK) component of the NF-κB transduction pathway by PHD1, and to a lesser extent PHD3 (Cummins, Berra et al. 2006). (iii) A more recently elucidated possible mechanism is *via* the hypoxic activation of calcium/calmodulin-dependent kinase 2 (CaMK2) which leads to the activation of the NF-κB signal transduction pathway (Cai, Liu et al. 2008; Culver,

Sundqvist et al. 2010). These are just a few of the reported possibilities of hypoxic NF-κB activation, regardless their potential importance is in the ability to integrate NF-κB signalling into the canonical HIF system (*via* crosstalk mechanisms). There have been several studies detailing crosstalk mechanisms, demonstrating the NF-κB regulation/modulation of the HIF system. The foremost idea is the regulation of HIF-1α mRNA by the activity of NF-κB (Belaiba, Bonello et al. 2007; Rius, Guma et al. 2008). It is therefore conceivable that the cellular NF-κB status can serve to prime the canonical HIF response. A lesser-characterised mechanism is centered around the sequestering of FIH by IκBα. FIH has been shown to bind to a range of ankyrin repeat domain containing proteins, including IκBα (Cockman, Webb et al. 2009). It has been suggested that increased expression of IκBα leads to the sequestration of FIH away from HIF-α and therefore promotes the transcriptional activity of HIF (Schmierer, Novak et al. 2010). These regulatory events and their effect on the output of the HIF system is further complicated as HIF activity has been shown to also affect NF-κB (Walmsley, Print et al. 2005). This complexity is made more overwhelming when the temporal arrangements of both pathways are considered, especially regarding the elucidated oscillatory nature of NF-κB signalling (Nelson, Ihekwaba et al. 2004).

1.6.3 Translational regulation of HIF-α

Hypoxia is cited to cause a global change to cellular protein synthesis (Koumenis, Naczki et al. 2002). During periods of hypoxia the energy status of the cell changes and several adaptive responses occur to minimise the expenditure of ATP. One such event is to reduce the energy used in the process of translation. Change in global protein synthesis could be expected to affect the steady-states/equilibria in several signalling arrangements, including that of canonical HIF regulatory systems. This mechanism itself can mediate some forms of hypoxic response. Additionally, in periods of hypoxia reduced protein synthesis itself may be beneficial to preferentially maintain/induce the synthesis of proteins relevant to the hypoxic stress (Young, Wang et al. 2008). This has been proposed to occur for HIF-α mRNAs in a IRES-mediated (internal ribosome entry sequence) fashion, of which IRES elements are described to promote the translation initiation within the mRNA nucleotide sequence (Lang, Kappel et al. 2002). However, a further paper has refuted the proposed function of IRES elements in mediating translation of stress pathway proteins,

suggesting that the observed increased in protein expression correlates mainly with increased mRNA production (Young, Wang et al. 2008). Despite this there are other suggested posttranscriptional regulatory events that are in some way O_2-sensitive. The first of these is mediated through the interaction of HIF-1α mRNA with the RNA-binding protein, Human Antigen R (HuR) (Sheflin, Zou et al. 2004; Galban, Kuwano et al. 2008). HuR has been shown to affect HIF-1α mRNA trafficking and stability, depending on the activating conditions; one such activating stimuli is hypoxia (Sheflin, Zou et al. 2004). Furthermore HuR has been implicated in regulating a number of mRNAs in a hypoxia-mediated fashion, including pVHL (Masuda, Abdelmohsen et al. 2009). The hypoxic regulation of HuR may therefore work in tandem with the canonical HIF response, although this mechanism is probably sensitive to crosstalk events as HuR is implicated in regulating many signalling systems (Lebedeva, Jens et al. 2011). The final O_2-sensitive posttranscriptional regulatory mechanism is the role of microRNA and the hypoxic response. MicroRNAs are short non-coding RNAs that are capable of destabilising mRNA or repressing translation of mRNA. Since their official discovery in 1993, microRNAs are increasingly accepted in the central dogma of the flow of information from DNA and as such have been implicated in regulating a vast array of cellular processes (Lee, Feinbaum et al. 1993; Lu, Li et al. 2009; Robinson 2009). Unsurprisingly there has been a series of emerging evidence implicating microRNA in the hypoxic response; both in response to hypoxia and modulation of the canonical HIF response (Kulshreshtha, Ferracin et al. 2007; Huang, Le et al.). Firstly, many microRNAs are known to change expression pattern in response to hypoxia and this postulates microRNAs as a broad component in the cellular response to hypoxia (Kulshreshtha, Davuluri et al. 2008). More specifically several microRNAs have been revealed to target HIF-1α mRNA, such as miR-199a, mir-155, miR-20b and microRNA cluster miR 17-92 (Taguchi, Yanagisawa et al. 2008; Lei, Li et al. 2009; Rane, He et al. 2009; Bruning, Cerone et al.). miR20b has been shown to be down-regulated in response to hypoxia and this is in accordance with data also showing HIF can repress expression of miR20b. However, HIF-1α is down-regulated by this microRNA and therefore forms a double-negative feedback loop which has implications for the HIF response to hypoxia. More recently it has been shown that microRNA-155 is HIF-1 inducible and as well as destabilising HIF-1α, constituting a feedback loop cited to

oscillatory potential to the HIF system (Bruning, Cerone et al. 2011). As a near fundamental aspect of gene expression, microRNAs represent a broad mechanism of regulation, sensitive to widely varied stimuli. It is therefore likely that alongside the oxygen-dependent regulation of HIF that microRNAs feature also in the O_2-independent regulation of HIF (Cha, Chen et al.).

1.7 O_2-independent regulation of the HIF pathway

Though most research centred on HIF concentrates on the response and role of this transcription factor in hypoxia there are many studies detailing oxygen-independent regulation of the HIF pathway. These mechanisms therefore may serve to prime the HIF pathway, or to provide context, integrating various signal transduction networks into the HIF hypoxic response.

1.7.1 HSP90 and Rack1

A study by Liu *et al.* (2007) demonstrated that Heat shock protein 90 (HSP90) and receptor of activated kinase C (Rack1) compete for binding to HIF-1α and this competition regulates HIF-1α protein stability. HSP90 binding promotes stability and conversely Rack1 destabilises HIF-1α in a PHD/pVHL independent manner (Liu, Baek et al. 2007). Rack1 is known principally as a scaffold protein interacting with protein kinase C, though there are a host of other researched interactions affecting various cellular processes (McCahill, Warwicker et al. 2002). Both Rack1 and HSP90 have been shown to bind to the PAS domain of HIF-1α (**Fig 1.5**), in which Rack1 promotes the ubiquitination and subsequent proteasomal degradation of HIF-1α (Liu, Baek et al. 2007). HSP90 is an abundant stress-response protein involved in the folding, activation and stabilisation of target proteins both in stressed and basal conditions (Sreedhar, Kalmar et al. 2004). Dysregulation of HSP90 is a common hallmark in cancer, often leading to the stabilisation of overexpressed oncogenes (Hahn 2009). It is therefore possible that this pathway may have significant physiological/pathological implications on the HIF system, affecting the potential O_2-dependent response of HIF.

1.7.2 Deubiquitinases; VDU1 and VDU2

The O_2-dependent regulation of HIF-α protein stability hinges upon its sequential post-translational modification, culminating in its ubiquitination and ensuing degradation (Taylor and Pouyssegur 2007). The ubiquitination event is typically portrayed to occur in a one-way manner though there has been significant research into the regulated reversibility of this process *via* a class of

proteins known as deubiquitinases (DUBs). Currently there are almost 100 known human DUBs and two of these have been implicated in the HIF system, namely pVHL protein-interacting deubiquitinating enzyme 1 and 2 (VDU1 and VDU2) (also known as USP33 and USP20 respectively) (Li, Wang et al. 2002; Li, Wang et al. 2005). The initial characterisation of VDU1 and VDU2 by Li *et al* (2002a, 2002b)(Li, Na et al. 2002; Li, Wang et al. 2002) showed that these proteins are targeted for proteasomal degradation by pVHL. However a further paper by this group has shown that ectopic expression of VDU2 acts to stabilise HIF-1α protein and this is proposed to occur via the deubiquitination of HIF-1α (Li, Wang et al. 2005). There are still significant questions remaining as to the stimuli regulating VDU2 and whether this mechanism may play a significant role in the physiological and/or pathological context.

1.7.3 Growth factor regulation

The extensive signalling transduction network of mitogen-activated protein kinase has also been found to regulate HIF signalling, sensitising HIF activity to a number of intergratable stimuli, notably including growth factors. Of the numerous MAPK effectors, HIF-1 regulation has been chiefly attributed to the efforts of p38 and p42/44 (Mylonis, Chachami et al. 2006; Nys, Van Laethem et al. 2010). Various modes of HIF-α regulation by MAPK have been reported, including the contentious issue of p42/p44 phosphorylation of HIF-1α; a mechanism proposed to originally effect HIF-1α protein abundance and later reported to effect transactivation potential, involving the enhanced p300 recruitment to HIF-1α (Sang, Stiehl et al. 2003). It has even been suggested that p42/p44 does not directly affect HIF-1, but the potentiality of downstream gene expression as has been shown for the hypoxic expression of VEGF mRNA (Yang, Wang et al. 2009). Other modes of MAPK activation of HIF signalling include the p38/akt stimulated increase of HIF-1α mRNA, translation and protein stabilisation (Khurana, Nakayama et al. 2006; Nys, Van Laethem et al. 2010). The Phosphoinositide 3-kinase signalling has a similar role to the MAPK network, acting as a broadly activated transducing network also responsive to growth factors. Again similar to MAPK signalling, PI3K has also been shown to regulate the HIF system, though there is more clarity on how this is achieved. Growth factor activation of phosphoinosiltide 3-kinase signalling enables mammalian target of rapamycin (mTOR) to facilitate the translation of HIF-1α mRNA and this has been shown to be sufficient for the normoxic stabilisation of

HIF-1α (Dery, Michaud et al. 2005). This arm of regulation has also been found to function in response to re-oxygenation (Harada, Itasaka et al. 2009).

O_2-dependent	
PHDs	The PHDs hydroxylate HIF-α, a process which uses molecular oxygen. The hydroxylated HIF-α is then targeted for proteasomal degradation. PHD2 & 3 are HIF target genes.
ROS	ROS production increases during hypoxia, which then reduces the hydroxylation potential of the PHDs by affecting the redox state of the iron co-factor.
NF-κB	Hypoxia induces the NF-κB system *via* several potential mechanisms. NF-κB activation leads to an increase in HIF-1α mRNA.
microRNAs	Mir20b is down-regulated in response to hypoxia. This in turn leads to a stabilisation of HIF-1α mRNA, a known target of mir20b.
HuR	The protein HuR is responsible for stabilising and enhancing the trafficking of HIF-1α and possibly pVHL mRNA in response to hypoxia.
p53	A lot of contradictory information exists. Hypoxia induces p53 atypically. P53 is then able to either downregulate, upregulate or have no effect on HIF-1 (Sermeus and Michiels 2011).
HIF-3α	HIF-3α protein levels are increased in response to hypoxic inhibition of the PHDs and the activity of HIF-1/2. HIF-3α is then able to competitively inhibit HIF-1α&-2α for HIF-1β
O_2 consumption	Hypoxia leads to changes in mitochondrial O_2 consumption which affect cellular availability of molecular oxygen for use in PHD-mediated hydroxylation of HIF-α.
Chromatin Remodelling	Multiple mechanisms. Hypoxia causes changes to various HATs and HDACs affecting the promoters of several HIF target genes (Kenneth and Rocha 2008).
Nitric Oxide	iNOS is induced by HIF-1a increasing NO. NO has a diverse set of consequences, regulating HIF-1α protein stability as well as transcriptional activity (Brahimi-Horn, Mazure et al. 2005).
NRF2	NRF2 is a redox-sensitive transcription factor activated by intermittent hypoxia. NRF2-dependent Trx1 enhances HIF-1 signalling (Malec, Gottschald et al. 2010). HIF-1 is capable of downregulating NRF2 (Loboda, Stachurska et al. 2009).

O_2-independent	
HSP90 vs Rack1	HSP90 and Rack1 compete for binding to HIF-1α. HSP90 promotes protein stability and conversely Rack1 destabilises HIF-1α in a PHD/pVHL independent manner (Liu, Baek et al. 2007).
VDU2	VDU2 deubiquitinates HIF-1α, thereby reducing the extent of proteasomal degradation.
HAF	HAF is an E3 ubiquitin ligase targeting HIF-1α for proteasomal degradation. While also able to bind to HIF-2α, this interaction increases HIF-2α transactivation.
Cytokines and Hormones	A rich assortment of cytokine led regulation of HIF reviewed extensively by Haddad *et al* 2005. Expectantly occurs with a large degree of overlap with NF-κB regulation of HIF.
TCA Cycle Intermediates	Several TCA intermediates inhibit PHD activity, thereby stabilising HIF-α. This is considered a pathological mechanism rather than physiological (Fong and Takeda 2008).
pH	Acidosis promotes nucleolar sequestration of pVHL, thereby stabilising HIF-α. (Mekhail, Gunaratnam et al. 2004)
CommD1	CommD1 protein is able to bind to HIF-1α which disrupts HIF-1 heterodimerisation. This process also disrupts HSP90 binding. CommD1 is also able to inhibit NFκB signalling.

Table 1.2. Overview of several salient HIF regulatory mechanisms. Abbreviations used in the table (not used elsewhere); The Citric Acid Cycle (TCA), Hypoxia-associated Factor (HAF), Nuclear factor erythroid-derived 2 (NRF2).Though these mechanisms have been divided into O_2-dependent or independent, there is significant possibility of crossover, in that many oxygen-independent mechanisms may also activate NRF2, HuR, Chromatin Remodelling, p53, Nitric Oxide etc. further outlining the complexity of regulation supporting the HIF signalling network.

1.8 Protein members of the canonical HIF pathway

The canonical HIF pathway members are currently considered to be; the HIF-α isoforms (excluding HIF-3α which is included below for the sake of completion), HIF-β isoforms, PHD isoforms, pVHL and FIH.

1.8.1 HIF-α (HIF-1α, HIF-2α and HIF-3α)

HIF-α is the oxygen-labile subunit of the heterodimeric complex with HIF-β and is currently known to occur as three isoforms HIF-1α, HIF-2α and HIF-3α. Of these three isoforms, HIF-1α and HIF-2α form transcriptionally active heterodimers (when bound with HIF-β), whereas the role of HIF-3α is less certain. Understanding explicitly the roles and functions of these isoforms is a current aim within the field of hypoxia research.

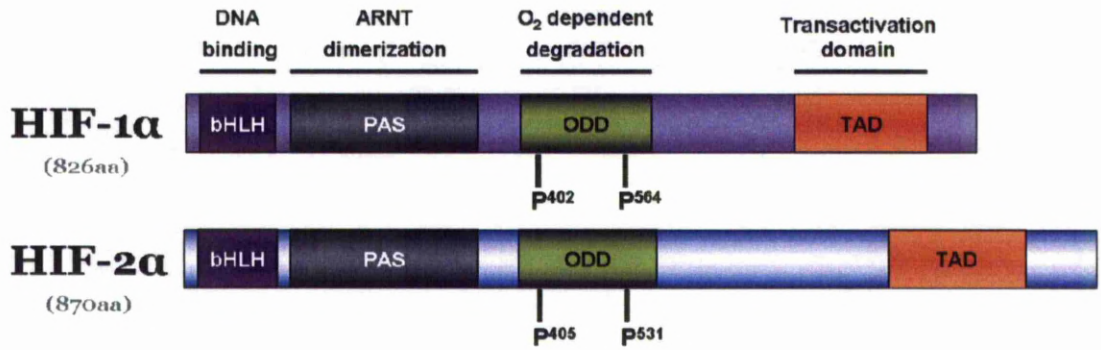

Fig 1.5. Domain representation of the transcriptionally active HIF-α isoforms with the hydroxylated proline residues labelled. Basic domain arrangement adapted from Lee *et al* (2004)

1.8.1.1 HIF-1α

The HIF-1α isoform is constitutively and ubiquitously expressed across all tissues and is therefore often thought of as the major α isoform (Gradin, McGuire et al. 1996). The gene is highly conserved and found as an orthologue in all multicellular life, which reinforces the importance of this transcription factor (Rytkonen, Williams et al. 2011). Furthermore, HIF-1α is necessary for healthy embryogenesis. HIF-1α knockout mice have been found to be embryonic lethal at E11 and this arises due to incorrect vasculature amongst other problems (Krishnan, Ahuja et al. 2008). The research interest in the HIF-1α isoform is further piqued due to the specific roles it appears to play in various pathologies, including the association of cancer malignancy, chemoresistance with increased HIF-1α expression (Lu and Kang 2010). There are two *Homo sapiens* mRNA transcript variants of HIF-1α: a 2481bp (NM_001530) and a 2208bp (NM_181054) variant, in which the longer transcript translates to

having an additional C-terminal sequence. Conventionally most research, including our own, has focused on the shorter transcript as the main variant. The translation of this shorter transcript results in an 827 aa, 120kDa protein that is found predominantly in the cell nucleus. The nuclear import of HIF-1α occurs in an importin-dependent manner via the nuclear localisation signal found in the C-terminal between residues 718-753 (**Fig 1.5**) (Depping, Steinhoff et al. 2008). Once inside the nucleus HIF-1α (as the heterodimeric complex) is free to bind to the target DNA consensus, the HRE. This consensus is shared by the transcriptionally active α units, nevertheless the different α subunits have overlapping and separable target gene expression profiles. A study examining the genome-wide analysis of HIF DNA binding in MCF7 cells found ~70% of HIF-α binding genes uniquely bound HIF-1α over HIF-2α and ~21% of genes bound both isoforms (Mole, Blancher et al. 2009). Further work by Imamura *et al.* 2009 examined the effect of HIF-1/2α siRNA knockdown in colon cancer cells and found HIF-1α was solely responsible for the hypoxia induction of ~30% of HIF-dependent genes and jointly responsible alongside HIF-2α for ~50% of HIF-dependent genes (Imamura, Kikuchi et al. 2009). So despite the similarities between the two transcriptionally active isoforms HIF-1α has distinct and broader roles.

The hypoxic sensitivity of HIF-α is underpinned by the hydroxylation and polyubiquitination of the protein and these are the most widely-regarded post-translational modifications of the α-subunits. However, emerging work has demonstrated the occurrence of other post-translational modifications including phosphorylation, SUMOylation and S-nitrosation (Brahimi-Horn, Mazure et al. 2005). Of these modifications phosphorylation is the best characterised. Phosphorylation of HIF-1α has been proposed to occur through a variety of kinases and to occur on a variety of residues. However a common consensus is that the phosphorylation of HIF-1α leads to the increase in transcriptional activity of the HIF heterodimer (Brahimi-Horn, Mazure et al. 2005). Conversely, more recent evidence indicates that the SUMOylation of HIF-1α has the opposite effect, repressing the transcriptional output of HIF-1 (Huang, Han et al. 2009; Kang, Li et al. 2010; Xu, Zuo et al.). The SUMOlyation of HIF-1α has been proposed to occur via the activity of the E3 ligase PIASγ, potentially on residues K391 and K477 (Kang, Li et al. 2010). Moreover, the SUMOylation of HIF has been suggested to be enhanced by the hypoxia-

inducible protein RWD-containing sumoylation enhancer (Carbia-Nagashima, Gerez et al. 2007). Finally S-nitrosation, the process of attaching a nitroso group to a sulphur atom, is also suggested to impact HIF-1α functionality. Once again, the clarity of this mechanism is lacking and it is suggested to increase and decrease HIF-1α stability as well as aiding the recruitment of the p300 co-activator to HIF-1α (Brahimi-Horn, Mazure et al. 2005).

HIF-1α is also known to have HIF-β independent functions, affecting the processes of differentiation, DNA repair and possibly elements of the circadian clock. HIF-1α is able to synergistically interact with the Notch pathway, an evolutionary-conserved signalling system with many roles in cell-to-cell communication and differentiation. This synergistic relationship, involves the heterodimerisation of HIF-1α with Notch intracellular domain. The HIF-1α-Notch heterodimer is then able to express a subset of Notch target genes (Gustafsson, Zheng et al. 2005). Though the exact mechanism hasn't been decisively proven, there is a wealth of publications which further imply a strong relationship between hypoxia and Notch, with HIF-1α likely to play an important role (Poellinger and Lendahl 2008; Mukherjee, Kim et al. 2011). Additionally, HIF-1α may also have a role in the circadian clock by means of a similar mechanism. HIF-1α synergistically acts with CLOCK in the induction of vasopressin mRNA, though it is possible that this mechanism acts via classical up-regulation of hypoxia-inducible genes in a HIF-β dependent manner. Finally, competition of HIF-1α with Myc for binding to Sp1 leads to a reduction in protein levels of NBS1, a component of the MRN trimeric complex responsible for recognising DNA breaks (To, Sedelnikova et al. 2006).

1.8.1.2 HIF-2α

In contrast to the ubiquitous tissue expression of HIF-1α, HIF-2α has more limited tissue expression profile (Wiesener, Jurgensen et al. 2003). Transcription of the HIF-2α gene, also known as EPAS1, leads to the production of a fully spliced 2613bp transcript (NM_001430) and the subsequent translation of this mRNA results in a 871aa ~90kDa protein. The HIF-2α protein maintains the same domain structure but shares a 48% overall amino acid conservation with HIF-1α, with a greater degree of conservation within the bHLH, PAS and transactivation domains (**Fig 1.5**) (Iyer, Leung et al. 1998). The modes of hypoxic regulation of HIF-2α are the same as for HIF-1α, in that protein stability and transcriptional output are regulated by the O_2-sensitive

activity of the PHDs and FIH. Despite utilising the same core signalling motif and proteins, the profile of hypoxic induction is apparently different between the two α-isoforms (Bracken, Fedele et al. 2006). HIF-2α is often cited as being stabilised at higher O_2-tensions and is often shown to accumulate at later time-points than HIF-1α (Holmquist-Mengelbier, Fredlund et al. 2006). Certainly both α-isoforms are non-redundant; mutations within HIF-2α are associated with differing pathologies; there are also high-instances of genetic variations in the HIF-2α gene within populations living at altitude amongst other non-redundancies (Peng, Yang et al. 2010). Furthermore HIF-2α knockout mice like HIF-1α are embryonic lethal but with differing phenotypes, not surviving past E16.5 partly due to impaired lung formation as opposed to cardiac defects found in the HIF-1α knockout condition (Loboda, Jozkowicz et al. 2010).

HIF-2α has not yet been as thoroughly researched as the HIF-1α isoform and therefore there is less known about the functional post-translational modifications of HIF-2α outside of the well-characterised hydroxylation and polyubiquinitation events. However there are several papers detailing evidence that expands the knowns of alternative post-translational modifications of HIF-2α. Phosphorylation is a commonly appreciated post-translational modification, understandably so as the genome is cited to encode 518 separate kinases (Manning, Whyte et al. 2002). This type of modification has been shown to occur for HIF-2α at Thr 234 mediated by protein kinase D1 (PKD1) and this interaction is exclusive to the HIF-2α isoform. The modification was shown to prevent the involvement of HIF-2α in affecting genomic instability, which in turn would explain some of the associated differences between the contributions of the α-isoforms to cancer progression (To, Sedelnikova et al. 2006). There has also been evidence suggesting the role of acetylation in regulating HIF-2α, wherein the redox-sensing deacetylase known as Sirtuin 1 (SIRT1) regulates the transcriptional output of HIF-2α *via* the deactylation of lysine residues within the HIF-2α amino acid sequence (Dioum, Chen et al. 2009). Lastly, there has been data to indicate that HIF-2α like HIF-1α is SUMOylated and this modification is catalysed by the HIF-1α acting enzyme SENP1 (van Hagen, Overmeer et al. 2010).

Essentially HIF-1α and HIF-2α exhibit significant functional and regulatory overlap. Nevertheless there is a continued drive to explore the divergent aspects

of these two isoforms with a view to more specifically targeted therapeutics involving the transcriptionally active HIF system.

1.8.1.3 HIF-3α

HIF-3α is currently at the fringes of our understanding of the HIF hypoxia-responsive signalling system. The most appreciated fact is that HIF-3α mRNA is subject to extensive splicing resulting in many transcript isoforms which all lack the C-terminal transactivation domain found in HIF-1/2α. HIF-3α splice forms are therefore generally regarded as being either transcriptionally inactive or at least weakly active (**Fig 1.6**) Currently there are 10 documented human splice forms, named HIF-3α1 through to HIF-3α10, though a recent study has failed to validate the predicted HIF-3α3 and HIF-3α5 forms (Pasanen, Heikkila et al. 2010). Several of the splice variants maintain the oxygen-dependent degradation domain and are therefore hypoxia-inducible, accumulating with decreased PHD activity. This is in spite of the HIF-3α ODD containing only a single prolyl hydroxylation site. It has been further shown that as well as hypoxia-induced protein stabilisation, the HIF-3α transcripts are up-regulated by HIF-1 activity (Pasanen, Heikkila et al. 2010). Most explored roles for HIF-3α are centred on the interaction of HIF-3α with the canonical HIF pathway. These interactions are inhibitory, exerted through competitive binding with HIF-β or potentially through inhibitory binding of HIF-3α4 to HIF-1α, an effect that has been shown for the mouse homolog of HIF-3α4 known as IPAS (Maynard, Evans et al. 2005). HIF-3α therefore potentially acts as a negative feedback in the regulation of the HIF-1α mediated hypoxic response, affecting and shifting the steady-state levels as well as managing the inducibility of the canonical system.

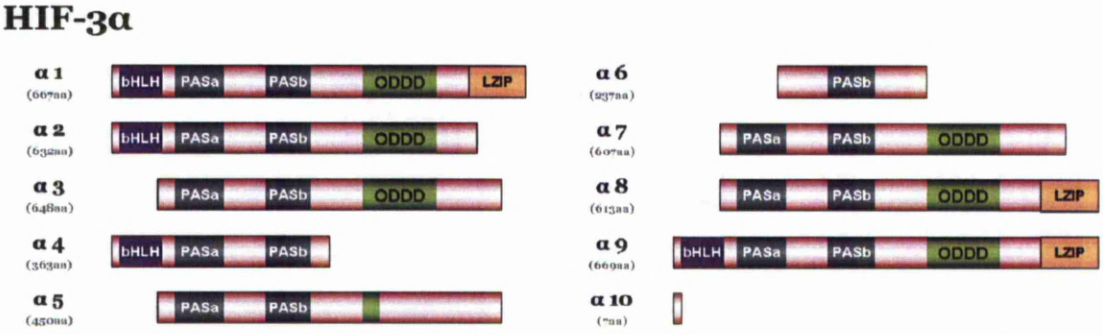

Fig 1.6 Domain representation of the HIF-3α isoforms, adapted from Pasanen *et al.* (Pasanen, Heikkila et al. 2010)

The exact roles and purposes of the HIF-3α transcripts are yet to be resolved. They are likely to be somewhat tissue-specific as suggested by the distinctive

expression pattern of transcripts (Pasanen, Heikkila et al. 2010). A final noteworthy potentiality is the involvement of HIF-3α in the promotion of adipogenesis, a result attained *via* the ectopic expression of HIF-3α in 3T3-L1 cells.

1.8.2 HIF-β/ARNT

HIF-β dimerises with HIF-1α/-2α to form transcriptionally active HIF-1/2. Though HIF-β is becoming synonymous with the cellular hypoxic response, it is not limited to this function and participates in several other pathways. Many biological products are known by several names and this is also the case with HIF-β which is commonly referred to as Aryl hydrocarbon receptor nuclear translocator (ARNT). In humans, HIF-β exists in two known isoforms HIF-1β and HIF-2β. These translate as a 790 aa and a 718 aa protein respectively that share a high-degree of sequence homology and are both localised in the cell nucleus (Hirose, Morita et al. 1996). Both isoforms are able to mediate the hypoxic response through the dimerisation to HIF-α, though whether the different HIF-1β dimerisation pairs have a functional consequence is currently unknown. It is known that the different isoforms have varied tissue expression patterns. Following in the same trend as for that of the α isoforms, HIF-1β is expressed ubiquitously and HIF-2β has a more limited expression profile, being predominantly found in embryonic, neural and kidney tissues (Maltepe, Keith et al. 2000). Unlike the α isoforms, HIF-β is considered insensitive to hypoxia, though there is some contention to this fact in certain cell lines (Stolze, Berchner-Pfannschmidt et al. 2002; Webb, Coleman et al. 2009). However, like the α isoforms, HIF-β is a member of the basic helix-loop-helix-PAS (bHLH-PAS) superfamily, a family of proteins sharing domain homology. A common property within this family is inter-family heterodimerisation. This heterodimerisation occurs between α-class subunits, such as HIF-α and the β-class subunits, such as HIF-β. Outside of HIF-α there are several other α binding partners of the α-subunits that interact with HIF-1β (Cowden and Simon 2002). The most widely cited of these is the aryl hydrocarbon receptor (AhR), a transcription factor with roles in metabolism of xenobiotics, mediated toxicity, development, cell-cycle, differentiation, the immune-response and UVB radiation sensing (Shimba, Wada et al. 2001; Puga, Xia et al. 2002; Esser 2009; Abel and Haarmann-Stemmann 2010). Here HIF-1β functions as a binding partner to activated AhR, facilitating DNA binding of the heterodimer to the

relevant xenobiotic response element (XRE) consensus sequence, a sequence different enough from HRE as to exhibit no cross binding (Kinoshita, Kikuchi et al. 2004). Murine and *Drosophila* based research has yielded two more HIF-β binding partners known as Single Minded 1/2 (SIM-1/-2). Both SIM versions are thought to be strongly involved in the process of neurogenesis, with SIM-2 having a suspected role in the causation of Down's syndrome (Chrast, Scott et al. 1997). With regards to the mode of action of these proteins, very little is understood. They are primarily characterised as transcriptional repressors, though there is limited evidence showing they are also able to act as transcription factors (Woods, Farrall et al. 2008). Interestingly, repression has been seen in the attenuation of the hypoxic induction of EPO. This reduction is suspected to come about through SIM1 and 2 competitive dimerisation with HIF-1β and then furthered by competitive binding of the SIM-HIF-β for the EPO gene (Woods and Whitelaw 2002).

1.8.3 Prolyl-hydroxylase domain proteins (PHD1, PHD2 and PHD3)

The prolyl-hydroxylase domain proteins are a class of intracellular enzymes that catalyse the hydroxylation of proline residues, most notably known for the hydroxylation of the HIF-α isoforms. In the HIF canon, there are 3 considered PHDs, which are all homologous and a less widely discussed but related isoform known as PHD4. These enzymes require Fe^{2+} as a cofactor which sits at the catalytic core, enabling the reaction of;

Proline + α-ketoglutarate + O_2 ➡ 4-hydroxyproline + CO_2 + succinate

The iron co-factor is perpetually recycled from ferric ions (Fe^{3+}) to the ferrous (Fe^{2+}) redox state, promoting the continuous hydroxylase activity of the PHDs (Pan, Mansfield et al. 2007). This has lead to several studies examining the role of vitamin C in the hypoxic response, both physiologically and with regards to cell cultures as they may be vitamin C deprived. Vitamin C deficiency would prevent the recycling of the ferrous element, in turn reducing the hydroxylase activity of the PHDs and subsequently stabilising HIFα (Pan, Mansfield et al. 2007). Contrary to this concern a recent publication demonstrated that vitamin C was not necessary as a co-factor for the HIF hypoxic response and could be substituted with glutathione (Nytko, Maeda et al. 2011). An additional necessity of the above reaction shown is the presence of the co-substrate α-ketoglutarate (also referred to as 2-oxoglutarate)(Gorres and Raines 2010). Interestingly α-ketoglutarate is produced as an intermediate of the citric acid cycle, thus tying

the PHD co-substrate to metabolism (**Fig 1.7.**) (Koivunen, Hirsila et al. 2007). The reactions of α-ketoglutarate in both the citric acid cycle and proline hydroxylation leads to the production of succinate which then acts to reduce PHD activity by feedback inhibition of the chemical reaction. Furthermore, another citric acid cycle intermediary, fumarate, is also capable of inhibiting PHD activity due to its structural similarity to succinate (King, Selak et al. 2006). This is a potentially important regulatory motif in which metabolic activity can modulate the hydroxylation of HIF-α (Qutub and Popel 2007). This mechanism is primarily considered of pathological importance rather than physiological due to the concentrations of the intermediates involved (Fong and Takeda 2008).

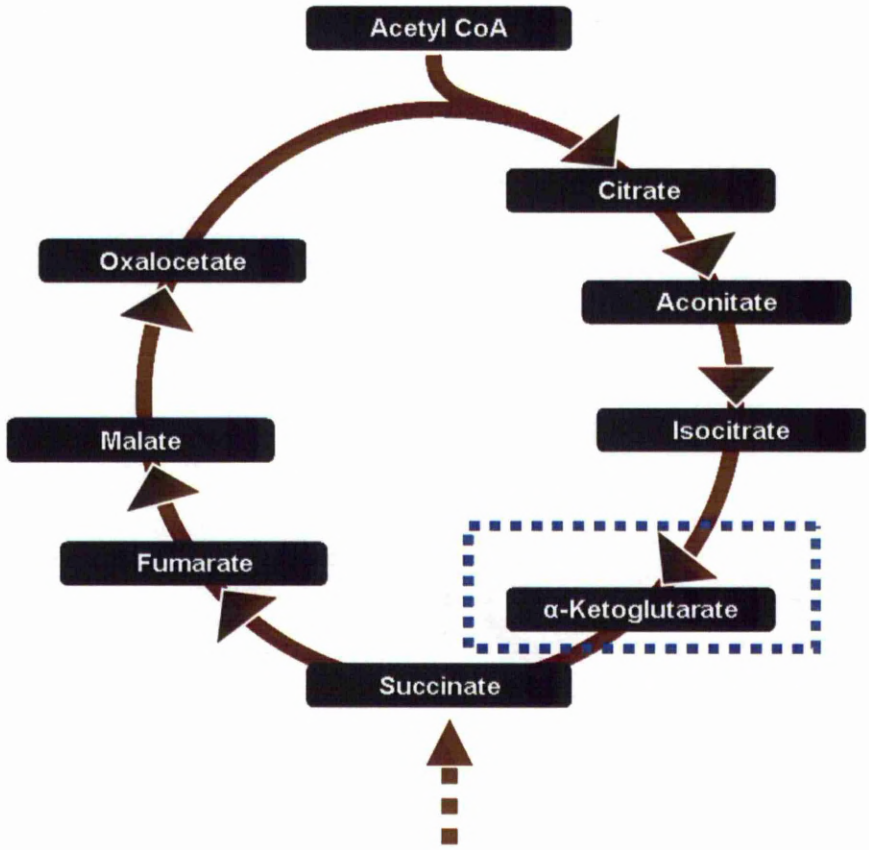

Fig 1.7. Simplified overview of the main intermediaries of the citric acid cycle. The intermediate, α-ketoglutarate is highlighted due to its other role as a co-factor of the PHD enzymes.

However, the most relevant regulatory aspect of the hydroxylation process is the requirement of the PHDs for molecular oxygen. It is from this chemical process that the O_2-sensitivity of the HIF transcription factor arises. The affinities of the PHDs for oxygen is apparently quite low, in the range of 230-250kM in contrast to the other known collagen modifying hydroxylase P4H, which has a kM value

of 40 (determined using peptide fragments) (Hirsila, Koivunen et al. 2003). These low affinities allow for physio/pathological oxygen conditions to be limiting for the PHDs as O_2 concentration ranges from an atmospheric limit of 200μM (Hirsila, Koivunen et al. 2003). Moreover, cellular components that utilise O_2 will compete when oxygen supply falls below demand; In cellular normoxic conditions ~90% of the available oxygen is used by the mitochondria. This figures rises to nearly 100% in hypoxic conditions, as the affinity of cytochrome C for the available oxygen exceeds that of other enzymes including the PHDs (Agbor and Taylor 2008).

Enzyme	kM	
	α-ketoglutarate	O_2
PHD1	60	230
PHD2	60	250
PHD3	55	230
C-P4H-1	20	40

Table 1.3. kM values of the intracellular hydroxylase and collagen hydroxylase for co-substrates, α-ketoglutarate and molecular oxygen. Values determined using peptide fragments. This table has been adapted from Hrsila *et al.* (2003).

Therefore, this leads ultimately to the paradigm that the rate of HIF-α hydroxylation by the PHDs is constrained by the cellular availability of O_2 and this rate is further diminished with additional hypoxic insult(s).

The PHDs all have the same overall mode of enzymatic action, but in spite of this the different isoforms are not entirely redundant and there is on-going work resolving their individual roles. This is of particular relevance to therapeutic design targeting the HIF system. The HIF system has become an attractive therapeutic target due to its involvement with angiogenesis, cancer progression and tumour malignancy as well as altitude acclimatisation (Nangaku, Kojima et al. 2006; Niatsetskaya, Basso et al. 2010; Smith and Talbot 2010). The relationship between the PHDs and HIF means that the PHDs are a common point to target compounds against and therefore understanding the individual roles of the PHDs is a desirable aim.

Cell/Tissue	mRNA expression			Protein expression		
	PHD1	PHD2	PHD3	PHD1	PHD2	PHD3
Brain	+	++	+	++	++	+
Heart	+	+++	+++	N/A	++	++
Skeletal Muscle	+	+++	++	N/A	+	N/A
Liver	++	++/+++	++	+/-	+/-	+/-
Kidney	+	++	+	++	++	++
Lung	+	+	+	+	-	+
Pancreas	N/A	++	N/A	+	+/-	+/++
Testis	+++	++	+	++	++	++
Placenta	+++	N/A	+++	++/-	++	+++
Adipose tissue	++	+++	N/A	-	_	-
Endothelium	N/A	N/A	N/A	-	-/++/+++	-/++
Epidermis, basal layer				N/A	++	N/A
Epidermis, upper layer				N/A	-	N/A
Carcinoma Cells				+	+	+
Breast Cancer				+	++	+/-
Testicular Cancer				++	+	+/-
Osteosarcoma Cells				+	++	+

Table 1.4. Tissue expression profiles of the different PHD isoforms (table adapted from Jokilehto *et al.* 2010). The criteria for the scoring of expression level was not included in the original publication. (Jokilehto and Jaakkola 2010)

1.8.3.1 PHD1/EGLN2

PHD1 mRNA and protein has been found to be expressed in numerous tissues and appears to have a more specialised requirement in the testis and placenta, where it is the most abundant PHD form with regards to mRNA. The PHD1 gene, known as EGLN2, has recently been shown to encode two isoforms via a mechanism of alternative translation initiation leading to PHD1p43 and PHD1p40 nuclear localised proteins (Tian, Mole et al. 2006). The nuclear localisation is determined by a functional bipartite nuclear localisation signal found within the N-terminus, between residues 89-134. PHD1 is the only PHD isoform with a predominant nuclear localisation and is therefore one of the distinguishing features amongst the PHDs (Metzen, Berchner-Pfannschmidt et al. 2003). The functional consequence or purpose of PHD1 nuclear localisation remains unclear, although the forced cytoplasmic expression of PHD1 shows no significant effect on HIF-1α hydroxylation (Yasumoto, Kowata et al. 2009). It is therefore a possibility that the nuclear localisation of the protein is of importance for other non-HIF related interactions. Indeed there is another suggested protein interaction partner for PHD1 outside of HIF-α, the inhibitory κ-B kinase β (IKKβ) protein of the NF-κB pathway. PHD1 has been postulated to hydroxylate proline P191 of IKKβ and this in turn is suggested to confer O_2-sensitivity to the NF-κB pathway (Cummins, Berra et al. 2006). This regulatory

mechanism, as is the case for HIF-α, depends on the hydroxylase activity of PHD1. Though the hydroxylase mode of action is the same for all PHDs, their enzymatic rates and binding affinities differ and this could potentially confer some functional differences. PHD1 has a lower measured HIF-α hydroxylation rate than the other PHDs, approximately 5-fold lower (Tuckerman, Zhao et al. 2004). This coupled to the lower abundance of PHD1 protein relegates PHD1 to having a reasonably minimal role in the down-regulation of HIF signalling.

1.8.3.2 PHD2/EGLN1

In contrast to PHD1, PHD2 is often considered the major regulator of HIF signalling and is the regulatory protein responsible for the suppression of HIF-α in normoxic conditions (Berra, Benizri et al. 2003). The protein is encoded by the EGLN1 gene, producing a transcript coding sequence of 1278bp (NM_022051) and a 42kDa 426aa protein. The tissue expression profile of this protein is seemingly ubiquitous and is also often the most abundant detectable PHD isoform, reinforcing the idea that PHD2 is the major isoform involved in HIF regulation (Jokilehto and Jaakkola 2010). This claim is further supported as PHD2, alongside PHD3, shows comparatively high rates of HIF-α hydroxylation compared to PHD1 and can therefore more significantly destabilise HIF. An interesting difference between the PHDs may be the differences in their affinity for the various HIF-α isoforms. It has been suggested that PHD2 preferentially hydroxylates HIF-1α over the HIF-2α form (Tuckerman, Zhao et al. 2004). Indeed the binding of HIF to the PHDs may be a regulated event as evidence has shown that osteosarcoma amplified 9 (OS-9) is able to facilitate HIF-1α and PHD2/3 binding (Baek, Mahon et al. 2005). More recently, this mechanism has been contested by Brockmeier *et al.* 2011 and shown to not occur on account of the different localisation of OS-9 to HIF-1α (Brockmeier, Platzek et al. 2011). Critically, PHD2 is cited to be the originator of PHD1 and PHD3 which arose from duplication of the EGLN1 gene (Taylor 2001; Rytkonen, Williams et al. 2011). This stated, it can be expected that the different PHD proteins have a strong degree of functional and characteristic overlap. Nevertheless unique characteristics for PHD2 exist, comparing to the other PHDs. One such is that PHD2 shows a different intracellular localisation, found predominately in the cytoplasm and this localisation is mediated by an N-terminus export sequence (Steinhoff, Pientka et al. 2009). The localisation of PHD2 appears to be of some significance as its been observed that the nuclear

accumulation of PHD2 promotes a malignant cancer phenotype by encouraging anchorage independent growth. This effect is not dependent on the hydroxylase activity of PHD2 and therefore possibly implicates other roles for PHD2 outside of the regulation of HIF stability (Jokilehto, Hogel et al. 2010).

As well as certain differences in the protein function of the variant PHDs there are differences in the transcriptional regulation and this is particularly critical for the canonical HIF response; hypoxia is able to induce the transcription of PHD2 and PHD3 but not PHD1. In accordance, a putative HIF binding site/HRE consensus (ACGTG) found in the PHD2 gene has been shown to be functional, occurring 412bp prior to translation start codon (Metzen, Stiehl et al. 2005). This hypoxia-inducibility is therefore HIF-dependent, forming a negative feedback loop in which HIF up-regulates its own inhibitor (Stiehl, Wirthner et al. 2006). Thus in the hypoxic situation HIF-α would become stabilised due to the reduced hydroxylation rate of the PHDs, PHD2 & 3 would be up-regulated compensating for their reduced activity with increased abundance which would then once again lead to destabilisation of HIF-α. This principal is of paramount importance to the current study described within this thesis as this motif has the potential to generate temporally meaningful response patterns. This will be discussed later in section **1.9.1**.

1.8.3.3 PHD3/EGLN3

PHD3 is the smallest protein of the PHDs, weighing at 25kDa and encoded for by a 720bp coding sequence. The expressed protein appears to be the dominant PHD form for the pancreas and the placenta, though for other tissues is less abundant than PHD2 (Jokilehto and Jaakkola 2010). Unlike the nuclear localisation of PHD1 and cytoplasmic localisation of PHD2, PHD3 is ubiquitous within the cell, found in both the cytoplasm and nucleus (Metzen, Berchner-Pfannschmidt et al. 2003). The tissue expression and intracellular expression patterns are the first discernible differences between PHD3 and the other PHDs, thus supporting the idea of a degree of non-redundancy. Additionally several publications have alluded to PHD3 specific phenomenon, including PHD3-regulated doxorubicin-induced apoptosis, TCP-1 ring complex association, neutrophil survival, α-ketoglutarate-induced apoptosis as well as the regulation of NF-κB via interaction with IKKβ (Masson, Appelhoff et al. 2004; Liu, Huo et al. 2010; Tennant and Gottlieb 2010; Xue, Li et al. 2010; Walmsley, Chilvers et al. 2011).

Within the HIF signalling pathway PHD3 plays a pivotal role, as alongside PHD2, PHD3 is up-regulated in a HIF-dependent manner and therefore forms another facet of the negative feedback regulation of HIF-α protein. The genomic region responsible for this up-regulation has been suggested to reside 12kb downstream of the transcription start site, an enhancer site within the first intron of the PHD3 gene. However, this may not be the only site to confer hypoxic sensitivity to the gene (Pescador, Cuevas et al. 2005). As is the case for PHD2, PHD3 binding to HIF-1α has also been suggested to be aided by the binding of OS-9 to HIF-1α. However, a possible discernible difference between PHD2 and PHD3 is the binding affinities for the HIF-α forms, in which PHD3 may have a higher binding affinity for HIF-2α (Tuckerman, Zhao et al. 2004).

1.8.4 Von Hippel-Lindau protein (pVHL)

pVHL is the E3-ubiquitin ligase responsible for targeting proline-hydroxylated HIF-α for degradation by the 26S proteasome. The full ligase activity is achieved through the complexing of pVHL with elongin B and C, cul2 and Rbx1 (Clifford, Astuti et al. 2001). The pVHL protein itself exists as a 214aa long form weighing 25kDa. The tissue expression pattern of pVHL mirrors that of HIF-1α in that it is ubiquitously expressed (Ohh 2006). On the cellular level pVHL is found in both the cytoplasm and nucleus and constantly shuttles between, enabling the degradation of HIF-α in both compartments (Berra, Roux et al. 2001). The importance of pVHL is mostly known due to its role in the disease of the same name, von Hippel-Lindau disease. Von Hippel-Lindau disease affects a patient's predisposition to several malignancies, notably tumour development in the form of renal cell carcinoma, haemangioblastoma and phaeochromocytoma (Barontini and Dahia 2010). The disease state is explained as an autosomal dominant disorder carrying various genetic abnormalities in the pVHL gene. These genetic abnormalities result in either the complete loss of pVHL or a missense mutation altering the functionality of pVHL. The exact nature of the genetic abnormality is used as a sub-typing identification; type 1 is characterised by gene loss and type 2 variants (A, B and C) by missense mutations. Consequently the loss or alteration of pVHL often leads to the pathological stabilisation of HIF-α and this pathological up-regulation of HIF-α is responsible for many maladaptive features of the resulting cancers. Despite the importance of HIF-α in pVHL disease progression, there are a number of HIF-independent aspects that have been witnessed in type 2c patients. Type 2c

patients have mutational defects in pVHL but no detectable change in HIF activity (Barontini and Dahia 2010). Part of the importance of this besides the clinical relevance, is that it implicates pVHL involvement in other pathways. Indeed, there is evidence supporting several pVHL interactions independent of the canonical HIF pathway. Firstly, pVHL has also been shown to interact with unassembled hydroxylated collagen IV chains (Grosfeld, Stolze et al. 2007). This postulates a role of pVHL in the maintenance of the extracellular matrix, something that is corroborated by observations in type 2c von Hippel-Lindau patients (Ohh, Yauch et al. 1998). Another elucidated pVHL interaction is with atypical protein kinase C λ (aPKCλ), a protein involved in cellular proliferation, survival and cell polarity. This interaction invokes the ubiquitin-ligase activity of pVHL and results in the degradation of PIP_3 activated aPKCλ. It is then suggested that pVHL regulation mat affect the role of aPKCλ complexes in cell adhesion (Okuda, Saitoh et al. 2001). Following the likes of the PHDs, pVHL is also implicated in part regulation of NF-κB signal transduction pathway. In this capacity pVHL is cited to act as an adaptor to promote the inhibitory phosphorylation of the NF-κB agonist caspase recruitment domain-containing protein 9 (Card9) by Casein-Kinase 2 (CK2) (Yang, Minamishima et al. 2007). A further suggested HIF-independent activity for pVHL, is the mimicking of mdm2 in the regulation of p53 protein stability. This is made additionally interesting by the reported prospect that murine double minute 2 (MDM2) is also able to mimic pVHL in HIF-α ubiquitination, though little published supportive data has arisen from this initial hypothesis (Roe, Kim et al. 2006).

The verity and scope of these HIF-independent functions are still yet to be fully understood and, though primarily relevant to pathological scenarios, physiological modulation of pVHL may also represent a mechanism for cells to tweak the HIF-response. In fitting with this, there are several detailed mechanisms regulating pVHL activity or availability. One such mechanism is the prior discussed hypoxia driven inactivation of pVHL via PIASγ-mediated small ubiquitin-like modification (SUMO) modification (Cai, Verma et al. 2010). A further mechanism purports pVHL protein levels to be positively regulated by increasing cell density. This was observed in human renal proximal tubule epithelial cells (RPTEC) and NIH3T3 fibroblast cells (Baba, Hirai et al. 2001). Finally, it has also been reported that pVHL protein levels fluctuate over the

course of cell cycle prompting a possibility in which the hypoxia-sensitivity of a cell is coupled to cell cycle progression (Liu, Xin et al. 2010).

1.8.5 Factor-inhibiting Hypoxia-Inducible Factor 1α (FIH)

The transcriptional activity of HIF is regulated by the hydroxylation of an asparagine residue within the C-terminus of the protein; Asn803 in HIF-1α and Asn851 in HIF-2α (Lando, Peet et al. 2002). This post-translational modification is performed by the asparignyl hydroxylase known as Factor-inhibiting Hypoxia-Inducible Factor 1α (FIH) and represents one arm of the major oxygen-sensitive regulations of the HIF transcription factor. FIH was initially identified and characterised as regulating HIF transcriptional activity by Mahon *et al.* (2001) (Mahon, Hirota et al. 2001). The 40kDa protein is the translated product of 1050bp coding sequence and in line with the fundamental HIF signalling system, is ubiquitously expressed across tissues (Lisy and Peet 2008). Once expressed, the protein is found to localise to the cytoplasm (Metzen, Berchner-Pfannschmidt et al. 2003). The catalytic mode of action of FIH is identical to the previously described prolyl hydroxylases with the only difference being the amino acid target. As the enzymatic activity occurs by the same reaction as the prolyl-hydroxylases, so to is the enzymatic activity of FIH dependent on the availability of oxygen, conferring another tier of O_2-sensitivity to HIF. An important difference between the PHDs and FIH are the reported affinities of the enzymes for molecular oxygen, whereby the PHDs have kM values of ~230-250μM FIH was measured to be 90μM (**Table 1.3**) (Fandrey, Gorr et al. 2006). This would indicate that FIH is less sensitive to milder hypoxic-insults than the PHDs and that only severe hypoxia would affect the transcriptional regulation of HIF (Stolze, Tian et al. 2004). This could potentially promote a stratified HIF response in which varying degrees of hypoxia have different transcriptional outputs.

There is considerable postulation of HIF-α independent functions of FIH. This concept has been spurred with the discovery that FIH binds to ankyrin repeat domains, a domain structure featured in many proteins notably IκBα of the NF-κB pathway (Cockman, Webb et al. 2009; Cockman, Webb et al. 2009; Schmierer, Novak et al. 2010). However, the exact purpose and validity behind the proposed sequestration remains unsolved; specifically with regards to the impact, the sequestration may have on the HIF signalling network. An issue theoretically approached by Schmierer *et al* 2010.

All of the prior discussed systems of HIF regulation, ranging from the alternate O_2 regulation, O_2-indepenent regulation as well as the individual roles of the proteins of the canonical system represent only a fraction of the integrated HIF network. The interconnected web of regulatory events that govern phenotypic responses via HIF are extensively complicated. The discussed regulatory components of the system underlie a potential for significant intricacy in HIF signalling; it will be an ongoing challenge for the field to begin to understand and account for some of this complexity. Specific fields of study are now in place that attempts this integration of signalling complexity and we hope to employ some of the methodology and ideas into our own investigation into the HIF system.

1.9 Complex signalling systems

Transduction pathways are often portrayed in a static uni-directional manner, whereas they are often better depicted as a *dynamic system*, in which the temporal profile of the system is just as important as characterising the proteins involved. The temporal profile/kinetics of a signal transduction pathway represents a further way for the system to encode information and can often affect downstream gene expression. This is perhaps somewhat intuitive, as a transcription factor is unlikely to activate the exact same genes from a range of stimuli and prolonged stimulation may require the cell to respond in a different way to acute stimulation. The temporal profile of the pathway is capable of integrating this information, as has been shown in lineage patterning by Oct-4, cell-to-cell communication in synthetic bacterial systems and gene expression following TNFα stimulation of NF-κB (Basu, Mehreja et al. 2004; Ashall, Horton et al. 2009; Plachta, Bollenbach et al. 2011). This can be achieved through temporally sensitive transcription, as a result of chromatin remodelling, changes in co-activators etc or through protein-thresholds, in which newly synthesised protein can change the phenotype of the response dependent on the amount of newly synthesised protein (Behar, Hao et al. 2008; Ashall, Horton et al. 2009; Schwartz, Sarvaiya et al. ; Plachta, Bollenbach et al.)

1.9.1 Delayed negative feedback loops

At the heart of temporally meaningful dynamic signalling systems are certain signalling motifs, one of which is a delayed negative feedback loop. With regards to the HIF system, there are several potential delayed feedback loops and the best characterised is the relationship between HIF-α and PHD2&3. The negative

feedback aspect arises from the arrangement that HIF-α induces its own repressor, PHD2 and PHD3. The delay arises from the time needed for the transcription, translation and protein-folding of the feedback PHD proteins before they're fully active. Thereby the activity of HIF affects its own protein stability in the future, in doing so also affecting its future activity – conveying a potential dynamism to the HIF regulatory circuit. The importance of this delay has been theoretically appraised in work from Qutub et Popel 2007 (Qutub and Popel 2007).

1.9.2 Biological oscillations

The most striking examples of known dynamic signalling systems are the various biological oscillators that have been discovered, ranging from the physiological level oscillations such as for ovulation and sleep-cycles to cellular level oscillations apparent for cell-cycle to a range of complex intracellular oscillators. There are several intracellular oscillators now described; one of the earliest characterised was calcium oscillations, in which calcium stores are released into the intracellular space upon stimulation and this in turn activates feedback mechanisms generating *sequential regenerative discharges* (Dupont, Combettes et al. 2011). Since then several transcription factors have been demonstrated to oscillate, including the nucleo-cytoplasmic oscillations found in the NF-κB pathway (Nelson, Ihekwaba et al. 2004) and the ERK pathway (Shankaran, Ippolito et al. 2009), the synthesis-degradation cycles of p53 (Geva-Zatorsky, Rosenfeld et al. 2006), and the oscillating gene-set under the control of the WNT pathway(Dequeant, Glynn et al. 2006; Mengel, Hunziker et al. 2010) It is these examples that have recently brought the delayed negative feedback motif to prominence. However, for oscillations to properly arise the system requires additional features on top of signalling motif. The system requires a sufficient degree of non-linearity, by which certain changes or measurements are not directly proportional to a driving-input (two interrelated values are not directly proportional to one another). There are many potential biological sources of non-linearity, including co-operative binding, reversible post-translational modification, multiple aa residue modification, stochiometric inhibition and saturated degradation points (Novak and Tyson 2008; Mengel, Hunziker et al. 2010). The importance of these oscillations hinges on the cell to decode meaning from the repetitive patterns of signalling and so subsequently much of the on-going work on these signalling systems aims at deciphering the

potentially functional consequences of the oscillations (Basu, Mehreja et al. 2004; Ashall, Horton et al. 2009). There has been headway towards this goal for some of the discussed intracellular oscillators. Work from our lab has showed the temporal profile of the NF-κB oscillations to affect downstream gene expression (Ashall, Horton et al. 2009). Although not a transcription factor, the frequency of calcium oscillations has also been shown to affect the downstream response (Dolmetsch, Xu et al. 1998). Though the biological oscillators are perhaps the most striking examples of temporally consequential signalling systems, they partly serve to illuminate the role timing and kinetics can have in determining the phenotype of a response – and this concept is not limited to oscillatory systems but is potentially applicable to any transitional state dynamics in a given signalling system (Covello, Kehler et al. 2006).

1.9.3 Integrated signalling systems

In addition to temporal complexity, transduction pathways are often portrayed as linear arrangements (as shown for the HIF system in **Fig 1.4**), whereby a single stimulus activates a single chain of events resulting in a defined response. However, they would be more accurately portrayed as *transduction networks*, integrating information from large volumes of separate and synergistic interactions which are translated into a meaningful biological response. As previously described, O_2 as a stimulus can be biologically detected in various ways and affects numerous integrated cellular and physiological processes i.e; bioenergetic status, ROS, post-translational modifications etc . This is further complicated as O_2 sensing does not act in an isolated fashion, but occurs alongside a plethora of separate stimuli activating a vast array of interconnected signalling systems.

These crosstalk events coupled with the aforementioned temporal aspects to cell signalling result in a significant degree of biological complexity, often to a level well beyond intuitive understanding. It is for this reason that scientific endeavour in biology has favoured dissecting this complexity, attempting to identify the biological interactions and components that constitute a living organism. However, research aimed at and addressing complexity has been made possible with the development of suitable tools and methods and this has lent momentum and credence to a several-decades-old-field that favours this less reductionist approach, namely the field of systems biology.

1.9.4 Systems biology approach

There are varying definitions of systems biology but they often incorporate the same core concepts, such as the focus on how interactions between components generates network level behaviour and the integration of complexity over the reduction. This has become a more applicable idea in the post-genomic era as many components of biological systems of interest have been identified. Furthermore the various –omics and bioinformatics approaches are also able to funnel into the systems biology approach due to their systems-wide approach in data acquisition. However, another common facet of systems biology is the use of computational models to pry details and predict system level behaviour, which is often difficult to discern by standard experimental methods. Complexity in signalling networks can be increasingly addressed using a computational approach, analysing systems that are larger than intuition can process. Many of the mathematical models are benefitted from high-resolution quantitative data and this has meant that often systems biology has become synonymous with technologies which offer this. A common such technique is the live-cell confocal imaging of single cells as it provides quantitative, high-temporal and spatial resolution data, allowing also for the detection of signalling events such as; protein-translocations, protein-diffusion, changes in protein-stability and/or transcription. Also the ability to image single-cells ensures the ability to measure events that may be asynchronous across a population of cells (Nelson, Ihekwaba et al. 2004). This is important as dynamic signalling events can often be difficult to detect using bulk-cell assays as they rely on averaging the state of many single cells.

This approach has gained significant momentum over the last decade and work is ongoing in shaping this field to maximise the potential. We hope to use many of the practices and principles in our approach of the HIF signalling network, specifically investigating the dynamic properties of the pathway with the aid of computational models and quantitative data.

1.10 Project Aims

This project aims to work towards the larger frame-work hypothesis that differing temporal patterns in transcription factor output have phenotypic consequences. **(i)** As part of the work towards this larger goal we aim to characterise any distinct single-cell spatio/temporal dynamics active within the O_2-sensitive HIF signalling system, with a specific focus on the transcription factors HIF-1α and HIF-2α. This first aim will also experimentally explore the potential of the signalling system to give rise to oscillatory behaviour, a common motif which would expectantly incorporate distinct temporal patterns. **(ii)** Secondly the project aims to support and drive the building of a mathematical model describing the core HIF hypoxic response with a view to using the mathematical model to probe various details of the signalling arrangement, such as the response to intermittent hypoxia, the response to acute and chronic hypoxia, the response to varying severities and rates of O_2-change as well as the aforementioned oscillatory potential of the system. This can hopefully provide new insights and/or to expand our current understanding on how the HIF system encodes information and this could potentially be used to strengthen the rationale in therapeutic drug design against this system.

Chapter 2: Materials and Methods

2.1 Chemicals and Reagents

All chemicals were purchased from BDH Chemicals Ltd. All DNA oligonucleotides were purchased from Invitrogen (UK) or Sigma-Aldrich (UK). Tissue culture media were purchased from Gibco (Invitrogen, UK) and foetal calf serum from Harlan Seralab (UK). All restriction and DNA-modifying enzymes were purchased from NEB (UK) or Roche (UK) unless otherwise stated.

2.2 Cell treatments

A range of various drug and chemical treatments were used, most extensively with the HeLa cell line. Chemical agents used were purchased from either Calbiochem or Sigma-Aldrich (**Table 2.1**).

Chemical	Purpose of use	Used concentration
Actinomycin D	Used to arrest transcription	5μg/ml
Cycloheximide	Used to arrest protein translation	10μg/ml
DMOG	Used to inhibit the intracellular hydroxylases	0.5mM
MG132	Used to inhibit the 26S proteasome	1μM
Nocodazole	Used to disrupt microtubule stabilisation	10μM
Thymidine	Used in G2/M cell synchronisation protocol	

Table 2.1. A list of drugs used throughout the project. Their common purpose of use and doses used for stimulation of HeLa cells is also shown.

2.2.1 Hypoxic Incubation

Hypoxic cell culture and sample preparation was performed using a Don Whitley H35 Hypoxystation. Growth conditions were maintained at 37°C and 5% CO_2 and the air humidified. Lysis and fixation protocols were carried out inside the incubator. The majority of hypoxic experiments were carried out at 1% O2 unless otherwise stated.

2.3 Plasmids

Plasmids were either purchased, donated or constructed during the project. Bought in plasmids came from one of three companies; SwtichGear Genomics, from the Addgene non-profit plasmid database or Clontech. A list of donated and purchased plasmids is shown below (**Table 2.2**). Additionally a detailed description (including cloning primers and diagnostic digests checks) of every plasmid used throughout the project is available in the **appendix 1.1**.

Plasmid name	Source
pHIF-1α	Donated by Prof. S. Edwards, Liverpool
pPHD1-EGFP	Retrieved from Addgene, reference 21400
pPHD2-EGFP	Donated by Prof. R. Depping, University of Lübeck
pPHD3-EGFP	Retrieved from Addgene, reference 21402
pcDNA3-hEPAS	Donated by Dr. S. McKnight, UT Southwestern Medical Centre
pYFP-HIF1β	Donated by Prof. J. Fandrey, Duisburg-Essen
pHIF1β-YFP	Donated by Prof. J. Fandrey, Duisburg-Essen
pRC-CMV-HA-pVHL	Donated by Dr. M. Ohh, Toronto
pEGFP-PHD2 Δ6-20	Donated by Prof. R. Depping, University of Lübeck
pEGFP-N1-PHD2 Δ181-220	Donated by Prof. R. Depping, University of Lübeck
pEGFP-PHD2 Δ1-100	Donated by Prof. R. Depping, University of Lübeck
pEGFP-N1-PHD2 Δ101-200	Donated by Prof. R. Depping, University of Lübeck
pEGFP-PHD2 Δ201-300	Donated by Prof. R. Depping, University of Lübeck
pEGFP-N1-PHD2 Δ301-426	Donated by Prof. R. Depping, University of Lübeck
PGL2.HRE-luc	Donated by Dr. G. Melillo, National Cancer Institute-Frederick
EGLN1-luc	Purchased from SwtichGear Genomics
EGLN3-luc	Purchased from SwtichGear Genomics
pIRES2-DsRedxp	Purchased from Clontech

Table 2.2. A list of plasmids acquired during the course of the project and the corresponding source.

2.4 Cell Culture

2.4.1 Cell line growth requirements

HeLa cells (human cervix carcinoma), HeLa ShPHD2 cells (stable knockdown for PHD2 abbreviated to ShPHD2) and SK-N-AS cells (human neuroblastoma) were cultured in Minimal Essential Medium (MEM) supplemented with 10% (v/v) fetal calf serum and 1% (v/v) non-essential amino acids (Invitrogen). Growth conditions were maintained at 37°C and 5% Co_2 in a humidified incubator (Sayo, Japan). HeLa and ShPHD2 cells were cultured for a maximum of 10 passages and SK-N-AS for 8 passages.

2.4.2 Cell line propagation

Cells were typically cultured in 75cm^2 tissue culture flasks (Corning, UK) and were grown to 80-90% confluence, mostly sub-culturing every other day. The media was removed from the flask prior to washing with Ca^{2+} free phosphate-buffered saline (PBS) (GibCo). Cells were then incubated at 37°C in the presence of 1ml of 1x trypsin/EDTA (Invitrogen) for 2-5 minutes. The trypsinisation process was inhibited through the addition of 9ml growth media. The total 10ml was then transferred and cells were pelleted by centrifugation for 5 minutes at 100g and the supernatant removed, to remove traces of trypsin. The cells pellet was re-suspended in growth media. The cell count was determined using a particle counter (Beckman Coulter). Between $8x10^5$ and $1.2x10^6$ cells were transferred to a new 75cm culture flask. The remaining cells were distributed to culture vessels for use in other experiment protocols (**Table 2.3**.).

Cell-culture vessel	Growth area (cm2)	Number of Cells plated
96-well	0.32-0.6	5×10^3
24-well	2	2.5×10^4
35mm dish	8	1×10^5
60mm dish	21	2×10^5
750ml Flask	175	~$1x10^6$

Table 2.3. Commonly used culture vessels and typical plating density(for a 2 days culture) used with the HeLa cell line.

2.4.3 Transfection

Cells were transfected using either FuGene®6, FuGene®HD, FuGene®HP Xtreme or Lipofectamine 2000 as per manufacturer's instructions. The DNA:reagent ratio was determined empirically, with the optimum conditions consisting of a cationic lipid (µl) to DNA (µg) ratio of 2:1 for HeLa and ShPHD2 and 3:1 for SK-N-AS. Transfection volumes were altered depending on the surface area of the tissue culture vessel to be transfected (**Table 2.4**).

Culture Vessel	FuGene (µl)	DNA (µg)	Total Volume (µl)
24-well plate	0.6	0.3	30
35mm dish	2	1	100
60mm dish	5	2.5	250

Table 2.4. Transfection volumes used with differing culture vessels. A ratio of 2:1 for FuGene to DNA was used for the transfection of HeLa cells.

2.5 Molecular Biology

2.5.1 Propagation of DNA

2.5.1.1 Production of Chemically Competent Cells

An aliquot of competent *E.coli* (DH5α or DB3.1) were mixed with 2.5ml LB and incubated overnight at 37°C with shaking. The culture was transferred to 100ml of LB and further incubated in the same conditions for ~3 hours (or when the culture OD_{600} reached 0.6). The culture was then chilled on ice for 10 minutes before being transferred into pre-chilled tubes. The bacteria were harvested by centrifugation at 3,000rpm at 4°C 10 minutes. The remaining protocol was carried out in a cold room maintained at 4°C. The supernatant was discarded and the bacterial pellets re-suspended in 20ml chilled transformation buffer (10mM acidic PIPES, 15mM $CaCl_2$, 250mM KCL, 87mM MnCL2 then adjust to pH 6.7 using KOH). The resuspended bacteria were centrifuged again for a further 10 minutes (3,500rpm, 4°C). The pellet was resuspended in 10ml TB buffer supplemented with 7% DMSO. It was incubated for 10 minutes on ice before being aliquoted. The aliquots were snap frozen by immersion in liquid nitrogen and then stored at -80°C.

2.5.1.2 Transformation of Chemically Competent Cells

Routine propagation of plasmid DNA was performed using a suitable strain of competent cells, typically DH5α, DB3.1. XL-10 blue commercial cells (Stratagene) were used in the transformation of mutagenesis reactions or ligation reactions as per the supplied protocol.

100ul of competent cells were thawed on ice and then incubated for 30-45 minutes in the presence of 1-25ng closed plasmid DNA in 1.5ml microfuge tubes. Cells were then heat-shocked at 42°C for 1 minute. Tubes were returned on ice for 2 minutes prior to the addition of a 900µl of LB (1% (w/v) bacto-tryptone; 0.5% (w/v) yeast extract; 1% (w/v) NaCl, pH 7.0). The tubes were incubated at 37°C with shaking for 45-60min. The cells were then pelleted in a micro-centrifuge at 11,000g for 1 minute and 900µl of supernatant then removed. The pellet was resuspended in the remaining ~100µl supernatant. 10µl and 90µl of the cell suspension were then plated onto LB-agar plates containing the appropriate selection antibiotic (50µg/ml ampicillin or kanamycin or 30µg/ml chloramphenicol as appropriate) and incubated overnight at 37°C.

2.5.1.3 Small Scale Purification of Plasmid DNA (Plasmid Mini Prep)

E.coli cells containing plasmid DNA were cultured in 5ml LB broth with an appropriate selection agent for a minimum of 8 hours, typically overnight at 37°C with vigorous shaking at 225rpm. 3ml of the culture was harvested by centrifugation at 6,800g for 3 minutes. The remaining culture was stored at 4°C for future use for a maximum of 8 hours. DNA was then extracted using a Qiagen Plasmid Mini Purification Kit or the PureLink kit (Invitrogen) according to the manufacturer's instructions. Plasmid DNA was eluted in either 50µl TE (10mM Tris-HCl (pH 8.0), 1mM EDTA) when using the Qiagen Kit or 100µl TE when using the Purelink kit. All purified plasmid DNA was quantified using spectrophotometry and confirmed using a suitable restriction endonuclease digest examined by gel electrophoresis (**Table 2.5**).

2.5.1.4 Large Scale Purification of Plasmid DNA (Plasmid Maxi Prep)

A 1L conical flask containing 200ml of LB broth was inoculated using 1ml from a Mini Prep culture and cultured overnight at 37°C with vigorous shaking at 225rpm. Cultures were harvested at 6,800g for 15 minutes at 4°C. The QIAfilter Plasmid Maxi Kit (Qiagen) was used in accordance with the supplied protocol. DNA eluted from the anion-exchange columns was relatively dilute and was concentrated by isopropanol precipitation. The eluted DNA/isopropanol solution was centrifuged at 5,000g for 60 minutes at 4°C. The supernatant was discarded and the DNA pellet washed with 1.5ml 70% (v/v) ethanol, then further centrifuged at 15,000g for 15 minutes at 4°C. The pellets were air-died for 10-30 minutes and dissolved in 100µl TE. The concentration of the plasmid was then determined using spectrophotometry and adjusted to a final concentration of 1µg/µl, divided into 100µl aliquots (**Table 2.5**).

2.5.1.5 Small Scale Purification of Bacterial Artificial Chromosome DNA (BAC mini prep)

E.coli cells containing BAC DNA were cultured in 5ml LB broth inoculated with chloramphenicol (30µg/ml) overnight. Cultures were then harvested in a benchtop centrifuge. The various buffers used for this protocol were taken from the Qiagen Mini Prep Kit. The supernatant was removed and the pellet resuspended in 250µl buffer P1 before being transferred to a fresh tube. 250µl buffer P2 was added to the tube and gently inverted 4-6 times and then incubated for less then 4 minutes 30 seconds at room temperature. A 350µl

volume of buffer P3 was added to the tube and again gently inverted 4-6 times. The sample is then centrifuged for 20 minutes at 14,000rpm at 4°C and the supernatant transferred to a new centrifuge tube. 650µl of chilled isopropanol is mixed with the supernatant to precipitate the DNA. The isopropanol precipitated DNA is pelleted by centrifugation for 20 minutes at 4°C. The isopropanol is then removed and the resultant pellet washed with 200µl of 70% EtOH. Excess ethanol is removed via pipetting and the pellet left to air dry before being resuspended in 50µl water.

Technique	260/280	260/230	~ng
Gel Extraction	>1.8	0.00-0.2	5-30
PCR purification	>1.8	0.00-0.2	15-50
Mini Prep	~1.8	~1.8	7500
Maxi Prep	~2.00	~2.00	600000

Table 2.5. Used DNA purification kits and their typical purity and yield. Purity is determined by the 260/280 and 260/230 ratio, in which 260/280 assesses protein contamination and 260/230 assesses solvent contamination.

2.5.2 Manipulation of DNA

2.5.2.1 PCR cloning

PCR cloning was used extensively to amplify DNA sequences in preparation for insertion into a plasmid backbone. The two main approaches employed were to amplify the sequence of interest (i) flanked with DONOR recombination sites for gateway mediated cloning (ii) flanked with restriction endonuclease sites for classical cloning. The DNA polymerase used for both of these approaches was the high fidelity, high processivity enzyme, KOD Hot Start DNA polymerase (Novagen). The generic PCR conditions used are indicated in **Table 2.6**. The amplified product was analysed by gel electrophoresis and then gel extracted before being used in further applications.

Step	Temp °C	Duration	No. of Cycles
Denaturation	95	15 seconds	1 cycle
Denaturation	95	30 seconds	
Annealing	50-70	30 seconds	25-35 cycles
Extension	72	15-30 seconds/kb	

Table 2.6. Generic PCR cycling parameters used with KOD Hot Start polymerase.

2.5.2.2 Site-directed Mutagenesis

Point mutations and deletions were introduced into plasmid backbones using the Quik Change ® site-directed mutagenesis kit (Stratagene) as per manufacturer's instructions.

2.5.2.3 Restriction Endonuclease Digest

Restriction endonuclease digest was carried out as either a single digest, sequential digest or simultaneous digest. For all reactions, DNA was incubated with the restriction endonuclease(s) in the presence of a supplied or suitable 1X buffer. After the digestion, the cleaved DNA was either purified using the PCR purification kit (Qiagen) or ran electrophoretically on an agarose gel and extracted using a QIAspin kit (Qiagen).

2.5.2.4 5'phosphate removal

Linearised plasmid DNA was enzymatically modified to remove 5' –phosphate in order to reduce the occurrence of self-ligation. This was performed by incubation of DNA with 1U/µg of Shrimp Alkaline Phosphatase (SAP) for 15 minutes at 37°C in 1X concentration of the supplied buffer. DNA was then purified using the PCR purification kit (Qiagen).

2.5.2.5 DNA Ligation

The enzyme T4 DNA ligase (Roche) was used to anneal two complementary pieces of DNA to encourage the formation of a single circular plasmid. The ligation reaction was only performed for linear DNA containing compatible cohesive 'sticky' ends. The reaction was organised so that an appropriate amount of insert and vector DNA was used, typically a 3:1 molar ration of insert:vector. The 1:1 ratio was determined using the following equation;

Vector/Insert (ng/µl) X Insert/Vector (kb)

The resulting value was multiplied by three to determine the final 3:1 ratio. The reaction was made in a 20µl volume, using between 20-50ng of insert in the presence of 1X the supplied buffer and 1U T4 DNA ligase. Reactions were

incubated on melting ice overnight. 2-4µl of ligation reaction was transformed into competent *E.coli* cells, often commercial XL-10 blue cells (Stratagene), DH5α (invitrogen) for increased transformation efficiency.

2.5.3 DNA purification

2.5.3.1 Agarose Gel Electrophoresis and Gel Extraction of DNA

DNA fragments were separated by a suitable % (w/v) agarose gel using electrophoresis. The gel was made with 1X TAE or 1X TBE and run in the presence of the same corresponding buffer.

Agarose was added to either 1X TAE or 1X TBE and then heated for ~25-50 seconds in a microwave, until all agarose had dissolved. 1X SYBR safe (Invitrogen) was added to the agarose solution. DNA samples were combined with 1X DNA loading buffer (Bioline) and electrophoresed against Hyperladder I DNA Ladder (Invitrogen) at 100mA for 30 minutes. Gels were imaged using a G-box gel imaging system (Syngene). For gel extraction, the gel was visualised using 302nm wavelength light from a trans-illuminator. Desired DNA fragments were excised from the gel by scalpel blade and then purified using the QIAquick Gel Extraction Kit (QIAgen) as per manufacturer's instructions. The purified DNA fragment was eluted in either a 30µl or 50µl TE volume, depending whether yield or concentration of the fragment was more important.

2.5.3.2 Quantification of DNA yield and purity

Nucleic acid concentration was determined using a Nanodrop spectrophotometer (Labtech). Samples were suitably diluted to allow for a reading within a concentration range of 2ng/µl – 3,000ng/µl. The absorbance at 230, 260 and 280 was then determined for a 1.5µl volume of the sample/diluted sample. The ratio values for 260/280 and 260/230 were then noted, as they give an indication of the purity of the sample. The 260/230 measurement is affected by the presence of solvents such as ethanol and the 260/280 measurement is affected by protein contaminants.

2.5.3.3 DNA Sequencing

Automated DNA sequencing was carried out by the GATC biotech (Germany). Plasmid DNA templates were sent at a concentration of 30-100ng/µl in a 30µl volume, sufficient for 8 reactions. Oligonucleotide primers were sent at a concentration of 10pmol/µl, also in a 30µl volume. Sequence analysis was performed using a combination of the Vector NTI (InVitrogen) plasmid

database software, the MultiAlin online software (http://bioinfo.genotoul.fr/multalin/multalin.html) and NCBI BLAST searches.

2.5.4 Gateway® BP & LR reactions

The BP & LR reactions transfer the DNA of interest from amplicon to Entry vector and Entry vector to Destination vector respectively. Reactions were performed using the BP clonase™ ii and LR clonase™ ii kits (InVitrogen), used as per the supplied protocol. 2µl-5µl of the reactions was then used to transform into DH5α/DB3.1 cells and plated on LB agar inoculated with the appropriate antibiotic. Positive antibiotic-resistant colonies were selected and their plasmid digested to ensure accuracy of the reaction.

2.6 Single-cell Imaging

2.6.1 Luminescence microscopy

Luminescence imaging was carried out on transfected cells in 35 mm glass bottom dishes (Iwaki, Japan) using a Hamamatsu Back thinned ORCAII counting camera attached to the Keller port of a3 Zeiss Axiovert 135 TV with a 10x FLUAR objective (NA=0.5). Prior to imaging, cells were incubated on the microscope stage (37°C, 5%CO_2) for 1 h in the presence of 1mM luciferin (Biosynth AG, Switzerland). Oxygen levels were altered using a Pecon O_2 Controller attached to a small stage incubator.AQM Kinetic Imaging software was used for image acquisition and analysis of mean intensity luminescence over time was performed using AQM Advance (Kinetic Imaging, UK). Images were acquired using 10-30 min integration times.

2.6.2 Confocal microscopy

Confocal microscopy was carried out on transfected cells in 35mm glass bottom dishes in a humidified CO_2 incubator (at 37°C, 5% CO_2) using a Zeiss Axiovert 200 with a 63X phase contrast oil immersion objective (NA =1.3). Oxygen levels were altered using a Pecon O_2 Controller attached to a small stage incubator. Excitation of EGFP and EYFP was performed using an Argon ion laser at 488nm and 514nm respectively. EGFP emitted fluorescence was reflected through a 505-550nm bandpass filter from a 540nm dichroic mirror. EYFP emitted fluorescence passed through a 514nm dichroic mirror and was collected through a 530nm long-pass filter. DsRed-Express and mCherry fluorescence were excited using a green Helium Neon laser (543nm) and detected through a 560nm long-pass filter. For the majority of two-colour imaging experiments,

DsRed-express and EGFP were used as the FP tags. Data capture and extraction was carried out with LSM510 version 3.5 software (Zeiss, Germany).

2.6.3 Fluorescence Recovery After Photo-bleaching (FRAP)

Regions of interest in cells over-expressing EGFPHIF-2α were photo-bleached. This was performed by imaging the cells every 2 seconds for 5 repetitions before bleaching, then imaging for a minimum of 2 minutes post-bleaching. Bleaching was carried out by using an Argon ion laser at 488nm at 100% output power for 25-75 iterations. For these experiments an oil immersion objective was used with a numerical aperture of 1.3. The pinhole was set to 1 airy unit.

2.6.4 Immunocytochemistry

HeLa cells were plated at density of $1x10^5$ in 35mm glass bottom dishes (IWAKI). Transfection was performed the following day when required. Cells were grown to 70-80% confluence prior to fixing. Cells were rinsed three times with PBS. Two methods of fixation were employed (i) Paraformaldehyde fixation and (ii) Methanol fixation. Paraformaldehyde fixation consisted of treating cells with 4% paraformaldehyde for 15 minutes then rinsing the cells three times with PBS. Cells were blocked for 30 minutes (blocking buffer: PBS containing 1% BSA and 0.1% Triton). Alternatively for methanol fixation, cells were treated with ice-cold methanol for 6 minutes at -20°C. Cells were then rinsed three times with PBS and then placed in a blocking buffer (PBS, 1% BSA). After fixation by either method, cells were incubated for one hour with primary antibody diluted (as indicated in **Table 2.7**) in the blocking buffer. Cells were then washed three times with PBS and incubated for a further 30 minutes with Cy3 labelled anti-mouse secondary antibody, diluted 1:500 also in the blocking buffer. During and after labelling samples were kept dark to minimise photo-bleaching.

cells.

2.6.4.1 Imaging of fixed cells

Confocal microscopy was used to visualise stained cells. Cy3 conjugates were excited using a 543nm laser line and emitted signal detected by LSM510 photomultiplier detectors, after passing through a 560nm long-pass filter. FITC conjugates were excited using a 488nm laser line and emitted signal detected after passing through a 505-550nm bandpass filter, also using LSM510 photomultiplier detectors. For instances of quantitative comparison of fluorescence, all images were taken together using the same detector settings.

Fluorescence levels were quantified using either AQM Kinetic Tracker ver 6, LSM image browser or Cell Tracker Version 0.6.

Antibody	Source	Catalogue No	Dilution	Host Species
Anti-mouse Cy3	Jackson Lab.	C2181-1	1:500	
Anti-rabbit Alexa Fluor 555	Invitrogen	A21428	1:500	
Anti-rabbit Alexa Fluor 488	Invitrogen	A1101	1:500	
HIF-1α	BD Biosciences	610959	1:200	Mouse
HIF-2α	Abcam	Ab20654	1:200	Rabbit
RNA polII	Upstate	CTD4H8	1:100	Mouse
PML	Santa Cruz	Sc5621	1:200	Rabbit
PHD3	Novus Biologicals	NB 100-139	1:200	Rabbit

Table 2.7. List of primary and secondary antibodies used in immunocytochemistry with HeLa cells.

2.6.5 Image Analysis

Image analysis was performed using either AQM Kinetic Tracker, LSM image browser or Cell Tracker ver 6.

2.6.5.1 Image analysis by cell tracker

Concatenated time series data and single-images of fluorescence were analysed using Cell Tracker Version 0.6 to convert fluorescence images to quantified data (software website: www.dbkgroup.org/celltracker/) (Shen, Nelson et al. 2006). Two methods of using Cell Tracker were employed; full tracking or small circle tracking. Full tracking involved accurately drawing around either the cytoplasm or cell nucleus, whereas a small circle tracking used a drawn small region placed in a representative area of either the cytoplasm or cell nucleus. Small circle tracking is more prone to noisy measurements, but still provides largely similar data (Dr. D. Turner, thesis) Cell Tracker data was exported as mean intensity of fluorescence and saved in an excel format.

2.6.5.2 Image analysis by AQM kinetic tracker

AQM kinetic tracker was used to quantify wide-field luminescence data or to automatically detect and quantify speckle fluorescence from confocal images (see Chapter 6). Manual measurement of image intensity was performed by fixing a region of interest to the images. This method does not track the signal

over time, only all signals from a fixed location over time. AQM kinetic tracker was also used to automatically detect signal. This required the manual setting of detection criteria, including size of object, distance away from other objects, object brightness and how many frames the object appears in Once these are empirically determined the program automatically records any object within the detection criteria. This approach was predominantly used in quantification of speckle fluorescence (see Chapter 6).

2.6.5.3 Image analysis by LSMsoftware

LSM Imaging software (LSM510 ver 3 or Zen) was used for confocal data capture and also as a basic image analysis tools. The software was used to quantify fluorescence for co-localisation studies or to examine emission spectra of a fluorophore following a lambda scan.

2.7 Bulk-cell Analysis

Bulk-cell analysis is defined here as cell biology techniques that involve the single-measurement of a population of cells.

2.7.1 Western Blotting

2.7.1.1 Sample preparation

Cells were typically plated into 6cm dishes (see table 2.2) and prepared or incubated according to specific experimental design. Cells were lysed after treatment or incubation protocols, ideally when at 80-90% confluency. After 2x PBS washes, lysis was performed by adding 200µl of lysis buffer (Tris-HCL 50mM pH7.5, 1mM EDTA, 1mM EGTA, 1% Triton X-100, Sodium Fluoride 50mM, 5mM Sodium Pyrophosphate, 10mM Sodium β-glycerophosphate, 0.1mM phenylmethylsulphonyl fluoride, protease inhibitor cocktail -sigma: p8340), followed by scraping the cells and centrifuging the collected the supernatant.

2.7.1.2 Measurement of protein concentration

Protein levels were determined for the lysates, using the BCA assay (Thermo Scientific). The assay was performed in 96-well plates, using a sample volume of 20µl to 178.5µl of reagent. A triplicate standard curve was included using BSA protein at concentrations (µg/µl) of; 0.00, 0.25, 0.50, 1.00 and 1.50. The signal present in the blank control was subtracted from all other measurements prior to calculation of protein concentration for each measured sample.

2.7.1.3 Protein separation by SDS-PAGE

10% SDS-PAGE resolving gels were prepared in H_2O (0.38M tris base, 0.1% SDS, 10% acrylamide, 0.25ng/µl APS and 0.125% Temed) and 4% stacking gels (0.14M tris base, 4% acrylamide, 0.75ng/µl APS and 4% Temed). SDS-PAGE gels were cast using the Mini-PROTEAN 3 system alongside glass plates and 0.75 mm spacers. Samples were boiled in the presence of an equal volume of 2x Laemlli buffer (25% v/v 0.5M tris, 20% v/v glycerol, 10% SDS, 0.1% w/v bromophenol blue and 5% v/v β-mercaptoethanol) 5 minutes before gel loading. Sample volume to load was determined using the calculated concentration, aiming to load even protein amounts for samples (on average 30-60µg/well). The gel was then resolved at a voltage of 120V submerged in running buffer (25mM Tris, 192mM glycine and 3.4mM SDS).

2.7.1.4 Transfer to nitrocellulose

Proteins were electrophoretically transferred from acryalmide gels to 0.2µm nitrocellulose membranes (Bio Rad) at 300mA for 90-minutes using a Bio Rad transfer tank filled with chilled transfer buffer (20% (v/v) methanol, 25mM Tris, 200mM glycine). Transfer was performed in 4°C cold room.

2.7.1.5 Detection of protein

Nitrocellulose membranes were washed by submersion in buffer (TBS-T; 20mM Tris, 140mM NaCl, adjusted to pH7.6, 0.1% Tween), in blocking buffer (5% w/v dried milk protein, 20mM Tris, 140mM NaCl, adjusted to pH7.6, 0.1% Tween) for 60-minutes. Blocking buffer was then removed and residual blocking buffer washed from the nitrocellulose membrane using TBS-T. Membranes were then incubated in the presence of primary antibody overnight at 4°C. All primary antibodies were made-up in a solution of 5% BSA in TBS-T, used concentrations and commercial sources of the antibodies are shown in **Table 2.8**. After primary antibody incubation, membranes were washed as previously and then submerged in secondary antibodies (conjugated with horse-radish peroxidase) solutions for 60-minutes and then re-washed; secondary antibodies were made in blocking buffer (**Table 2.8.**).

Antibody	Source	Catalogue No	Dilution	Host Species
Anti-mouse HRP	Abcam	Ab6808	1:15000	
Anti-rabbit HRP	Cell Signalling	7074	1:5000	
HIF-1α	BD Biosciences	610959	1:1000	Mouse
HIF-2α	Santa Cruz	Sc13596	1:500	Mouse
pVHL	BD Biosciences	556347	1:500	Mouse
PHD1	Novus Biologicals	NB 100-137	1:1000	PHD1
PHD2	Novus Biologicals	NB 100-138	1:1000	PHD2
PHD3	Novus Biologicals	NB 100-139	1:1000	Rabbit

Table 2.8. List of antibodies used for western blotting and the corresponding source, dilution used and species raised in.

Membranes were then covered in a commercially available high sensitive chemiluminscent substrate reactive (SuperSignal®West Dura Extended Duration Substrate, Thermo Scientific)to HRP for 1-minute and excess substrate removed. Membranes were then imaged using a Syngene Gel Imaging G:Box, imaging every two-minutes and integrating subsequential images for up to 40-minutes. The integrated intensity of the bands was quantified using AQM kinetic tracker version 6.

2.7.2 Cell Proliferation Assay (MTS)

The CellTiter 96® Aqueous Non-Radioactive Cell Proliferation Assay (Promega) was used to determine an arbitrary count of viable cells in a population. The assay uses the change in absorbance of a tetrazolium compound [3-(4,5-dimethylthiazol-2-yl)-5-(3-carboxymethoxyphenyl)-2-(4-sulfophenyl)-2H-tetrazolium due to mitochondrial reductase activity as an indication of viability. Cells in suspension were prepared prior to plating, using a density of a 50,000 cells/ml. Cells to be transfected were incubated with the transfection mixture at this stage prior to plating. Cells were dispensed into transparent 96-well plates, plating 100µl of cell suspension per well. Plates were then incubated as indicated. For the proliferation assay, 20µl of room temperature reagent B was added to each well. The plates were incubated for 90 minutes before being

analysed using a Multiskan* plate reader (Thermo scientific) at 492nm. Results shown were subtracted by a media and MTS reagent blank.

2.7.3 Luminometry

Cells in 24-well plates were transfected a day after plating with the indicated luciferase reporter construct with or without additional expression vectors and treated in triplicate After a determined incubation period, the media was removed and the cells were washed with Ca2+-free PBS. Cells were then treated directly in the 24-well plate with 250µl per well of lysis buffer (0.04g DTT, 1.6g BSA, 123.12ml H_2O, 4ml 1M Tris-phosphate pH 7.5, 1.6ml Triton X-100, 30ml 80% glycerol, 32µl 0.5M EDTA and 1.28ml 1M $MgCl_2$). Cells lysis was performed at room temperature under gentle shaking. ATP was then added to a final concentration of 1mM before 90µl of the lysate was transferred to a white opaque 96-well plate (Greiner). An Envision 2103 Multilabel reader (Perkin-Elmer) was used for the assay protocol. 200µl 25mM luciferin (buffered in pH8 10mM Tris-phosphate) was added to each sample. Luminescence signal was recorded every 0.1 seconds for 5 seconds. All measurements were summed for a final value.

2.7.4 RT-qPCR

2.7.4.1 RNA extraction

The RNeasy Mini Kit (Qiagen, Germany) was used in the extraction of RNA from HeLa cells. The RNA extraction was performed on cells grown in 6cm dishes. Upon extraction, the media was removed and the cells rinsed with PBS. 350µl of lysis buffer RLT containing β-mercaptoethanol (1% (v/v)) was added directly onto the cells. The cells were then scraped and the lysate was frozen at -80°C. All lysates from a single time course were collected before resuming the extraction protocol. Homogenisation of the lysate was performed using a QIAshredder (Qiagen), as detailed in the kit protocol. Samples were eluted in 30µl of RNAse free water. The elute was assessed for RNA quantity and purity as detailed using spectrophotometry.

2.7.4.2 Reverse Transcription

Reverse transcription of extracted RNA (to cDNA) was carried out using the SuperScript® VILO cDNA Synthesis Kit (Invitrogen). The reaction consisted of 1µg sample RNA, 1X SuperScript® Enzyme Mix, 1X VILO™ Reaction Mix made up to a 20µl total volume using DEPC-treated water. Reactions were then performed using a Px2 Thermal Cycler (Thermo) for 10 minutes at 25°C, then

60 minutes at 42° and finally 5 minutes at 85°C. The resulting cDNA was then diluted 20-fold prior to use in quantitative-PCR.

2.7.4.3 Q-PCR

Q- PCR reactions were carried out in triplicates. 20µl reaction mixtures were made using 1µl of cDNA combined with 300nM forward and reverse primers (primers used shown in **Table 2.9**), 1x SYBR Green PCR master mix (Roche) and Raze free H20. Temperature cycling was performed using a LightCycler 480 (Roche) using the parameters in **Table 2.10**.

RT-qPCR primers			
Cyclophillin A (for)	gctttgggtccaggaatgg	HIF-1α (for)	tgctcatcagttgccacttc
Cyclophillin A (rev)	gttgtccacagtcagcaatggt	HIF-1α (rev)	tcctcacacgcaaatagctg
pVHL (for)	ggtcacctttggctcttcag	HIF-2α (for)	gccacccagtaccaggacta
pVHL (rev)	gctgtccgtcaacattgaga	HIF-2α (rev)	ggcagcaggtaggactcaaa
FIH (for)	ctttaagccgaggtccaaca	PHD2 (for)	tgcagatgagagagcacg
FIH (rev)	caacctctcttcccctcctc	PHD2 (rev)	ttagcgaccgaatctgaagg
PHD1 (for)	actgggacgttaaggtgcat	SIAH1 (for)	gcagtcctgttttggctttc
PHD1 (rev)	aaatgagcaaccggtcaaag	SIAH1 (rev)	tcagctgtacgattgcgaag
PHD3 (for)	agatcgtaggaacccacacg		
PHD3 (rev)	ttctgccctttcttcagcat		
SIAH2 (for)	agccgagaactttgcctaca		
SIAH2 (rev)	cacaccgtcatgaatcgaac		

Table 2.9. RT-qPCR primers used. Target transcript indicated by primer name with corresponding sequence adjacent. For denotes forward primer (5'-3') and Rev denotes reverse primer (3'-5').

Results were analysed using the Advance Relative Quantification function the LightCycler® 480 software (version 1.5.0.39) to calculate the fold change based on the threshold cycle for each PCR reaction using the 2-ΔΔCT method (Pfaffl, Horgan et al. 2002). The target gene was normalised to house-keeping gene cyclophillin A, with time 0 used as the calibrator.

Step	Temp	Duration	Ramp Rate (°C/s)	Cycles
Pre-Incubation	95°C	300 s	4.4	1
Amplification	95°C	10 s	4.4	45
	60°C	30 s	2.2	
Melt Curve	95°C	5 s	4.4	
	65°C	61 s	2.2	1
	97°C	continuous	0.11	
Cooling	40°C	10 seconds	1.5	1

Table 2.10. RT-qPCR cycling parameters used with LightCycler 480 (Roche).

2.8 Mathematical Modelling

Mathematical modelling and simulations were performed using Matlab software, version 7 and later. All model simulations and operations were carried out using the ODE45 numerical solver. Parameter fitting was performed using the 'fminsearch' function to determine minimum variables.

Chapter 3: Protocol optimisation and generation of molecular tools

3.1 Introduction and Aims

A fundamental aim of the project was to examine canonical HIF signalling at the single-cell level using live-cell time-lapse confocal microscopy in ambient and hypoxic O_2 levels. In order to achieve this it was necessary to determine a suitable cell line, to generate relevant fluorescent fusion plasmids, to optimise and validate imaging in hypoxia as well as optimising image analysis protocols.

3.2 Results

3.2.1 Optimisation of experimental protocols

3.2.1.1 Choice of cell line

In our lab, cell behaviour in hypoxia has never been examined and therefore the suitability of the available cell lines was uncertain. One of the initial aims of the project therefore was to determine a cell line that can be used for the majority of the project, paying heavy consideration to the hypoxic response and ease-of-use for confocal microscopy. Our lab currently uses two cell lines considered to be highly suitable for live-cell confocal microscopy; the neuroblastoma cell line SK-N-AS and the cervical epithelial HeLa cell line (Gey GO 1952; Sugimoto, Tatsumi et al. 1984). The criteria that underpin their suitability are their ease-of-transfection, adherence, low instance of migration and clear cell morphology (which aids software image analysis). Additionally, both the SK-N-AS and HeLa cell line have been characterised and optimised for use with several transfection reagents including Amaxa electroporation, FuGene 6 and Lipofectamine 2000. From these two cell lines, HeLa cells have been most widely used in hypoxic research (Chilov, Camenisch et al. 1999; Taylor, Furuta et al. 2000; Hofer, Desbaillets et al. 2002). In an effort to keep our data comparable with others in the field, the HeLa cell line was initially chosen as a cellular model.

Oxygen functions as a complex stimulus affecting many important cellular processes such as cell cycle progression, cell death, migration, cellular energy production, transcription and translation (Lee, Bae et al. 2004; Van Hoecke, Prigent-Tessier et al. 2007). This project aims to utilise hypoxia extensively and so it was therefore necessary to broadly characterise the effect of reduced O_2 on our HeLa cell line and to account for any potentially experimentally compromising changes to cell viability (Gardner, Li et al. 2001; Gordan, Bertout et al. 2007; Van Hoecke, Prigent-Tessier et al. 2007; Lomb, Desouza et al. 2009). Alteration to growth and death rates would impact experimental design reducing our ability to account for cell-density between normoxic and hypoxic

samples. Furthermore, significant changes to cell death would impact the duration we would be able to examine the HIF response. We therefore sought to measure whether cell viability is perturbed by reduced oxygen over the course of 24 hours.

3.2.1.2 Cell growth in hypoxic conditions

To measure cell viability, the commercially available MTS assay was employed (Cory, Owen et al. 1991). HeLa cells were plated into 96-well plates at two different densities and incubated at either 1% O_2 or atmospheric O_2 (performed in air, where O2 tensions are above 19%) for up to 48-hours. By using two densities we are able to negate changes in viability that may occur due to confluency. The results of the MTS assay indicate that cell viability increases for the first 24 hours when cells are incubated at 1% O_2 (**Fig 3.1**). Cells exposed to 48 hours of hypoxia showed a reduction in viability compared to the control when plated at a high density and cells plated at a lower density showed a similar degree of viability compared to control. This is perhaps indicative of an increased proliferation rate leading more rapidly to confluency which is then detrimental to the viability of the cells.

Examination of cells by light microscopy did not agree with results obtained by the MTS assay (data not shown). Similar growth rates and increased cells death were observed prompting us to question the accuracy of the MTS assay in determining cell viability for these experimental conditions. The MTS assay is a colourimetric assay in which the MTS reagent (3-(4,5-dimethylthiazol-2-yl)-5-(3-carboxymethoxyphenyl)-2-(4-sulfophenyl)-2H-tetrazolium) is reduced to produce formazan which has a known absorbance at490-500nm. The reduction of the MTS reagent is catalysed by cellular reductases, predominantly mitochondrial reductases. An elevated amount of functional mitochondria therefore result in an increased absorbance signal which serves as a proxy variable for viability. However, the hypoxic environment used will possibly affect the redox state of the cell as well affecting the mitochondria and therefore disturb the reduction of the MTS substrate to formazan (Makarov, Wiswedel et al. 2002). To address this issue cell growth was also assessed using a simple cell-count method. HeLa cells were plated into 6cm dishes and grown for 24-hours at either 1% O_2 or atmospheric O_2. After incubation cells were removed into suspension by trypsinisation and counted using a Coulter Particle cell counter. In contrast to the ~25% increase in viability as measured by the MTS

assay, hypoxia was found to reduce the cell count by 7.7% (n=1 repetition). This finding is in accordance with a more extensive investigation into hypoxia and cell fate (Fan *et al.* unpublished).

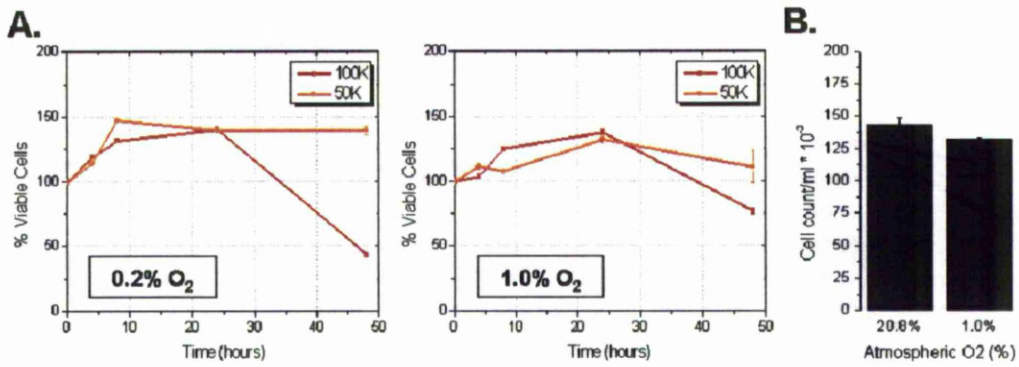

Fig 3.1. HeLa cells were cultured in 96-well plates at either 0,2% or 1% O2 for up to 48-hours. To measure cell viability, MTS reagent was added to the cells and after 30 minutes the 492nm absorbance of the cell culture measured. Measurements are normalised to to as a percentage of viable cells. (**A**) MTS viability assay of cells shown as a percentage of hypoxia over normoxia. (**B**) Cell count of HeLa cells grown in hypoxia or atmospheric conditions for 24-hours. Count was performed automatically using a Coultier particle counter set to detect objects between 7 and 22µms.

3.2.1.3 Is HRE-luciferase inducible in HeLa and SK-N-AS cells by incubation at 1% O_2?

The next important criterion was to determine whether SK-N-AS and HeLa cells were HIF inducible and if the response occurred in accordance with published data.

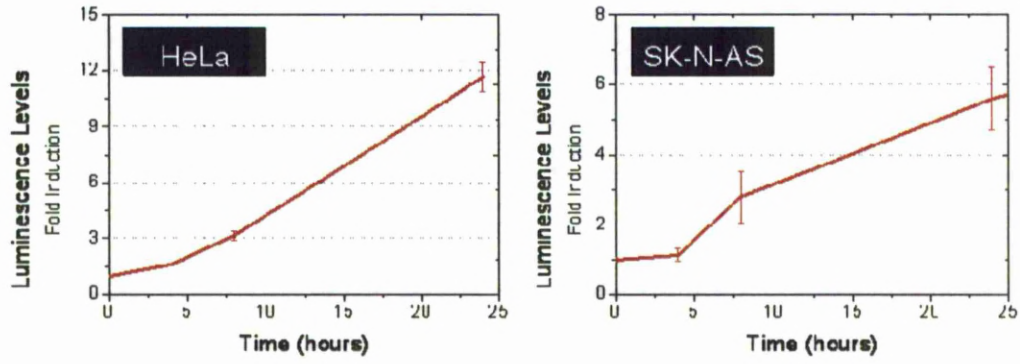

Fig 3.2. HeLa cells and SK-N-AS cells were plated into 24-well plates and then transfected to express the PGL2-TK-HRE-luc reporter. After 24 hours of transfection, cells were incubated at staggered time points for up to 24 hours in 1% O2. All cells were lysed simultaneously and samples prepared for measurement by endpoint luminometry. Graphs show measurement of measured luciferase signal normalised to the normoxic control.

To determine HIF-inducibility cells were transfected to express a HIF responsive luciferase reporter termed PGL2-TK-HRE, incubated at 1% O_2 up to 24 hours and then the luciferase signal was measured by endpoint luminometry (**Fig 3.2**). We were able to measure a significant increase in luciferase signal after a minimum of 8 hours incubation, indicating that the cell-line is HIF-

inducible despite existing in atmospheric culture conditions for several decades. (Gey GO 1952; Sugimoto, Tatsumi et al. 1984). The result verifies the PGL2-TK-HRE luciferase reporter plasmid which was kindly donated to our lab by Dr. Giovanni Mellilo and also serves to validate the recently installed Don Whitley hypoxystation which was used to incubate the samples.

3.2.1.4 Does the use of pre-equilibrated hypoxic medium affect the HRE-response to hypoxia?

Both HeLa and SK-N-AS cells are adherent and therefore are cultured as a monolayer submerged in growth media. Any manipulation of atmospheric oxygen would need to translate to a change in the dissolved O_2-environment immediately surrounding the cell monolayer to achieve cellular hypoxia. There was an initial uncertainty as to whether the duration of time needed for O_2 gas exchange when using hypoxia or re-oxygenation could significantly affect the assessed behaviour. The majority of this study is concerned with the HIF response to hypoxia and therefore we decided to assess the inducibility of the HRE-luciferase when using de-oxygenated media versus oxygenated media. HeLa cells were grown in 24-well plate format from a density of $12.5x10^5$ cells/cm^2 and transfected with PGL2-TK-HRE for 24-hours prior to hypoxic incubation (1% O_2). Upon incubation the media was removed from the cells and replaced with either media equilibrated in atmospheric normoxia or media equilibrated for 24 hours in 1% O_2. No significant difference was found comparing the use of de-oxygenated media versus oxygenated media on the signal output of the HRE-luciferase reporter (**Fig 3.3**). Although the speed of de-oxygenation would be dependent on the culture vessels and depths of media, the difference was considered negligible for evaluating the HIF response (which occurs in the order of hours), theory and our data therefore encouraged us to disregard the use of pre-equilibrated media to induce hypoxia.

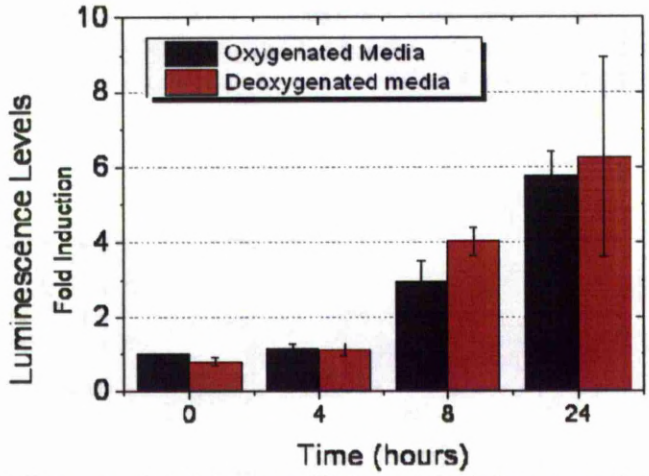

Fig 3.3. HeLa cells were plated in 24 well format and then transfected with pGL-TK-HRE-luciferase. After 24 hours of transfection, cells were incubated in either atmospheric unequilibrated media or 24-hour 1% O_2 equilibrated media. Cells were lysed simultaneously and samples prepared for luminometry analysis. Results show the luminescence levels normalised to the normoxic control(n=1 repetition in triplicate).

3.2.1.5 Analysis of HIF-1α and HIF-2α protein response in HeLa cells exposed to 1% O_2

Previous experiments using the HRE-luciferase had indicated the HeLa cell line as a suitable model to study the hypoxia-inducible HIF system (**Fig 3.1.** & **Fig 3.2.**). The HRE-reporter does not resolve whether the transcriptional activity is attributable to HIF-1α and/or HIF-2α and so we therefore have little idea of the kinetics of the population wide-accumulation of these factors. Furthermore, before engaging in the single-cell imaging of the separate α-isoforms it was prudent to characterise the bulk-cell response of these factors to hypoxia. This is underlined by reports of the different sensitivities and response patterns of both isoforms to hypoxia (Bracken, Fedele et al. 2006). HeLa cells were plated at a density of $3.5*10^5$ per 6cm dish and incubated at 1% O_2 for several periods of time up to 24 hours. Additionally one sample incubated for 24 hours at 1% O_2 was further exposed to a 15-minutes re-oxygenation back to atmospheric O_2. Western blot analysis was carried out using these samples probing for HIF-1α and HIF-2α protein (**Fig 3.4.**). HIF-1α was detected at 120kDa and showed a transient accumulation over the 24-hour hypoxia time-course as well as showing the effective rapid degradation of protein upon re-oxygenation. Examination of HIF-2α protein levels yielded varied results between repetitions, showing no distinct accumulation or re-oxygenation sensitivity. A similar finding was reported by Bracken et al. when also examining HeLa cells (Bracken, Fedele et al. 2006). Nevertheless, the cellular response to hypoxia was observable when probing for HIF-1α and the accumulation kinetics are in

accordance with published data (Wang, Jiang et al. 1995; Stiehl, Wirthner et al. 2006).

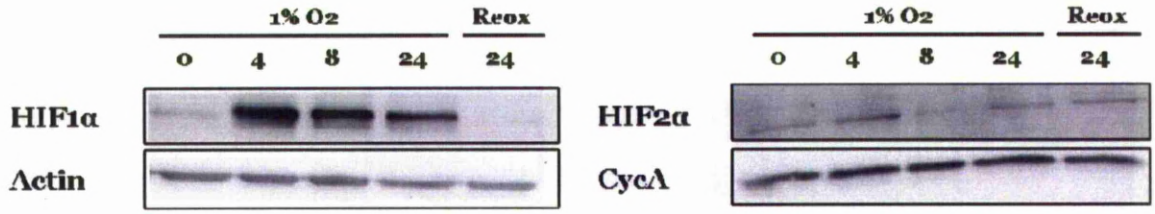

Fig 3.4. Western blot of HIF-1α/-2α protein levels for samples prepared form HeLa cells incubated at 1% O_2 over a course of 24 hours. An additional sample was prepared from cells incubated for 24 hours at 1% O_2 and then exposed to a 15-minute re-oxygenation back to atmospheric conditions.

3.2.1.6 Dose-response of HeLa cells treated with DMOG

Due to the wide-reaching effects of reduced O_2 on various cellular processes we considered use of dimethyloxallyl glycine (DMOG); a chemical mimic of hypoxia that inhibits the hydroxylases of the canonical HIF system. DMOG acts as a competitive inhibitor of hydroxylases activity, inhibiting their ability to bind the co-substrate α-ketoglutarate (Rey and Semenza 2010). This drug could be used to corroborate and further explore some of the claims or data arising from study using hypoxia. This is of particular relevance to the live-cell imaging by wide-field luminescence and confocal microscopy as the generation of signal requires O_2, an issue further discussed later in **section 3.2.2.**

Before we could begin to use this chemical agent, it was necessary once again to characterise the effects of DMOG use (again assessing if there were detrimental affects to cell viability which may compromise experimental design). We once again used the MTS assay and performed a dose-response curve in which HeLa cells were plated into 96-well format 1-day prior to treatment. Cells were then treated with varying concentrations of DMOG ranging from 0.01mM to 2mM for 24-hours (**Fig 3.5**.). Concentrations above 0.1mM caused a significant reduction to cell viability, in which the viable population was reduced by 75% at 1mM. As well as determining the effects of DMOG on viability it was necessary to also determine the suitable DMOG dose to induce the HIF system. HeLa cells were transfected for 24-hours using the HRE-luciferase reporter and then treated with a range of DMOG concentrations for 6 hours before lysis and analysis by luminometry. We found that concentrations from 0.1mM to 1mM significantly induced the reporter with 0.5mM proving to be the most substantially inducing dose (**Fig 3.5**). With regards to the previous experiment of DMOG on viability, 1mM and 2mM most likely show a reduced HRE-

induction accredited to the reduced cell viability. For future experiments we therefore decided to use doses of 0.5mM and we tested the effect of this dose by time-course, again looking at cell viability and HRE-luciferase induction. The MTS assay showed a 37%±18 reduction in viability within 8 hours of treatment which was followed by some degree of recovery as cells reached 90%±1.6 viability compared to control (**Fig 3.5**.). In comparison, the fold induction of HRE-luciferase persistently increased across 24 hours of treatment reaching a total 37±10 fold increase.

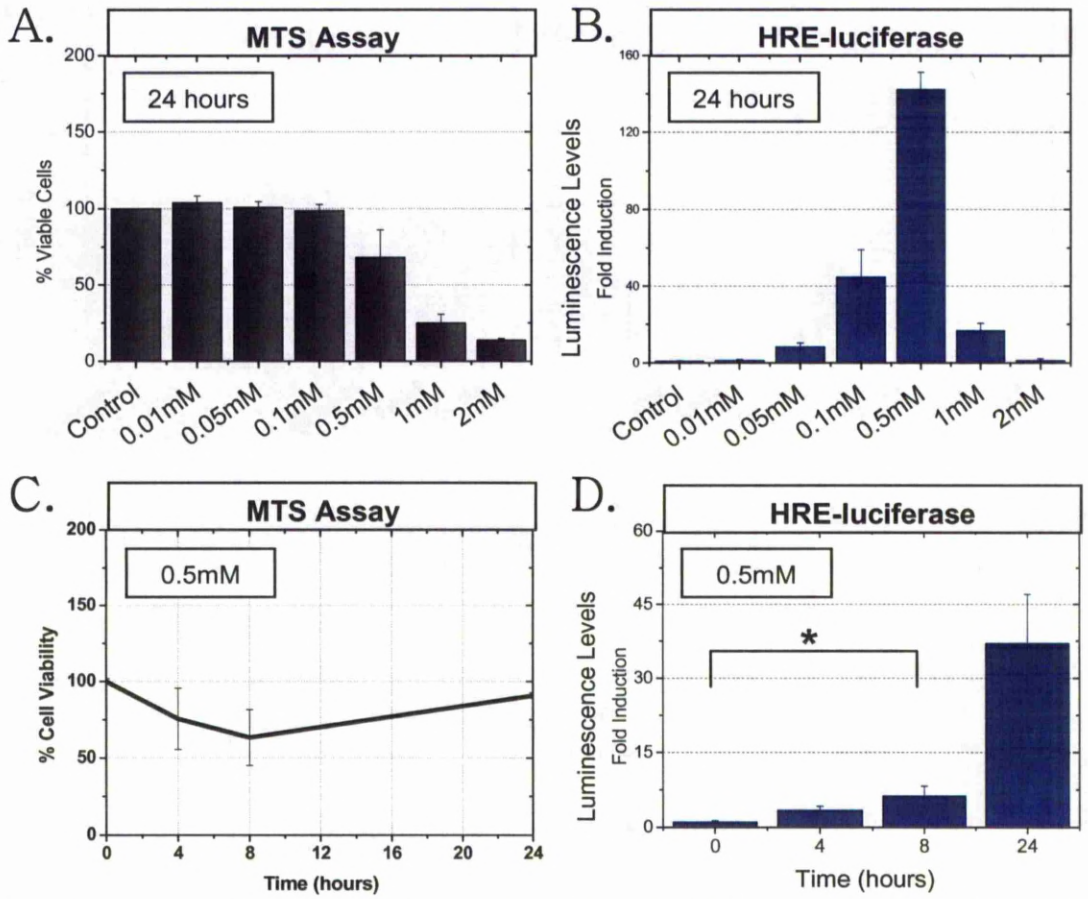

Fig 3.5. The effect of DMOG doses on HeLa cells measured by (**A**) MTS cell viability assay showing standard error of the mean (SEM) and (**B**) luminometry using cells ectopically expressing the HRE-luciferase reporter, showing standard deviation of triplicate measurements. (**C**) Time-course of HeLa cells treated with 0.5mM DMOG measuring effects on cell viability by MTS assay and shown as a percentage viability of treated over untreated cells. Error bars are calculated using the propagation of uncertainty to merge error bars from sextuplicate normoxic measurements and hypoxic measurements. Viability calculated as a % of treated over untreated. Treatment duration and doses are indicated (N=3 repetitions for A, B and D, N=2 repetitions for **C**). (**D**) Luminometry using cells ectopically expressing the HRE-luciferase reporter to assess HRE-inducibility by DMOG.

3.2.1.7 Is HRE-luciferase inducible by DMOG in HeLa and SK-N-AS cells?

During the course of previous experiments, we aimed to evaluate the effect of DMOG on various luciferase reporters in both HeLa and SK-N-AS cells. This

was performed with the goal of further verifying the use of the HeLa cell line as the main model to use throughout the project and as a limited control on the specificity of DMOG. HeLa cells and SK-N-AS cells were plated into 24-well plates at a density of 25k/well and 50k/well respectively and immediately transfected with a luciferase reporter sensitive (canonically) to either HIF, p53, NF-κB or CyclinD. Cells were then treated with 0.1mM DMOG for 8-hours before lysis and subsequent endpoint luminometry analysis. DMOG was found to only significantly activate the HRE-luciferase (**Fig 3.6.**). This is perhaps in contradiction to several publications suggesting crosstalk mechanisms with p53, NF-κB and cell-cycle (Cummins, Berra et al. 2006; Wen, Ding et al. ; Sermeus and Michiels 2011).

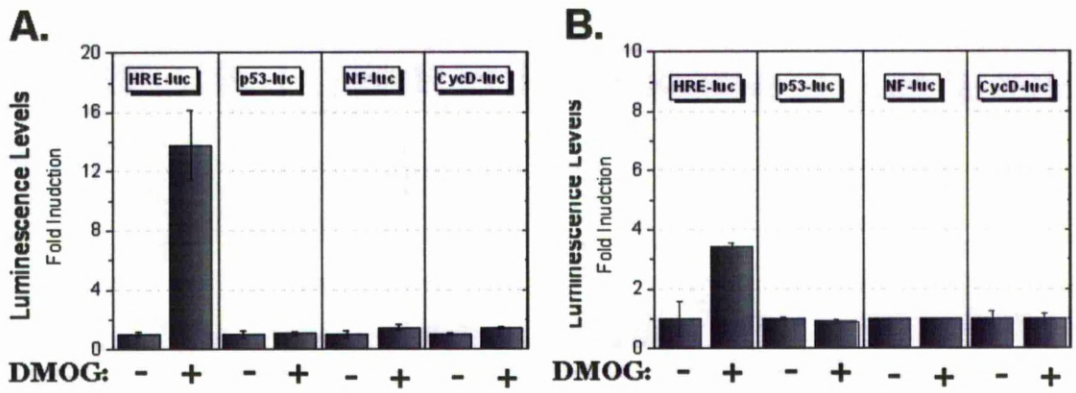

Fig 3.6. Endpoint luminometry analysis of samples prepared from (**A**) HeLa cells and (**B**) SK-N-AS cells ectopically expressing either HRE-luc, p53-luc, NF-luc or CycD-luc. Cells were stimulated for 8 hours using 0.1mM DMOG, denoted with +. Unstimulated control denoted with -. (n=1 repetition performed in triplicate)

3.2.2 Oxygen sensitivity of reporter and expression molecular tools

Many commercially available expression plasmids are driven by the human cytomegalovirus immediate early promoter (CMVie promoter), a strong viral promoter/enhancer that has been in use as a research tool for several decades (Qin, Zhang et al. 2010). Its suitability as a generic promoter for the expression of proteins of interest stems from an accepted view that the promoter activity is constitutive and unchanged by experimental conditions. Nevertheless, there are several known human transcription factor binding sites contained within the CMVie promoter such as CREB/ATF, NF-1, SP-1, MDBP and of particular interest, NF-κB (Loser, Jennings et al. 1998). This project aims to image single-living cells transfected with various fluorescent tagged proteins of the HIF pathway and the expression of these will be driven by the CMVie promoter. We we're therefore concerned whether the CMVie promoter would be a suitable

system for driving the expression of our fluorescent-tagged proteins, especially with regards to the use of hypoxia (Doran, Kulkarni-Datar et al. 2010) (Ramanathan, Hasko et al. 2005).

3.2.2.1 Does hypoxia regulate the CMV promoter?

To address this HeLa cells were plated into 24-well plate format and then transfected with CMV-luciferase. After 24 hours post-transfection, cells were then incubated at 1% O_2 as part of a time-course up to 24 hours before analysis by endpoint luminometry. We found no significant change in fold induction over the time-course (**Fig 3.7.**). This endpoint assay is a measurement of changes in fold induction over a population of cells, where as our work concerning the HIF system will focus on attaining data from the single-cell level. Single-cell asynchrony can be masked when using population-level measurements, we therefore looked at the CMV-luciferase response on the single-cell level using wide-field luminescence (Levsky and Singer 2003). Here HeLa cells were transfected for 24 hours with the CMV-luciferase before being imaged. Time-lapse data was then analysed using Kinetic Tracking Analysis as detailed in **section 2.6.1**. We found evidence of single-cell heterogeneity of light production, though the calculated population average of all cells showed a similar trend to that observed by endpoint luminometry.

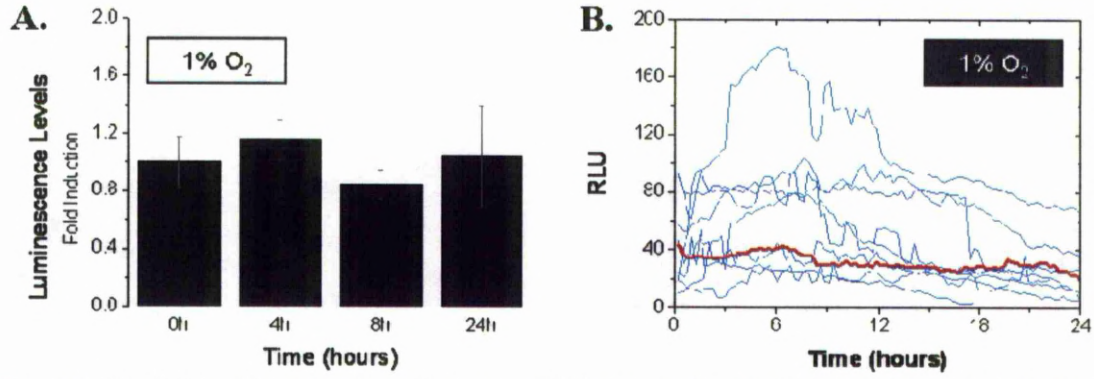

Fig 3.7. (**A**) HeLa cells were plated into 24-well format and transfected with CMV-luciferase. After 24 hours of transfection cells were incubated for up to 24-hours in 1% O2. Cells were then lysed simultaneously and samples prepared for analysis by endpoint luminometry. Measurement shows luminescence signal normalised to normoxic control. (**B**) HeLa ells were plated into 35mm imaging dishes and transfected with CMV-luciferase. After 24 hours of transfection cells were incubated in the presence of 1mM luciferin for 1 hour and then imaged for 24 hours by wide-field luminescence using a 20x objective. Image analysis was performed using AQM kinetic tracker to quantify single-cell level luminescence. Plots of single cell level luminescence are shown in blue and the calculated population average as a bold red line.

3.2.2.2 O_2-dependent luciferase reaction

Additionally, the previous experiments (**Fig 3.7.**) provide information on the oxygen-dependent sensitivity of the luciferase catalysed reaction, a reaction

requiring O_2 in the conversion of luciferyl adenylate to oxyluciferin, AMP and light (Moriyama, Niedre et al. 2008). By comparing the signal trend for CMV-luciferase between luminometry (as performed in atmospheric conditions) and wide-field luminescence (as performed in hypoxic conditions) we can see no significant loss of signal, suggesting the technology to be suitable for hypoxic conditions as low as 1% O_2 (**Fig 3.7.**). In fact, published work from Imamura et al. (2009) suggests luciferase to be functional at tensions as low as 0.2% O_2.

Luciferase reaction schematic:

1. luciferin + ATP ⟶ luciferyl adenylate + PPi
2. luciferyl adenylate + O_2 ⟶ Oxyluciferin + AMP + light

3.2.2.3 O_2-dependent fluorophore maturation

Alongside luminescence, fluorescent proteins also have an oxygen-dependent step that underlies their abilities as detectable reporters, specifically the maturation of fluorescent proteins requires molecular oxygen (**Fig 3.8**) (Tsien 1998; Zimmer 2002). This prompted concern that hypoxic conditions may impair the function of the fluorescent proteins and thereby their use as fluorescent fusion reporters. To explore this issue we characterised the several available fluorophores across a range of oxygen conditions.

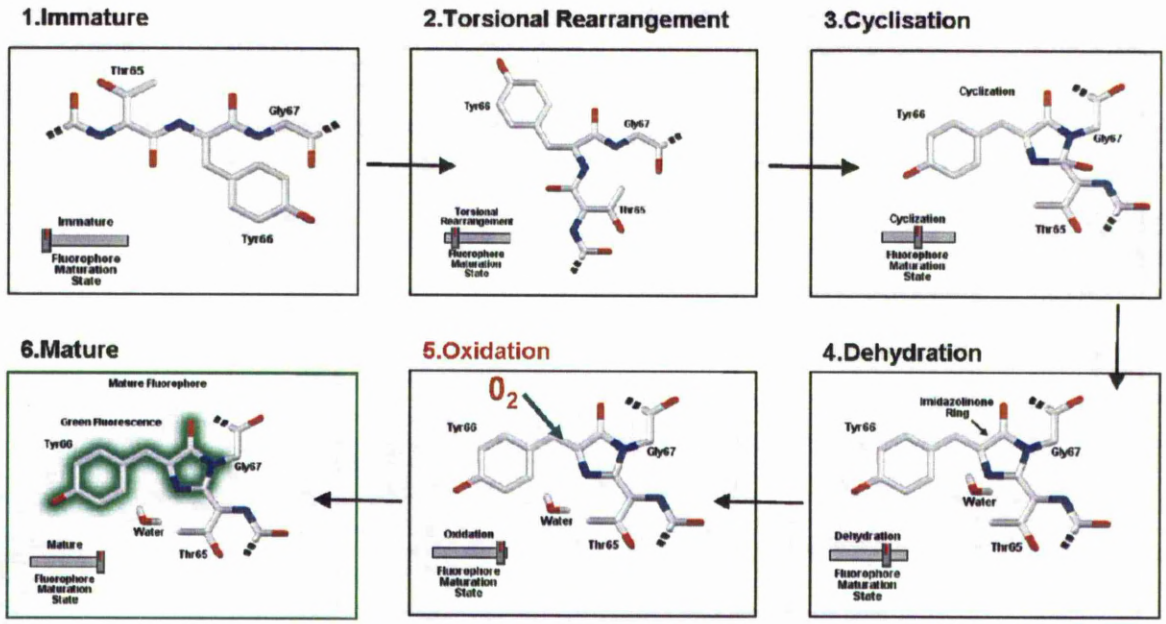

Fig 3.8. Fluorophore maturation process for Threonine-66, Glycine-67 and Tyrosine-68 of EGFP. Oxygen, Nitrogen and Carbon atoms are coloured red, blue and white respectively. Figure adapted from http://www.olympusmicro.com

Cells were transfected with either expression plasmids for unfused EGFP, EYFP, DsRedxp or mCherry. Immediately after addition of the transfection reagent,

cells were incubated in either 0.2%, 0.5% or 5% O_2 on the microscope stage, so that the initial fluorescence expression would occur in an oxygen-deprived environment. After 24 hours post transfection, cells were imaged for a total of 6 hours, switching oxygen back to atmospheric levels after an hour of imaging. Whole cell fluorescence levels were quantified using Cell Tracker. Analysis of fluorescence indicated that EGFP was the most suitable fluorophore to use when imaging in hypoxia, as fluorescence was observed at as low as 0.2% O_2 (**Fig 3.9.**). EYFP was also seen to be applicable to imaging in hypoxia and was visible at 0.5% O_2. DsRedxp and mCherry fluorescence was found to be severely impaired at tensions of 0.5% O2 and lower. Both these fluorophores require an additional oxidation event compared to the GFP variants (Gross, Baird et al. 2000). An additional consideration for imaging mCherry in hypoxic to atmospheric conditions is that the high quantum efficiency of the fluorophore (compared to DsRedxp) can more easily lead to detector saturation (Chudakov, Matz et al. 2010).

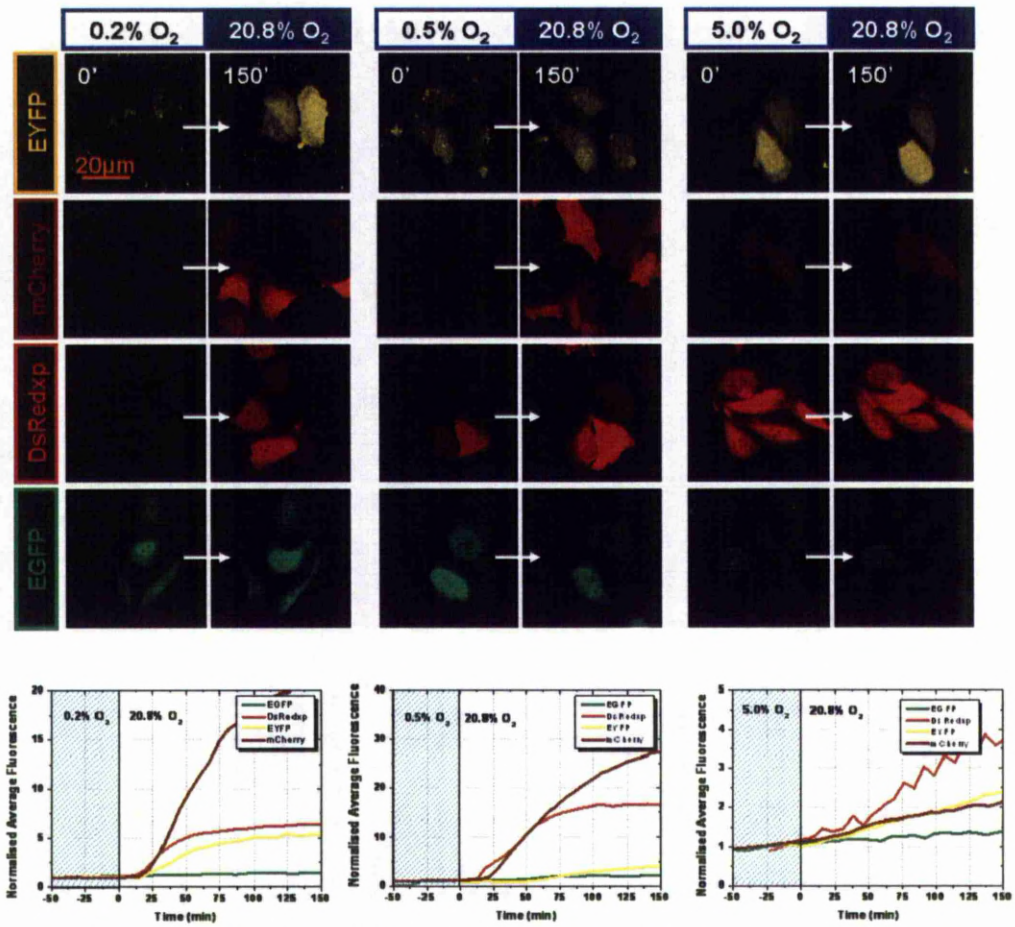

Fig 3.9. Time-lapse imaging of HeLa cells transfected to express an unfused fluorescent protein: EGFP, EYFP, DsRedxp or mCherry. Immediately after addition of transfection reagent, cells were incubated in hypoxia so initial fluorophore expression occurred in an O2-deprived environment. After 24-hours post transfection, cells were imaged through a re-oxygenation step.

Graphs depict mean average cellular fluorescence normalised to t0. (n=>10 cells for each condition)

3.2.3 Molecular tools to investigate HIF signalling

3.2.3.1 Gateway® Cloning Rationale and Principle

A primary aim of this project is to image protein dynamics of the HIF signalling system. As we are employing a confocal microscopy approach, it was necessary to have access to expression plasmids encoding fluorescent fusion proteins of the canonical HIF pathway. Plasmids encoding fluorescent fusions for the intracellular prolyl-hydroxylases were kindly donated by Dr. E. Metzen and Dr. R. Depping. These molecular tools are used and described in Chapter 5. Despite having access to other fluorescent fusion proteins of interest, kindly donated from a variety of sources, these fusion forms were unsuitable for multiplexing and difficult to validate the impact of the fused fluorophore. In order to achieve this ambition, we employed the Invitrogen Gateway® System, as it allows for quick and efficient cloning as well as flexibility in terms of fluorophore orientation (N- or C- terminal) and fluorophore choice for multiplexed imaging (**Fig 3.10**). It was therefore an aim to use this system to produce fluorescent fusion expression vectors encoding HIF-1α, HIF-2α, pVHL as well as FIH. Each protein was to be either fused in an N-terminal, C-terminal or to be separately translated from the fluorescent protein using an internal ribosome entry sequence (IRES) contained within the plasmid. The IRES carrying plasmids are used as a control, as they allow the co-expression of both the protein-of-interest and EGFP from a single promoter, but the independent translation of the products (Pelletier and Sonenberg 1988; Hellen and Sarnow 2001).

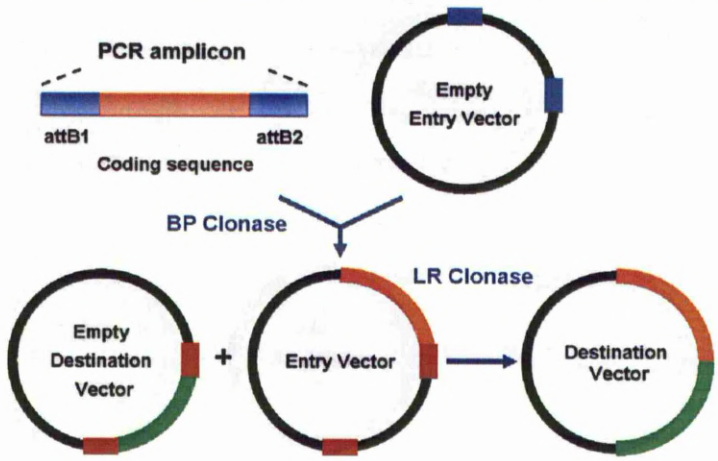

Fig 3.10. Schematic representation of the Gateway® Invitrogen homologous recombination cloning strategy, which was employed to generate plasmids encoding fluorescent tagged proteins. Orange indicates coding sequence of interest and green denotes fluorescent protein coding sequence. The recombination sites are shown as blue and red.

3.2.4 Fluorescent fusion HIF-1α plasmids

3.2.4.1 Cloning of HIF-1α

HIF-1α is the major oxygen labile isoform of the HIF-1 transcription factor (Semenza 2003; Lee, Bae et al. 2004). The previous O_2-dependent fluorophore maturation data indicated (**Fig 3.9.**) that the EGFP was the most suitable fluorescent protein to couple to HIF-1α. EGFP was also the preferred fluorophore of choice due to a well characterized short folding time and higher quantum yield, which may compensate for the HIF-1α short half-life (Chudakov, Matz et al. 2010). To introduce HIF-1α into the gateway vectors the 2481bp HIF-1α coding sequence was PCR amplified from a previously donated (Professor S. Edwards, University of Liverpool) HIF-1α expression plasmid using the Gateway® primers (**appendix 1.1**) and protocols. These amplicons were then used to produce a C-terminally tagged HIF-1α, N-terminally tagged HIF-1α and an IRES containing plasmid. The three plasmids produced are referred to as; pG-HIF1α-EGFP, pG-EGFP-HIF1α and pG-HIF1α-IRES-EGFP (left to right is in the N- to C- orientation in all plasmid names throughout the thesis). In these three plasmids, transcriptional control of the HIF-1α coding sequence is under the viral CMV promoter (**Fig 3.11**). All plasmids were confirmed by restriction digest (data not shown) and the coding sequences for HIF-1α and EGFP were sequenced (detailed maps and information for the plasmids are available in **appendix 1.1**).

3.2.4.2 Transcriptional activity of expressed HIF-1α plasmids

The function of fused proteins may be compromised due to the presence of the additional amino acid sequence, effectuated through alterations to protein folding as well as domain and recognition site exposure (Yewdell, Lacsina et al. 2011). Subsequently, it is necessary to validate the functionality of the fused proteins. Luminometry was used to examine the ability of exogenous HIF to activate the HRE-luciferase reporter plasmid (**Fig 3.11**). HeLa cells were transfected with the pG-TK-HRE-luciferase reporter and either an unfused EGFP control or one of three HIF-1α expressing plasmids. After 24 hours transfection, cells either were exposed to 1% O_2, 0.5mM DMOG or remained unstimulated for 8 hours.

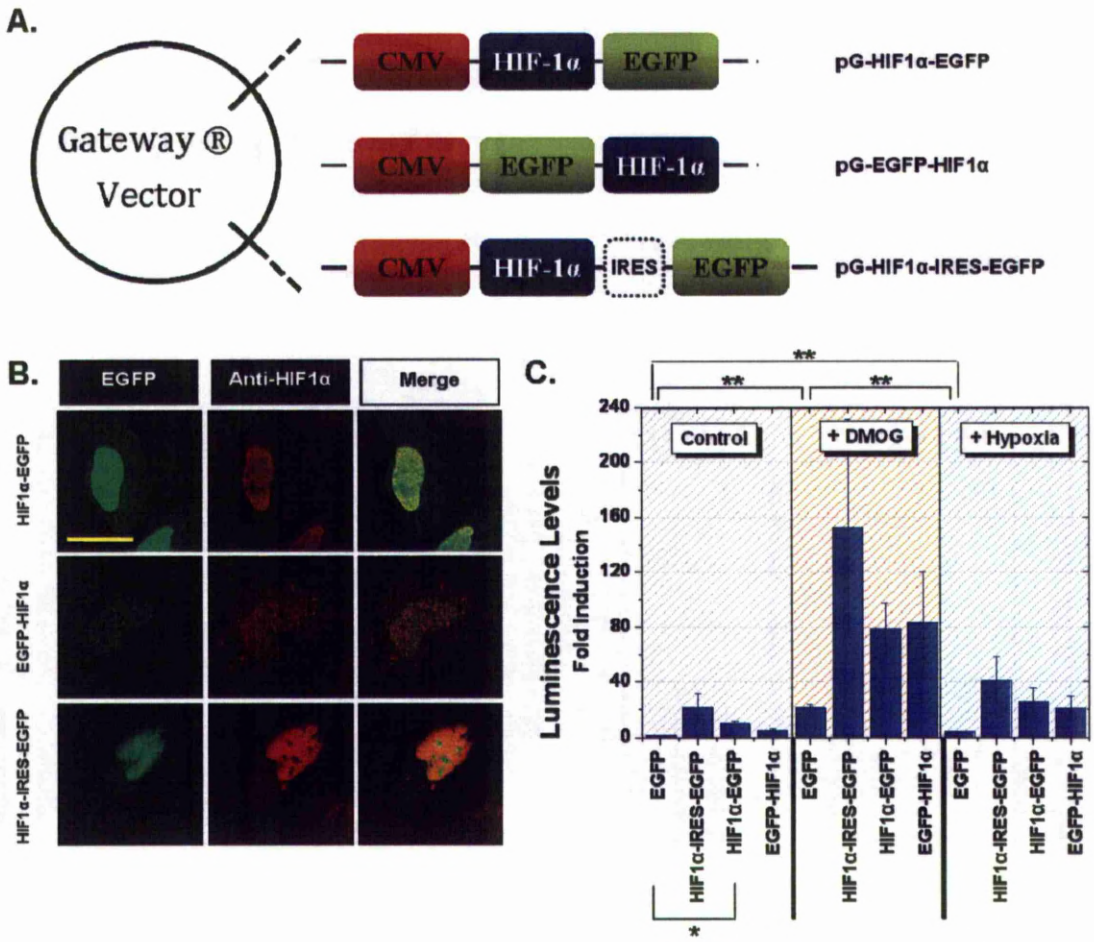

Fig 3.11. (**A**) Diagram of developed fluorescent HIF-1α encoding plasmids. Detailed plasmid maps can be found in the **appendix 1.1**. (**B**) Immunocytochemistry of HeLa cells expressing fluorescent fusion HIF-1α encoding plasmids. Yellow scale bar denotes 20μm. Cells were fixed 24-48 hours after transfection. (**C**) Endpoint luminometry analysis of samples prepared from HeLa cells co-expressing HIF-1α fluorescent plasmid variants alongside the pG-TK-HRE luciferase reporter. Additionally, transfected cells were exposed to either 1% O2 or 0.5mM DMOG for 8-hours. Results are normalised to unfused EGFP normoxic control. Statistical significance assessed using one-way ANOVA; p-values ≤0.05 are shown as * and p-values ≤0.01 are shown as **. (n= 3 repetitions)

Both hypoxia and DMOG stimulation were found to significantly induce the HRE-luciferase signal, though 0.5mM DMOG showed significantly more potency to do so than 1% O_2. Expression of all HIF-1α plasmids elevated the HRE-luciferase signal over the EGFP control. In normoxia induction was found to be 21±11 fold for pG-HIF1α-IRES-EGFP, 10±2 fold for pG-HIF1αEGFP and 5±1 fold for pG-EGFP-HIF1α. The difference between the IRES plasmid and the fused forms was found to be statistically insignificant.

3.2.4.3 Localisation of expressed HIF-1α plasmids

Although luminometry data strongly suggested that the HIF-1α expression plasmids were functional, all expression plasmids were additionally assessed by immunocytochemistry (**Fig 3.11**) to ensure that the construct was fluorescent

and the localisation in accordance with previously reported work. HeLa cells were transfected with each one of the HIF-1α expression plasmids and after 24-48 hours post transfection, were fixed and antibody labelled using anti-HIF1α (methodology detailed in **section 2.6.4**). All expression plasmids produced nuclear localised fluorescence and the EGFP signal and antibody detected signal correlated appropriately. There was some concern that the IRES expression plasmid also led to a perceived nuclear localised fluorescence where as the unfused EGFP would be expected to be ubiquitous. To confirm whether this was an issue with the fixation protocol used all plasmids were transfected and expression imaged in a live-cell context using HeLa cells (**Fig 3.12**). In this instance, pG-HIF1α-IRES-EGFP fluorescence was found to be ubiquitous throughout the cell, in contrast to the fusion forms which were again found to be suitably localised to the cell nucleus (Chilov, Camenisch et al. 1999; Wotzlaw, Otto et al. 2007).

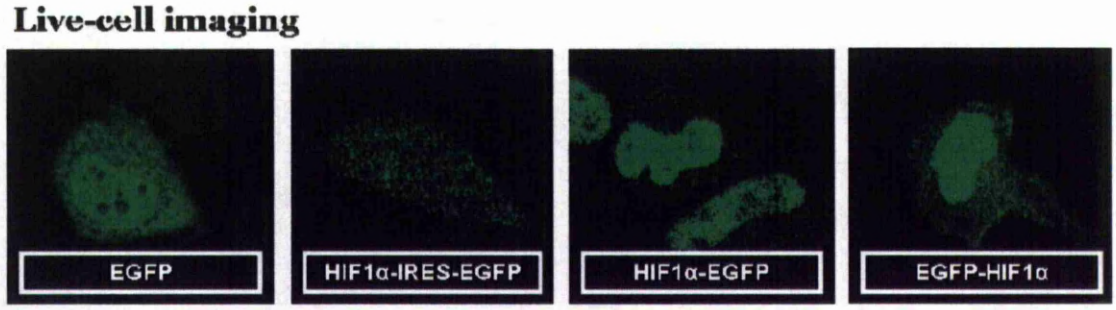

Fig 3.12. Live-cell confocal microscopy of HeLa cells ectopically expressing one of several HIF-1α expression plasmids or an unfused EGFP control plasmid. Images shown are 24 hours post transfection. Image width is representative of 60μms.

3.2.5 Fluorescent fusion HIF-2α plasmids

3.2.5.1 Cloning of HIF-2α

HIF-2α is the second transcriptionally active oxygen labile isoform of the heterodimeric HIF transcription factor, originally characterised by Ema *et al.* in 1997 (Ema, Taya et al. 1997). The potential protein dynamics of HIF-2α, as well as any observable differences compared to HIF-1α are also of interest to the study. HIF-2α was to be cloned and coupled to EGFP for the same reasons outlined for the cloning of HIF-1α. Nevertheless we were interested in potentially imaging cells co-expressing both fluorescent HIF-α isoforms, in which case we would need to couple one isoform to a fluorophore spectrally distinct from EGFP. The most common option is to use a fluorophore of the red-spectrum. As HIF-2α is cited to show greater protein stability and stabilisation at higher O_2-tensions, we thereby decided that HIF-2α would be the most suitable to attach to the red fluorescent protein, specifically DsRed-express. The

2613bp HIF-2α coding sequence was PCR amplified from the hEPAS myc-pcDNA3 expression plasmid (appendix 9.1), again using the Gateway® primers and protocols and these amplicons were then used to produce pDONR entry vectors suitable for generating N-terminal, C-terminal and IRES-containing expression plasmids. The entry vectors were then used to produce three expression plasmids; pG-EGFP-HIF2α, pG-DsRedxp-HIF2α and pG-HIF2α-IRES-EGFP (**Fig 3.13**) (detailed maps and information for the plasmids are available in **appendix 1.1**).

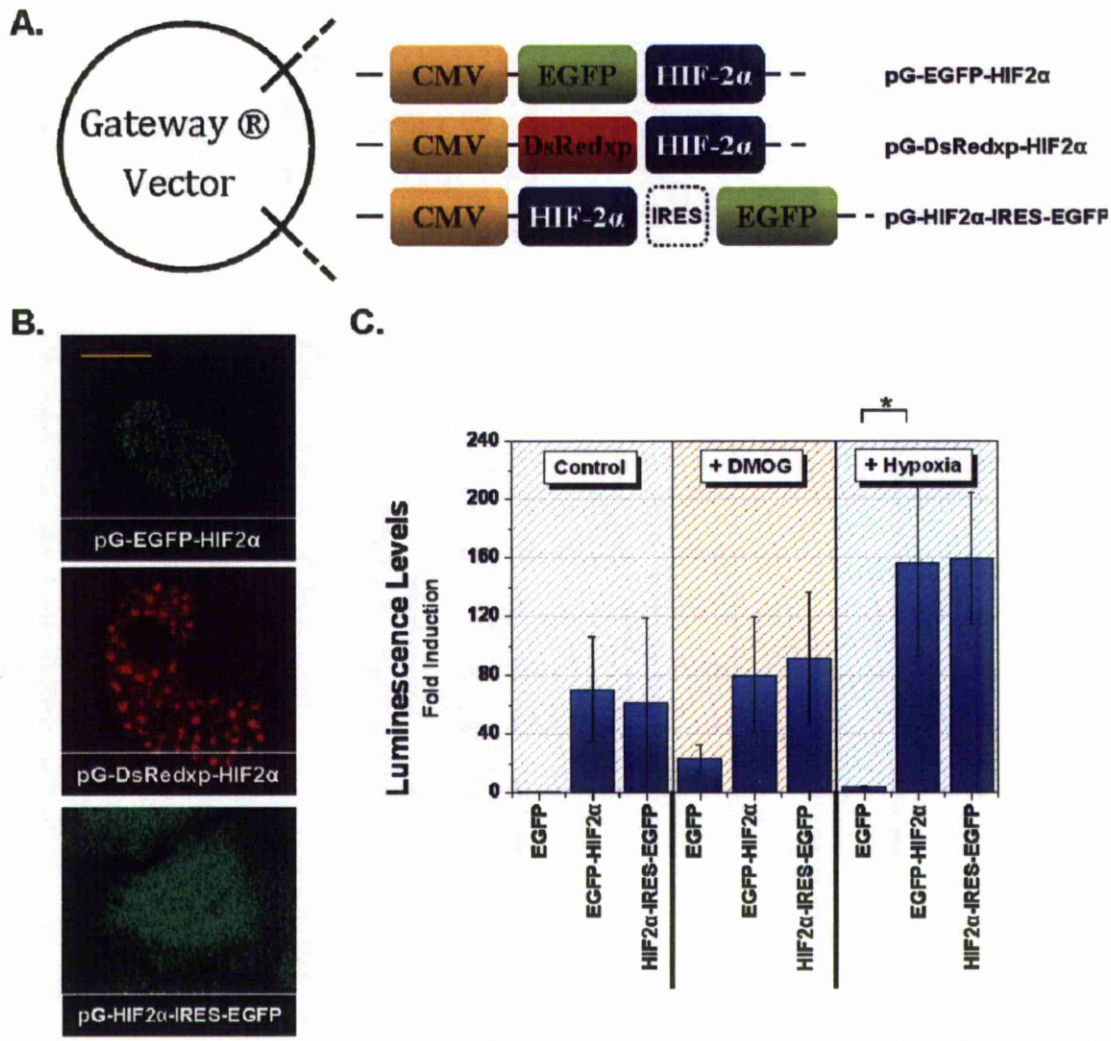

Fig 3.13. (**A**) Pictorial representation of developed fluorescent HIF-2a encoding plasmids. (**B**) Live-cell confocal microscopy of ectopically expressed HIF-2α plasmids in the HeLa cell line. Scale bar denotes 10μms (**C**) Endpoint luminometry analysis of HeLa cells co-tranfected with a HIF-2α fluorescent plasmid variant alongside the pG-TK-HRE luciferase reporter. Additionally, cells were exposed to either 1% O2 or 0.5mM DMOG for 8-hours. Results are normalised to unfused EGFP normoxic control. Statistical significance assessed using one-way ANOVA; p-values ≤0.05 are shown as * and p-values ≤0.01 are shown as **. (n= 3 repetitions)

3.2.5.2 Live-cell confocal imaging of HIF-2α expression vectors

The newly generated HIF-2α expression vectors were initially assessed by transfection into HeLa cells and observation by live-cell confocal microscopy

(**Fig 3.14**). In accordance with expectations evenly distributed green fluorescence was observable in normoxic conditions following transfection with the IRES containing plasmid. Fluorescence signal was also detected in normoxic conditions after transfection with tagged HIF-2α and the expressed protein was found to be nuclear, with few cells showing instances of cytoplasmic only localisation (Hara, Kobayashi et al. 1999; Konietzny, Konig et al. 2009). However, in startling contrast to HIF-1α, high-resolution imaging of fluorescent HIF-2α showed a non-homogenous localisation pattern, a phenotype characterised by the occurrence of punctate regions of high fluorescence intensity (*speckles*). This localisation pattern has been previously (though passively) reported and is the focal point of Chapter 6 (Hara, Kobayashi et al. 1999; Konietzny, Konig et al. 2009).

3.2.5.3 Transcriptional activity of expressed HIF-2α plasmids

Cells were co-transfected with the pGL2-TK-HRE plasmid as well as a HIF-2α or an unfused EGFP expression vector. After 24-hours cells were then treated for 8-hours with 0.5mM DMOG or incubated in 1% O_2. Cells were then lysed and samples prepared for luminometry analysis. In all instances, expression of the HIF-2α plasmid resulted in elevated luminescence compared to the expression from the unfused EGFP control vector. No significant difference was found between the fused and unfused forms of HIF-2α (**Fig 3.13.**) (detailed maps and information for the plasmids are available in **appendix 1.1**).

3.2.6 Fluorescent fusion pVHL plasmids

3.2.6.1 Cloning pVHL

pVHL is a necessary component in the sequence of events that confers oxygen-sensitivity to HIF-α protein stability (Maxwell, Wiesener et al. 1999). Alongside this main role, there are several other regulatory points of interest including the transcription and posttranslational sensitive nuclear-cytoplasmic trafficking of pVHL and the implications of this on HIF-α regulation (Lee, Neumann et al. 1999; Groulx and Lee 2002; Cai and Robertson). We were therefore interested in any identifiable pVHL dynamics, as well as engineering the ability to express the HIF-α alongside pVHL. The latter reasoning would require pVHL to be fused to a fluorescent protein with an emission spectra discernable from EGFP coupled HIF-α. To this end we further employed the gateway cloning system to generate three expression vectors; pG-pVHL-DsRedxp, pG-DsRedxp-pVHL and pG-pVHL-IRES-DsRedxp (**Fig 3.14.**). The pVHL coding sequence was

amplified from the plasmid pRC-CMV-HA-pVHL, a gift kindly donated by MD William G. Kaelin. All plasmids were checked by restriction digest and the coding sequences verified by DNA sequencing.

3.2.6.2 Live-cell confocal imaging of pVHL expression vectors

pVHL expression vectors were characterised by live-cell confocal microscopy using HeLa cells ectopically expressing one of the several pVHL expression plasmids. Transfection of the pVHL-IRES-DsRedxp plasmid resulted in a uniform cellular distribution of fluorescence, where as transfection of tagged pVHL though also apparent in both the cytoplasm and nucleus was visibly more cytoplasmic, albeit marginally (**Fig 3.14.**). The localisation pattern was the same for all observed cells indicating no asynchronous or heterogenous resting state. Importantly the cellular localisation pattern of pVHL agrees with published material, though as the localisation is not particularly distinct it is difficult to conclude whether the expressed protein is functional from this data alone (Lee, Neumann et al. 1999).

3.2.6.3 Assessment of pVHL expression vectors using the HRE-luciferase reporter

In order to further examine the generated pVHL expression vectors, luminometry using the pGL2-TK-HRE-luc reporter was once again employed. HeLa cells were transfected with either a pVHL expression vector or a DsRedxp control plasmid before cultures were exposed to 8 hours of either control conditions, hypoxic incubation (1% O_2) or 0.5mM DMOG treatment. Expression of pVHL led to a reduction in luminescence signal in all measured instances, when cells were stimulated with DMOG (**Fig 3.14**). The reason for this remains unknown. In all instances, the IRES form and fused forms were found to function similarly.

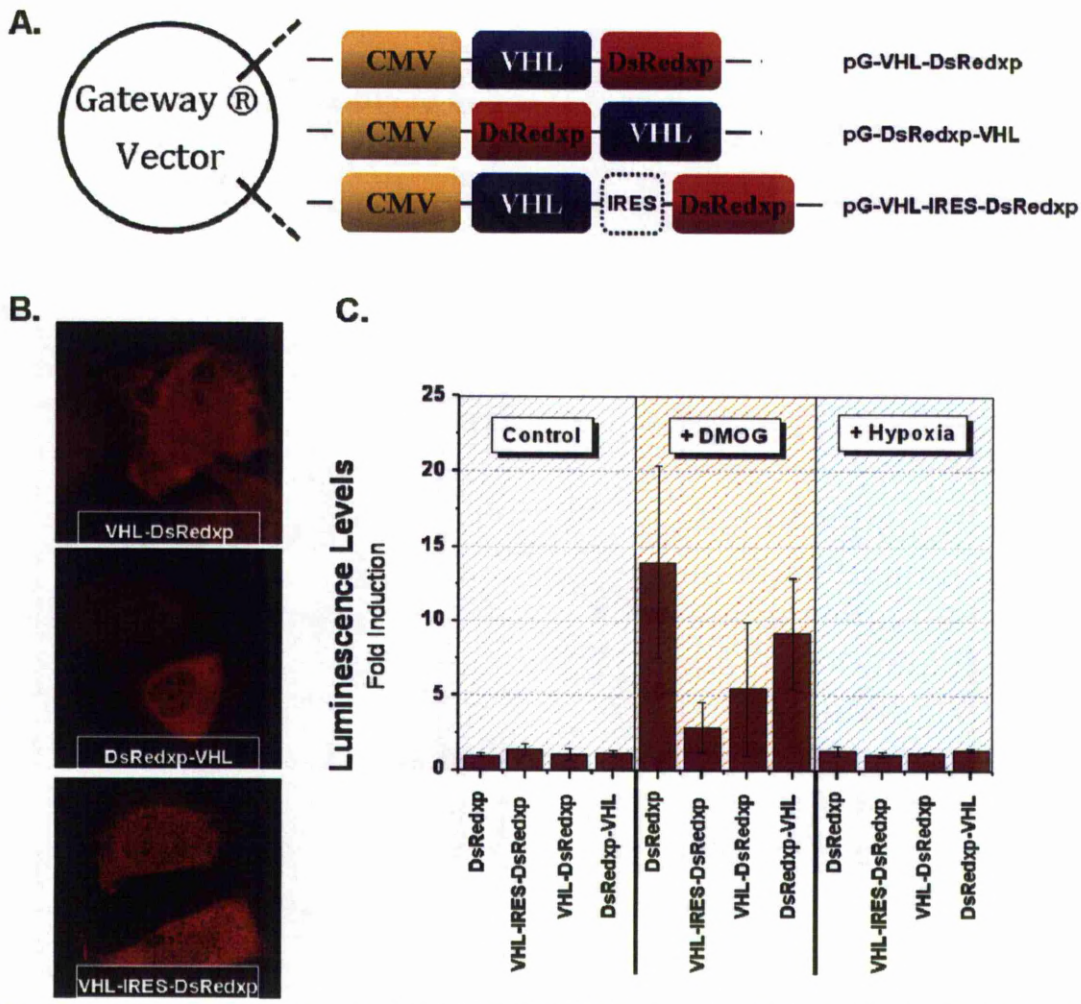

Fig 3.14. (**A**) Pictorial representation of developed fluorescent pVHL expression plasmids. (**B**) Live-cell confocal microscopy of expressed HIF-2α plasmids in the HeLa cell line. Scale bar denotes 10μms (**C**). Endpoint luminometry analysis of HeLa cells co-expressing pVHL fluorescent plasmid variants alongside the pG-TK-HRE luciferase reporter. Additionally, transfected cells were exposed to either 1% O2 or 0.5mM DMOG for 8-hours. Results are normalised to unfused EGFP normoxic control. Statistical significance assessed using one-way ANOVA; p-values ≤0.05 are shown as * and p-values ≤0.01 are shown as **. (n=2 repetitions)

3.2.7 Fluorescent fusion FIH plasmids

3.2.7.1 Cloning FIH

FIH regulates the transcriptional activity of HIF-1α and HIF-2α in an oxygen-dependent manner, an activity that can be speculated to modulate the transcriptional feedback potential of the HIF system (Mahon, Hirota et al. 2001). Investigating whether co-expression of FIH with either HIF-1α /-2α affects HIF-α protein dynamics was therefore of interest. As per pVHL, FIH was cloned into entry vectors after PCR amplification from pEGFP-FIH1 (donated from Dr. E. Metzen) before recombination into a DsRed-xp expression plasmid. Two FIH expression plasmids were produced from this; pG-FIH-IRES-DsRedxp and pG-DsRedxp-FIH (**Fig 3.15.**). Both plasmids were checked by restriction

digest and the coding sequences verified by DNA sequencing (detailed maps and information for the plasmids are available in **appendix 1.1**).

3.2.7.2 Live-cell confocal imaging of FIH expression vectors

HeLa cells were transfected with either FIH expression plasmids for 24 hours and then imaged by live-cell confocal microscopy. Transfection of the IRES vector led to relatively evenly distributed red fluorescence throughout the cell (**Fig 3.15.**). Fluorescence from DsRedxp-FIH was found to be cytoplasmic and thereby similarly localised to previous publications (Metzen, Berchner-Pfannschmidt et al. 2003). However, fluorescence expressed from the fused form was often found to form *'blob-like'* aggregates around the cytoplasm that were unlike the punctate structures seen for HIF-2α (**Fig 3.15**). This may be the result of the fusion of DsRedxp, as this red fluorescent protein is known to exist weakly as a tetramer or is simply a result of protein aggregation following the expression of un-physiologically high levels of protein (Wall, Socolich et al. 2000; Mayer and Buchner 2004).

3.2.7.3 Assessment of FIH expression vectors using the HRE-luciferase reporter

The effect of ectopic FIH expression upon the transcriptional output from the HRE-luciferase was investigated. HeLa cells were transfected with either a FIH expression vector or a DsRedxp control plasmid before cultures were exposed to 8 hours of either control conditions, hypoxic incubation (1% O_2) or 0.5mM DMOG treatment. No significant change to luminescence levels was seen from the ectopic expression of FIH compared to the unfused DsRedxp control vector (**Fig 3.15**). Additionally no significant difference was measured between the fused and unfused forms of FIH.

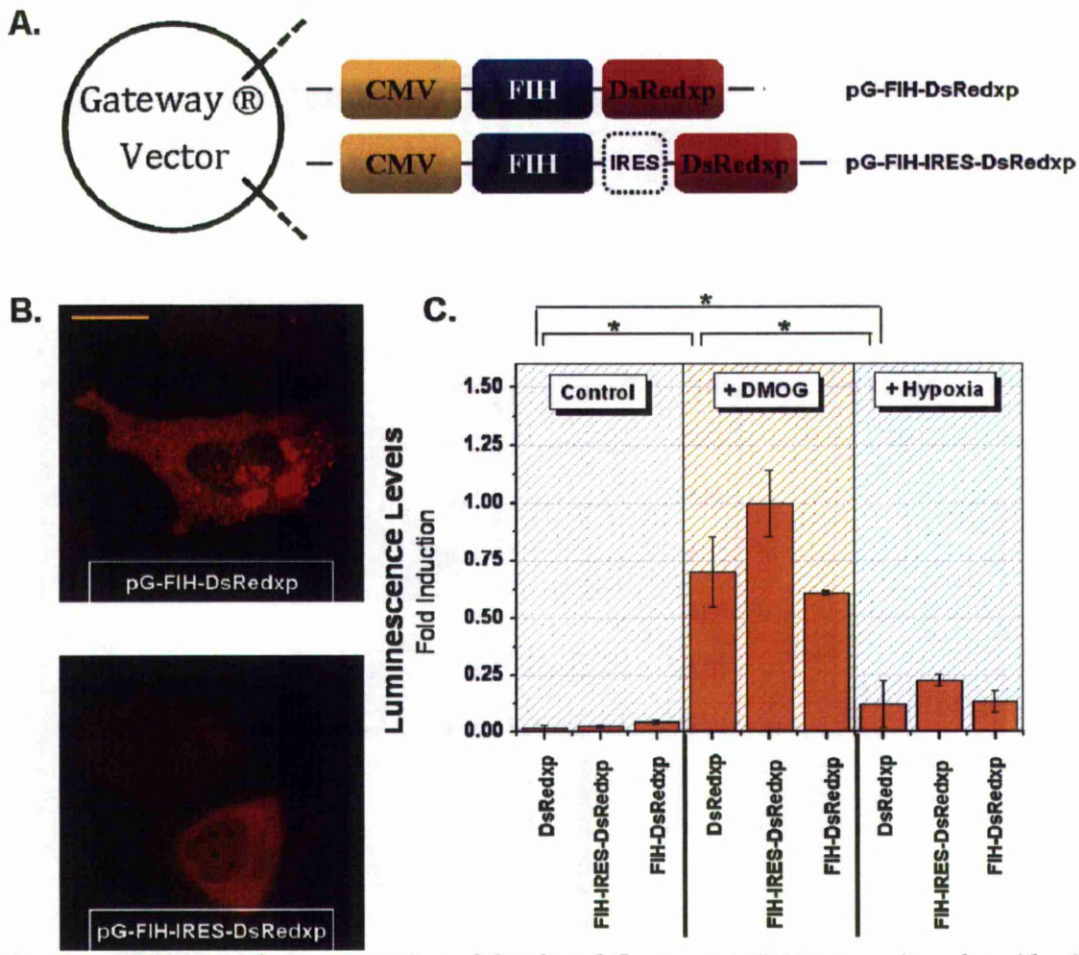

Fig 3.15. (**A**) Pictorial representation of developed fluorescent FIH expression plasmids. (**B**) Live-cell confocal microscopy of ectopically expressed FIH plasmids in the HeLa cell line. Scale bar denotes 10μms (**C**). Endpoint luminometry analysis of samples prepared from HeLa cells co-expressing a FIH fluorescent plasmid variant alongside the pG-TK-HRE luciferase reporter. Additionally, transfected cells were exposed to either 1% O2 or 0.5mM DMOG for 8-hours. Results are normalised to unfused EGFP normoxic control. Statistical significance assessed using one-way ANOVA; p-values ≤0.05 are shown as * and p-values ≤0.01 are shown as **. (n=3 repetitions)

3.3 Discussion

The purpose of this chapter was to determine and optimise a suitable experimental system for the investigation of single-cell dynamics within the HIF pathway. To this end, I believe the aims were met; (i) the HIF-1α response was found intact in our HeLa cell line, confirmed by western blot analysis and luminometry (ii) hypoxia and DMOG were shown to not significantly affect cell fate within a 24-hour time period (iii) the use of fluorescent proteins in a hypoxic environment was addressed and EGFP concluded as the most suitable (iv) and finally the gateway system was utilised to rapidly develop a range of molecular tools for use in later confocal microscopy experiments.

3.3.1 Suitability of the HeLa cell line for investigation into HIF-α dynamics

A common cause for concern within the field of cell biology is whether the often-immortalised research grade cell line is truly representative. This concern is furthered with regards to the response to hypoxia, as many laboratory available cell lines have existed in near atmospheric O_2 conditions for decades. This propelled the current study to examine the HIF-α response using both western blot analysis and an endpoint luminometry assay. We concluded that the HeLa cell line was indeed suitable (despite almost 6-decades of atmospheric O_2), as an intact transient HIF-1α response was observed comparable with other published examples, including in vivo assays (**Fig 3. 4**) (Gey GO 1952; Wang, Jiang et al. 1995; Stiehl, Wirthner et al. 2006). Though hypoxic accumulation of HIF-1α protein was visible, we failed to detect a robust and convincing accumulation of HIF-2α protein, despite HIF-2α being detectable in HeLa cells (**Fig 3. 4**). A measured increase in HIF-2α was considered not to be a critical criterion in cell line selection; partly due to the 'secondary role' HIF-2α is cited to play in the cellular hypoxic response. Principally, the aim is to investigate and mathematically model the HIF-1α response, though it could be expected that HIF-2α may interject with and affect the PHD feedback loop (Aprelikova, Chandramouli et al. 2004). It is therefore of interest to hypothesise an explanation for the lack of hypoxic HIF-2α accumulation (or loss up on re-oxygenation). There are several plausible possibilities that may explain the lack of measured HIF-2α induction. Firstly, HIF-2α accumulation has been cited to occur more slowly than HIF-1α in HeLa cells meaning that we may not observe as distinct stabilisation of protein within the 24-hour experiment time period used (Bracken, Fedele et al. 2006). The response may also be transient and asynchronous, making bulk-cell measurements of induction difficult (Nelson, Ihekwaba et al. 2004; Burrill and Silver 2011).

3.3.2 Imaging technologies in hypoxia

A mainstay of this project is the ability to measure events at the single-cell level in living cells. The main technological approaches employed towards this goal are wide-field luminescence and confocal microscopy, technologies based on bioluminescence and fluorescence respectively. A potential caveat with this approach is that bioluminescence and fluorescent proteins both require molecular oxygen in order to produce signal.

3.3.3 Use of bioluminescence

Bioluminescence catalysed by luciferase is dependent on molecular oxygen. Additionally, the luminescence signal produced is also dependent on available molecular oxygen but also available cellular pool of ATP, which can be depleted or altered by hypoxia (Hara 2009). With regards to bioluminescence, endpoint luminometry assays do not suffer from O_2-dependency as the reaction can be performed post lysis and thereby in an oxygen rich environment. However, bioluminescence is often applied to live-cell imaging in hypoxia, including the *in vivo* imaging of tumour growth (Jost, Collins et al. 2009; Hawes and Reilly 2010). In this context, we attempted to validate the use of luminescence for live-cell measurements in hypoxia finding levels as low as 1% O_2 suitable. An extensive study into this issue was undertaken by Moriyama *et al.* 2008 in which they found a 32% loss of luminescence signal comparing atmospheric oxygen to 1% O_2. The loss of luminescence was chiefly attributed to decreased cellular ATP. This finding may suggest the hypoxic sensitivity of bioluminescence to be cell-type dependent, arising from the cellular energy status. In this context, the high mitochondrial mass of HeLa cells may explain the relative insensitivity of bioluminescence to hypoxia observed in our own measurements (Ryan, Taylor et al. 2005). Nevertheless, the effect of hypoxia on cellular ATP remains an interesting prospect that can have diverse repercussions of the physiology of the cell (Matveev, Vinokurov et al. 1996; Tsujimoto 1997; DiGregorio, Ubersax et al. 2001). Creative methodologies have been recently developed allowing for the cellular and subcellular measurement of ATP levels over time, enabling the live-cell measurement of ATP levels following hypoxia (Imamura, Nhat et al. 2009). Using such methodology it would be possible to further address the use of bioluminescence in hypoxic cells and tissues as well as gaining a broader understanding of the contribution altered cellular ATP to the hypoxic response.

3.3.4 Use of fluorescent proteins

The other imaging technology employed, namely protein fluorescence, is also dependent on the availability of molecular oxygen. Furthermore the technology is widely relevant to many avenues of hypoxic research (including our own) as well as the in vivo imaging of tumour growth, tumour oxygenation and angiogenesis (Hoffman 2002; Hoffman 2004; Kuchimaru, Kadonosono et al.). The chemistry of fluorescent protein maturation has been the topic of several

papers, in which the different fluorescent proteins have different maturation processes; GFP variants require a single oxidation event in order to fluoresce whereas RFP variants require two events (Gross, Baird et al. 2000; Zimmer 2002). Interestingly, single oxidised RFP proteins are thought to fluoresce with a green emission and it is the second oxidation which is responsible for the characteristic red fluorescence (Gross, Baird et al. 2000). However, it has also been suggested that the maturation of DsRed is a branched process in which the fluorophore can mature to a green form, or red form. The maturation to a red fluorescent form is oxygen-dependent and so periods of sufficient hypoxia would shift DsRedxp fluorescence from red to green (Strack, Strongin et al. 2010). These mechanisms may have implications for multiplexing GFP and DsRed variant proteins in hypoxic conditions.

However, to address the most pressing point, GFP variants are suitable for hypoxic imaging in tensions as low as 0.5% O_2. This is in accordance with a paper published by Vordermark *et al.* 2001 which found EGFP fluorescence to be sensitive to near anoxic conditions of ~0.02% O_2. This reinforces the use of GFP for hypoxic imaging, whether for research purposes, *in vivo* or *ex vivo* and/or clinical applications (Hoffman 2005). For example, *in vivo* assessment of tumour oxygenation is considered important due to the correlation with prognosis and even potential hypoxia-sensitive drug delivery (Avni, Cohen et al. 2011) (Thorwarth and Alber 2010) (Shinae Kizaka-Kondoh 2009). There are a number of methodologies in place to measure tumour oxygenation as common non-invasive techniques include the use of magnetic resonance imaging (MRI), positron emission tomography (PET) and single-photon emission computed tomography (SPECT) (Sun, Niu et al. 2010). Though measurements are also made on other features of the tumour, and a number of these markers utilise fluorescent protein technologies (Yu, Timiryasova et al. 2003; Ma, Taruttis et al. 2009; Serebrovskaya, Edelweiss et al. 2009).

Chapter 4: Single-cell imaging and initial mathematical modelling of O_2-stimulated HIF-α dynamics

4.1 Introduction

Many intracellular processes exist in a state of dynamic flux which often results in a perceived resting steady-state. This is suspected to be true for the HIF system, in which HIF molecules are continuously produced and degraded while at the same time also continuously shuttled between the nucleus and cytoplasm (Irisarri, Lavista-Llanos et al. 2009; Purvis, Radhakrishnan et al. 2009). Perturbations to the resting steady-state have the potential to cause a temporary transitional period as the system re-establishes a new steady-state, as has been addressed in the NRF2 response to oxidative stress (Zhang, Pi et al. 2010). This is the hypothesised process that governs the transient accumulation of HIF-α in response to a hypoxic-insult or any other HIF-α acting stimulus. Moreover it is hypothesised that the kinetics of the transitional state are meaningful and are able to encode differing contexts (Ni, Bruce et al. 2009). To properly address this issue it is necessary to characterise the kinetics of the HIF-α response. To this end, inhibition of the PHDs will be used to stimulate HIF-α accumulation and the ensuing accumulation will be visualised using time-lapse confocal microscopy of cells expressing fluorescent-tagged HIF-α. Currently, only a few attempts have been made at the live-cell imaging of the HIF hypoxic response; several of these have been live-cell measurements of HIF protein interactions, others include the *in vivo* imaging of tumours and reperfusion injury using HIF-orientated reporters (Serganova, Doubrovin et al. 2004; Liu, Qu et al. 2005; Wotzlaw, Otto et al. 2007; Choi, Chan et al. 2008; Konietzny, Konig et al. 2009). This leaves the single-cell level response over the course of hypoxia unexplored. The absence of these measurements is given more importance by the purported role of localisation dynamics in the HIF response as well as providing highly quantified data suitable for the movement towards mathematical modelling of pathways (Groulx and Lee 2002; Nakayama, Qi et al. 2009; Cai and Robertson 2010; Hughey, Lee et al.). The mathematical modelling of the HIF signalling network has been of interest to several studies, initially in 2004 by Kohn *et al.* These mathematical tools complement our core biochemical understanding of the signalling proteins, allowing for the appreciation of the network behaviour in a range of contexts. This has important implications for the HIF-signalling systems given the range of pathological and physiological situations where HIF is activated (briefly summarised in section 1.3) (Eungdamrong and Iyengar

2004; Krohn, Link et al. 2008; Toffoli and Michiels 2008; Taylor and McElwain 2010).

4.2 Results

4.2.1 Validation of methodology for the single-cell imaging of HIF-α

4.2.1.1 Is HIF-α mRNA production regulated by hypoxia?

Several reports have suggested that not only is HIF-α abundance regulated at the protein level but also at the level of transcript, reporting both positive and negative regulation (Uchida, Rossignol et al. 2004; Mojsilovic-Petrovic, Callaghan et al. 2007; Bruning, Cerone et al. 2011). This would have important ramifications in our understanding of the signalling arrangement as well as future experimental design concerning the use of expression plasmids (if regulation was at the HIF-1 promoter level). We investigated the hypoxic sensitivity of HIF-1α and HIF-2α transcript using quantitative real-time PCR. HeLa cells were plated at a density of 350k/6cm dish in 5ml media then cultured over 24-hours at either 1% O_2 or atmospheric conditions. Samples were lysed and prepared for time points; 0h, 0.5h, 1h, 2h, 4h, 8h and 24h. No significant changes were measured for both HIF-α isoforms, indicating no discernible population-wide regulation of either promoter within 24-hours (**Fig 4.1**). This data suggests therefore that use of the CMV driven HIF-α expression vectors should be suitable with regards to hypoxic promoter regulation and also refutes attention to transcript level regulation within the first 24 hours of hypoxia in our cell line.

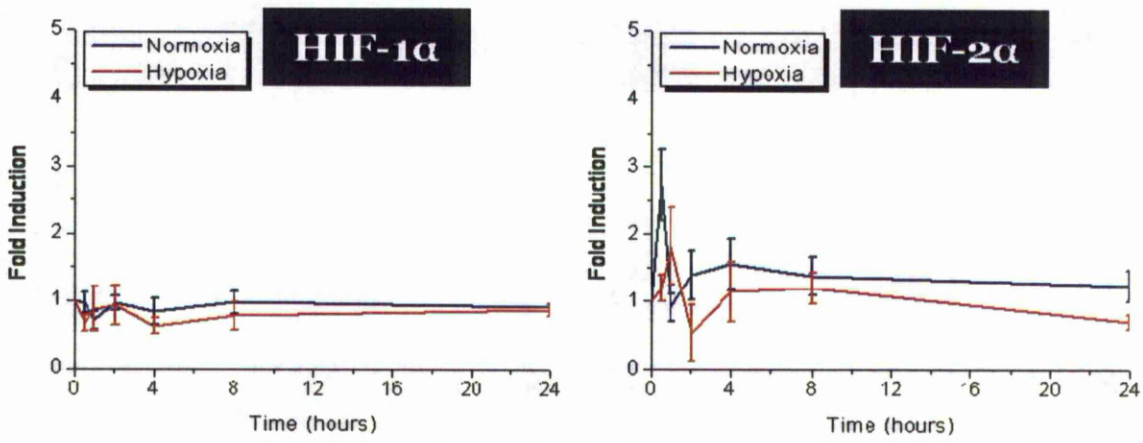

Fig 4.1. RT-qPCR measurement of samples prepared from HeLa cells that were incubated for a time course of 24-hours at either 1% O_2 or atmospheric O_2. (n=3 repetitions hypoxia and n=1 repetition normoxia)

4.2.1.2 Consequence of HIF-1αEGFP expression on hypoxic accumulation of endogenous HIF-α

A common concern when employing the CMV promoter is the relatively high expression level, especially as ectopic expression is often additional to the endogenous expression of a protein-of-interest (Mayer and Buchner 2004) (Qin, Zhang et al. 2010). To address this concern in our own experimental system, the population-wide accumulation of HIF-1α in HeLa cells expressing pG-HIF1α-EGFP was investigated in order to determine whether the normal response was intact (and whether the endogenous response was comparable to the exogenous response). HeLa cells plated into 6cm dishes were transfected with pG-HIF-1αEGFP prior to their incubation at 1% O_2 for up to 24-hours. Samples were then lysed and analysed by western blot, probing with a HIF-1α antibody. The HIF-1α antibody detected both the 120kDa endogenous protein and the heavier fluorescent tagged HIF-1α found at about ~147kDa (**Fig 4.2**). The accumulation pattern for both tagged and untagged was found to be similar to one another. Furthermore, the accumulation pattern was similar to that observed for non-transfected (assessed earlier in **Fig 3.4.**) and to previous reported accumulation profiles (Stiehl, Wirthner et al. 2006). However, there was a slightly elevated signal observed when comparing HIF-1αEGFP to untagged HIF-1α in the normoxic sample and re-oxygenated sample. Endogenous and exogenous HIF-2α protein was detected at 90kDa and 117kDa respectively and was already apparent in the normoxic sample. The response profile for both species of HIF-2α was indistinct, similar to the untransfected response seen previously in **Fig 3.4.** This result suggest the lack of endogenous HIF-2α induction is not specific to either the promoter activity or mutations within the HIF-2α sequence, as the exogenous HIF-2α also showed no increase, in accordance with observations by Bracken *et al.* (2006) in HeLa cells.

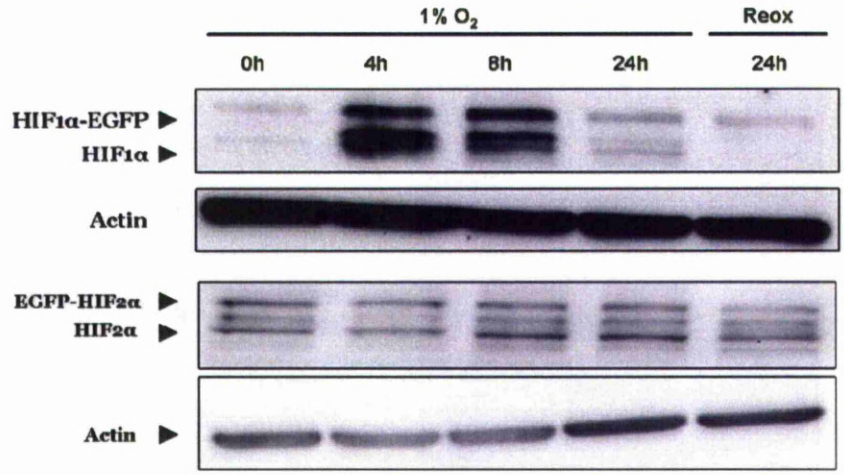

Fig 4.2. Western blot analysis of HIF-α protein accompanied with a corresponding actin loading control. Samples were prepared from HeLa cells transfected with either HIF-1αEGFP or EGFPHIF-2α and incubated in 1% O_2 over 24 hours with an additional sample being re-oxygenated (labelled as Reox) for an additional 15-minute period.

4.2.2 Single-cell imaging of HIF-1α stimulated using 1% O_2

The real-time single-cell accumulation of HIF-1α protein in response to hypoxia has never been directly imaged (Liu, Qu et al. 2005; Krohn, Link et al. 2008). The presence of a delayed-negative feedback regulating this accumulation has prompted this study to investigate and characterise any potential dynamic events within this signalling network. To this end, HeLa cells were plated into 35cm imaging dishes and transiently transfected with pG-HIF-1αEGFP. Cells were also co-transfected with a DsRedxp expressing vector which aids in the detection of transfected cells in the normoxic condition when HIF-1α is extensively degraded and thereby difficult to detect. After 24-48 hours transfection, locations expressing red fluorescence were selected and then imaged every 5 minutes over the course of 20 hours. Cells were either imaged as a normoxic control (~21% O_2) or hypoxic perturbation (1% O_2). For the hypoxic condition, cells are initially imaged for an hour in atmospheric O_2 conditions and then switched to 1% O_2 for the remanding 15 to 25 hours (**Fig 4.3**).

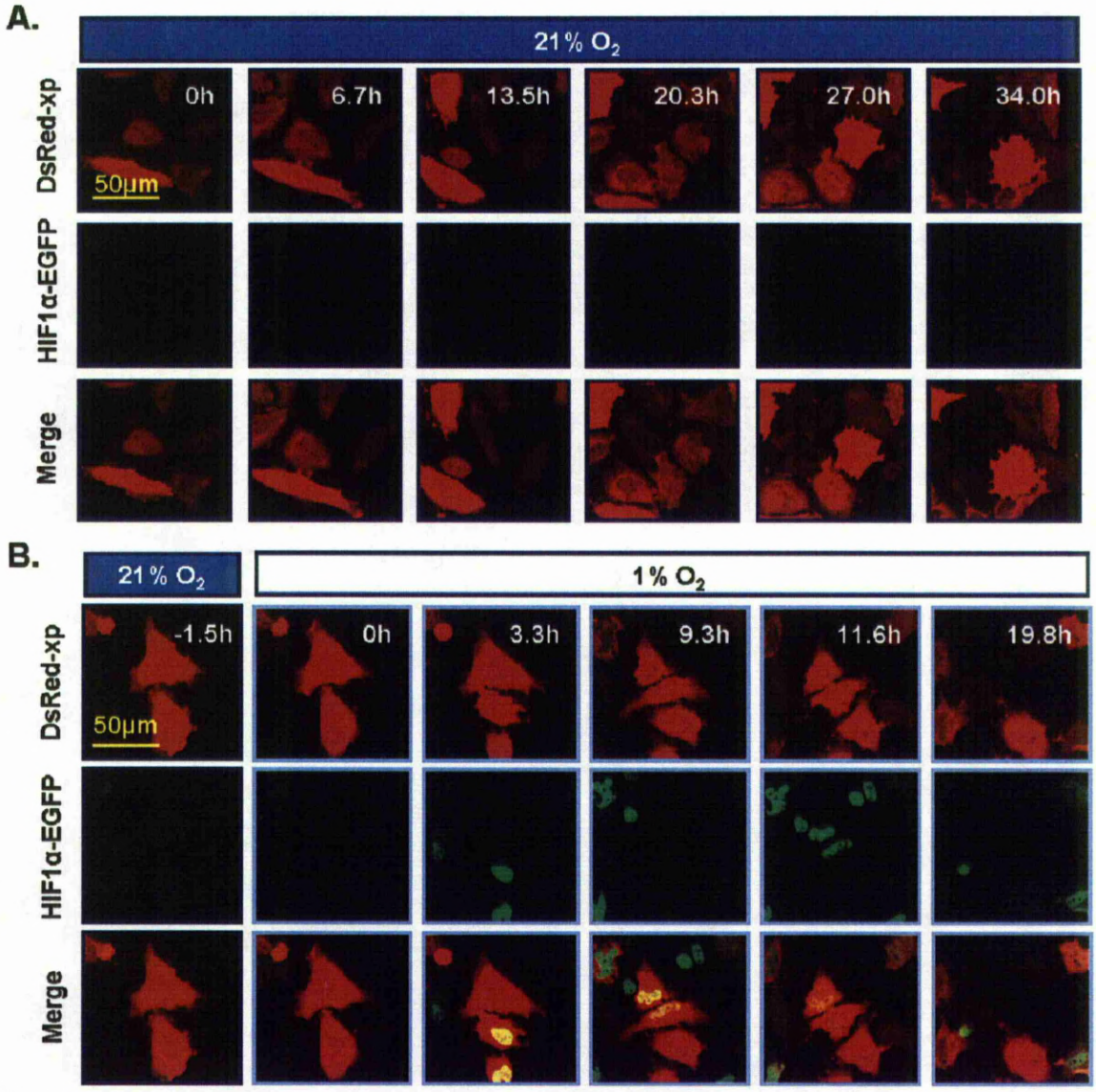

Fig 4.3. HeLa cells were co-transfected with pG-HIF-1αEGFP and pG-DsRed-xp. After 24 hours of transfection, cells were imaged by time-lapse confocal microscopy in either (**A**) atmospheric O_2 or (**B**) 1% O_2. Images are of a single location over time, chosen from a selection of 15 locations per experiment repetition, from a total of three t repetitions.

4.2.2.1 Number of responding cells and method of calculation

We have assessed the cell responsiveness by eye. A consideration for this calculation is the loss of observable cells during the experiment, which can occur from cell death and cell migration (as the imaged location is fixed in position). Therefore strict criteria addressing cell loss needs to be in place. Here we decided that any cell dying or migrating out of the field of view within 200 minutes of the first image were not counted. Ideally a more robust measurement method would be employed, one that is less open to experimenter bias. The robust measurement of responding cells would require use of strict quantitative criteria, such as a threshold equation to address whether a change in fluorescence intensity is meaningful or within experimental noise as well as

improving the repeatability of the measurement method. However, this practice would require all visual information to be processed into a quantitative format. This is a very time-intensive step due to the manual to semi-automated functioning of the cell tracking software used and is therefore a difficult task to approach in an entirely systematic manner. And so we elected to use the less reliable but time wise by eye method, recording the categorisations for each experiment and dish-location so that the findings are open to dispute.

Prior to time-lapse imaging, it was evident that there was a greater ratio of detectable red fluorescence expressing cells compared to green, possibly indicating that exogenous expression of HIF-1α was not sufficient to saturate the degradation pathway for the majority of observed cells. Upon hypoxic exposure, 42% of red expressing cells (n=66 of 159 cells) showed an increase in green fluorescence over the experiment time period compared to 19% observed in the control condition (n=20 of 105 cells) (**Fig 4.4**). Only cells visibly transfected in the first images were considered for this calculation and only single daughters from dividing cells were counted to the total. This was considered justifiable as an increase in fluorescence in one daughter correlated with an increase for the other in 97% of instances (n= 37 of 38 daughter pairs).

Suitable cells that showed changes in green fluorescence and did not die or migrate out-of-view within 200 minutes were analysed by Cell Tracker, converting visual data into a quantitative format (cell tracking analysis described in methods). Many references describing the HIF-1α response to hypoxia suggest that HIF-1α dimerises with HIF-1β in the cytoplasm and then translocates to the nucleus (Chilov, Camenisch et al. 1999; Kaur, Khwaja et al. 2005). By eye examination of the images indicated that the accumulated HIF-1αEGFP was predominantly nuclear in almost all cases (**Fig 4.4**). The nuclear translocation of HIF following stabilisation was initially and convincingly demonstrated by Kallio *et al.* 1998 and since then been repeated in various reviews of the pathway (Kallio, Okamoto et al. 1998; Webb, Coleman et al. 2009). Quantitative examination of cytoplasmic fluorescence versus nuclear fluorescence in our data disagrees with the dogma that a translocation of HIF-1 occurs upon hypoxic stimulation as no loss of cytoplasmic fluorescence was observed. In contrast cytoplasmic fluorescence could be seen to increase in several cases, only ever alongside nuclear fluorescence (**Fig 4.4**).

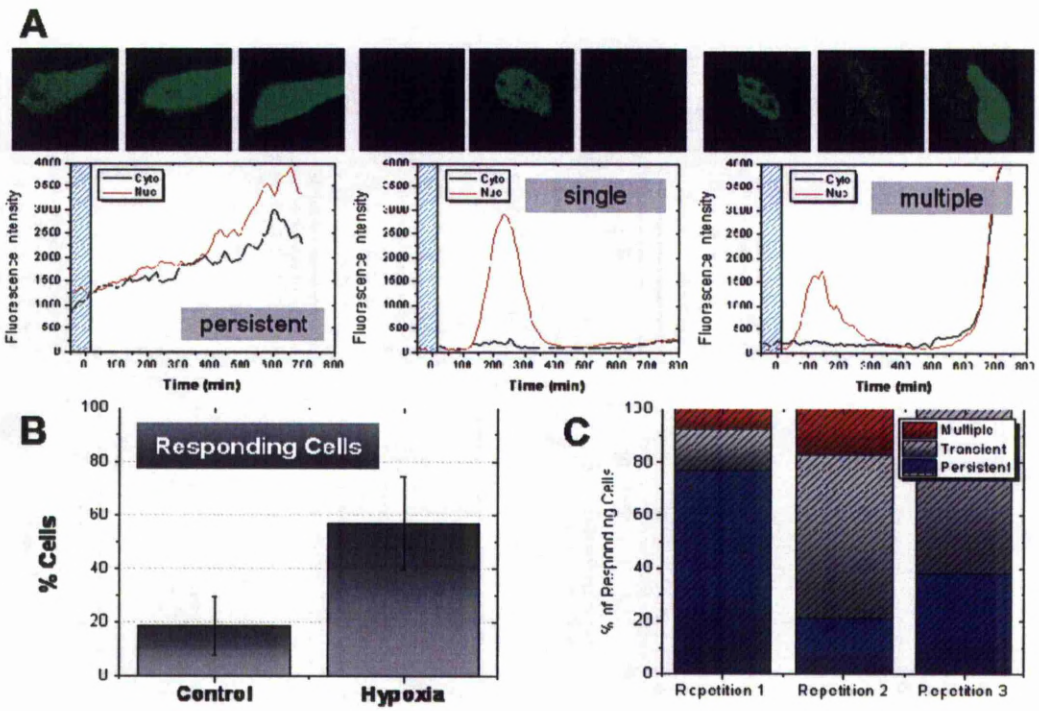

Fig 4.4. (**A**) Live-cell confocal images and corresponding fluorescence intensity traces of cytoplasmic and nuclear HIF1αEGFP from HeLa cells exposed to 1% O_2. The three cells shown depict the representative classifications of response kinetics. (**B**) % of red-fluorescent cells that show a visible change in HIF-1αEGFP intensity over the course of the experiment. Measurement of responding cells as determined by visual counting. (**C**) Classification of HIF-1αEGFP response kinetics observed and percentage cells calculated to belong to each classification. Repetition 1, 2 and 3 are experimental repetitions, each reflecting a number of cells from imaging 15 locations.. (All nuclear cell traces are shown in the **appendix 1.2**)

A recent review by Majmundar *et al.* of HIF regulatory mechanisms omits entirely translocation as a regulatory event (Majmundar, Wong et al. 2010). Here, there were observed instances of spontaneous nuclear-to-cytoplasmic translocations (for less than 10 cells). This phenomenon is later explained in chapter 7 as a result of rupturing nuclear herniations, a feature unrelated to the HIF system. An additional observation was the common occurrence of a rapid increase in green fluorescence preceding cell death (**Fig 4.5**). This occurred in both the normoxic and hypoxic conditions. Using a similar counting criteria as previously outlined, it was found that up to 40% of HIF-1α expressing cells died (no significant difference was found between normoxic and hypoxic conditions) (**Fig 4.5**). The cause-and-effect relationship of this event in our data remains unexplored, but it does perhaps support the various papers implicating HIF in cell death (Volm and Koomagi 2000; Piret, Mottet et al. 2002).

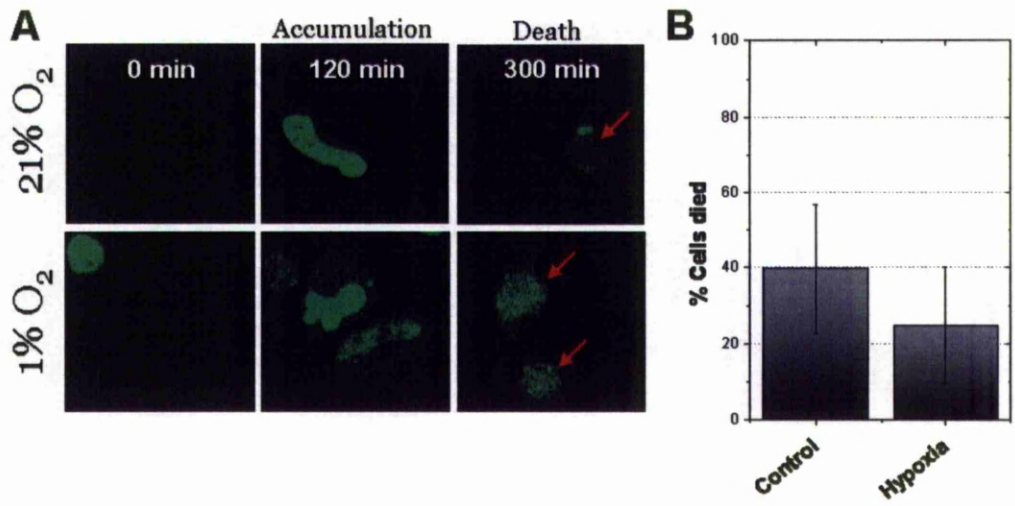

Fig 4.5. Images are taken from live-cell confocal microscopy of HeLa cells expressing HIF1αEGFP and then imaged in either 1% O_2 or 21% O_2. Chosen images highlight the nuclear accumulation of HIF1αEGFP prior to cell death. Percentage of dying cells is calculated and shown as an average from all three repetitions.

4.2.2.2 Analysis of single-cell response

Quantitative analysis of HIF-α fluorescence showed a very heterogeneous response. This heterogeneity was observed with regards to the accumulation pattern, timing, and. The range of accumulation patterns was visually counted and broadly categorised into (1) persistent accumulation (2) single-transient event and (3) multiple accumulations (**Fig 4.4**). A persistent increase in fluorescence was characterised as a slow ongoing increase and occurred in 45.5% (n=30 of 66 cells) of responding cells; single-transient events were characterised by a increase and subsequent decrease in HIF-α fluorescence intensity, this often presented as a distinctive peak, observed in 44.0% (n=29 of 66 cells) of responding cells; additionally multiple-peak accumulations were also present in the data-set with this response making up a small fraction of 10.6% (n=7 of 66 cells) (see **appendix 1.2** for all traces of nuclear fluorescence). Cell-to-cell variance has been suggested to be an important aspect of the tissue level response and so we pursued addressing this issue in our own data (Sigal, Milo et al. 2006; Cohen, Kalisky et al. 2009; Paszek, Ryan et al.). Such studies are only made possible using single-cell level technology; however, this also limits the range of corroborative evidence and so some degree of caution must be applied to the inferences made (potential sources of artefact are discussed later).

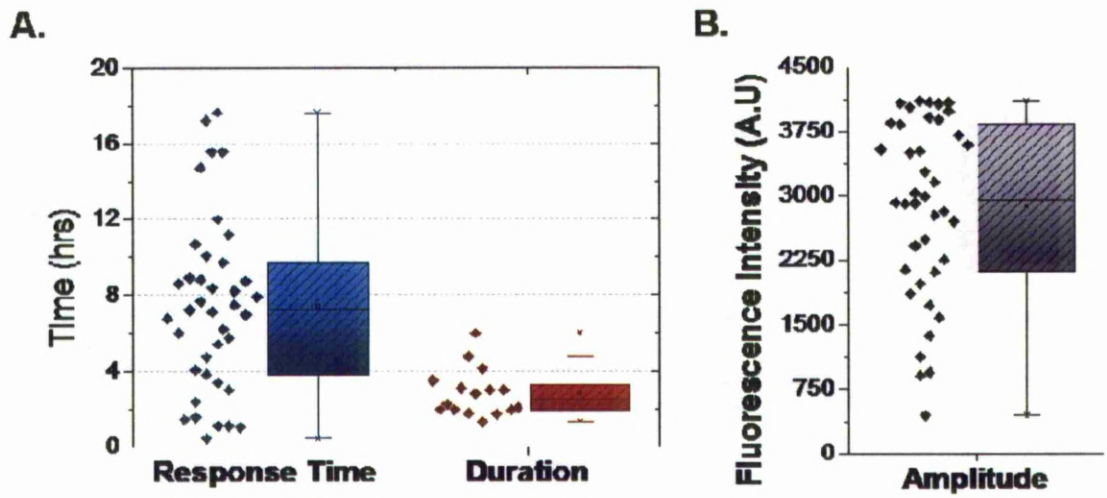

Fig 4.6. Analysis of HIF-1αEGFP fluorescence from ectopically expressing HeLa cells stimulated with hypoxia. (**A**) Time to 1st response and duration of single-transient response. (**B**) Maximum amplitude of all cells Time-to-1st-response was calculated as the point in which fluorescence values reach half maximum. The duration was calculated as the time between the point at passing half maximum fluorescence and returning below this value.

Quantified data was then handled to address heterogeneity within features of the response, namely the time-to-1st-response, duration-of-1st-response and the maximum amplitude of response (**Fig 4.6**) amplitude (plots of all quantified nuclear fluorescence are available in appendix). To assign these values a thresholding system was applied to the data. A cell's time-to-1st-response was determined at the time-point when fluorescence intensity crosses it's;

Minimum fluorescence + (Maximum Fluorescence - Minimum Fluorescence)/2

Rationale for threshold (**i**) Calculating a threshold for each individual cell was found to be the most ideal method due to the high population variance in values. (**ii**) minimum fluorescence was used to determine the resting steady-state of the system, used instead of prestimulus fluorescence due to the occurrence of un-stimulated dynamics

The duration was also calculated using this, corresponding to the difference in the time-point above the threshold to the drop below the threshold. The time-to-1st-response was shown to vary considerably, spanning from ~1-hour up to ~20-hours. This was in contrast to the duration of the transient response, which was found to be more robust ranging from ~2-hours to ~6-hours, with an average timing of ~3-hours (**Fig 4.6**). Again, in contrast the maximum amplitude of response was also found to be highly variable with values measuring across the entire dynamic range of the microscope detector. The relative heterogeneity between duration and timing was confirmed using the

fano factor (variance over the mean) measurement of dispersion around the mean (Masuda and Doiron 2007; Paszek, Ryan et al.).

4.2.3 Single-cell imaging of HIF-2α stimulated using 1% O_2

Although no clear hypoxic accumulation (or re-oxygenation loss) of HIF-2α protein was detected in the bulk cell population, we aimed to examine whether a response was visible at the single-cell level, testing the hypothesis whether single-cell variability masks any population measurement. HeLa cells appropriately plated and incubated were transfected with pG-EGFP-HIF2α, as well as an unfused DsRedxp transfection control vector. After 24-48 hours of transfection cells were imaged in the same manner as HIF-1α (**Fig 4.7**). There were many more instances of visible/stabilised HIF-2α prior to hypoxic incubation as there were for HIF-1α. To counteract cell selection bias, cells for imaging were selected by red fluorescence only. As with HIF-1α, the majority of fluorescence was localised to the nucleus and there was no distinct change in localisation upon hypoxic stimulation. Remarkably accumulations of HIF-2α protein were visible and occurred primarily in the nucleus. All quantified measurements of HIF-2α used the nuclear fluorescence as a readout to compare to the imaging data from HIF-1α. Although one confounding variable for these measurements was the repeat presence of spontaneous nuclear to cytoplasmic translocations as well as the speckle-like localisation patterns, to be discussed in chapters 7 and 6 respectively. The occurrence of translocations was more pronounced for HIF-2α than HIF-1α, partly as the amplitude of the translocation was greater than a nuclear:cytoplasmic ratio of 1, therefore a loss in nuclear fluorescence was sometimes attributable to these localisation events.

4.2.3.1 Analysis of single-cell response

In the normoxic condition, 18.5% of red fluorescing cells (n=17 of 92 cells) showed a response with respect to changes in HIF-2α fluorescence over time compared to 52.5% of cells (n=62 of 114 cells) stimulated with hypoxia (**Fig 4.8**). Variability was seen in the response pattern, manifesting as differing rates of accumulation and degradation occurring at differing times and with differing frequencies. To partly address the heterogeneity, the visualised hypoxic data was again classified into the categories; (1) persistent accumulation, (2) single-transient accumulation and (3) multiple-accumulations. The single-transient category was the largest, accounting for 56.5% of responses (n=35 cells), the second-largest was the multiple-accumulations category, describing a further

30.7% (n=19 cells) and persistent accumulation was recorded for the remaining 12.9% (n=8 cells) (**Fig 4.8**).

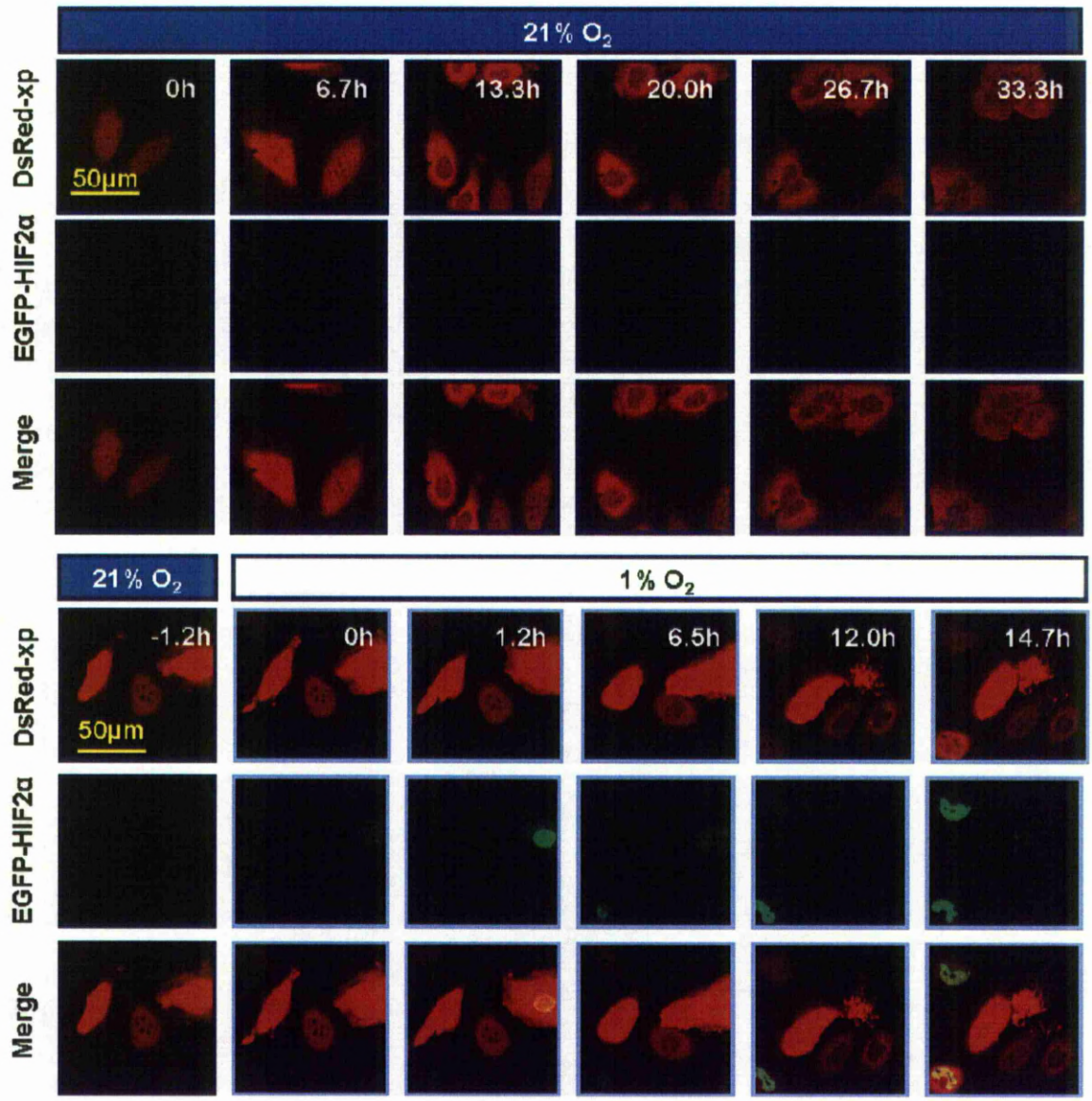

Fig 4.7. Time-lapse microscopy of HeLa cells co-transfected to express EGFPHIF-2α and DsRed-xp. After 24-48 hours of transfection cells were imaged in either atmospheric O_2 (**A**) or 1% O_2 (**B**). Images are of a single location over time, chosen from a selection of 15 locations per experiment repetition, from a total of three t repetitions.

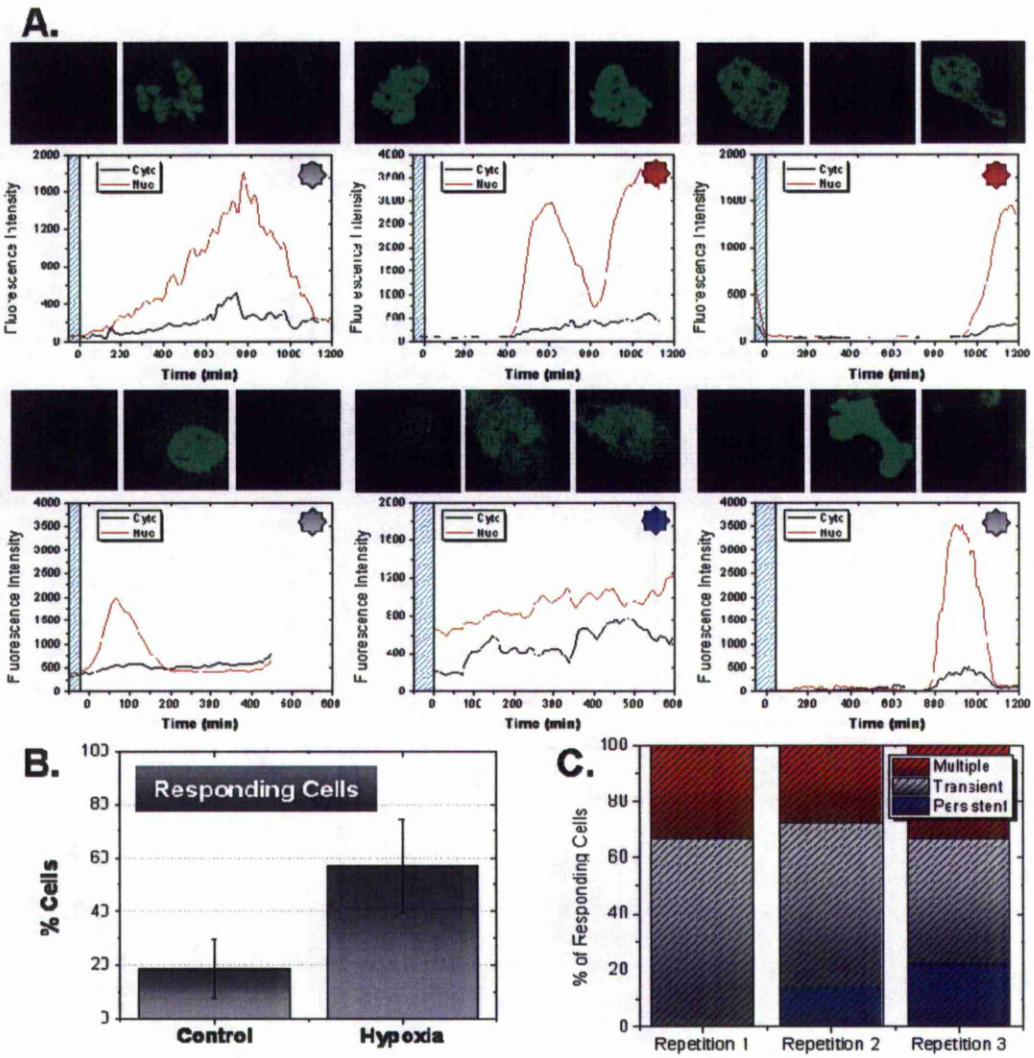

Fig 4.8. (**A**) HeLa cells ectopically expressing EGFP-HIF2α were imaged by confocal microscopy while stimulated by hypoxia (1% O_2) Traces of fluorescence intensity of cytoplasmic and nuclear EGFPHIF2α from HeLa cells exposed to 1% O_2 accompany corresponding images. (**B**) % of red-fluorescent cells that show a visible change in HIF-1αEGFP intensity over the course of the experiment. (**C**) Classification of EGFPHIF-2α response kinetics observed and percentage cells calculated to belong to each classification. The classification of the cell traces shown are indicated using a circular graphic of the same colour scheme. Repetition 1, 2 and 3 are experimental repetitions, each reflecting a number of cells from imaging 15 locations (All nuclear cell traces are shown in the **appendix 1.3**)

The quantified HIF-2α data was subjected to analysis of time-to-1st-response, duration and max amplitude (**Fig 4.9**). The results matched those observed for HIF-1α; time-to-1st-response was found to be heterogeneous ranging across 20-hours of experimental time whereas durations of the transient peaks were found to be more robust lasting 2-4 hours (confirmed again by fano factor measurement). Also the maximum amplitude was again found to vary across the maximum dynamic range of the microscope photo-multiplier detector.

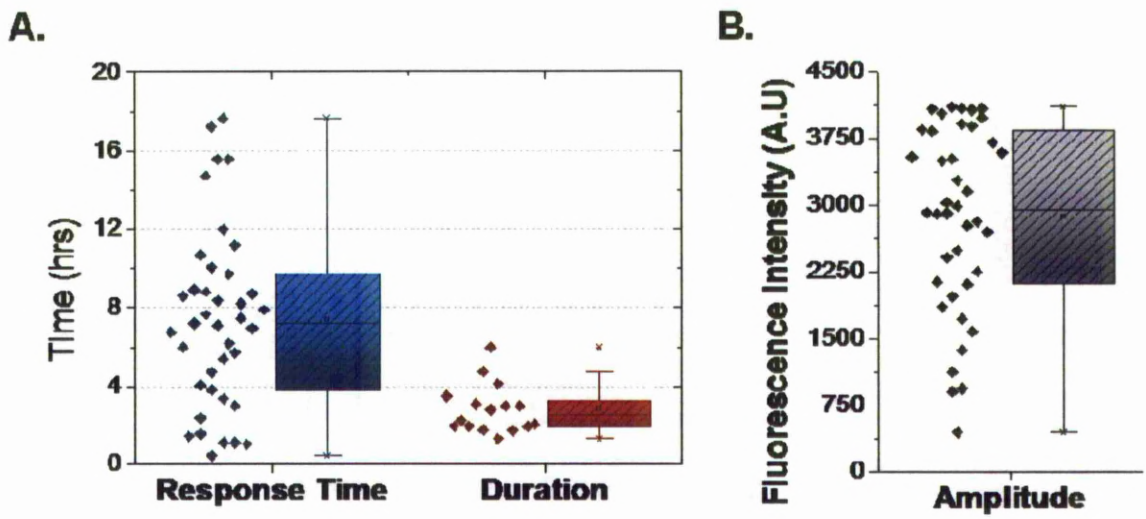

Fig 4.9. Analysis of EGFPHIF-2α (fluorescence) response kinetics from HeLa cells stimulated with hypoxia. (**A**) Time to 1st response and duration of single-transient response. (**B**) Maximum nuclear fluorescence of all cells. The duration was calculated as the time between the point at passing half maximum fluorescence and returning below this value.

4.2.4 Single-cell imaging of HIF transcriptional activity in hypoxia

In response to hypoxia, there is a transient accumulation of HIF-1α protein by western blot accumulation. The single-cell imaging of both HIF-1α and HIF-2α also depicted a transient response profile characterised with a robust duration and an unexpectedly heterogenous response time. To test whether this was similar with endogenous HIF activity, HeLa cells were transfected with the luciferase reporter, pGL2-TK-HRE. After 24-hours transfection, 1mM luciferin was added to the cells for a further hour and then cells were imaged by wide-field luminescence. The imaging data was quantified to the single-cell level response using the AQM kinetic tracker software as described in chapter 2. Once again, transiency and heterogeneity were aspects of the response profile. After analysing 60 cells, the time-to-1st-response was found to range from 0.5hrs to 50hrs with an average of 20hrs (**Fig 4.10**). Multiple responses were also observed, characterised by multiple transient accumulations. There was no evidence of robustness to the multiple responses in terms of; peak-to-peak timing, time-of-occurrence or relative peak amplitude (all traces of nuclear fluorescence can be found in **appendix 9.3**).

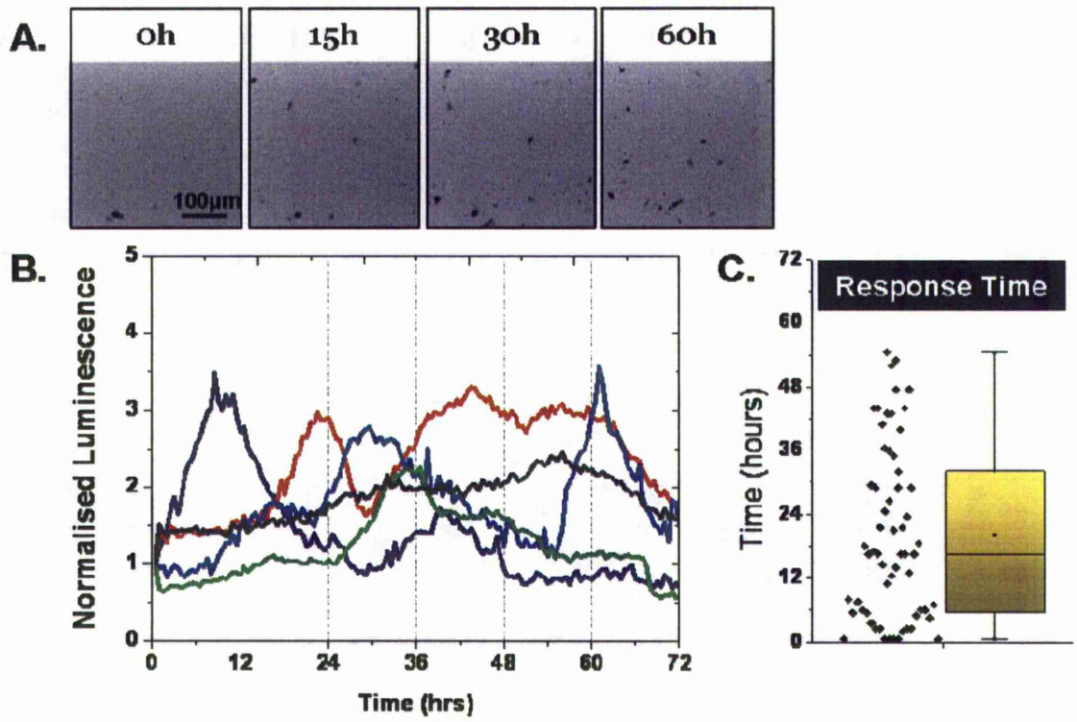

Fig 4.10. HeLa cells were transiently transfected with the HRE-luciferase reporter, pGL2-tk-HRE-luc. After 24-hours transfection cells were incubated for an hour with 1mM luciferin and imaged by wide-field luminescence in (**A**) normoxia or (**B**) hypoxia; images show the light intensity detected. (**C**) Quantification of luminescence levels was performed using AQM kinetic tracker. Representative traces of 5 cells luminescence levels for the hypoxic imaging time-course are shown. (**D**) Box-and-whisker plot showing the response time, as calculated at the point of 50% maximum increase in luminescence levels.

4.2.5 The response of HIF-α protein levels to re-oxygenation

4.2.5.1 Bulk-cell response of HIF-α protein to re-oxygenation

The observed heterogeneity in HIF-α response time is not entirely concordant with the known governing molecular mechanisms, lacking receptor level stochasticity and are expectantly determined by a rapid inhibition of the intracellular prolyl hydroxylases (Lipniacki, Puszynski et al. 2007; Taylor 2008). This prompted work to investigate the reverse scenario, rather than the hypoxic accumulation examine the re-oxygenation driven degradation of HIF-α. HeLa cells plated into 6cm dishes were incubated at 1% O_2 for 6-hours, then lysed throughout a re-oxygenation (back to atmospheric O_2) time-course of 120-minutes. Analysis of samples showed that HIF-1α protein is reduced to below detectable levels within 10-minutes, a similar value was reported by Marxsen *et al.* (2004) (**Fig 4.11**). On the other hand, HIF-2α showed no decrease upon re-oxygenation over the 120 minutes and perhaps even a subtle increase in protein.

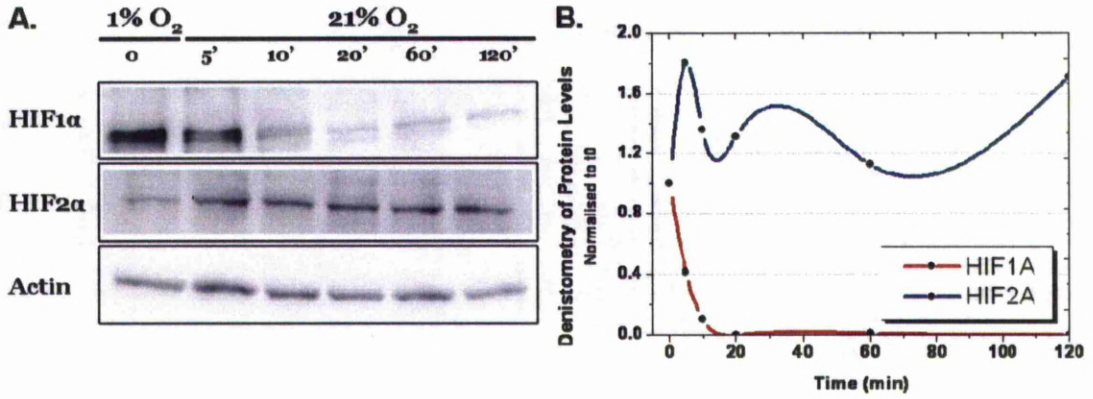

Fig 4.11. HeLa cells were incubated at 1% O_2 for 6-hours and then exposed to a re-oxygenation time-course back to atmospheric O_2 levels. (**A**) Western blot analysis of samples throughout re-oxygenation, probing for HIF-1α and HIF-2α and an actin loading control. (**B**) Densitometry analysis of HIF-1α and HIF-2α western blot protein bands. Values are normalised to to.

4.2.5.2 Single-cell response of HIF-1α protein to re-oxygenation

The same experimental re-oxygenation protocol was performed at the single-cell level, using time-lapse confocal microscopy of HeLa cells transiently transfected with HIF1α-EGFP for 24-48 hours. Cells were then incubated on the microscope stage hypoxic incubator for 5-hours at 1% O_2. Cells showing a visible nuclear green fluorescence signal were selected for imaging and imaged for an hour in hypoxia before reverting to atmospheric oxygen, imaging for a minimum further 300-minutes. In this instance, 82% of cells (n=66 of 80 cells) visible for HIF-1αEGFP at to were found to show a significant reduction in fluorescence intensity after re-oxygenation (**Fig 4.12**). The half-life of HIF-1α protein in response to re-oxygenation was found to be 26±14 minutes from a data set of 48 cells.

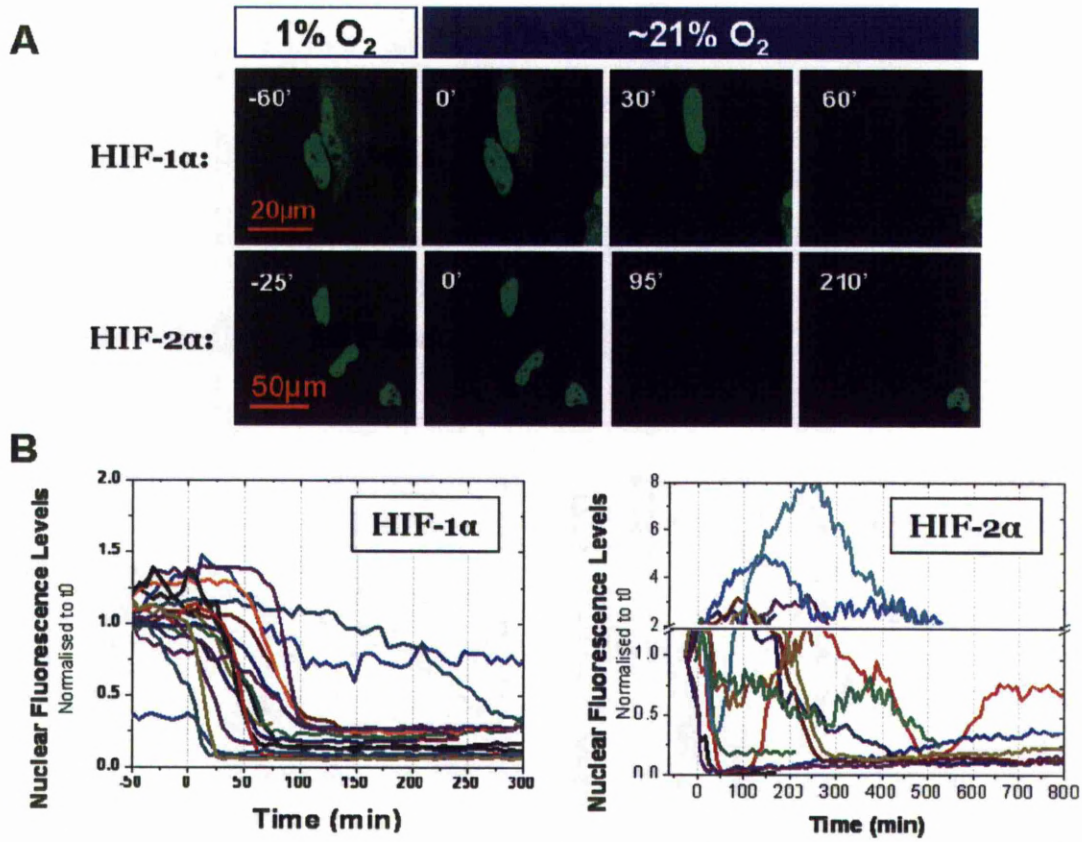

Fig 4.12. HeLa cells ectopically expressing EGFP fused HIF-1α or HIF-2α were imaged by confocal microscopy through the re-oxygenation from 1% O_2 to atmospheric O_2 after a 6-hours 1% O_2 hypoxic incubation. (**A**) Shows representative images from the time-course and (**B**) shows the cell traces of normalised nuclear fluorescence for some of the cells. Additionally, the y-axis for HIF-2α traces has been broken to better show the loss and re-accumulation of fluorescence.

4.2.5.3 Single-cell response of HIF-2α protein to re-oxygenation

Confocal microscopy imaging of HIF-2α in hypoxia suggested a degree of O_2-sensitivity not convincingly seen when examining the response by western blot analysis (shown previously in **Fig 3.4 & 4.2**). We sought to further investigate the oxygen sensitivity of HIF-2α by transfecting HeLa cells with the pG-EGFP-HIF2α expression vector and imaging expressing cells through a re-oxygenation event. Again, cells were selected that demonstrated green fluorescence after 5-hours of incubation at 1% O_2. Cells were then imaged in the same manner as per HIF-1α re-oxygenation. Surprisingly, 82.6% of HIF-2α cells (n=62 of 77 cells) showed a strong reduction in fluorescence after re-oxygenation (**Fig 4.12**). The measured decrease of HIF-2α gave a half-life value of 29±10 minutes. It is worth noting, that HIF-2α protein showed a greater range of dynamism in response to re-oxygenation than observed for HIF-1α. Several cells showed a short increase in fluorescence following re-oxygenation prior to the major reduction. The point of decrease was used in the calculation of half-life. Upon further observation, 15% of cells also showed re-accumulation events occurring after initial

degradation. The increased dynamism and asynchrony of HIF-2α, observed in both re-oxygenation and hypoxic imaging, may explain the lack of bulk-cell level detection of oxygen-dependent regulation of HIF-2α.

4.2.5.4 The effect of ectopic expression of HIF-α on cell fate during re-oxygenation

An encountered issue when evaluating single-cell data was the accounting of cell division and cell death. Both issues effect the data as cell death prevents long term measurements and cell division results in the doubling of possible number of cells. This was an important issue when evaluating the single-cell imaging data of re-oxygenation. A large degree of cell death was present when imaging over-expressed HIF-α cells (**Fig 4.13**). When imaging HIF-1α the average occurrence of cell death was found to be 71% (total data set of 80 cells over three repetitions). For HIF-2α this average was found to be lower at 60% (total data set of 77 cells over three repetitions), but not significantly lower than HIF-1α. These data were compared to an EGFP control, in which 11% of imaged cells were found to undergo cell death during imaging (concluding data from 94 cells). The low instance of cell death when imaging unfused EGFP disregards the possibility of laser induced ROS contributing towards cell death (Dixit and Cyr 2003).

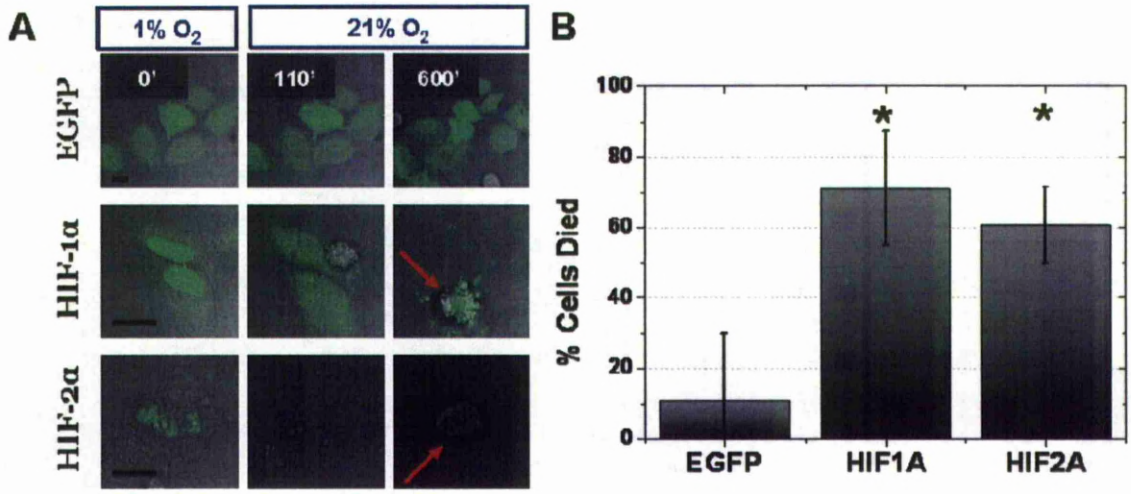

Fig 4.13. (**A**) Confocal imaging of HeLa cells ectopically expressing un-conjugated EGFP, HIF-1αEGFP or EGFP-HIF2α, showing the merge of bright-field and green channel. Cells were exposed to re-oxygenation following 6-hours of hypoxia. (**B**) Calculated average % of cells died during re-oxygenation (n = >77 cells per condition). (n=3 repetitions) Statistical significance assessed using one-way ANOVA; * = <P0.05

The results prompted us to revisit the observed relationship between HIF-α expression and the advent of cell death, as detailed in the single-cell hypoxic imaging (measured earlier in **Fig 4.5**) (Carmeliet, Dor et al. 1998). From the re-

oxygenation data we can see that the ectopic expression of either HIF-α vectors increases the propensity of a cell for re-oxygenation mediated cell death, essentially sensitising the cell to re-oxygenation apoptosis. This has important implications in ischaemia-reperfusion injury, a pathological scenario characterised by the resurgence of oxygen after a hypoxic episode (Loor and Schumacker 2008).

4.2.6 Constructing the mathematical model

The advent of mathematical modelling provides another useful tool in understanding and addressing biology. To this end mathematical equations are used to describe an arrangement of biological interactions and components (Eungdamrong and Iyengar 2004; Eungdamrong and Iyengar 2004; van Riel 2006). Often for these models to be of meaning, they need to be informed and tested against biological data (van Riel 2006). The live-cell imaging data acquired throughout this chapter is one such type that is very compatible with mathematical modelling, on account of the highly quantitative nature of the data (Bartfeld, Hess et al.). The single-cell HIF-α data therefore provided us with an insight into the HIF hypoxic response as well as preparing a platform from which to build a mathematical model detailing the HIF system.

Mathematical models are artificial constructs that attempt to recreate phenomenon through abstraction (Eungdamrong and Iyengar 2004). It is therefore critical to sensibly determine the extent of the abstraction and this requires the rational conception of the interactions, components and features the model is to encompass. Ideally the scope of the model should be relative to the known constraints i.e. biological measurements pertaining to the model. If more terms are included than constrained, then the parameter space of the model enlarges, increasing the models' flexibility. This can lead to the scenario in which a model may be able to mimic network level behaviour but for the wrong reasons, undermining the model as a tool (Eungdamrong and Iyengar 2004). Previous attempts at modelling HIF have ambitiously attempted to detail many of the relevant processes, yet lack high-resolution data pertaining to the assumptions; often fitting to several bulk-cell analysis time points (Kohn, Riss et al. 2004; Dayan, Roux et al. 2006). These abstractions represent a 'top-down' approach, in which the essential behaviour of the system is expected to arise from the complicated network topology. We propose a 'bottom-up' approach, building the simplest model able to capture the single-cell imaging of HIF-1α

transiency. From this model, a cycle of hypothesis and improvements can be made, essentially building the model (van Riel 2006). Starting from a more thorough conception of the HIF signalling network, we aimed to reduce the description to a minimal system designed to recapitulate HIF-α transiency (**Fig 4.14**).

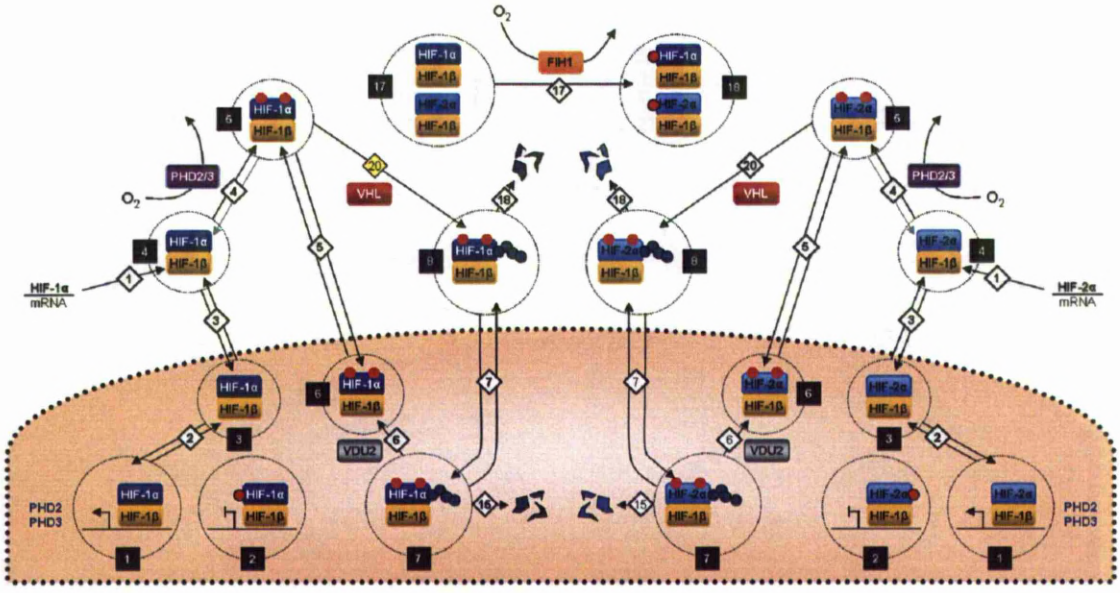

Fig 4.14. Early conception of HIF-model abstraction. Species to mathematically define are indicated numerically with black squares. Reaction kinetics to define are indicated with white diamonds. This topology is similar to those used in previous HIF-models produced by Kohn *et al.* 2004 and Dayan *et al.* (2009).

The data-set provided by the single-cell imaging provides us with an initial constraint with which to build the model around. The principle behaviour we attempt to capture is the hypoxia-induced transiency observed by both western blot and single-cell imaging (**Fig 4.2** & **Fig 4.4**) We therefore needed to detail the oxygen sensitive regulation of HIF-α protein that can give rise to transiency. The favoured hypothesis is that the feedback actions of PHD2 and PHD3 convey this transiency; in which PHD2 is cited to exert the majority of regulation (Berra, Benizri et al. 2003). It was therefore decided to mathematically model this regulatory sequence. The PHD-mediated destruction of HIF-α protein is a multi-step process involving the proteins pVHL, Ubiquitin as well as the 26S proteasome multi-protein structure. We decided to disregard the role of ubiquitin and the 26S proteasome under the assumption that they are not limiting or dynamic due to their extensive role in cellular biology. Previous modelling efforts by Kohn *et al.* and Dayan *et al.* had determined HIF-1β to only weakly impact HIF-α accumulation. Also work by Chilov *et al.* 1999 found HIF-1β to not effect HIF-1α translocation to the nucleus. For these reasons we also

disregarded explicitly modelling HIF-1β. Inhibition of FIH hydroxylase activity occurs in severe instances of hypoxia, remaining near fully functional in tensions below 1% O_2 (Stolze, Tian et al. 2004). As our experimentation will only regard tensions from 20% to 1% we ruled out including FIH in the first incarnation of the model. Finally, pVHL was disregarded from the model abstraction on the assumption that the rate limiting step in HIF O_2-dependent degradation is the hydroxylation of HIF-α and not ubiquitination (Berra, Benizri et al. 2003).

This leaves the model abstraction with the PHD proteins and the HIF-1α isoform. To further reduce the initial free parameter space, the HIF-α isoforms and PHD isoforms were reduced to a generic single form, a transcriptionally viable HIF-α and a feedback $PHD^{generic}$. This model is referred to as the 2-component model (2C-model) or the generic feedback model, on account of the 2 ordinary differential equations (ODEs) (**Fig 4.15**).

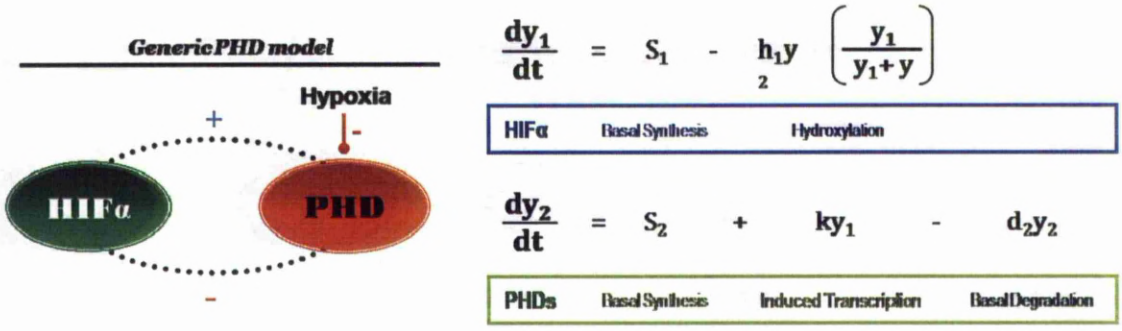

Fig 4.15. Finalised HIF model abstraction. The signalling motif to model is depicted on the left with the corresponding ODEs (with described biological function) on the right.

4.2.6.1 Initial fitting of imaging data to 2C-model

After the 2C-model architecture was decided we could now begin to integrate our imaging data into the model framework. This work was carried out by Joseph Leedale, a PhD student of mathematics under the supervision of Dr. Rachel Bearon and Dr. Kieran Sharkey of the University of Liverpool maths department. Therefore my role in this section of work was peripheral, though there was a large degree of consultation and discourse between us. The aim for this body of work was to simulate the HIF-1α imaging data using the 2C-model to determine parameter values in process known as *fitting* (**Fig 4.16**). For this purpose the only parameter that was fixed was *h*, the parameter corresponding to the hydroxylation rate. To represent the switch from normoxia (21% O_2) to

hypoxia (1% O_2) the *h* value was reduced by 87%, a value derived for PHD2 by Tuckerman *et al.* 2004. The reverse was performed to simulate re-oxygenation.

For the model to fit the hypoxic and re-oxygenation perturbations, the model requires a steady-state value to initialise from. As part of this fitting procedure, the pre-perturbation state of the model (the concentrations of y1 and y2) was determined for each individual cell, calculated by using the mean values of all HIF fluorescence recorded before perturbation. After determining the initial conditions, it is then possible to perform the parameter search. This was performed using the matlab 'fminsearch' function; an algorithm that searches for the minimum values of several variables in order to recapitulate a numerical solution, in this instance to find the minimum values of model parameters needed to trace our experimental data. As only HIF-α fluorescence was imaged, the kinetics and response of PHD in relation to HIF-α are left open and unconstrained. For the model to aptly account for this, PHD was rescaled by the hydroxylation rate resulting in the equation;

$$\frac{dy1}{dt} = S - \sigma y2\left(\frac{y1}{Y1 + y}\right) \qquad \frac{dy2}{dt} = kh_N y1 - dy2$$

A series of fitting was then performed; initially parameter estimates were fitted to the single-cell imaging of hypoxic transiently responding HIF-1α cells without constraint (n = 11 cells) (**Fig 4.16**). The parameter estimates were then used in a constrained round of fitting for all HIF-1α confocal imaging data, allowing up to a 50% shift in value from the median value of the original estimates. For this purpose the median values were used over the mean due to the order of magnitude variance of parameters and thereby the excessive weighting of outliers. The median was also considered acceptable as the parameter estimates indicated an observable median consensus. Evaluation of the parameter variance showed the most deviation for γ, followed by *d*, *s* and then *k*. The second round of fitting elucidated the final parameter set to be used to finalise the 2-component model (**Table 4.1**).

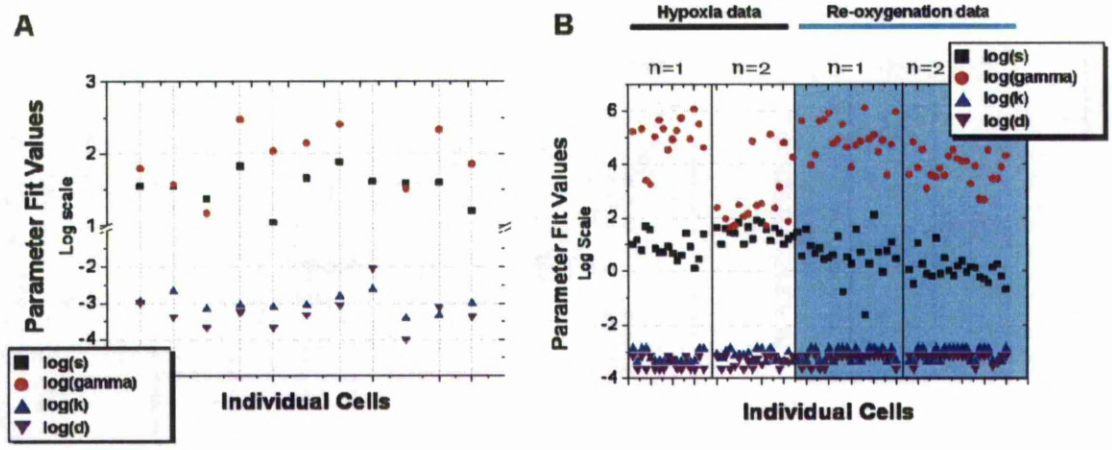

Fig 4.16. Results for the fitting of the 2-component model to single-cell HIF-1α imaging data. (**A**) Shows initial unconstrained fitting of the model to eleven cells from the single-cell hypoxic imaging data of HIF-1α transiently accumulating cells. (**B**) Values derived from the unconstrained fitting were used for the constrained fitting of all single-cell HIF-1α imaging. Only values within 50% of the initial estimates were allowed. The hypoxic and re-oxygenation data sets are indicated, with an additional line break to indicate repetition of data (data together totals 88 cells).

For both rounds of fitting, a criteria was established to determine a *good fit* or *bad fit*. An envelope was drawn around each measured cell trace, using the equation;

$$\mathbf{EXP(t) \pm \beta * (max(EXP)-min(EXP))}$$

β = 0.35 (width of error envelope)

EXP(t) = Fluorescence levels at a given time point

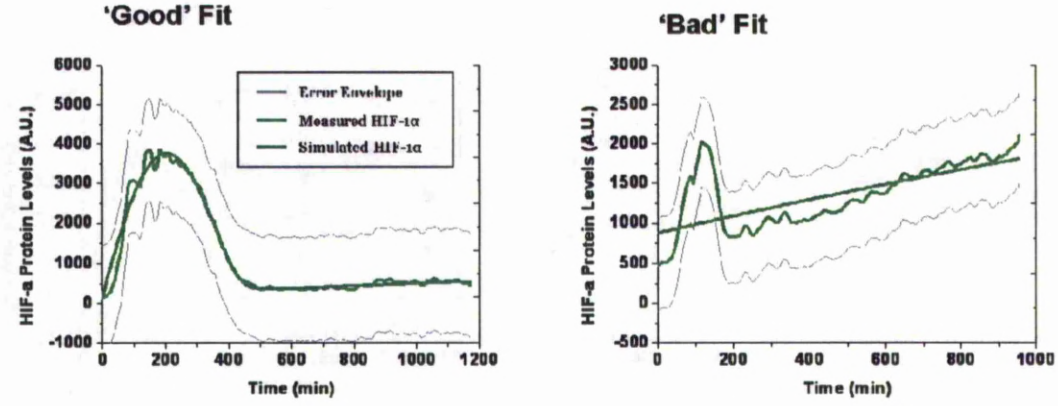

Fig 4.17. Model fitting solutions were compared against the experimental data. To determine a good fit versus bad fit an error envelope was defined around the experimental data. If the fit fell outside of this envelope for several time points, the fit was considered bad.

Fits deviating outside of this envelope for a defined number of data points relevant to the time-course, were considered *bad*. Using this criteria, all 11 cells from the initial unconstrained fitting were considered good (**Fig 4.17**). The constrained fitting resulted in 79% (n= 31/39 cells) good fits for the hypoxic data set and 74% (n = 31/42 cells) good fits for the re-oxygenation data set.

	Parameters	Units	Value
S	'*synthesis rate*'	$AUmin^{-1}$	5.14
γ	'*saturation function*'	AU	1.83×10^{4}
K	'*Induction rate*'	min^{-1}	7.10×10^{-4}
d	'*Degradation rate*'	min^{-1}	7.07×10^{-4}

Table 4.1. Table of parameters, units and values fitted in the 2-component model.

The parameterised model was then used to simulate perturbation by exposure to hypoxia (reducing 20% O_2 to 1% O_2) and also the reverse re-oxygenation (**Fig 4.18**). The hypoxic profile showed a HIF accumulation profile qualitatively maintaining a transient accumulation. Transiency in both HIF and PHD settled to a new steady-state 24 hours after perturbation. The model output for re-oxygenation showed the rapid loss of HIF-1α, with a half-life of 25.8 minutes, a value very comparable to the 26 minutes observed experimentally (measured in **section 4.2.5.2**) After re-oxygenation, the model finally reaches a steady-state solution after 40 hours. The 2C-model was deemed to behave appropriately, in line with measurements and thereby can be used for further analysis.

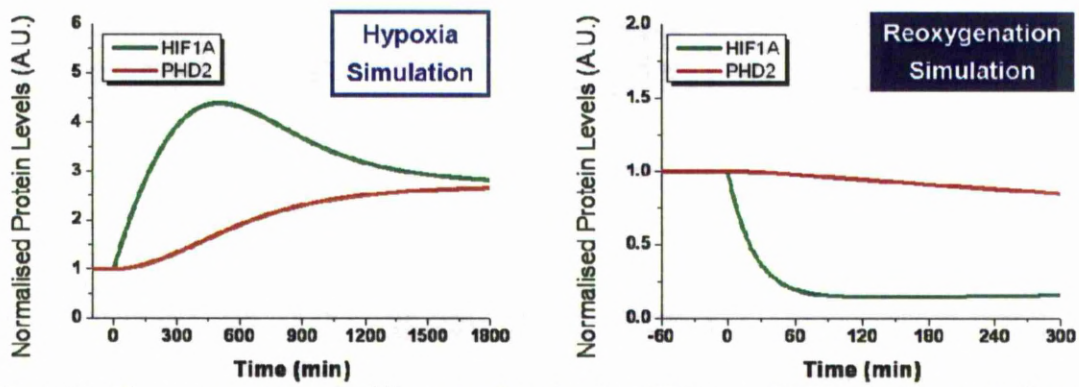

Fig 4.18. The 2-component model was used to simulate HIF-1α and PHD2 levels responding to a hypoxic perturbation (1% O_2) and a re-oxygenation event, in which the simulation details the HIF system at a steady-state solution in 1% O_2 before re-oxygenation back to 20.8% O_2.

4.2.7 Heterogeneity and cell cycle

The model has been informed by our single-cell imaging data of HIF-α dynamics following hypoxic and re-oxygenation events. The model does not attempt to recapture all events seen, especially with regards to the heterogeneity observed. The experiments described in the following section attempt to validate and quantify the heterogeneity, while also investigating potential sources. These results were designed to impact our decision at including descriptions of heterogeneity in future model expansions.

4.2.7.1 A Cell-cycle component explains some heterogeneity in response time

The known molecular mechanisms governing the O_2-dependent accumulation of HIF-α do not lend to response-time heterogeneity as seen by wide-field luminescence of the HRE-reporter and time-lapse imaging of fluorescent HIF-α. Especially given the sharp profile of the transient accumulations imaged.

The confocal data set afforded us one important observation; often cell division preceded the nuclear accumulation of HIF-α fluorescence (**Fig 4.19**). We re-evaluated the data-set in this context and found that 50% of the responding cells (for both α-isoforms) fell into this category, in which fluorescence accumulation occurs within 3-hours after cytokinesis. The asynchrony of cell division therefore drives some of the asynchrony in HIF-α accumulation; this mechanism partially explains some of the heterogeneity observed. This evidence suggested that if the cells were to be cell cycle synchronised, so to would a large portion of the HIF accumulations be synchronised.

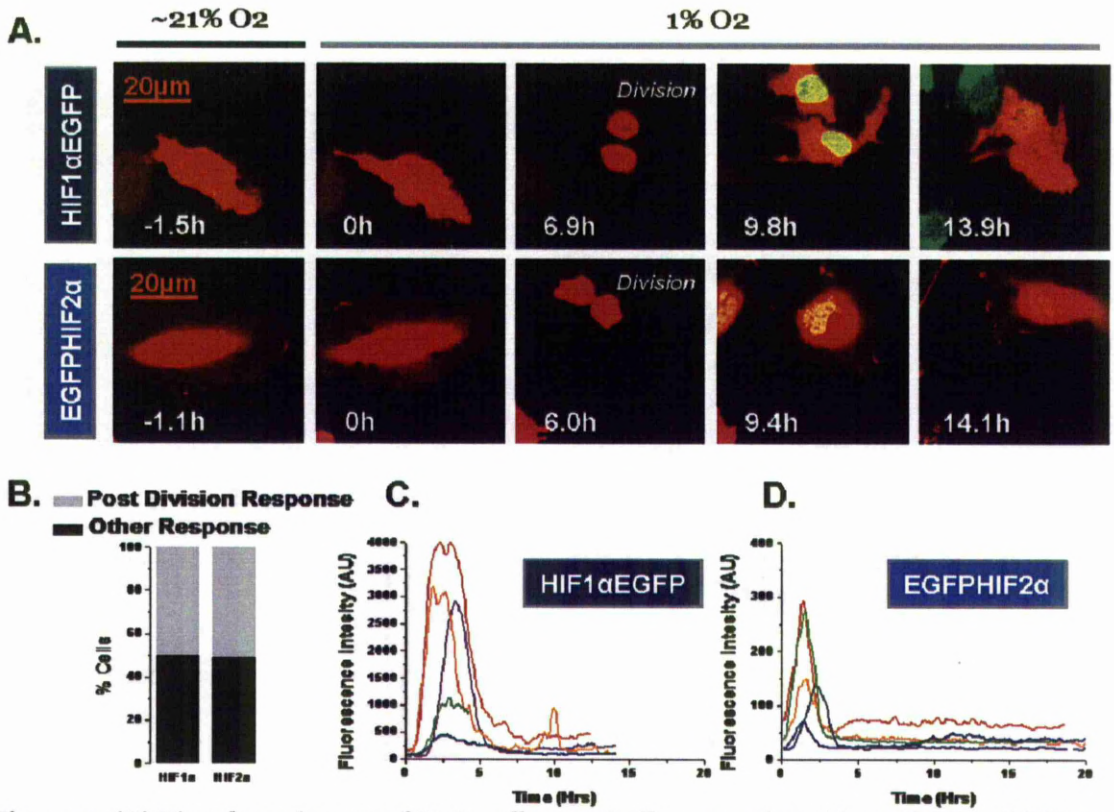

Fig 4.19. (**A**) Time-lapse images of HeLa cells ectopically expressing either pG-HIF1αEGFP or pG-EGFP-HIF2α as well as a DsRedxp unfused control. The point of cell division is indicated in text. (**B**) Transiently accumulating cells were classified as occurring within 3 hours after metaphase (post division response) or not (other). (**C** & **D**) Corresponding traces of nuclear fluorescence for representative cells where to is the division time.

4.2.7.2 Double Thymidine Block synchronises HIF response

The cell cycle can be chemically synchronised using a method referred to a the double thymidine block (Whitfield, Zheng et al. 2000). The addition of extraneous thymidine to a cell culture disrupts the normal ratio of dNTPs and this promotes problems with the fidelity of DNA replication, causing either G1/S checkpoint arrest or apoptosis depending on the genetic status of the cell line (Hyland, Keegan et al. 2000; Pietenpol and Stewart 2002). HeLa cells were synchronised using the double thymidine block protocol, during which cells were also transfected with the expression vectors pG-HIF1αEGFP and pG-DsRedxp. Cells were released from cell cycle arrest and immediately imaged in hypoxic conditions (1% O_2). The nuclear fluorescence levels of suitable cells were quantified using Cell Tracker. Cells were found to only accumulate HIF-1α after cell division, which occurred on average 7-hours after release from the thymidine block (**Fig 4.20**). All visualised responses were transient and occurred with a tightly constrained duration with an average time of ~4hrs, a value comparable with the non-synchronised data. The time-to-1st-response was more constrained than seen in previous asynchronously dividing cells, occurring with a normal distribution around 9-hours. The majority of variance in response time was attributable to variance in division time, as even with chemical synchronisation the timing of cytokinesis spanned approximately 2-hours. A recent publication by Hubbi *et al.* 2011 has produced exciting evidence to suggest this link between the HIF system and the cell cycle, citing that the MCM proteins act as negative regulators on HIF stability (Hubbi, Luo et al. 2011). However, within our own data the validity of this claim remains unclear due to the use of the transient transfection with cationic lipid. Cationic lipid transfection reagents such as FuGene use the cell-cycle nuclear envelope breakdown to gain access and deliver plasmid to the nucleus. Therefore transfection occurs in a cell-cycle dependent fashion in which the newly acquired plasmid is first expressed during mitosis (Zabner, Fasbender et al. 1995). This mechanism would account for the occurrence of HIF-αEGFP accumulation within 3 hours of cytokinesis, the criteria used to determine a HIF cell cycle related response.

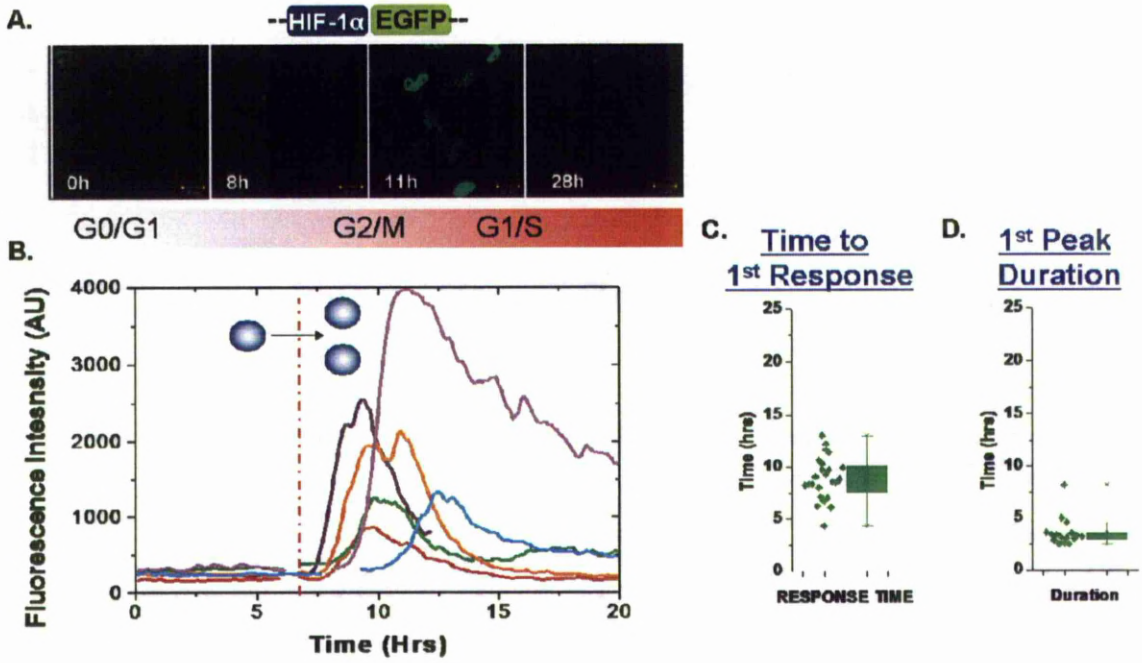

Fig 4.20. Results for the live-cell confocal imaging of HIF-1αEGFP expressing cells, chemically synchronised in the cell cycle to Go/G1 (**A**) Confocal images of HIF1αEGFP fluorescence with time indicated in hours. The corresponding average cell cycle progression is shown. (**B**) Representative plots of EGFP nuclear fluorescence intensity with the average division time of the cells indicated. Box-and-whisker plots of data; (**C**) time to 1st response and (**D**) 1st peak duration for all imaged cells.(n=1 repetition)

4.2.7.3 Transient-transfection as a source of heterogeneity

As well as potential cell cycle artefacts, transient transfection has the capacity to introduce a degree of heterogeneity as the method may load uneven quantities of plasmid into individual cells. This would lead to different expression levels from cell-to-cell and thereby varying initial concentrations of exogenous protein. Varied protein levels are a source of heterogeneity (Cohen, Kalisky et al. 2009). Typically the impact of this heterogeneity is experimentally reduced by imaging cells displaying a similar signal level, using the assumption that signal level corresponds to plasmid concentration. However a technical difficulty prevented us taking the same precaution when imaging the HIF system. Prior to hypoxic stimulation HIF-α is extensively degraded and the fluorescent form near undetectable (in most cases). Those cells that showed sufficiently detectable HIF in normoxia may not be a suitable and are perhaps a consequence of saturated degradation arising from overexpression, possibly stabilised from a number of O_2-independent crosstalk events (outlined in **Table 1.2**) or are currently transfecting, a scenario in which fluorescent HIF protein is initially expressed before being reduced by the activity of the feedback mechanisms. To counteract these issues for confocal microscopy cells

expressing an unlabelled DsRedxp fp were selected and imaged, thereby removing a degree of bias. To achieve this, cells were co-transfected with a DsRedxp encoding plasmid and a separate HIF-α encoding plasmid. Unfortunately, the plasmid content of DsRedxp is not expected to correlate well with the plasmid content of HIF-α and therefore red fluorescence was not used as a proxy for HIF-α expression level.

To address the myriad of concerns with transient transfection, we aimed to produce cells stably expressing fluorescent for HIF-1α and HIF-2α. HeLa cells were transfected with either pG-HIF1αEGFP or pG-EGFPHIF2α in a $75cm_2$ flask using FuGene 6. After 48 hours of transfection, the cell media was replaced with selection media containing 1mg/ml G418 sulphate. After 2-3 weeks the majority of cells had died and small colonies had begun to form. At this point cells were trypsinised from the flask, counted and plated into 96-well format at a density of 1 cell/well. From this we started with an initial selection of 192 clones each for HIF-1αEGFP and EGFPHIF-2α. After a week of growth, clones were inspected by light microscope, selecting 24 clones to propagate for each transfection. At this point cells had grown sufficiently to be assayed for stable expression of the fluorescent HIF-α isoforms.

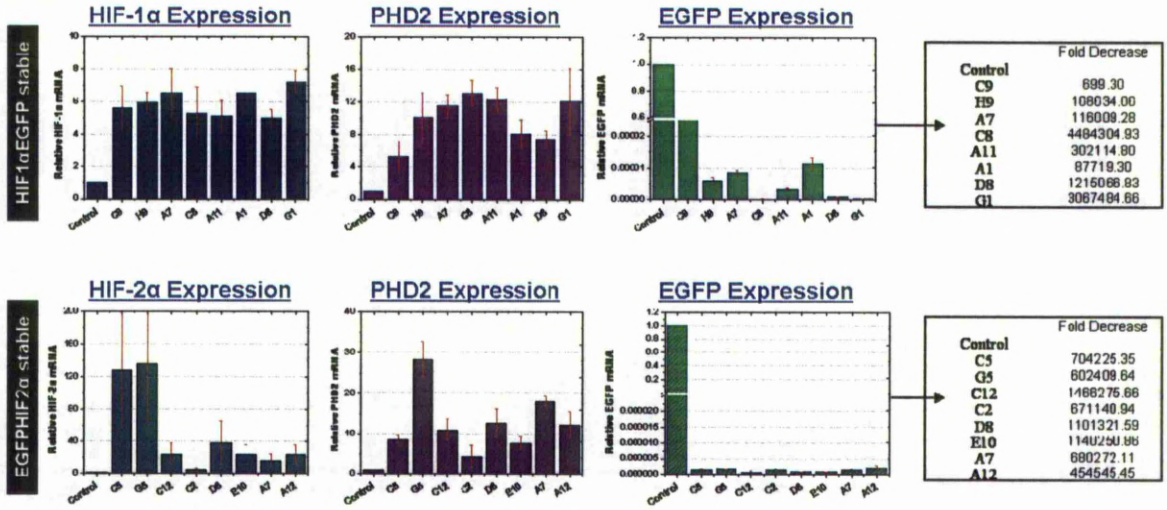

Fig 4.21. Clones of HeLa cells (named as 'letter'+'number') stably expressing either HIF-1αEGFP or EGFHIF-2α were assessed for HIF-α, PHD2 and EGFP mRNA via qRT-PCR. All clones examined were found to have suppressed EGFP mRNA below detectable limits. Control samples were prepared from HeLa cells ectopically expressing EGFP.

Eight clones for each condition were grown in 6cm format and then lysed and samples prepared for RT-qPCR. Unfortunately, all were found to have suppressed the expression of EGFP below detectable limits (**Fig 4.21**).

Nevertheless, we remained interested to estimate the heterogeneity in the system using stable expressing cells. Fortunately, a cell line stably expressing HRE-luciferase (C51 mouse carcinoma cells) were kindly donated by Dr S. Lehmann and Prof. R. Wenger. C51 cells were plated and prepared for imaging by wide-field luminescence and then imaged either at 1% O_2 or atmospheric O_2. The luminescence levels were quantified at the single-cell level using AQM kinetic tracker. From this data, we can contrast to the transient transfection of HeLa cells using the pGL2-tk-HRE-luciferase vector in **Fig. 4.10**. Here we found the response time to be more homogenous and still transient (**Fig 4.22**).

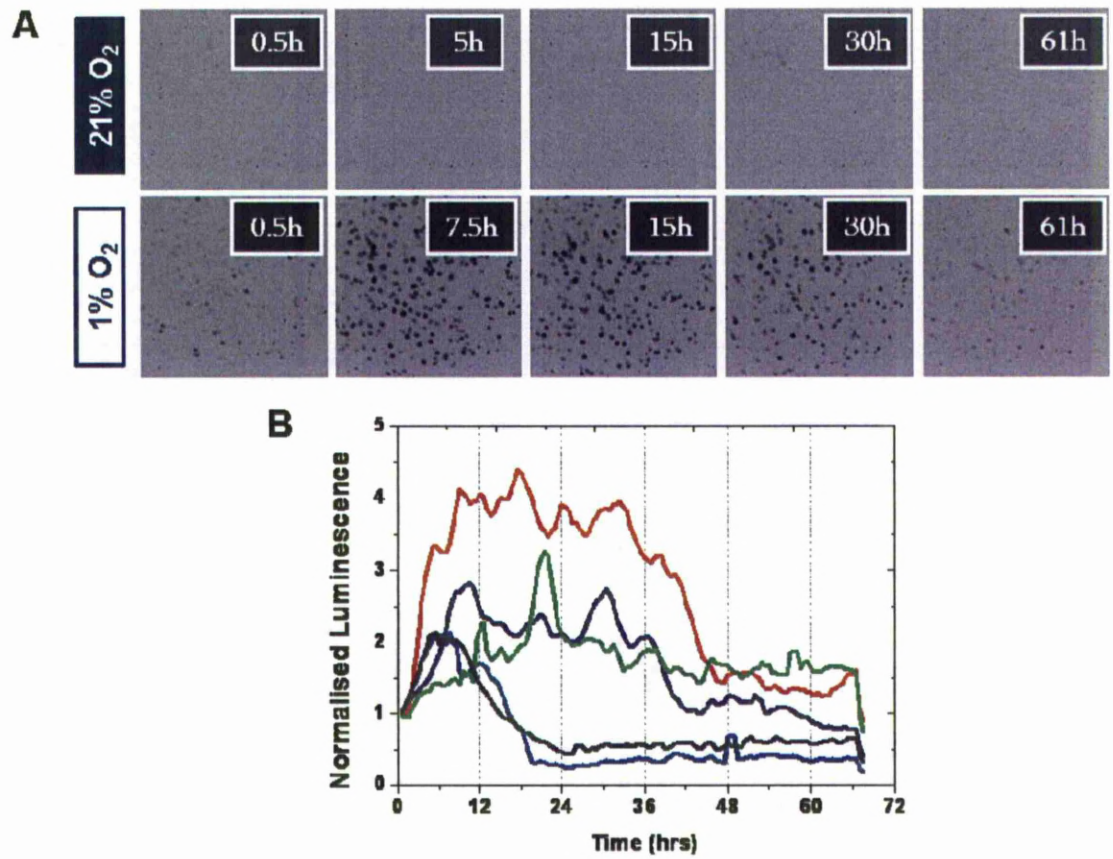

Fig 4.22. (**A**) Wide-field luminescence imaging of C51 mouse carcinoma cells stably transfected with a HRE-luciferase reporter plasmid. Cells were imaged either in atmospheric O_2 of hypoxic conditions of 1% O_2. Luminescence levels of responding cells were automatically measured using AQM kinetic tracker software. (**B**) Single-cell traces for 5 representative cells are shown.

4.2.7.4 Cloning fluorescent fusion reporters of HIF-1α ODD domain

Overexpression of HIF-α induces a significant degree of cell death and is therefore one argument against the use of these constructs (as shown in **Fig 4.13**) The increased cell death or sensitivity to cell death indicates that the overexpressed cell does not function entirely as it would in a native state. This is further confirmed when examining the effect of ectopic expression HIF-α upon

the HRE-luciferase, the signal is significantly higher than control cells expressing unlinked EGFP (shown previously in **Fig 3.11**). HIF signalling is therefore higher than the native, untransfected state and thus the negative feedback may be over represented. The over representation of the PHD2 and PHD3 feedback, coupled with the different expression levels associated with the transient transfection method may experimentally introduce a degree of heterogeneity. To address some of these issues we decided to make a plasmid vector expressing a reporter of HIF-1α O_2-dependent stability which was transcriptionally inert. This new molecular tool could then be used to enhance the data of the current study as well as function as a suitable O_2-sensor for other studies. To achieve these goals we decided to clone several portions of the HIF-1α sequence without including the DNA binding domain. This approach has been previously been used in the generation of hypoxic reporters, often coupling the ODD domain to an EGFP (D'Angelo, Duplan et al. 2003; Kuchimaru, Kadonosono et al. 2010). A similar system has been commercialised for investigation into cell cycle progression, fusing fluorescent proteins to degradation domains of several cell cycle proteins (Sakaue-Sawano, Kurokawa et al. 2008). As this study is one of the first to concentrate on the kinetics of the transient accumulation of HIF-1α, these previous tools have not been validated in this context. We aimed therefore to clone several versions of the HIF-1α coding sequence, preserving the ODD domain in each. Three versions were cloned using the gateway procedures outlined in chapter 3; the first version includes residues 217 aa - 374 aa (termed pG-ODD-EGFP), preserving only the first p402 hydroxylase site; the second version is extended to include the p564 hydroxylation site, taking from residues 271 aa to 652 aa (termed pG-frODD-EGFP). Both these two forms lack the nuclear localisation domain, found in the c-terminal, this may have implications for the *correct* degradation of the protein (Fandrey, Gorr et al. 2006; Chachami, Paraskeva et al. 2009; Nakayama, Qi et al. 2009). A final version therefore was cloned, including almost all coding sequence except the DNA binding domain, including therefore residues 217 aa – 826 aa (termed pG-nucODD-EGFP) (**Fig 4.23.**). To assess the impact of the ODD expression vectors on HIF signalling, all three plasmids were transfected into HeLa cells alongside the pGL2-TK-HRE-luciferase for 24-hours. After this period, samples were lysed, prepared and analysed by endpoint luminometry. No induction of the HRE-luciferase was detected, confirming the loss of

transcriptional activity (**Fig 4.23**). All expression plasmids were then transfected into HeLa cells and imaged by confocal microscopy, assessing the localisation in normoxic conditions. As to be expected, the ODD-EGFP and frODD-EGFP expression was mostly detected in the cytoplasm and the nucODD-EGFP predominantly found to be localised to the cell nucleus (**Fig 4.23.**).

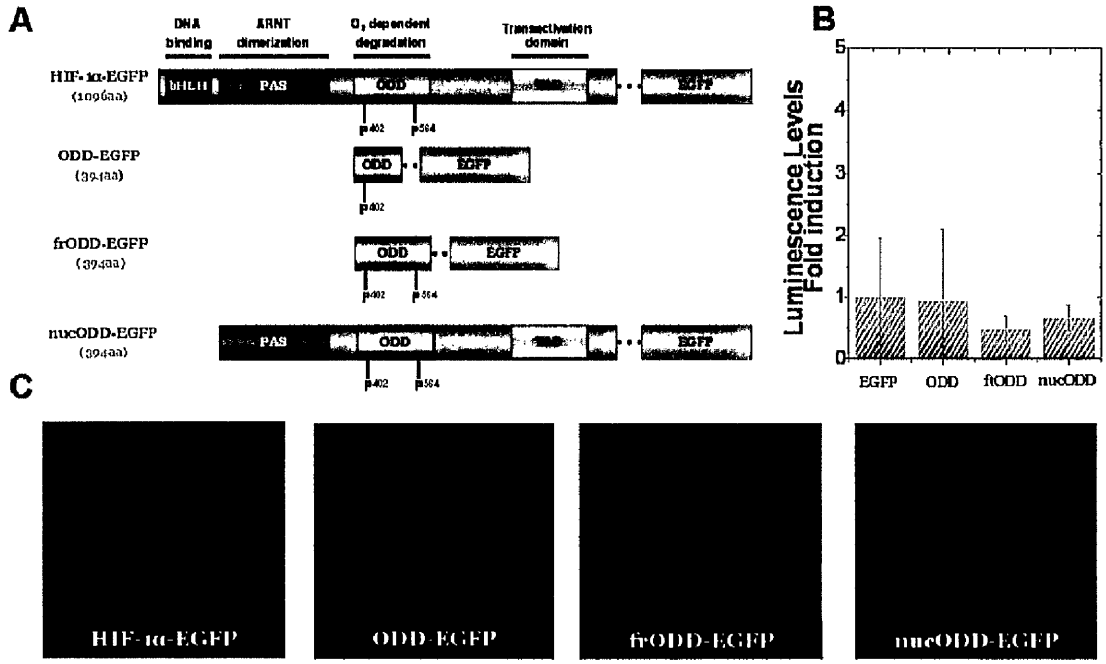

Fig 4.23. (**A**) Protein domain structure of full length HIF-1α and the ODD-variants. (**B**) Luminometry measurement of HeLa cells co-expressing the HRE-luciferase reporter and either an ODD-variant, an unfused EGFP expression vector or full length HIF-1αEGFP. (C) Live-cell confocal microscopy of HeLa cells expressing either an EGFP fused ODD-variant or full length HIF-1αEGFP imaged 24-48 hours after transfection. Scale bar denotes 10μms.

4.2.7.5 Confocal imaging of ODD-EGFP

In the time-line of this project, these endeavours were towards the end and so results remain in the preliminary stages, therefore only the ODD-EGFP response kinetics have been investigated to date. HeLa cells were plated into 35mm dishes and transfected with the ODD-EGFP expression vector for 24-hours, then imaged by confocal microscopy, imaging either at atmospheric O_2, 1% O_2, treated with 0.5mM DMOG or imaging through re-oxygenation (back to atmospheric O_2) following 6-hours at 1% O_2. All fluorescence levels were quantified using Cell Tracker. Dynamic changes in fluorescence were evident within the normoxic control (n= total 8 cells), further supporting the previous data suggesting a degree of normoxic stabilisation witnessed both by confocal imaging of the HIF1αEGFP and wide-field luminescence imaging of HRE-luciferase (**Fig 4.24**). Several O_2-independent mechanisms of HIF regulation

have been postulated, but the dynamic response of the ODD-EGFP reporter suggests that these can be integrated through the protein stability of just the ODD domain; also of note was the transient accumulation of fluorescence following cell division (Li, Wang et al. 2005; Liu, Baek et al. 2007; Liu, Xin et al.). Hypoxic imaging of the ODD-EGFP showed fluorescent levels to accumulate (n = 28 of 34 cells), although the distinctive sharp peak present when imaging full length HIF-1α was lost, replaced with a broader curve. Four of the total 34 cells were also found to show multiple accumulations. In contrast to our previous experiments, here we also used DMOG treatment to stimulate the accumulation of ODD-EGFP. A transient profile was present and the response profile found to be homogeneous, reaching peak max at 300 minutes. Finally, the kinetics of re-oxygenation degradation of ODD-EGFP were measured, in which a broader range of half-lives were found for the ODD-EGFP compared to the full length HIF-1α results (attained earlier in **section 4.2.5.2).** An average of 100 minutes was observed for the ODD-EGFP compared to 28 minutes for full length HIF-1α. The different kinetics observed throughout the imaging of ODD-EGFP are explainable by the lack of pro564 hydroxylation site, as it was reported by Chan *et al.* 2005 that pro564 is necessary for efficient O_2-dependent destabilisation of HIF-1α (Chan, Sutphin et al. 2005). This hypothesis will be tested in future work by imaging the frODD-EGFP, which contains both p402 and p564 hydroxylation sites. Finally, when imaging re-oxygenation using the ODD-EGFP only 10.5% (n = 2 of 19 cells) were observed to die compared to 73.75% (n = 64 of 87) for full length HIF-1αEGFP. These preliminary results highlight the potential usefulness of the ODD reporter constructs for future work investigating the single-cell response.

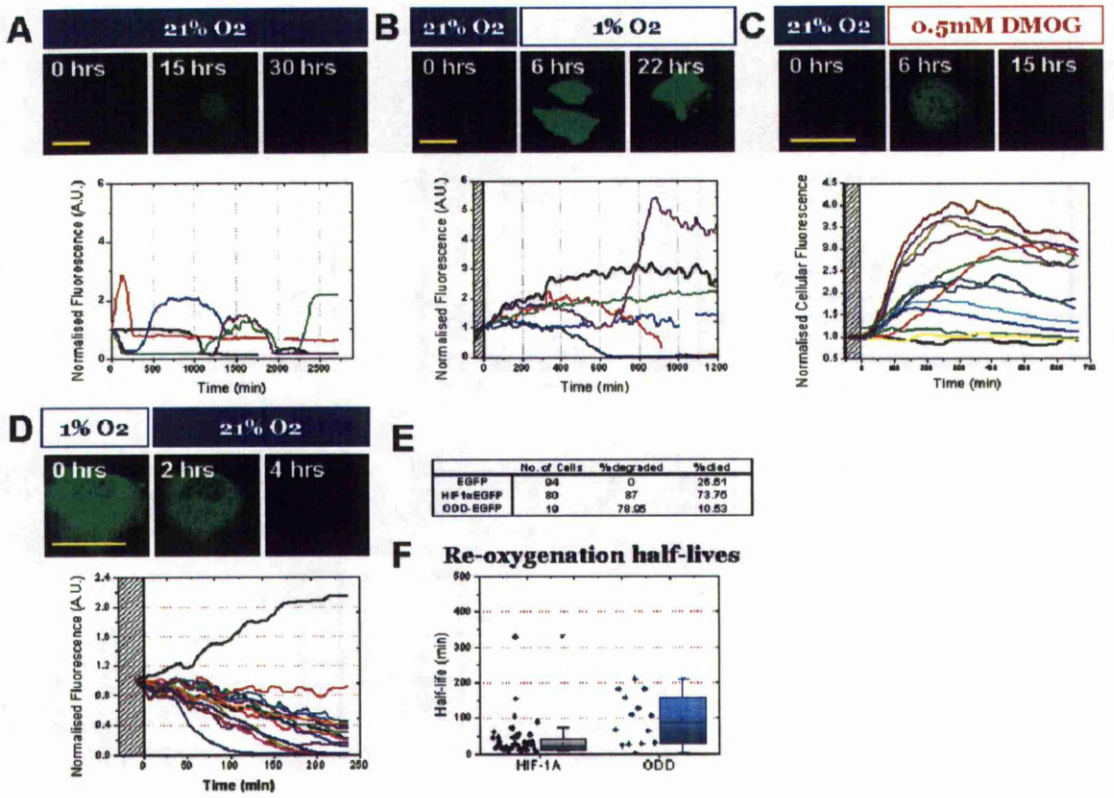

Fig 4.24. HeLa cells were transfected with pG-ODD-EGFP for 24-48 hours before imaging by confocal microscopy. (**A-D**) Representative images and several quantified traces of cellular fluorescence are shown for each condition. Scale bar denotes 50μm. Conditions used were (**A**) atmospheric O_2 for ~48 hours, (**B**) atmospheric O_2 for 1-hour followed by 20-hours of 1% O_2 (**C**) atmospheric O_2 for 1-hour followed by 16-hours 0.5mM DMOG treatment and (**D**) a re-oxygenation switch in which cells are incubated on the microscope stage at 1% O_2 for 6-hours and then returned to atmospheric O_2. (**E**) Shows the percentage cells died and where fluorescence was reduced following re-oxygenation, comparing unfused EGFP, HIF1αEGFP and ODD-EGFP transfections. (**F**) Shows the calculated half-life of fluorescence following re-oxygenation, comparing HIF1αEGFP against ODD-EGFP transfections.

4.3 Discussion

In summary, here we have undertaken the task of live-cell imaging of fluorescently labelled and ectopically expressed HIF-1α and HIF-2α in HeLa cells, exposed to either hypoxia or the reverse scenario, re-oxygenation. To our knowledge this is the first time the HIF-α system has been assessed for intracellular dynamic properties, as previous studies have made either tissue resolved measurements or have assessed protein binding using FRET studies (Serganova, Doubrovin et al. 2004; Liu, Qu et al. 2005; Wotzlaw, Otto et al. 2007; Choi, Chan et al. 2008; Konietzny, Konig et al. 2009). Our data have provided several insight into possible novel understandings of the HIF system; (1) ectopically expressed HIF-2α is similarly sensitive to oxygen as HIF-1α and HIF-2α dynamics may mask bulk-cell measurements (2) the possibility that a rich-assortment of single-cell accumulation patterns contributes to a population-wide response to hypoxia (3) that the duration of transient

accumulation was found to be robust indicating it may be an important property (4) and finally that a simple 2C mathematical model of a transcription factor directed feedback loop is sufficient to explain the majority of transient response profiles. The next chapter continues the work investigating HIF transiency and the PHD feedback, so several issues arising from this chapter are discussed later. However, a prominent feature of our single-cell data here was the manifestation of cell-to-cell variance. Our findings with regard to this will be discussed.

4.3.1 Heterogeneity and Asynchrony in the HIF system

An emerging paradigm shift is an appreciation of the role of cell-to-cell variability, especially in managing a robust population-wide response (Rausenberger, Fleck et al. 2009; Paszek, Ryan et al. 2010). It is therefore considered that heterogeneity is an important feature in many biological processes. Cell-to-cell variance was a prevalent part of the single-cell imaging data-set within this thesis, evident via the imaging of HIF-α protein and HRE transcriptional response. Such cellular heterogeneity is readily discernible via the time-lapse imaging of single living cells. This means the techniques employed here can offer powerful insights into fundamental aspects of cellular processes, albeit caution must be taken without corroborative evidence. It is therefore important to assess the validity and extent of the observed cell-to-cell variability in the HIF system and comment on the possible sources. A relationship between the cell cycle and HIF has been reported several times, though solely on the influence HIF-1/-2 has on cell cycle progression, cited that HIF-1α induces G1/S arrest and HIF-2α promotes progression (Hackenbeck, Knaup et al. 2009). Only very recently has the reverse scenario been proposed, in which the cell cycle phase influences both HIF-α signalling. A paper published by Liu *et al.* in 2010 reports that pVHL protein levels vary during the course of cell cycle, though our own data fails to support this (data not shown). More recently a paper published by Hubbi *et al.* 2011 has suggested that the cell cycle phase influences both HIF-α protein stability and transactivation via the activity of the MCM proteins (Hubbi, Luo et al. 2011). The paper also reports that the activity of HIF affects the expression of a subset of the MCM proteins, presenting then a complex arrangement of feedbacks. These results lends credence to our own findings that the cell cycle stage has a role to play in HIF protein stability, although more ideally explored without potential artefact from

transient transfection (Zabner, Fasbender et al. 1995). The conceptual relationship between the cell-cycle and the HIF system remains an interesting and plausible scenario, in which the cell balances proliferation against hypoxic responsiveness. Regardless, the cell cycle only partially explained the asynchrony and heterogeneity observed. Transient transfection was identified as a further source of heterogeneity, introducing different protein expression at both the level of HIF and downstream feedback motifs (Cohen, Kalisky et al. 2009). In spite of this, a degree of asynchrony was seen when imaging cells stably expressing HRE-luciferase (**Fig 4.22**). We would speculate that this asynchrony arises from a combination of cell-to-cell variance in crosstalk mechanisms (extrinsic events) and stochastic processes (intrinsic events). There are numerous routes for crosstalk with the HIF system and other signalling systems. And as prior mentioned, cell-to-cell variance at the protein level is to be expected, it can therefore be expected that several of the crosstalk mechanisms are operating at different levels, sensitising the HIF response differently between different cells (Cohen, Kalisky et al. 2009; Majmundar, Wong et al. 2010). Additionally, stochastic processes may also contribute to the measured heterogeneity and asynchrony. Stochasticity arises from processes revolving around small numbers in which the probability of an interaction is a dominant/important characteristic. The opposite appreciation is determinism, in which there are sufficient numbers of species interacting to treat the process as an average. In cell biology two common sources of stochasticity are receptor activation and gene expression (Alarcon and Page 2007; Lipniacki, Puszynski et al. 2007) (Cai, Friedman et al. 2006); of these only transcription is relevant to HIF signalling. The stochasticity of protein expression exists as a consequence of the low copy number of genes (normally 2) and mRNA (~$1x10^2$ molecules) (Cai, Friedman et al. 2006). From this we could expect a degree of asynchrony in the accumulation of both HIF and PHD. This concept is in line with the relative homogeneity of the half-life for loss of HIF-α protein following re-oxygenation, as the degradation of protein falls more into the realms of determinism (Chen, Niepel et al.).

4.3.2 Response kinetics; transient duration and possible implications

In stark contrast to the extensive heterogeneity observed, the duration of the transient response was found to be robust. This is an easily identifiable

temporal signature of the HIF-α response, indicating that hypoxia-induced gene expression via HIF is time limited in response. This has been proposed to be protective and enacted by the feedback activity of PHD2 (Ginouves, Ilc et al. 2008; Henze, Riedel et al.). Biological systems are capable of encoding meaningful information in a numbers of ways; a commonly appreciated form is in the amplitude of a response (Roach, Lee et al. 2005; Turner, Paszek et al. 2010; Schodel, Oikonomopoulos et al. 2011). However, there is an emerging appreciation and hypothesis for the ability of temporal kinetics to carry more contextual information (Nashat and Langer 2003; Banerjee and Slack 2005; Behar, Hao et al. 2008). The duration of HIF-α accumulation may therefore be an important aspect to the phenotype of the response, assuming that modulation of the duration of the response is possible. The observed cell-to-cell variance in response kinetics supports the possibility of modulation, in which the slow and persistent accumulation of HIF-α will lead to a varying duration of gene expression. The characterisation of transiency in both the accumulation and transactivation profile of HIF-α is far from novel and has been shown to occur at the population-wide response in several studies (Stiehl, Wirthner et al. 2006; Moroz, Carlin et al. 2009). However, the high-resolution imaging of HIF-α transiency is conducive to the development of a mathematical model, providing us with a tool to better explore the feedback responsible for transient HIF-α; previous HIF modelling attempts have suffered from lack of available suitable data as suggested by Heiner and Siriam 2010 (Heiner and Sriram 2010). Our imaging data set alongside the feedback model encourages a novel appreciation of the meaning and implication of the temporal arrangement of HIF signalling. Several studies over the last decade have begun to suggest ways in which duration of transcription factor activity can translate to phenotypic consequences. The two encompassing modes-of-action occur at the level of gene expression and/or in the threshold response to levels of protein (Vousden 2006).

The genomic landscape is dynamic, switching between active and inactive conformations bound at different times to different proteins and complexes (Xie, Yang et al. 2007). Over the course of transcription factor activation, the genomic landscape can therefore change leading to different gene expression (Boellmann, Zhang et al. 2010). In support the possible role of HIF in this level mechanism, HIF has been several times cited to affect the histone

acetyltransferases and histone deacetylases, modulators of chromatin (Johnson and Barton 2007). Specifically, it has been reported that jumonji domain containing 1a (JMJD1A) is a HIF-target gene and which acts to alter the epigenetic status of a subset of other HIF genes, thereby creating a feed-forward method in which HIF gene expression is altered over time (Perez-Perri, Acevedo et al. 2011). Alternatively, the duration of activation of a transcription factor such as HIF may exert different phenotypes through the triggering of downstream protein sensitive thresholds (Callus, Moujallad et al. 2008). For example, ongoing expression of a pro-apoptotic protein will need to occur for a specific period of time until a threshold decision is reached and the cell commits to apoptosis. This has been demonstrated by Schwartz *et al.* (2011) in glutocorticoid signalling of cell death (Schwartz, Sarvaiya et al. 2010). Whether these concepts are important with regards to HIF-signalling hinges upon whether or not the duration of HIF accumulation can be physiologically or pathologically altered to a significant enough degree. In the introduction of this thesis, the differing ways a hypoxic episode may take place was discussed. The insult was described to occur in an acute, prolonged or intermittent manner. This represents a very simple way to modulate the duration of the hypoxic episode, possibly resulting in differing durations of activated HIF signalling.

Chapter 5: Dissecting the role of the individual PHD proteins on the transient accumulation of HIF-α

5.1 Introduction & Aims

The accumulated results from the previous chapter directed the abstraction and parameterisation of a 2-component model detailing the HIF-PHD negative feedback motif. However, the data underpinning this has focused only on the measurement of the HIF-α component. To increase the fidelity of the model an approach was devised to measure parameters pertaining to the PHD feedback. Currently the model-described-feedback is a concatenation of all PHD proteins, and so the relation of experimental measurements into model terms is difficult as we are unable to directly measure the concatenation of parameters with confidence. The next rational step was therefore to separate the model-described-feedback into the separate PHD components, detailing each individual protein.

5.1.1 Sensitivity analysis of 2C-model to support aims

The rationality for this step was further strengthened as parameter analysis of the 2-component model indicated that the most sensitive values were both the PHD induction rate (k) and PHD protein degradation rate (d) (**Fig 5.1**) A PHD-resolved model can act as a starting point in understanding the role of the individual PHDs and the consequences of their pharmacological inhibition/induction. This is relevant to the large amount of work designing pharmacological agents targeting downstream HIF activity. A common way to achieve this is via the targeting of PHDs (Nangaku, Kojima et al. 2006; Niatsetskaya, Basso et al. 2010; Smith and Talbot 2010). For all these reasons, the model was expanded into a 4-component form describing a generic transcriptionally active HIF-α interacting with or influencing PHD1, PHD2 and PHD3. This model is referred to as the 4C-model or resolved PHD model.

5.1.2 Expanded model architecture; The resolved PHD model

The expansion of the 2C-model requires little re-formulating of the model architecture. The abstractions generally remain untouched for all species involved; protein and mRNA remain constrained as a single entity (**Fig 5.2**). The ODE depicting HIF-α (**dx/dt**) has been expanded to incorporate the degradation from the hydroxylase activities of all 3 PHD proteins. This in turn requires the resolution of several parameters. The hydroxylation rate now has three terms, $h1$, $h2$ and $h3$.

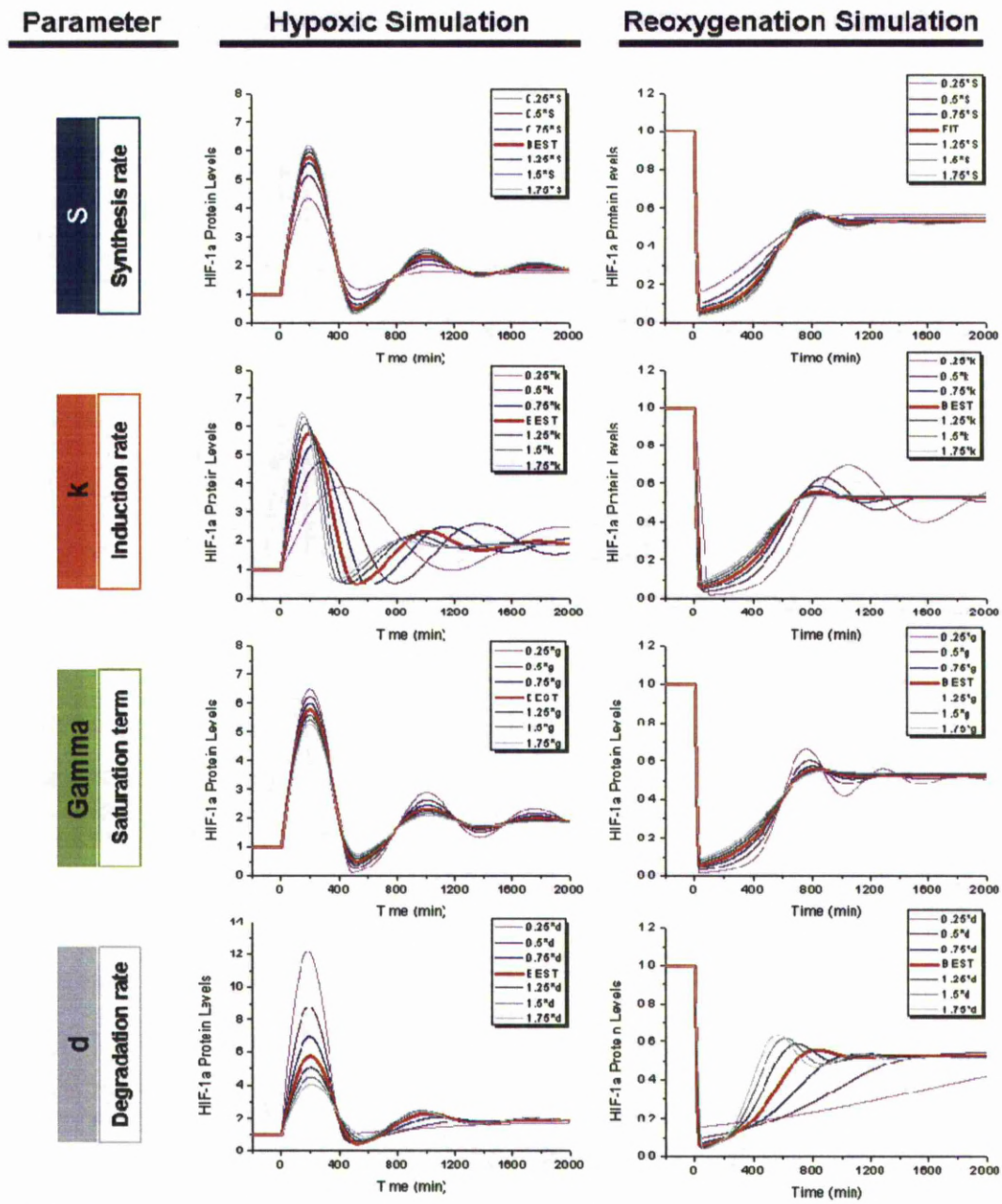

Fig 5.1. Parameter sensitivity analysis of the 2C-model. Parameter values *S*, *k*, *γ* and *d* were altered and the corresponding response profile for HIF-α plotted for both hypoxic and re-oxygenation simulations. Equilibration value was normalised to 1. (NB. This parameter sensitivity was performed on a previous fitting of the 2C-model. Though the parameter values have now changed the sensitivity remains the same for the current parameterisation)

Previous publications have suggested the hydroxylation rate to be different between the three PHDs and so to take this into account it was necessary to separate these terms (Tuckerman, Zhao et al. 2004; Stiehl, Wirthner et al. 2006). In contrast, the saturation function for all three PHDs is maintained using the single parameter γ. The rationale behind the use of a single γ is the apparent insensitivity of the term, having a more qualitative function than quantitative (**Fig 5.1**). Finally, the ODE detailing the generic PHD has been

resolved to three separate ODE's describing non-inducible PHD1 (**y1/dt**), inducible PHD2 (**y2/dt**) and inducible PHD3 (**y3/dt**). This gave rise to an important change to the architecture of the model; in the previous model PHD synthesis was solely attributable to HIF-α. The inclusion of PHD1 and the aim to quantify PHD2 and PHD3 inducibility led us to include a synthesis rate for each PHD, *S1*, S2 and S3.

$$\frac{dx}{dt} = S - h_1 y_1 \left(\frac{x}{x+\gamma_1}\right) - h_1 y_1 \left(\frac{x}{x+\gamma_1}\right) - h_1 y_1 \left(\frac{x}{x+\gamma_1}\right)$$

HIFα — Basal Synthesis — PHD1 Hydroxylation — PHD2 Hydroxylation — PHD3 Hydroxylation

$$\frac{dy_1}{dt} = S_1 - d_1 y_1$$

PHD1 — Basal Synthesis — Basal Degradation

$$\frac{dy_2}{dt} = S_2 + k_2 x - d_2 y_2$$

PHD2 — Basal Synthesis — Induced Transcription — Basal Degradation

$$\frac{dy_3}{dt} = S_3 + k_3 x - d_3 y_3$$

PHD3 — Basal Synthesis — Induced Transcription — Basal Degradation

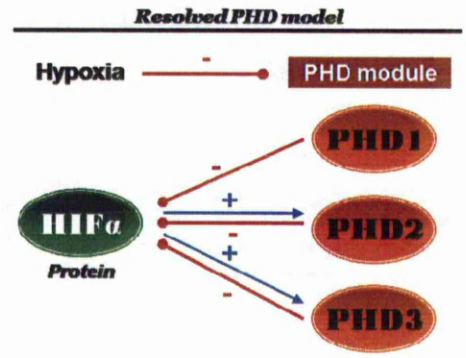

Fig 5.2. The ODE's for the resolved PHD model are shown with the corresponding biological process highlighted underneath. (**Right**) A diagrammatic representation of the resolved PHD model.

5.2 Results

5.2.1 New molecular tools to investigate PHD feedback

5.2.1.1 Functionality of PHD fluorescent fusion expression vectors

Ideally the 4-component model would be parameterised against single-cell data in the same vein as for the HIF-1α component. In order to do this, we aimed to attain and validate the use of fluorescent fusion vectors for PHD1, PHD2 and PHD3. All three expression vectors were kindly donated to our lab courtesy of Dr. Eric Metzen (PHD1 and PHD3) and Professor Reinhard Depping (PHD2). All PHD expression plasmids were transfected into HeLa cells and the localisation of the protein assessed by live-cell confocal microscopy (**Fig 5.3**). As has been previously shown by Metzen *et al.* (2003), we found PHD1 to be strongly localised to the cell nucleus, PHD2 to be predominantly cytoplasmic and PHD3 to be ubiquitous throughout the cell (Metzen, Berchner-

Pfannschmidt et al. 2003). Also observed for the expression of PHD3, were small punctate fluorescent speckles found in the cytoplasm. A 2008 publication from Rantanen *et al.* have shown this localisation for PHD3, suggesting these structures to be oxygen-dependent aggregates related to the proteasomal machinery (discussed further in chapter 6) (Rantanen, Pursiheimo et al. 2008). To further confirm the functionality of the expressed fluorescent PHD proteins, endpoint luminometry was used to assay the effect of co-expression of the PHD fusion vectors alongside the HRE luciferase reporter. HeLa cells were plated into 24-well plates at a density of 1x105 cells per ml and a volume of 0.5ml per well. Cells were then transfected to co-express the HRE-luciferase together with either PHD1-EGFP, PHD2-EGFP or PHD3-EGFP. After 24 hours transfection, cells either remained un-stimulated or were additionally treated for 6-hours with 0.5mM DMOG or incubated at 1% O_2. After this period, cells were lysed and samples analysed by luminometry (**Fig 5.3**).

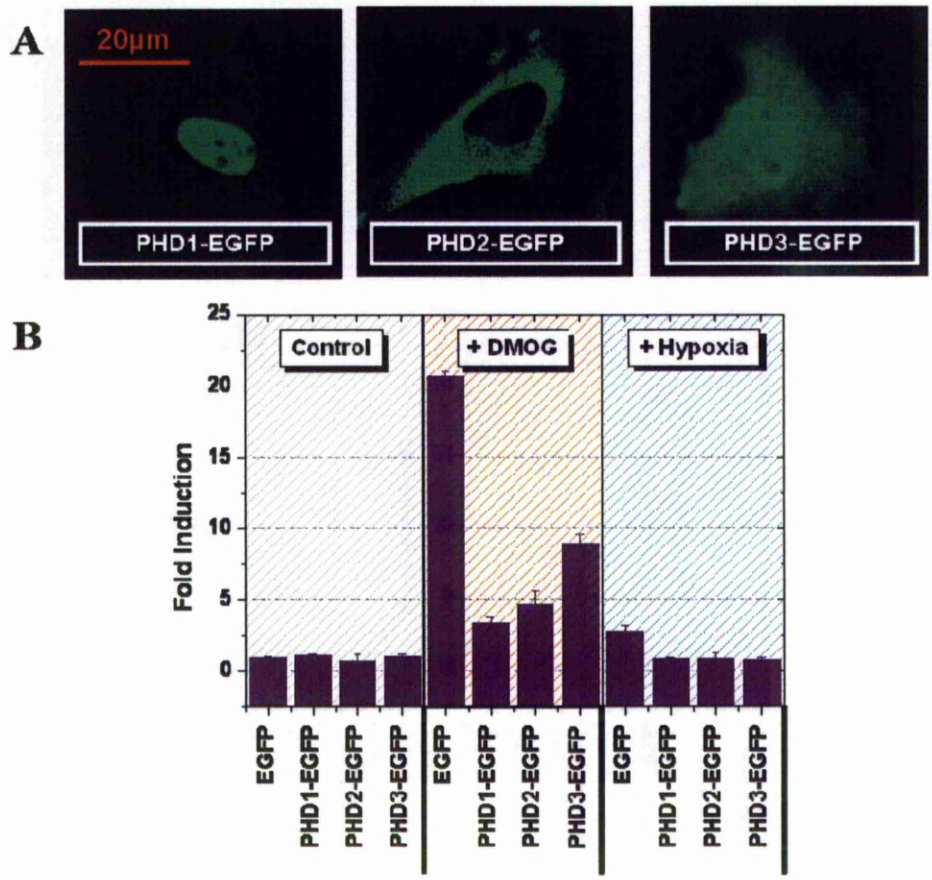

Fig 5.3. (**A**) Confocal images of HeLa cells ectopically expressing fluorescent fusion PHD isoforms. (**B**) Endpoint luminometry assay of samples prepared from cells co-transfected with pG-TK-HRE-luc and a PHD isoform expression vector then further treated with either 0.5mM DMOG or 1% O_2 for 8 hours. (n=1 repetition performed in triplicate)

Co-expression of all PHD vectors reduced the stimulated induction of the HRE-luciferase reporter compared to the EGFP control. For the unstimulted condition, no significant difference was observed between the co-expression of the PHDs versus the unfused EGFP. This may suggest that the hydroxylase-dependent degradation has reached maximal rate and that the addition of more PHDs are surplus to requirement. In hypoxia all PHDs were seen to reduce luciferase signal equally, although when stimulating the cells with DMOG, PHD1 was seen to reduce HRE-luciferase to the greatest degree, followed by PHD2 and then PHD3. This is perhaps surprising given that PHD1 has been cited to only weakly hydroxylate HIF-α compared to PHD2 and PHD3 (Appelhoff, Tian et al. 2004; Tuckerman, Zhao et al. 2004).

5.2.1.2 Generation of HIF-inducible PHD2 and PHD3 expression plasmids

In this chapter we aim to image the PHD2 and PHD3 feedback kinetics using fluorescent fusion expression plasmids. However, whereas HIF-α accumulation kinetics are determined at the protein level PHD protein accumulation requires mRNA upregulation and therefore the CMV promoter is unsuitable to drive expression. To address this we proposed to replace the CMV promoter of the PHD fluorescent fusion vectors with a HIF inducible promoter, either proximal promoters or consensus promoters. As consensus reporters only have a minimum amount of promoter architecture (~5-15bp) the preferential aim was to synthesise expression vectors that use a functional proximal promoter sequence (~100-4000bp). Two luciferase reporter plasmids were purchased from SwitchGear Genomics that contain 1000bp sequences upstream of the transcriptional start sequence for PHD2 and PHD3. Before using these sequences as templates to generate inducible PHD expression vectors, the luciferase reporters were assessed under hypoxic stimulation for up to 24 hours by endpoint luminometry (**Fig 5.4**). HeLa cells were transfected for 24 hours with either PHD2-luciferase or PHD3-luciferase. Samples were then introduced at staggered time-points over the course of 24-hours into a 1% O_2 hypoxic chamber. After incubation cells were lysed simultaneously and samples prepared for endpoint luminometry analysis. PHD2-luciferase was found to significantly increase after 8 hours of incubation whereas no significant inducibility was seen when using the PHD3-luciferase. This is in accordance with the literature, which indicates that the functional PHD2 HRE consensus is

0.5kb upstream of the translational start site and the functional PHD3 HRE site is 12kb away, therefore outside of the 1000bp proximal promoter sequence contained within the PHD3-luciferase (Metzen, Stiehl et al. 2005; Pescador, Cuevas et al. 2005).

Concluding from these results, a HIF-inducible PHD2 fusion vector was made using the 1000bp proximal promoter from PHD2-luciferase as a template and this sequence was used to replace the existing CMV promoter from the pPHD2-EGFP expression plasmid; this new plasmid is termed p-pro-PHD2EGFP. However, we decided against doing the same using the PHD3-luciferase signal as the promoter architecture was shown to be hypoxia insensitive (**Fig 5.4**). For future work, there are several options available to enable the imaging of the PHD3 feedback. Firstly a bacterial artificial chromosome could be employed and this would have the advantage of endogenous promoter architecture, encompassing on an average 200kb of sequence (Tunster, Van De Pette et al. 2010). However, there are disadvantages with this approach, most notably the construction of a fluorescent protein expressing BAC is considerably more difficult and time consuming than a plasmid (Adamson *et al.* 2011, in preparation). For this purpose I have disregarded the imaging of the PHD3 feedback within the timeframe of my own project.

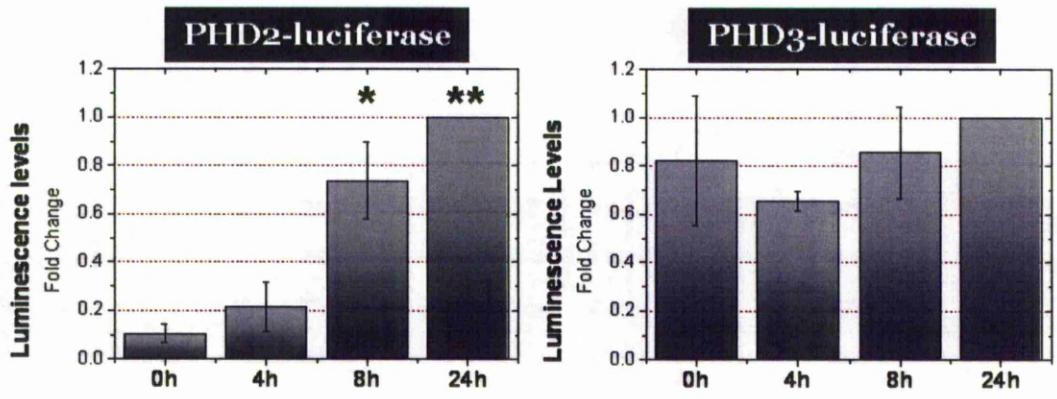

Fig 5.4. Endpoint luminometry assay of samples prepared from HeLa cells that had been transfected with either a PHD2 or PHD3 luciferase reporter for 24 hours and then exposed to 1% O_2 for up to a further 24-hours. Results are normalised to t24. Significance was determined using one-way anova; values lower than 0.05 are denoted * and values lower than 0.01 as **.

5.2.2 Parameterising the model

The expansion of the model has led to the creation of 10 new parameters and thereby has increased the parameter space. The following section describes experiments aimed at constraining these parameters to measured values.

5.2.2.1 Measurement of basal synthesis values for PHDs: *S1*, *S2*, *S3*

The 4C-model has introduced a HIF-independent term for synthesis of the PHDs, *S1, S2 and S3*. These function as an encompassing term allowing for a degree of non-dynamic PHD expression from other sources, essential for PHD1 which is not HIF-inducible (Treins, Giorgetti-Peraldi et al. 2005; Fong and Takeda 2008; Jokilehto and Jaakkola 2010). RT-qPCR can provide evidence to the relative abundance of mRNA within a sample and from these values we can extrapolate values for protein synthesis rates, as has been performed in a recent publication by Harper *et al.* (2010) (Harper, Finkenstadt et al. 2011). Following this principal, we aimed to relatively measure PHD1, -2 and -3 mRNA using RT-qPCR. HeLa cells were plated into 6cm dishes at atmospheric O_2 and cultured for 24 hours. The rationale behind using a normoxic sample was to minimise contamination of the estimation of basal synthesis (*S2* and *S3*) with induced synthesis (*k2* & *k3*). At ~80% cell confluency cells were lysed. RNA was extracted from the lysates and then used for cDNA conversion. The cDNA templates were then used alongside PHD1, 2 and 3 targeting primers for RT-qPCR measurements (**Fig 5.5.**). Using this approach, PHD3 was found to be the most abundant mRNA passing the threshold point 1.57±0.15 cycles before PHD1 and 8.48±0.49 cycles before PHD2. These differences were then raised to the power of the measured efficiency of the primers used in order to determine the relative difference in mRNA abundance. *Via* this calculation, we concluded that in relation to PHD3, PHD1 and PHD2 are 2.3 and 38.9 fold less abundant. We then applied this relationship to the corresponding *S* values used in the model.

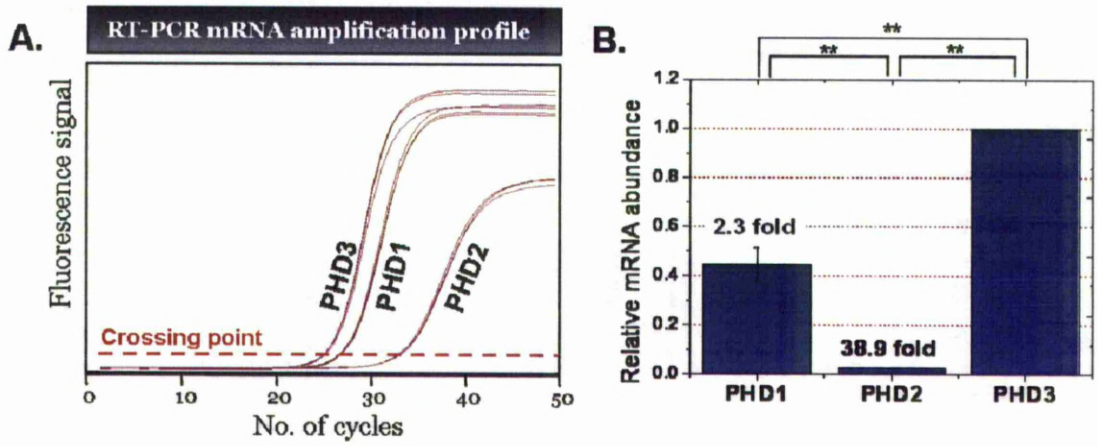

Fig 5.5. HeLa cells were plated and maintained in atmospheric oxygen prior to sample preparation for RT-qPCR analysis. (**A**) RT-qPCR comparing amplification profile of mRNA in which the crossing point has been added on manually and (**B**) the calculated relative abundance of mRNA compared to PHD3; value of reduction is also shown. All conditions are found to be significantly different (p=<0.01 = **) by one-way ANOVA. (n=3 biological repetitions, S.E.M. is shown)

In further support of these findings, the luminometry results attained using PHD2-luciferase and PHD3-luciferase were revisited (previously measured in **Fig 5.4**) and the signal ratio for the normoxic samples compared (**Fig 5.6**). Mimicking the trend observed by RT-qPCR, signal from PHD3-luc was found to be on average 35-fold greater than signal from PHD2-luc.

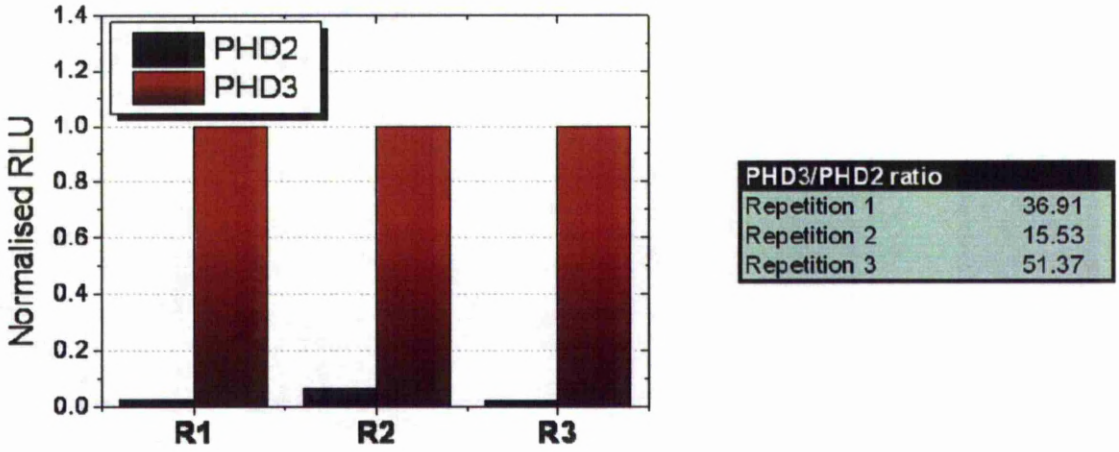

Fig 5.6. Endpoint luminometry assay of samples prepared from HeLa cells that had been transfected with either a PHD2 or PHD3 luciferase reporter for 24 hours. Cells were left unstimulated before lysis and sample preparation. Data shows three repetitions of luminescence measurement normalised to PHD3 signal. Statistical significance of PHD2 vs PHD3 is <0.05 measured by one-way ANOVA.

5.2.2.2 Induction of feedback: *k2* & *k3*

The PHD feedback loop hinges upon the assumption that hypoxia up-regulates PHD mRNA production in a HIF-dependent manner. This principle is given as the rate term k in the 2-component model. Previous reports by Stiehl *et al.* (2006) and Appelhof *et al.* (2004) suggest that the level of rate of induction may differ between PHD2 and PHD3, moreover this difference was found to vary across cell types (Appelhoff, Tian et al. 2004; Stiehl, Wirthner et al. 2006). Additionally a publication by Erez *et al.* (2004) suggested PHD1 mRNA to be down-regulated by hypoxia and this would have ramifications on the 4C-model topology (Erez, Stambolsky et al. 2004). As these are critical issue for the parameterisation of the model, we sought to investigate the hypoxic induction kinetics (and potential) of the individual PHD proteins. Samples were prepared from HeLa cells incubated over a time-course of 1% O_2. The relative mRNA profile was then measured by RT-qPCR for PHD1, PHD2 and PHD3 (primers listed in chapter 2) (**Fig 5.7**).

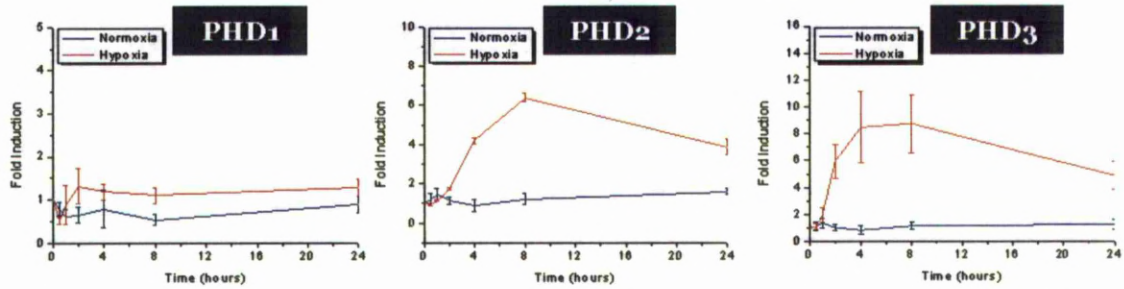

Fig 5.7. RT-qPCR measurement of samples prepared from HeLa cells that were incubated for a time course of 24-hours at either 1% O_2 or atmospheric O_2. (n=2 hypoxia and n=1 normoxia; error bars are from the technical quadruplicates from a single biological repetition)

Both PHD2 and PHD3 were found to be inducible whereas PHD1 mRNA levels remained largely unchanged, thereby conforming to the general published consensus (Epstein, Gleadle et al. 2001; Treins, Giorgetti-Peraldi et al. 2005; Stiehl, Wirthner et al. 2006). In contradiction to the findings of Stiehl *et al.* (2006) and Appelhof *et al.* (2004), the kinetics of PHD2 and PHD3 induction were found to be largely similar, suggesting that *k2* and *k3* rate terms can be kept equal.

5.2.2.3 Measurement of degradation rate of the PHD proteins: *d1*,*d2* & *d3*

Parameter sensitivity analysis on the 2-component model indicated that variance in the degradation rate of the feedback protein is important for the HIF-α accumulation profile (as shown previously in **Fig 5.1**). The expansion of the 2-component model to resolve the individual PHD proteins may require the use of three separate intrinsic degradation rates (*d*) depending on how significantly different these values may be. To our knowledge the relative protein stabilities of all three PHD isoforms have not been reported, although Tian *et al.* (2006) showed PHD1 and PHD3 to differ significantly using cells treated with cycloheximide and analysing samples by western blot (Tian, Mole et al. 2006). Additionally it has also been shown that PHD1, PHD2 and PHD3 protein stabilities are regulated by different mechanisms. PHD1 and PHD3 are subject to destabilisation by the activities of seven in abstentia homology 1 and 2 (SIAH1 & 2) and PHD2 is destabilised by FKBP38 (Barth, Nesper et al. 2007; House, Moller et al. 2009). These findings support the likelihood that the PHD protein stabilities differ between isoforms and that the controlling parameter values would need to be properly resolved for the mathematical model.

Currently the degradation rate (*d*) fit for the 2-component model can be considered as a concatenation of both PHD2 and PHD3, however without

additional information this value cannot be rationally split and any attempt at refitting the expanded model may be subject to excessively free parameter space. Thus, to constrain the model appropriately we aimed to measure the degradation rate of the individual PHDs. To achieve this we utilised the single-cell imaging of HeLa cells ectopically expressing fluorescently labelled PHD1, -2 or -3 and treated cells with cycloheximide, a drug commonly employed to induce translational arrest in eukaryotes (Siegel and Sisler 1963; Schneider-Poetsch, Ju et al. 2010). The loss of fluorescence was then monitored for up to 16 hours. All visualised fluorescent cell data was quantified and the half-life of fluorescence for each cell calculated. PHD3 was found to degrade the fastest with a mean half-life of 98±33 minutes, followed by PHD1 at 618±303 minutes and then PHD2 at 669±369 minutes (**Fig 5.8**). These values were converted to rate constants then subsequently used to parameterise the model (values used are shown later in **Table 5.1**). Once again the single-cell approach also afforded us the ability to see cell-to-cell variance in the degradation profiles, indicating that average behaviour must be taken with caution as many cells were not average (Levsky and Singer 2003). The observed heterogeneity in degradation was quantitatively assessed by calculating the Fano factor (variance over the mean) for each PHD (Masuda and Doiron 2007; Paszek, Ryan et al. 2010). PHD3 was found to have the most homogenous degradation profile with a Fano factor of 9, followed by PHD1 with 96 and PHD2 with 295.

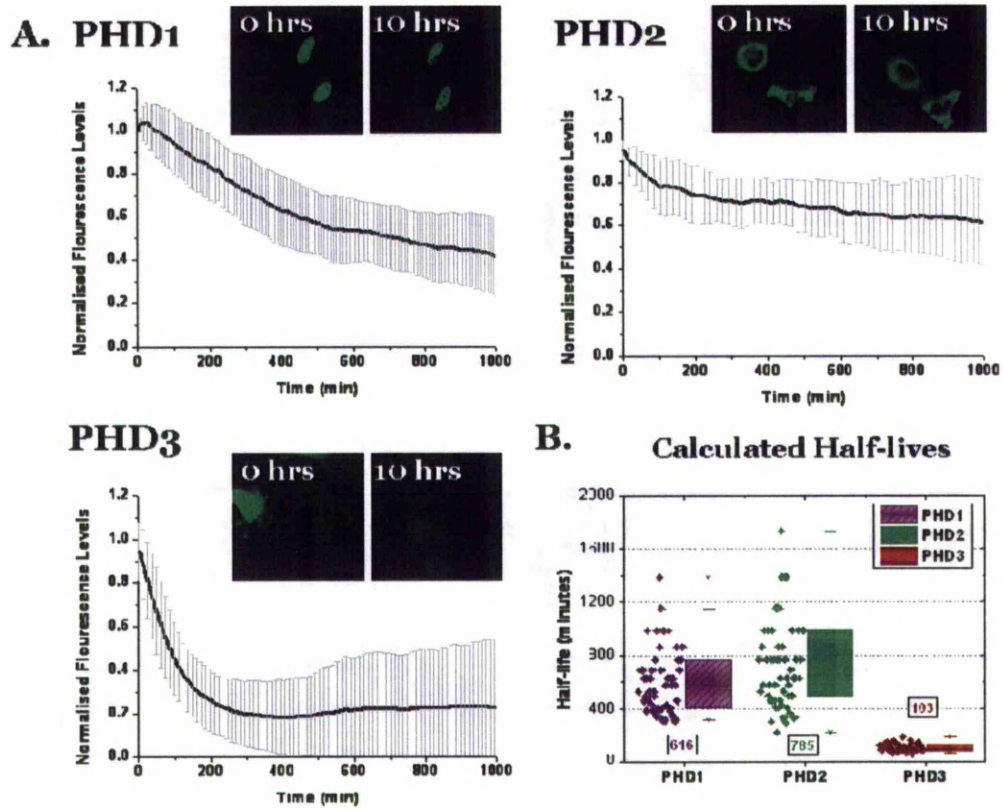

Fig 5.8. (**A**) Time-lapse imaging of HeLa cells ectopically expressing fluorescent PHD and treated with 10μg/μl cycloheximide. A plot of the normalised average cell fluorescence is shown for each condition (showing a single repetition of three), with standard error indicated. (**B**) A box-and-whisker plot shows the calculated half-lives with the mean average half-life numerically stated.

Our results concerning PHD protein stability are in agreement with the limited selection of other published values (Tian, Mole et al. 2006; Barth, Nesper et al. 2007). However, our approach taken to measure PHD degradation rates remains open to criticism. Firstly, rather than measuring endogenous PHD stability we have measured the fluorescent fusion form and it is therefore possible that the novel protein degrades differently to the native form (Schwanhausser, Busse et al. 2011; Yewdell, Lacsina et al. 2011). Secondly cycloheximide is often used as a standard approach towards the measurement of protein stability in spite of the possibility of detrimental or confounding issues. Cycloheximide is unable to completely arrest translation of the specific protein of interest. This means that some degree of protein synthesis is ongoing and thereby confounds an accurate measurement of degradation. Also, as cycloheximide acts on all protein synthesis it equally acts on proteins that may be responsible for the degradation or regulation of the measured protein. Loss of a negative regulator would undoubtedly lead to an extended half-life of the measured protein of interest (Yewdell, Lacsina et al. 2011), a concept made

prominent by the purported destabilisation of PHDs by the SIAH proteins (House, Moller et al. 2009). Following these concerns, future efforts should be made to reinforce these measurements using one of many available methodologies, including the recently outlined global protein stability profiling by Yen *et al.* (2008) and the dynamic stable isotope labelling with amino acids (dynamic SILAC) reported by Doherty *et al.* (2009) (Yen, Xu et al. 2008; Doherty, Hammond et al. 2009).

5.2.3 Single-cell imaging of HIF-inducible PHD2-EGFP

Constraining the degradation terms (*d1*, *d2*, *d3*), basal synthesis rates (*s1*, *s2*, *s3*) and induction terms (*k2*, *k3*) still leaves the PHD feedback kinetics unexplored and unaccounted for. In the case of the 2-component feedback model all parameters were fit against HIF-1α imaging data, leaving the feedback un-visualised. The next aim was to therefore image the PHD2 feedback kinetics and then use this data to fit against the 4-component model. The proximal promoter driven PHD2EGFP expression vector constructed earlier in this chapter was used for this purpose. The expression vector was transfected into HeLa cells alongside a unfused DsRedxp control vector and after 24-48 hours transfection, imaged by confocal microscopy (**Fig 5.9**). The expression level of PHD2 appears to have been greatly reduced compared to the CMV version and is thereby more difficult to detect. Therefore fields containing DsRedxp expressing cells were chosen and these were then imaged for ~20h in either 1% O_2 or 21% O_2. An increase in green fluorescence was observed in 6.98% (n=6 of 86 cells) of red expressing cells at 20.8% O_2 and 34.6% (n=44 of 131 cells) of instances at 1% O_2. Cells showing a change in green fluorescence had their cytoplasmic fluorescence intensity quantified. In contrast to the diverse kinetics seen for HIF-α, PHD2 showed a consistent increase which in several cases reaches a plateau within the experiment time-frame. Despite the robust accumulation pattern the response time was again found to vary over the entirety of the experiment time frame. The amplitude was also found to vary though no strong correlation was found between amplitude and time of response (data not shown). An interesting facet of this experiment is that the PHD2-EGFP response is driven by endogenous HIF, this may partially explain the relatively subtle amplitude of response when using the p-pro-PHD2-EGFP compared to imaging HIF-1α/-2α.

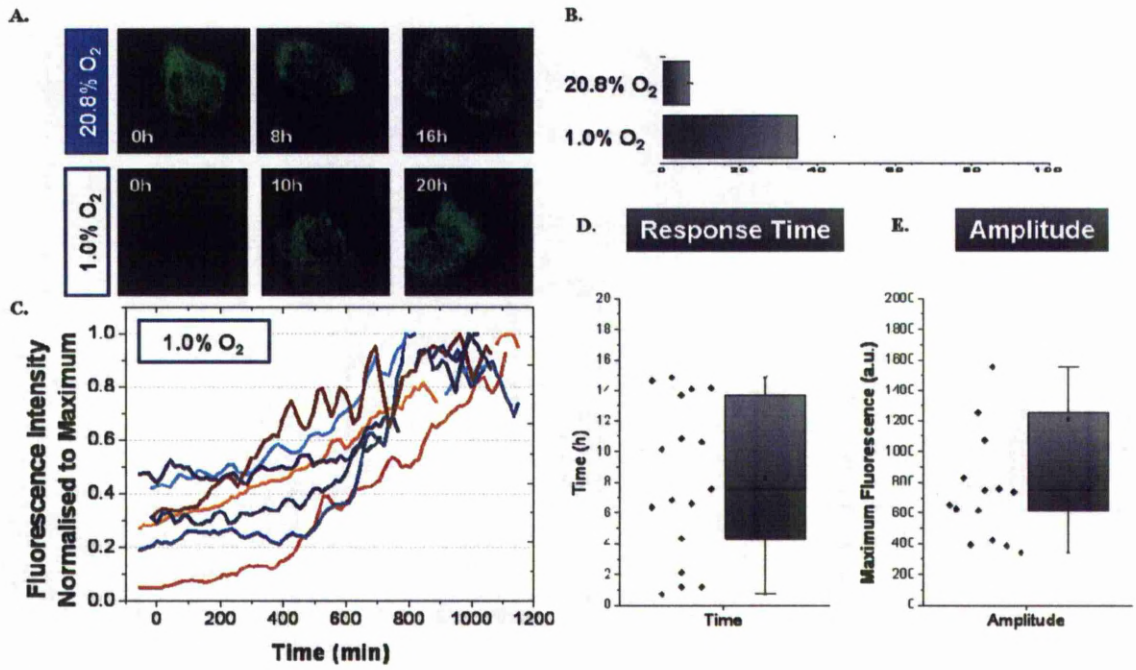

Fig 5.9. (**A**) EGFP channel images from time-lapse microscopy of HeLa cells transfected with p-proPHD2EGFP and DsRedxp then either incubated in normoxic (~21% O_2)or hypoxic (1%O_2) conditions. (**B**) Percentage of average red cells that show an induction in PHD2EGFP. (**C**) Representative traces of cellular PHD2 fluorescence during hypoxia. Analysis of quantified cells, calculating (**D**) response time and (**E**) maximum amplitude.

The 2C-model was raised against imaging of HIF-1αEGFP and this model served as the basis for the expansion to the 4C-model. Originally therefore, the HIF-1α creation rate (S) was derived from a CMV expressed version of HIF-1α and this is likely to be very different to the endogenous value (Qin, Zhang et al. 2010). To keep the model in line with the HIF-α imaging data we decided to continue using the 2C-model fitted S value and decided against pursuing a measurement of endogenous HIF-1α synthesis rate. However, using the imaged PHD2 feedback data it is very possible to refit this endogenous *S* value. Previously in the 2C-model, the PHD feedback was fit using the HIF1α-EGFP imaging data (**Fig 4.16.**). In the same manner, the HIF-1α profile could be reconstructed using the pro-PHD2-EGFP data. Importantly, the pro-PHD2-EGFP feedback is driven by the endogenous HIF-α and so the endogenous creation rate could therefore be suggested from this data.

5.2.4 4C-model parameterised and outputs generated

The parameter measurements carried out throughout this chapter were introduced into the 4C-model, leading to the total measurement of eight of twelve criteria and six of ten parameter rates (**Table 5.1**). Additionally the hydroxylation rates were expanded to include hydroxylation of HIF-1α by all

three PHD isoforms, using data published by Tuckerman *et al.* (2004). Using these values PHD1 has a slower hydroxylation rate than PHD2 and PHD3 by almost five-fold. Finally several unmeasured values were either carried across from fitting in the 2C-model or refit using the 4C-model framework; including S^* (PHD synthesis rate), Sx (HIF-1α synthesis rate), k (PHD induction rate) and γ (saturation of hydroxylation term).

Parameters		Units	Value	Source
S1:S2:S3=S*	'Synthesis ratios'		0.44:0.03:1	**Measured** (section 5.2.2.1)
S*	'HIF Synthesis rate'	$AUmin^{-1}$	7.6×10^{-11}	Fitted in 4-component model
d1	'PHD1 degradation rate'	min^{-1}	1.13×10^{-3}	**Measured** (section 5.2.2.3)
d2	'PHD2 degradation rate'	min^{-1}	8.83×10^{-4}	**Measured** (section 5.2.2.3)
d3	'PHD3 degradation rate'	min^{-1}	6.74×10^{-3}	**Measured** (section 5.2.2.3)
k2:k3 = k	'Induction ratios'		1:1	**Measured** (section 5.2.2.2)
k	'PHD Induction rate'	min^{-1}	7.10×10^{-4}	Fitted in 2-component model
γ	'Saturation function'	AU	1.83×10^{4}	Fitted in 2-component model
h1	'PHD1 hydroxylation rate'	min^{-1}	0.25 →0.035	**Measured** (Tuckerman *et al.* 2004)
h2	'PHD2 hydroxylation rate'	min^{-1}	1 → 0.135	**Measured** (Tuckerman *et al.* 2004)
h3	'PHD3 hydroxylation rate'	min^{-1}	1.25 → 0.133	**Measured** (Tuckerman *et al.* 2004)

Table 5.1. Table of parameters, units and values used in 4C-model. Also included is a list of the method of parameter rate determination and corresponding reference to the measurements. The hydroxylation rate values are shown for the switch from 21% O_2 to 1% O_2. (NB. A revision to the parameters is underway and so the values for k and s* are likely to change)

After parameterisation, the 4C-model was used to simulate the protein level response of HIF-1α, PHD1, PHD2 and PHD3 following an episode of 1% O_2 (dropping from atmospheric oxygen) (**Fig 5.10**). The simulated response retained all the qualitative features of the biological response; HIF-1α protein accumulated transiently, PHD2 and PHD3 were up-regulated and PHD1 levels remained constant throughout. The response to re-oxygenation was also simulated; occurring as 1% O_2 for 6-hours and then re-oxygenation back to 21% O_2.

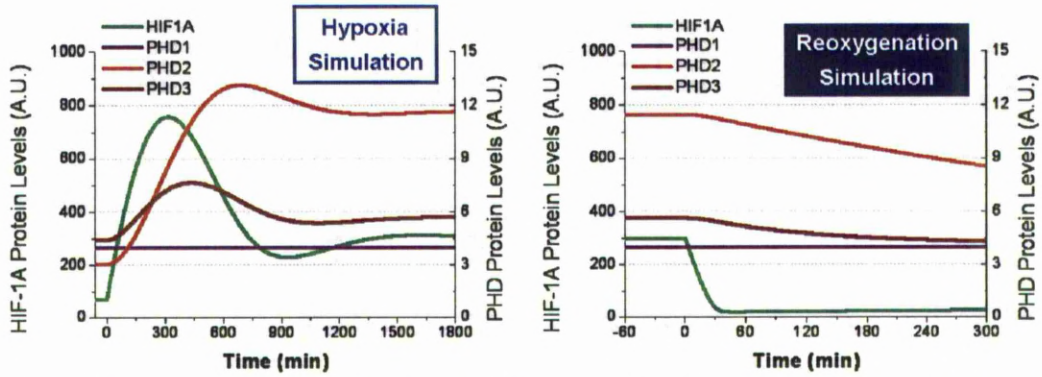

Fig 5.10. The 4c-model was used to simulate the protein level response of HIF-1α, PHD1, PHD2 and PHD3 following an episode of 1% O_2 (dropping from atmospheric oxygen). The response to re-oxygenation was also simulated; occurring as 1% O_2 for 6-hours and then re-oxygenation back to 21% O_2.

5.2.5 Removal of PHD2 feedback

With the completion of the 4C-model, it was considered prudent to further validate the model against biological data. The 4C-model is capable of assessing the impact of removing PHD2 *in silico* and this is also readily performed biologically. HeLa cells stably expressing short hairpin RNA targeted against PHD2 (ShPHD2 cells) were kindly donated by Dr. D. Stiehl and Prof. R. Wenger (Zurich). Our initial goal after receiving these ShPHD2 cells was to confirm the knockdown of PHD2.

5.2.5.1 Validation of knockdown

Knockdown of PHD2 was confirmed using western blot analysis (**Fig 5.11**). ShPHD2 and HeLa cells were plated into 6cm dishes and later incubated for 4 hours in either atmospheric conditions or 1% O_2 prior to lysis and sample preparation. The absence/reduction of PHD2 protein was confirmed and no accumulation of PHD2 protein in hypoxia was seen. Furthermore PHD3 was not seen to strongly compensate for the loss of PHD2. Though it is worth noting we were unable to convincingly detect an upregulation of PHD2 protein in either ShPHD2 cells or wild-type cells, most likely on account of the short time course used and low amplitude of response. Both cell lines were found to be inducible for HIF-1α within this time frame. The ShPHD2 cells were deemed suitable for further experimentation.

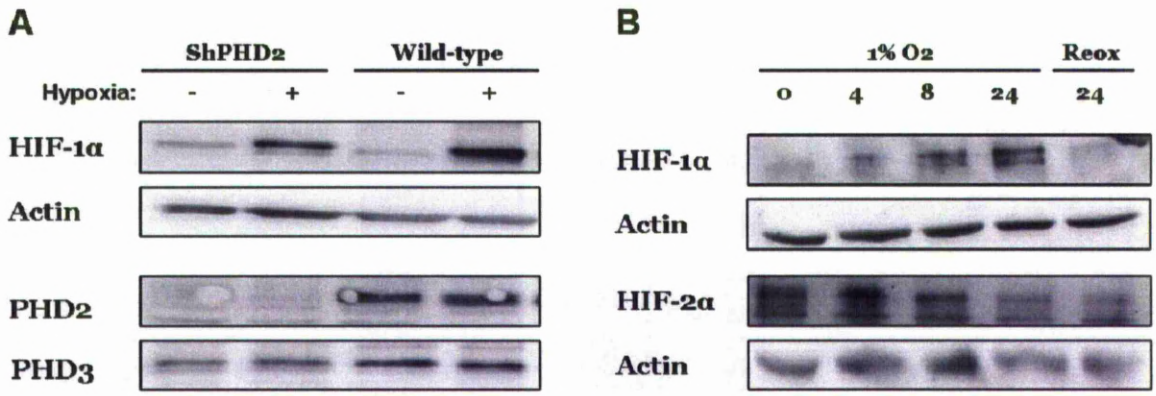

Fig 5.11. (**A**) ShPHD2 and HeLa cells were plated into 6cm dishes and later incubated for 4 hours in either atmospheric conditions or 1% O_2 prior to lysis and sample preparation (+) for 4 hours. Prepared samples were then analysed by western blot, probing for HIF-1α, PHD2 and PHD3.protein (**B**) Samples prepared from ShPHD2 cells were analysed by Western blot to examine the HIF-α response to hypoxia and a subsequent 15-minute re-oxygenation back to atmospheric levels.

5.2.5.2 Western blot analysis of HIF-α accumulation in ShPHD2 cells

Next, using the ShPHD2 cells we examined the population-wide accumulation kinetics of both HIF-α isoforms in response to hypoxia (**Fig 5.11**). A time-course of 24 hours with an additional 15 minute atmospheric re-oxygenation was used. Once again the HIF-2α response was found to be ambiguous, generally indicating no response as can be expected from a HeLa lineage cell line (Bracken, Fedele et al. 2006). Importantly, HIF-1α transiency was abolished as accumulation continued up to the 24 hour time point. Despite the loss of PHD2, HIF-1α protein was effectively reduced to pre-hypoxic levels following 15 minutes re-oxygenation. The loss of HIF-α transiency on the population-level inspired the pursuit at the single-cell level, again using time-lapse microscopy and wide-field luminescence.

5.2.5.3 Time-lapse imaging of HIF1-α expressing ShPHD2cells in hypoxia

Following conformation of knockdown, ShPHD2 cells were transfected with pG-HIF1αEGFP and an unfused DsRedxp expression plasmid. After 24-48 hours transfection cells were imaged for up to 20-hours by confocal microscopy, either at atmospheric O_2 or 1% O_2 (**Fig 5.12**). Using the same criteria as outlined in **section 4.2.2.1**, the % responding cells was calculated for both conditions. From the normoxic condition, 14.4% of cells (n= 18 of 125 cells) were determined to show changes in HIF-1αEGFP fluorescence compared to 36.14% of cells (n= 30 of 83 cells) for the hypoxic scenario. These values are comparable with those observed for the wild-type HeLa cells imaged in Chapter 4.

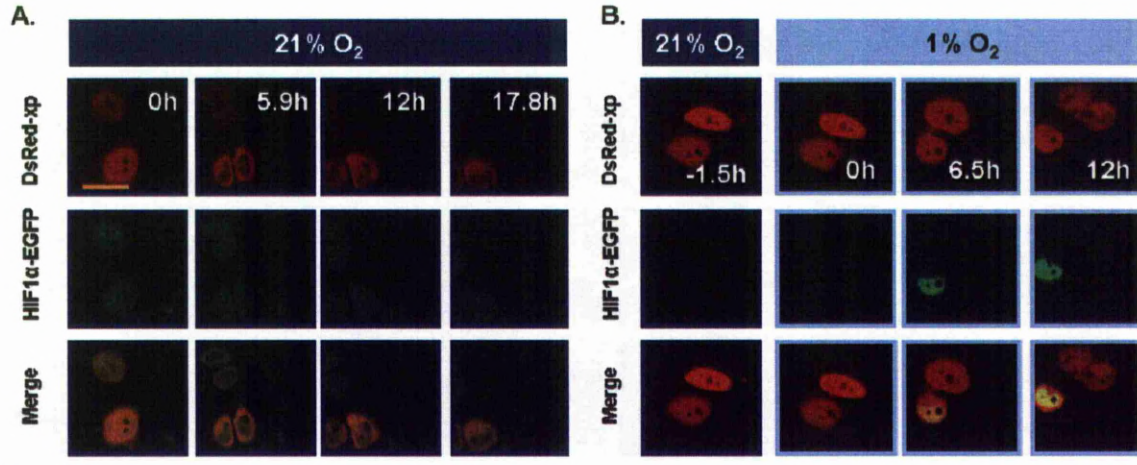

Fig 5.12. Time-lapse microscopy of ShPHD2 cells co-expressing vectors encoding HIF-1αEGFP and DsRedxp. Cells were imaged at either 21% (**A**) or stimulated with hypoxia using 1% O_2 (**B**). Orange scale bar indicates 20μm.

Responding cells were analysed using Cell Tracker and nuclear fluorescence converted into a quantitative format (**Fig 5.13**). Analysed cells were then categorised in a similar manner to the wild-type responding cells, using the classifications (1) persistent accumulation and (2) transient accumulation. There were no recorded instances of multiple accumulations of HIF-1α when imaging the ShPHD2 cell line. Within the existing classifications, it was found that 63.3% (n= 19 of 30 cells) of cells adhered to persistent accumulations and 36.7% (11 of 30 cells) belonged to transient accumulations. The reduced instances of transient accumulations are in line with the observed loss of transiency by western blot analysis (**Fig 5.11**). The maintenance of some degree of transiency can be explained by either the still intact PHD3 feedback, or one of the many other reported feedback mechanisms (Stiehl, Wirthner et al. 2006; Qutub and Popel 2007; Horak, Crawford et al. 2010; Moslehi, Minamishima et al. 2010).

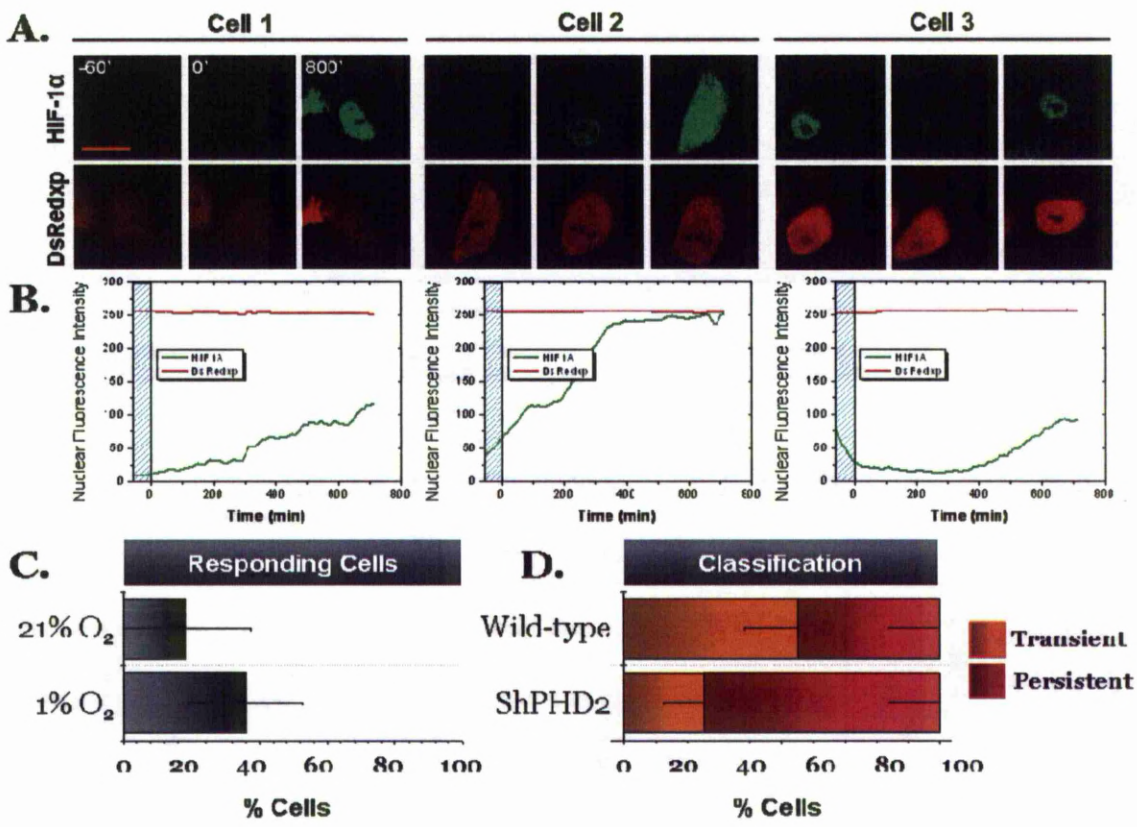

Fig 5.13. Time-lapse microscopy of ShPHD2 HeLa cells co-expressing vectors encoding HIF-1αEGFP and DsRedxp. Three representative cells are shown above and the corresponding cell traces below. Scale bar denotes 20μms and time-steps shown are the same for all three cells. A figure of all responding cells is shown in appendix 1.4.

5.2.5.4 Model prediction of ShPHD2 re-oxygenation

The loss of PHD2 from the feedback network is expected to not only affect HIF-α transiency following hypoxia, but to slow the clearance of HIF-α protein upon re-oxygenation. The 4C-model output of ShPHD2 reinforces this hypothesis, predicting a near ~4-fold increase in HIF-α protein half-life to 101 minutes from 25 minutes (**Fig 5.14.**). This model output was generated assuming a 6h 1% O_2 incubation preceding the re-oxygenation back to atmospheric O_2.

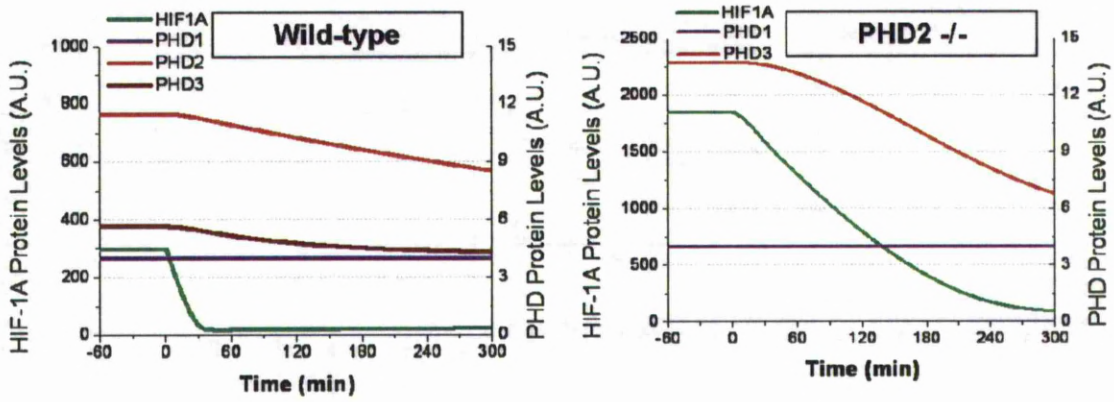

Fig 5.14. 4C-model outputs simulating wild-type cells and ShPHD2 cells experiencing re-oxygenation after 6 hours incubation at 1% O_2. Both simulations were run to equilibrium either in with the intact PHD2 feedback or without before simulating hypoxia and re-oxygenation.

5.2.5.5 Time-lapse imaging of HIF-1α expressing ShPHD2 cells through re-oxygenation

To validate the model prediction, we used time-lapse imaging to experimentally address the re-oxygenation mediated loss of HIF-α protein in ShPHD2 cells. Cells were plated into 35mm IWAKI dishes and co-transfected with pG-HIF1αEGFP and an unfused DsRedxp expression vector, as has been performed previously. After 24 hours of transfection cells were placed into the microscope stage mounted incubator, which was then set to an oxygen tension of 1%. After 6 hours of incubation, cells selected for green fluorescence were imaged through the re-oxygenation back to atmospheric O_2. From this data, 56.76% (n=21 of 37 cells) of cells showed a loss of green fluorescence as counted by eye, a value lower than wild-type but not statistically significant when assessed by one-way ANOVA. All green fluorescent cells (that didn't die or migrate from field of view within 150-minutes) were analysed using Cell Tracker to quantify nuclear fluorescence levels. The profile of loss of fluorescence was very comparable to the model simulation comparing to several cells analysed (**Fig 5.15**). The slope of decreasing fluorescence was used to calculate the half-life values as was

previously performed on wild-type HeLa cells (measured earlier in **Fig 4.12**), deriving a half-life average value of 300±145 minutes for the ShPHD2 cells. However, a degree of caution must be exercised when comparing these averages as a large degree of heterogeneity was once again observed. The half-life values for wild-type HeLa cells ranged from 8.6 minutes to 330 minutes, where as data from the ShPHD2 cells were seen to vary from 49 minutes to an outlier at 1300 minutes. The calculated fano factor further confirmed this heterogeneity, in which a value of 139 was contrasted to 497 for wild-type against ShPHD2 cells.

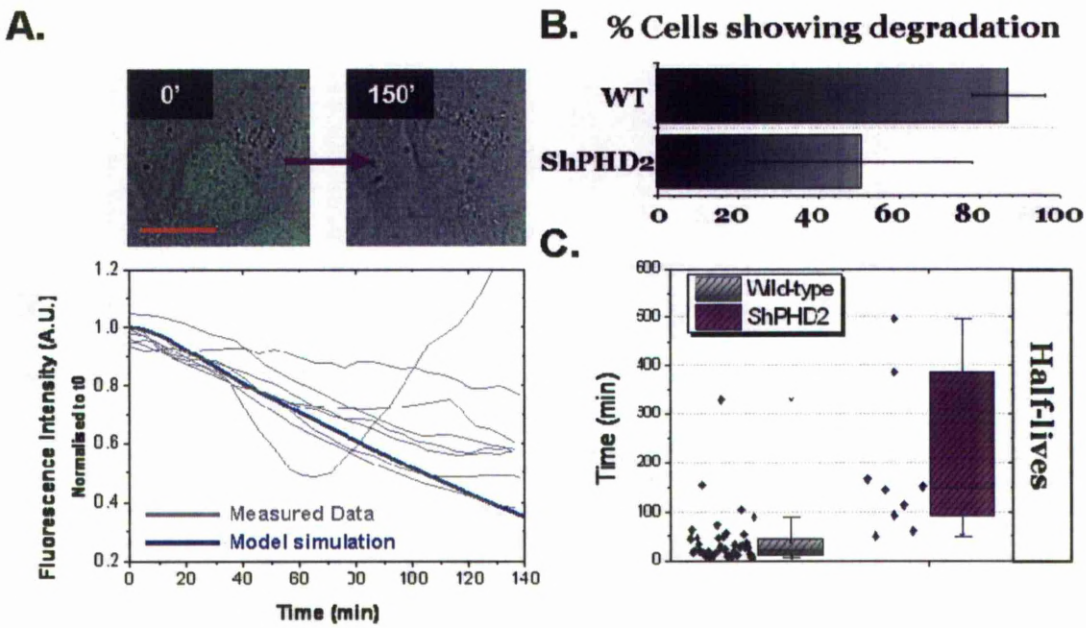

Fig 5.15. Time-lapse microscopy of ShPHD2 cells co-expressing vectors encoding HIF-1αEGFP and DsRedxp. (**A**) Cells were incubated in 1% O_2 for 6 hours before imaging through the re-oxygenation back to atmospheric conditions. Nuclear fluorescence was quantified and a selection of cells shown. Also indicated is the model simulation of HIF-1α levels from the same experiment performed *in silico* (**B**) Chart depicting the % of cells visibly degrading within a 150 minutes of re-oxygenation; previous data from wild-type cells is included for comparison (data from **section 4.2.5.3**). (**C**) Box-and-whisker plot shows the calculated half-lives comparing wild-type cells to ShPHD2 cells.

5.2.6 Sensitivity analysis of the 4C-model; Model Predictions

Mathematical models of cell signalling systems are built as tools to complement biological experiments, achieved through a combination of model predictions and insight. The completion of the 4C-model enabled the systematic investigation into the model architecture, investigating the sensitivity of the signalling features in differing scenarios *in silico*, making predictions that can later be experimentally verified or refuted (Ihekwaba, Broomhead et al. 2004).

5.2.6.1 Parameter Sensitivity Analysis and the Importance for potential crosstalk events

Model simulations were run to explore the sensitivity of the parameters and their relationship to the HIF-1α hypoxic response profile. In order to achieve this, we quantified the features of transient response profile, detailing amplitude, duration, steady-state levels and response time. The amplitude of response was calculated as the difference between maximum HIF-1α levels minus steady-state levels. The duration of response in this instance was calculated as the time from the initiation of response until the re-establishment of steady-state; otherwise referred to as the transitional period. The steady-state levels are calculated as the post-perturbation HIF-α levels when the level of changes in values is below 1%. Finally, the response time was determined as the time taken to reach maximum response amplitude. Using these criteria, each parameter value was doubled and the effect on the outlined signalling features scored, normalised to the unaltered 4C-model output. The scoring of the different parameter alterations is depicted in a heat map format as has been similarly performed in the analysis of the NF-κB model by Ashall *et al.* 2009 (Ashall, Horton et al. 2009) (**Fig 5.16.**). The analysis of the system showed that the doubling of HIF-1α synthesis affected only the amplitude and steady-state levels, elevating them both by a factor of 2.57. In contrary, the doubling of the PHD synthesis rate terms negatively affected these features, in which PHD1 and PHD3 exerted the most influence on account of their substantially higher rate values. The only parameter which distinctly affected all signalling features was the PHD2 induction rate *k2*, negatively scoring for all and most prominently affecting steady-state levels. In contrast, doubling the PHD3 induction rate *k3* affected only amplitude and response time, decreasing them mildly in comparison to *k2*. An observation that has been reported several times in the literature, first reported by Berra *et al.* 2003 (Berra, Benizri et al. 2003; Natarajan, Salloum et al. 2006). Interestingly, doubling PHD2 degradation rate strongly and solely increased steady-state levels where as doubling PHD3 degradation rate increased both amplitude and steady-state. A feature perhaps relevant to FKBP38 mediated destabilisation of PHD2 (Barth, Nesper et al. 2007).

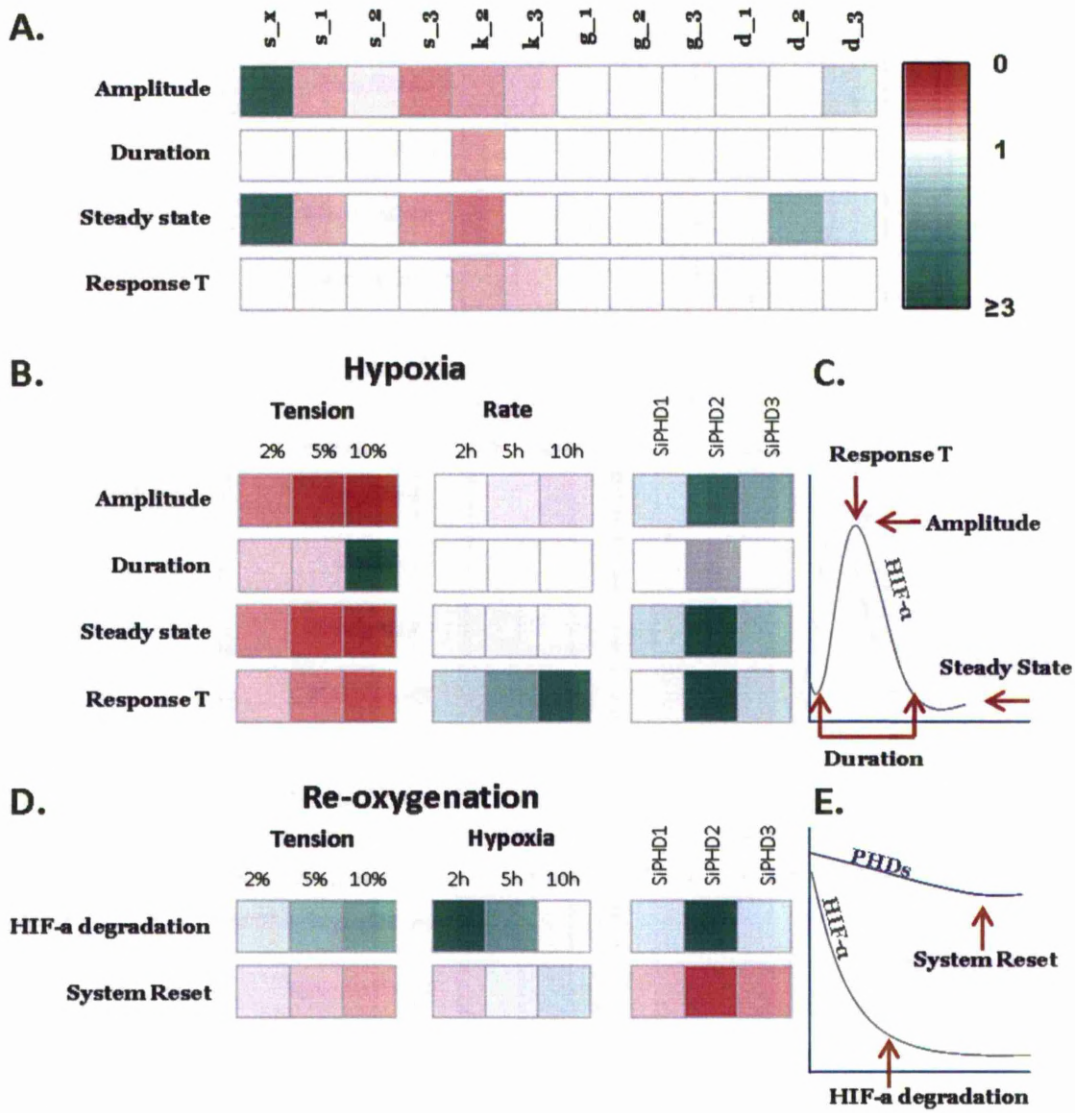

Fig 5.16. 2D heat map showing the sensitivity analysis of the 4C-model. A pictorial definition of these response features are shown for hypoxia (**C**) and re-oxygenation (**E**). (**A**) All parameter values were increased by 2-fold and the corresponding changes to response features plotted. (**B**) Shows how the manifestation of hypoxia affects response features, including the oxygen tension, the rate of de-oxygenation and removal of individual PHDs. (**D**) Shows how the manifestation of re-oxygenation affects the response features, including the oxygen tension switch, the prior duration of hypoxia and the removal of individual PHDs. (horizontal arrows indicate features measured by amount, vertical arrows indicate features measured by time)

5.2.6.2 4C Model sensitivity to oxygen kinetics and levels

Disruption to cellular oxygen homeostasis can occur in numerous ways (Gainer 1987; Toffoli and Michiels 2008; Shi 2009). In spite of this hypoxia is often considered or reduced to an encompassing and single term. We therefore investigated the sensitivity of the 4C-model to differing hypoxic and re-oxygenation scenarios, using a similar heat map sensitivity analysis as previously described. The HIF-1α response to hypoxia was assessed using the same criteria outlined for the parameter sensitivity analysis, namely; amplitude, duration, steady-state levels and time-to-peak-max. However in this analysis,

rather than altering parameter values, the mode-of-hypoxia was altered. Three different severities of hypoxia were arbitrarily selected and used, switching from atmospheric 21% to 10%, 5% or 2% O_2. Results were normalised and scored against a model output using the standard tension switch of 21% O_2 to 1% O_2 (**Fig 5.16.**). Reducing the O_2 tension switch was found to reduce amplitude, duration, post-perturbation steady-state as well as the time to peak-max. The model outputs thereby provide evidence that the severity of the hypoxic switch can translate into differing HIF-α response profiles, suggesting that this information is perhaps purposefully encoded. A corroborative result for this prediction was published by Jiang *et al.* (1996), in which they used western blot densitometry to determine a HIF-α dose response curve to varied oxygen tensions (Jiang, Semenza et al. 1996). Next the model was used to investigate the HIF-α response to different rates of de-oxygenation, investigating the effect of the hypoxic switch from 21% to 1% O_2 spanning 2 hours, 5 hours or 10 hours. In this instance, the model predicted that the kinetics of HIF accumulation were largely insensitive to the rate of de-oxygenation, marginally affecting only amplitude although dramatically affecting time-to-peak-max. This sensitivity is the result of the non-linear relationship of the hydroxylation rates to oxygen tension, creating a switch like mechanism when the tension reduces to values of ~2%. These results suggest that the HIF-α response does not encode rate of de-oxygenation on the cellular level when the rate of de-oxygenation is within the time frame of a day. However, some tumours may take longer than this to reach hypoxia (Ilangovan, Bratasz et al. 2005). In this case the amplitude of response may have been sufficiently damped as to be meaningfully different.

As well as investigating hypoxia, the reverse scenario of re-oxygenation was also explored by sensitivity analysis as was similarly investigated by Schmierer *et al.* (2010). We explored the sensitivity of HIF-α degradation and HIF-PHD reset following re-oxygenation under varying oxygen conditions. HIF-α degradation was scored as the time to maximal loss of HIF-α protein and the HIF-PHD reset as the time for the system to reach a steady-state solution. First the model examined whether the hypoxic tension preceding re-oxygenation altered the response kinetics, using 2%, 5% and 10% O_2. Results were scored and normalised against the model output for 6 hours of 1% O_2 followed by a re-oxygenation to 21% O_2. The reduced severity of hypoxia translated to increased times for HIF-α degradation and decreased times for HIF-PHD reset. As well as

assessing hypoxic severity, the preceding duration of the hypoxic episode was also investigated. Here three durations of 1% O_2 hypoxia were simulated by the model, 2 hours, 5 hours and 10 hours. A hypoxic episode of 2 hours was found to increase by greater than 3-fold the time for HIF-α degradation when compared to 6 hours. This prediction is in line with a report from Marxsen *et al.* (2004) who showed a similar sensitivity of HIF-α re-oxygenation mediated degradation to the preceding duration of hypoxia (Marxsen, Stengel et al. 2004).

5.2.6.3 4C Model sensitivity to individual PHD isoforms

Finally the model was used to quantify the *in silico* loss of each individual PHD on the hypoxic and re-oxygenation profiles of the system. Removal of PHD1 had the least impact, marginally increasing HIF-α amplitude, steady-state levels, degradation time and decreasing system reset time. Loss of PHD3 had a similar but more pronounced effect, additionally increasing the time-to-peak-max. Lastly, loss of PHD2 affected every feature in the same manner as PHD3 but far more substantially. The loss of PHD2 also resulted in the loss of transiency and so therefore an alteration to duration could not be calculated (**Fig 5.16**).

In summary, the 4C-model provides supportive evidence, predicting that the oxygen tensions and kinetics of hypoxia, re-oxygenation and intermittent hypoxia can translate in the response kinetics of the HIF-PHD feedback axis. This alludes to the importance of HIF-α kinetics in relation to gene expression and phenotype, a concept that has been suggested for the yeast pheromone pathway, ERK oscillations and p53 response pathway (Behar, Hao et al. 2008; Shankaran, Ippolito et al. 2009; Batchelor, Loewer et al. 2011). For the following systems, the importance of kinetics in phenotype has moved away from hypothesis and been directly shown for lineage patterning by Oct-4 in embryo development, cell-to-cell communication in synthetic bacterial systems and gene expression following TNFα stimulation of NF-κB (Basu, Mehreja et al. 2004; Plachta, Bollenbach et al. 2011). This thesis has a strong interest in the propagation of information through the signalling arrangements such as the HIF-PHD signalling motif. It will be interesting for future work to validate the encoding of contextual information and to investigate to what extent it may affect the HIF-mediated response to hypoxia.

5.2.7 Oxygen-dependent destabilisation of PHD proteins explored

Within the last seven years several publications have reported on an additional level of O_2-sensitive regulation which negatively impacts the protein stability of PHD1 and PHD3 (Nakayama, Frew et al. 2004; Calzado, de la Vega et al. 2009). This destabilisation of PHD1 and PHD3 is carried out by the activity of the E3-ubiquin ligases, SIAH1 & -2, targeting the PHD proteins for proteasomal degradation. Importantly, both SIAH1 and SIAH2 have been shown to be activated by hypoxia (and DNA damage), thereby incurring a double negative feedback loop to the HIF-PHD motif (Matsuzawa, Takayama et al. 1998; Nakayama, Qi et al. 2009). This scenario carries with it the possibility to dramatically enrich the dynamics and explain the observed variety of HIF-α accumulation kinetics. Also as the SIAH proteins do not act equally on all PHD isoforms, it may be a prominent mechanism to incorporate into the resolved PHD model. We therefore decided to investigate the potential role of the SIAH proteins in our own experimental system.

5.2.7.1 Are SIAH1 and SIAH2 induced at the transcriptional level

Conflicting information exists describing the mode of hypoxic activation of the SIAH proteins. It has been suggested that the ubiquitin ligase activity of the proteins is augmented during hypoxia though there has also been evidence to suggest that the proteins are up-regulated at the mRNA level following hypoxia (Nakayama, Qi et al. 2009). We investigated whether SIAH1 or SIAH2 mRNA levels changed in response to hypoxia. HeLa cells were incubated at either 21% O_2 or 1% O_2 for a time-course of 24 hours and then cells were lysed and samples prepared for measurement by RT-qPCR (**Fig 5.17.**). No significant change to mRNA levels was found for either SIAH1 or SIAH2. This may imply that the SIAH proteins are augmented at the post-translational level in our system. This has been suggested by Khurana *et al.* (2006), reporting the phosphorylation of SIAH2 by p38 MAPK to enhance SIAH2 binding to PHD3 (Khurana, Nakayama et al. 2006).

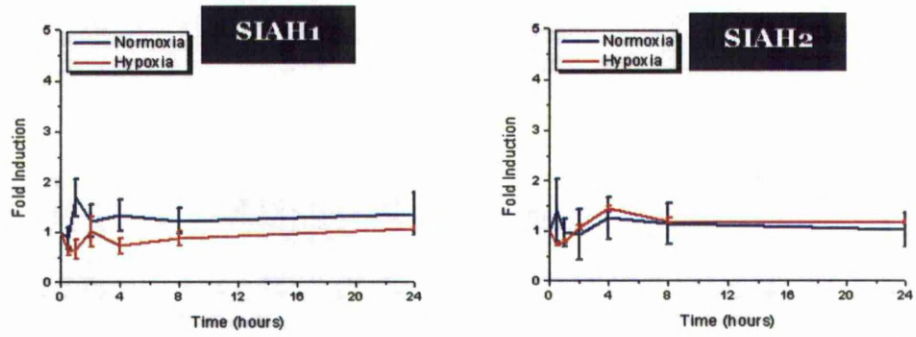

Fig 5.17. RT-qPCR measurement of samples prepared from HeLa cells that were incubated for a time course of 24-hours at either 1% O_2 or atmospheric O_2. (n=2 hypoxia and n=1 normoxia)

5.2.8 Evidence of O_2-sensitive PHD protein destabilisation

Cells expressing fluorescent fused PHD were used to assay whether an O_2-sensitive regulatory mechanism exists in our cell line and whether this may impact on PHD protein stability following hypoxia. HeLa cells were transfected with either an unfused EGFP expression vector or a plasmid encoding PHD1-EGFP, PHD2-EGFP or PHD3-EGFP. After 24 hours transient transfection, cells were imaged by confocal microscopy (imaging once every ~5-minutes) for an hour at atmospheric O_2 before switching to 1% O_2 and imaging for a further 300 minutes (**Fig 5.18**). All imaged cells were analysed using Cell Tracker. From this data we calculated the % cells showing a greater than 50% loss of fluorescence within 300 minutes and found 39% (n=9 of 23 cells) for PHD1 and 10% (n=2 of 20 cells) for PHD3. No extensive loss was seen for either PHD2 (n=total 15 cells) or unfused EGFP (n=total 13 cells).

Additionally, the source of SIAH hypoxic sensitivity is suggested to be ROS related rather than via the transcriptional activity of HIF-α. ROS can be produced from both a hypoxic episode and re-oxygenation episode (Morita-Fujimura, Fujimura et al. 2001; Hamanaka and Chandel 2009). Furthermore, ROS can lead to DNA damage and this is cited to also activate SIAH1 (Wiseman and Halliwell 1996; Matsuzawa and Reed 2001). This led us to consider the possible re-oxygenation sensitivity of the PHD protein stability.

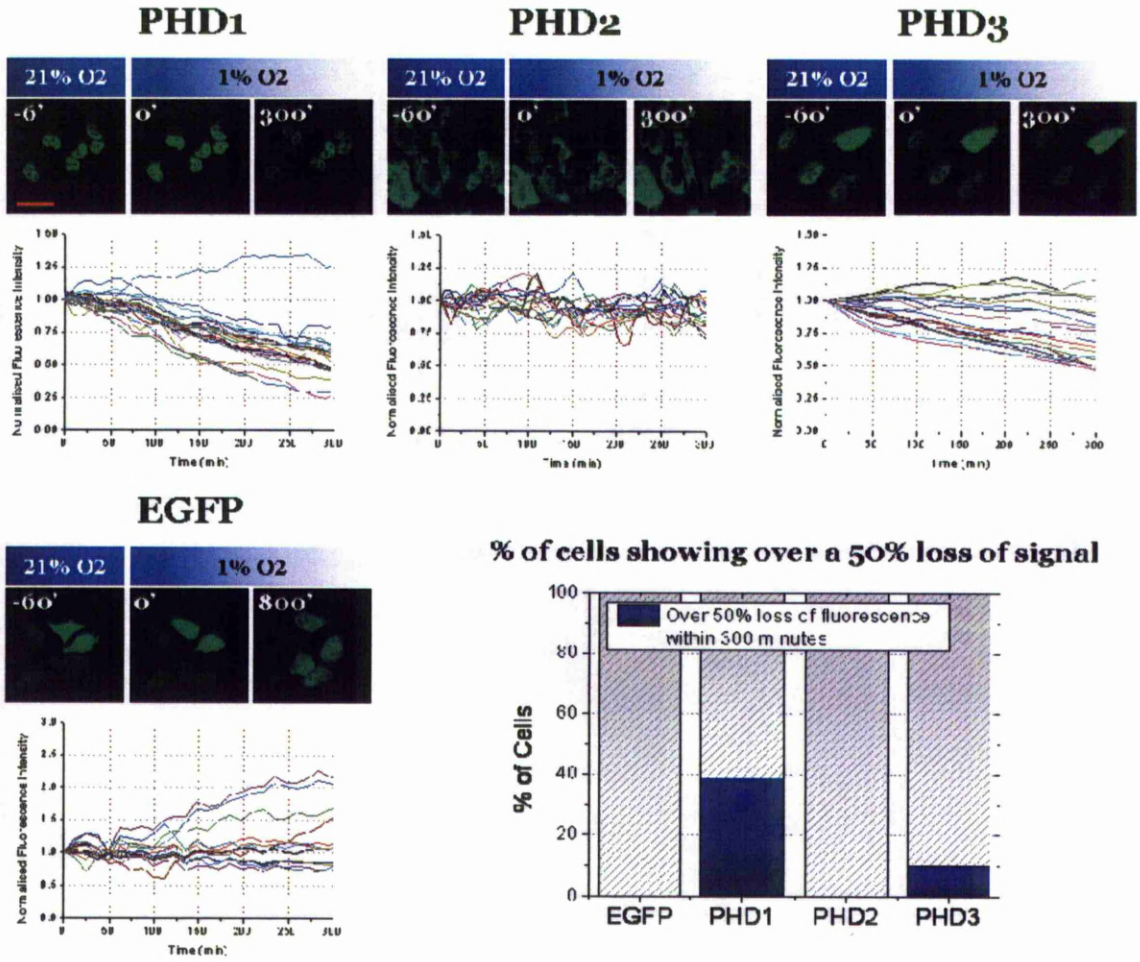

Fig 5.18. HeLa cells were transfected with either un-conjugated EGFP, PHD1-EGFP, PHD2-EGFP or PHD3-EGFP. After 24 hours of transfection cells were imaged by time-lapse confocal microscopy for 1 hour in atmospheric O_2 and then several hours in 1% O_2. Time-lapse images are shown next to the corresponding quantifications of cell fluorescence. Cell traces of fluorescence are normalised to to. Stacked bar chart shows percentage of cells showing more than a 50% loss of fluorescence within 300 minutes of experimental start point No. of cells quantified; EGFP (n=total cells 13), PHD1 (n=total 23 cells), PHD2 (n=total 15 cells) and PHD3 (n=total 20 cells). Scale bar denotes 50μm

For these reasons we also decided to image the PHD expression vectors through re-oxygenation. HeLa cells were transfected in the same manner using the same expression vectors. This time however, after 24 hours of transfection cells were incubated at 1% O_2 on the microscope stage for 6 hours before confocal imaging through the re-oxygenation back to atmospheric O_2 and continuing imaging for further 1000 minutes. Here 50% loss of signal was calculated for the 1000-minute time-point. Using this criteria, 100% (n=20 of 20 cells) of PHD3 cells showed a greater than 50% loss of fluorescent signal, 74% (n=31 of 42 cells) for PHD1, 36% (n=9 of 25 cells) for PHD2 and 5% (n=1 of 21 cells) for EGFP (**Fig 5.19**).

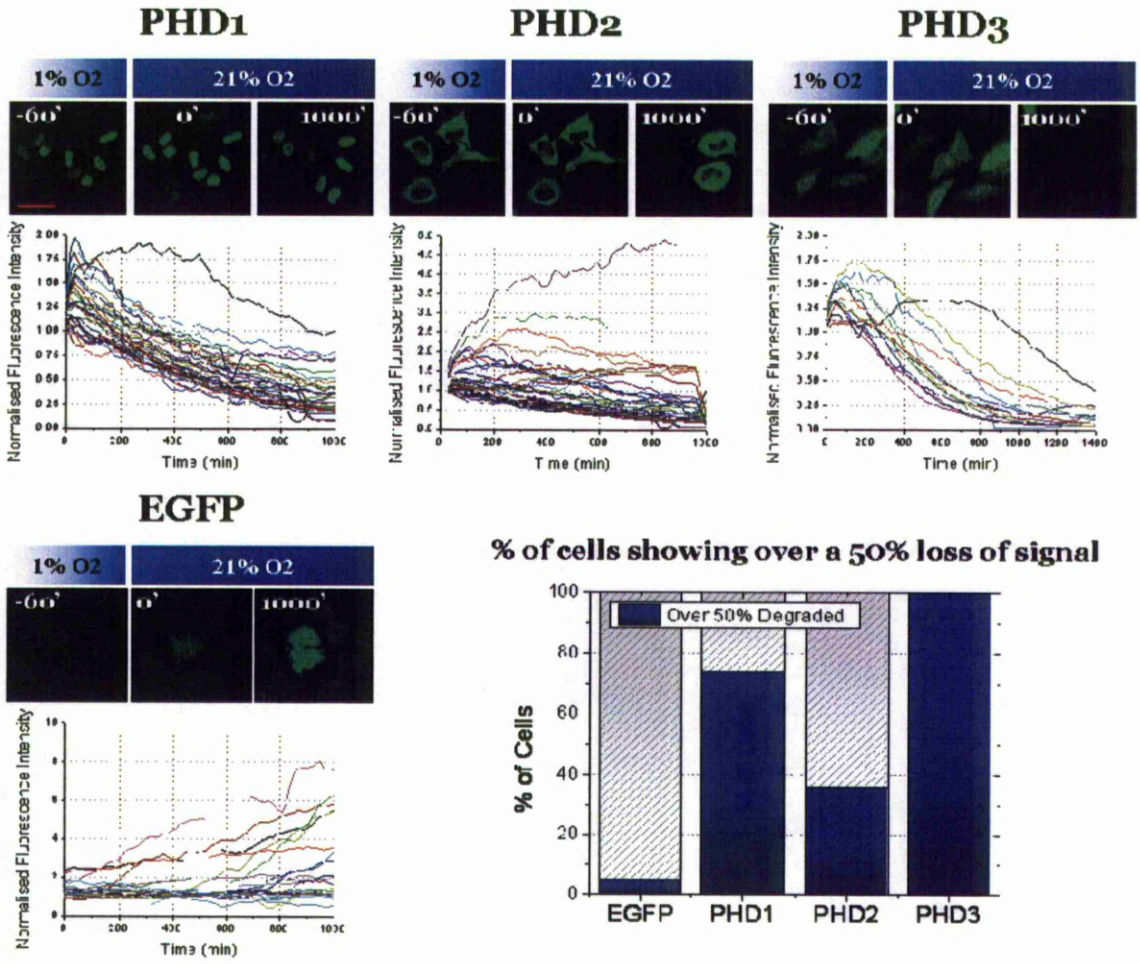

Fig 5.19. HeLa cells were transfected with either un-conjugated EGFP, PHD1-EGFP, PHD2-EGFP or PHD3-EGFP. After 24 hours of transfection cells were incubated at 1% O2 for 6 hours then imaged by time-lapse confocal microscopy, re-oxygenating the cells back to atmospheric O_2 and then several hours in 1% O_2. Time-lapse images are shown next to the corresponding quantifications of cell fluorescence. Cell traces of fluorescence are normalised to t0. Stacked bar chart shows percentage of cells showing more than a 50% loss of fluorescence within 1000 minutes of experimental start point No. of cells quantified; EGFP (n=total cells 13), PHD1 (n=total 23 cells), PHD2 (n=total 15 cells) and PHD3 (n=total 20 cells). Scale bar denotes 50μm

These results provide preliminary evidence to warrant further investigation of the HIF-PHD-SIAH motif. However, this avenue of work investigating the O_2-destabilisation of the PHDs remains as of yet incomplete and has therefore not been included in the most recent version of the 4C-model. The discovery of the hypoxic and re-oxygenation sensitivity of PHD1 protein could be explored by western blot analysis on the endogenous protein as no compromising hypoxia-inducibility would be present. Or the imaging of re-oxygenation could be performed in an SIAH knockout background to see if the loss of fluorescence is abated. If the O_2-sensitive SIAH feedback was validated the imaging data again could be readily used alongside the model to drive the parameterisation of the new model architecture. These results have the capacity to be very interesting as

the additional feedback will introduce additional non-linearity into the system and provide a more detailed tuning of the HIF-α response to disrupted oxygen homeostasis.

5.3 Discussion

In this chapter, the generic PHD model was expanded to include all PHD isoforms and this expansion was performed along biological measurements aimed at constraining several of the new parameters. This new model is the first of the HIF signalling models to attempt the resolution of the individual PHD isoforms. This task is likely to be ongoing as highlighted by the preliminary data garnered concerning the O_2-dependent destabilisation of PHD1 and PHD3. However, despite room for further development we believe the current 4C-model to have been sufficiently developed and constrained as to warrant the experimental testing of model predictions, especially with regards to the arising hypothesis that the HIF-α kinetics are sensitive to the context of disrupted oxygenation.

5.3.1.1 Hydroxylation rates: h1, h2 and h3

Ideally all model parameters would be constrained accurately to biological measurements, though this can often be cumbersome and difficult to thoroughly perform (Kim and Tidor 2003). Despite effectively measuring and estimating the combined synthesis and degradation rates for the 4C-model, we did not attempt the measurement of the individual hydroxylation rates of the PHDs. Oxygen-sensitive hydroxylation is a critical aspect of HIF-signalling, responsible for conferring hypoxia-inducibility to the system. An accurate measurement of this process with regards to rate of hydroxylation would therefore be ideal. For the purpose of the model the values used were not measured by us, but taken from available literature, specifically using measurements from a capture pVHL assay performed by Tuckerman *et al.* 2004. The findings here suggested a non-linear relationship between oxygen tension and hydroxylation rate, where this non-linearity is most pronounced for PHD3. The results further suggested that HIF-1α was most rapidly hydroxylated by PHD3, though at a similar rate to PHD2 and that PHD1 hydroxylation occurred near 5-fold slower in comparison. The hydroxylation rate in the model is normalised and arbitrarily set at 1 (PHD2 rate), when simulating hypoxia these values are scaled down accordingly. The values published by Tuckerman *et al.* (2004) were used to inform the scaling for each individual PHD. The values reported by Tuckerman *et al.* (2004) have only

been contested (as far as I'm aware) by one publication, Stiehl *et al.* (2006), in which the oxygen-sensitivity of hydroxylation was inferred *via* the antibody detection of HIF-α hydroxyproline. Where as Tuckerman *et al.* (2004) reported a ~10-fold reduction in hydroxylation following a switch from 20% O_2 to 1% O_2, Stiehl *et al.* (2006) found a milder ~3-fold reduction. However, both were in agreement with the apparent non-linearity of hydroxylation in relation to oxygen availability. The exact fold-reduction will not change dramatically the behaviour of the model only alter other values attained through fitting. However, the exact non-linearity of the oxygen tensions used may have more of an effect, especially regarding the models prediction that response time is encoded in the rate of de-oxygenation. A possible caveat of these measurements made by Tuckerman *et al.* (2004) is the use of *in vitro* biochemistry in determining hydroxylation rate. The extension of these values into the model framework might not provide a detailed and accurate enough picture of the interactions between the individual PHDs and HIF-α. For instance, we are unaware if the intracellular localisations of the PHDs and thereby proximity to HIF-1α may significantly influence the effective hydroxylation rate (Metzen, Berchner-Pfannschmidt et al. 2003). This issue was partially addressed in a publication by Yasumoto *et al.* (2009) who reported that the forced cytoplasmic expression of PHD1 had no effect on HIF-1α hydroxylation.

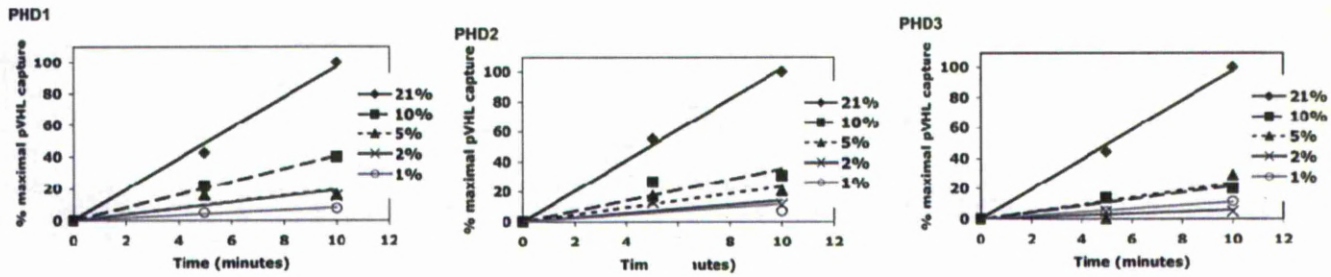

Fig 5.20.Oxygen dependence of PHD isoforms. In vitro enzyme assays were performed using HIF-1α, for each PHD isoform at varying oxygen concentrations. The assay measures captured pVHL to quantify level of hydroxylated HIF-1α, making use that only hydroxylated HIF-1α binds pVHL. Values are expressed as a percent of maximal pVHL captured. Figure taken from Tuckerman *et al.*

5.3.1.2 Role of the individual PHDs

The resolution of individual roles of the PHD isoforms has been often queried (Appelhoff, Tian et al. 2004; Fong and Takeda 2008; Thirstrup, Christensen et al. 2011). Since the original postulation of these questions a range of mechanisms, characteristics and regulatory events specific to each PHD has been shown or suggested, including the aforementioned intracellular

localisations, the role of PHD1 in regulating IKKβ, PHD3 in mediating apoptosis and PHD2 anchorage-independent carcinoma cell growth (Metzen, Berchner-Pfannschmidt et al. 2003; Cummins, Berra et al. 2006; Rantanen, Pursiheimo et al. 2008; Jokilehto, Hogel et al. 2010). In the framework of the 4C-model, it would be an interesting proposition to begin to address these crosstalk activities. For example, the model predictions of PHD3 protein concentration following hypoxia could be extended to infer the effects on PHD3 aggresomes and the associated disposition to cell death (Rantanen, Pursiheimo et al. 2008). Or the nuclear levels of PHD2 could be deduced in relation to anchorage-independent cell growth (Jokilehto, Hogel et al. 2010). The separable roles of the individual PHDs has been further postulated by the reported different abundances of PHD mRNA and protein across differing tissues (Jokilehto and Jaakkola 2010). Sensitivity analysis of the 4C-model would suggest this to alter the characteristics of HIF-α signalling and this may therefore underpin an aspect of the cell-type specific hypoxic response, especially relevant given the range of physiological normoxia (Carreau, El Hafny-Rahbi et al. 2011). Computational investigations into these scenarios amongst others are only possible when using a resolved PHD model as a foundation module. To our knowledge, the 4C-model is the first model of the HIF system to explicitly resolve the PHD isoforms (other models are discussed below) (Kohn, Riss et al. 2004; Qutub and Popel 2007; Dayan, Monticelli et al. 2009; Schmierer, Novak et al. 2010; Bruning, Cerone et al. 2011).

In spite of the emerging divergent functions of the PHD isoforms their remains significant overlap and a degree of redundancy in their regulation of HIF-α. This is partly due to the evolutionary history of the proteins, evolving from the duplication of the PHD2 gene (Taylor 2001; Rytkonen, Williams et al. 2011). This evolutionary history supports the near widely accepted dominant role of PHD2 in the regulation of HIF-α protein levels (Berra, Benizri et al. 2003). Our model produced predictions in line with these findings, suggesting HIF-α hypoxic transiency to be chiefly regulated by PHD2 (**Fig 5.16**). A feature made prominent by the reported protective role HIF-α transiency has following chronic hypoxia (Ginouves, Ilc et al. 2008).

Additionally, separable roles were found between PHD2 and PHD3 determined by their intrinsic degradation rates. A significant difference was found between the protein stability of PHD2 versus PHD3, in which the latter is more rapidly

turned over. 'Memory' of a stimulus can be carried in several forms, one of which is the stability of downstream proteins (Locasale 2007). This concept was extensively considered by Locasale (2007), in regards to T-cell activation and can be extended in shedding light on a functional component of the HIF-PHD feedback and a resolving difference between the PHD proteins. After a hypoxic episode and subsequent re-oxygenation, HIF-α levels are rapidly degraded but do not settle at pre-perturbation concentrations for hours. This is due to the elevation of PHD2 and 3 levels. PHD2 levels will remain elevated above the resting steady-state for up to 24 hours. The system therefore retains a memory of a hypoxic episode dependent on the turnover rate of PHD2. However, though PHD2 compromises a long-term memory, PHD3 with a half-life of ~100 minutes, is a component of a short-term memory. This idea is ratified by the work of Maxrsen *et al.* (2004), who found that PHD2-levels remained elevated 24-hours after re-oxygenation (Marxsen, Stengel et al. 2004). Finally, a similar concept of "hypoxic memory" has been suggested before in work from Kamat *et al.* (2007). In this publication it was found that HMEC-1 cells exposed to several weeks of mild hypoxia retained elevated HIF-1 dependent gene expression up to a week after return to normoxia. The characterisation of memory in this instance is therefore different to our own, though the idea is similar. The concept of memory in the HIF system is possibly of importance in instances of intermittent hypoxia, in which cells are repeatedly exposed as is found in some tumours as well as obstructive sleep apnoea (Toffoli and Michiels 2008; Belaidi, Joyeux-Faure et al. 2009). In relation to the feedback PHD proteins, it is becomingly increasingly important to regard their individual roles, both to the regulation of HIF-α and the reporter crosstalk events.

5.3.1.3 Existing HIF-models

At the onset of this project only a single mathematical model regarding the HIF regulatory system had been published by Kohn *et al.* 2004. Since then a handful of models have emerged, each focusing on and detailing certain features of the regulatory motifs (**Table 5.2**). The model produced by Kohn *et al.* (2004) details a complex topology involving 23 species, including HIF-α mRNA, HRE binding sites, pVHL, HIF-β, PHD and in-between binding arrangements (Kohn, Riss et al. 2004). These species are governed by an extensive arrangement of 32 reactions. A fundamental question of their proposed model is, how the switch-like response of HIF-α protein to decreased oxygen arises. The model suggested

the affinity of HIF-α to PHD was a determining factor, influenced and modulated to some degree by the remaining network topology. In comparison to our own model, the switch-like response arises from the non-linear relationship of hydroxylase activity to oxygen availability as measured by both Tuckerman *et al.* (2004) and Stiehl *et al.* (2006). The aim of the Kohn model meant that little attention was given to response kinetics, except for the PHD mRNA kinetics in response to varied oxygen tensions. Furthermore, the limited available quantitative data at the time meant that the numerical assumptions and relationships within the model were left unconstrained. As such it would therefore be an interesting prospect to parameterise their model using our own data and existing published quantifications. However, I believe the parameter space of the model to still be too large for this to be sufficiently performed. In essence, Kohn *et al.* 2004 suggest a sensible abstraction of the core regulatory network which has been evolutionary conserved and were the first group to prepare this signalling system into a mathematical framework. Since then four more groups (to our knowledge) have attempted this; Qutub et Popel (2007), Yu *et al.* (2007) Dayan *et al.* (2009), Heimer *et al.* (2010)Schmierer *et al.* (2010) and most recently Bruning *et al.* 2011 (Qutub and Popel 2007; Dayan, Monticelli et al. 2009; Schmierer, Novak et al. 2010; Bruning, Cerone et al. 2011). Of these models, the works of Yu et al. Dayan et al. and Heimer et al. build on the original Kohn model. Yu et al. and Heimer et al. essentially perform analysis on the models, streamlining the equations and concluding aspects from the reduced models. A key point made from their work concerns the switch like response of HIF-α accumulation, as addressed by Kohn et al. Of the Kohn derived models, only the work of Dayan *et al.* 2009 adds to the original 2004 model (or alters the topology), extending the model to include FIH. The model abstraction remains similarly ambitious, detailing 16 species interacting across 23 reaction constants. Their analysis of the Kohn model suggested HIF-β to have a non-determinant role in HIF-α regulation and so was removed for the Dayan *et al.* model incarnation. A fundamental aim of the Dayan *et al.* model was to address the non-redundancy of the PHD and FIH mechanisms, in determining HIF activated gene expression. As such, FIH was introduced into the model abstraction. Many of the parameters from Kohn *et al.* were refit into the Dayan *et al.* model framework, including the total concentration of HIF-1α protein at different oxygen concentrations (western blot analysis) and

downstream gene expression profiles in response to FIH availability (RT-qPCR and luminometry analysis) (Dayan, Roux et al. 2006). The model predicted how the concentration of FIH determines individual hypoxic sensitivity of a subset of HIF activated genes. As in the previous Kohn *et al.* model, the steady-state solutions were the defining outputs and no emphasis was given to kinetics. The first model to attempt an overtly time-resolved HIF-α response to hypoxia was published by Qutub et Popel (2007). Here, the abstraction of HIF signalling was comprised of three feedback motifs. Negative feedbacks were provided by the HIF-PHD axis and the metabolically sensitive relationship between HIF and succinate production. An autocrine positive feedback was included which described HIF-1α regulating itself. The model is inclusive of many determining species, including; HIF-1α, hydroxylated HIF-1α, Fe^{2+}, succinate, PHD, 2-oxoglutarate and oxygen, pVHL binding and the constituent proteins of the pVHL ubiquitin ligase complex. The arrangement of species spans 6 equations and includes 18 parameters. Most relevant initial concentrations and rate kinetics are referenced to in three publications. A range of values are explored for unconstrained parameters. The Qutub et Popel model shares a similar ambition to our own, in that it explores how the duration of hypoxia affects intracellular concentrations of HIF-α over time, specifically addressing the interplay of the three feedbacks in determining the response. The kinetics of response hinge on delay terms for the HIF-1 production of HIF-1α and PHD2, using 3-hours and 4-hours respectively. The model outputs for total HIF-1α and PHD2 protein are fit to western blot data, capturing six time-points over the course of 72-hours. The model is not contradictory to our own and at a glance, is very detailed and considerate of many aspects of HIF-1α regulation. However, the model remains largely unproven against biological measurement. This is important as the model ambitiously attempts to predict the behaviour of many constituent species over the course of 72-hours of hypoxia. This is no trivial task given the measured and expected wide-spread changes to cellular biology in terms of cell-cycle, redox state, transcription, translation, DNA damage, cellular energy status and so on so forth (Gerald, Berra et al. 2004; Lee, Bae et al. 2004; Van Hoecke, Prigent-Tessier et al. 2007). The model proposed by Bruning *et al.* (2011) also investigates the HIF-1α protein response to hypoxia over a prolonged time-course. In contrast to the HIF-1α positive feedback of the Qutub et Popel model, Bruning *et al.* 2011 describe a negative feedback regulation of

HIF-1α mRNA and the functioning of this feedback alongside the HIF-PHD feedback loop. In this model, the arranged feedback motifs are able to convey an oscillatory profile to the downstream transcriptional output of the HIF-1. This finding is of interest for explaining the multiple transient accumulations within our own imaging data-set, an event left unexplained by our 4C-model. Finally, the model proposed by Schmierer *et al.* (2010) approaches the HIF regulation from a novel point; the regulation of HIF transcriptional activity by ankyrin protein sequestration of FIH. From a series of findings and publications, it is now known FIH is able hydroxylate other substrates beyond HIF-α (Cockman, Webb et al. 2009). To date, all identified FIH targets except HIF-1α contain an ankyrin repeat domain, a 33 aa residue protein motif found in 6% of eukaryotic protein sequences (Barrick, Ferreiro et al. 2008). Notable examples include p105, IκBα, IκBε and Notch-1 (Cockman, Webb et al. 2009). The exact purpose of the individual ankyrin hydroxylations has not yet been convincingly and assuredly stated. The model produced by Schmierer *et al.* reports on plausibility that the ankyrin repeat proteins can act as a *sink* for FIH, which in turn effects the transcriptional regulation of HIF-α by FIH. Similar to the models produced by Kohn *et al.* and Dayan *et al.* there is little suggested about the kinetics of response, but instead the steady-state solutions of varied oxygen tensions. Notably this model lacks the HIF-PHD feedback loop, the only HIF model to do so. It may be an interesting prospect to meld our 4C-model to this model and investigate the potential kinetics of FIH sequestration. In summary, although several other HIF models have been produced ours remains distinct in the central appreciation of the HIF-PHD feedback and the manner by which the model was informed against biological measurement. Unlike previous models, our own suggests the scope for the sensitivity of the transitional kinetics to encode the context of disrupted oxygenation, as well as making transparent potential significant crosstalk points. However, our model does not necessarily compete as we have attempted a much more restricted topology (a bottom-up approach) and only attempt to explain the first 24-hours of hypoxia. Ideally our model may work alongside the other existing models, serving as basis for further exploration and corroboration of the proposed regulatory mechanisms, whether it is the additional positive and negative feedbacks or the sequestration of FIH.

Reference	Model Details
Kohn *et al.* 2004	**Switch-like properties of HIF bio-regulatory network** The model details 23 species interacting through 32 reaction constants, which have either been arbitrarily set or qualitatively fit. The PHD2 & -3 feedback are contained within the depicted regulatory network.
Qutub *et* Popel 2007	**3-autocrine feedback model** The model describes three autocrine feedback loops using 17 species and 18 parameters. The signalling topology is comprised of two negative and one positive feedback mechanism, notably including the PHD feedback.
Yu *et al.* 2007	**Pathway switching to describe sharp response of HIF network** A model dissecting the contribution of the quantitative arrangements of the Kohn et al. model, suggesting how the number interplay results in a sharp response profile of HIF accumulation to hypoxia.
Dayan *et al.* 2009	**Non-redundant roles of PHD and FIH in regulating gene expression** An adaptation of Kohn *et al.* 2004. The model details 16 species interacting through 23 reaction constants. Parameters from Kohn *et al.* 2004 have been carried across and with some updating in accordance with western-blot and gene expression data. Notably HIF-1β has been removed from the signalling network.
Schmierer *et al.* 2010	**Hypoxia-dependent sequestration of FIH** The model describes 5 variables and 4 constant species acted upon via 13 parameters. The parameter values are derived in several ways, either estimated, ranged, arbitrarily set or used published values.
Heiner et Siriam 2010	**Structural Analysis to determine core HIF response network** Analysis and reduction of the Yu et al. model, a model originating from Kohn et al. A principal aim of this model was to reduce the model complexity and describe the core HIF module.
Bruning *et al.* 2011	**MicroRNA-155 feedback model** A model encapsulating the PHD2 feedback motif and a microRNA feedback (targeted against HIF-1α mRNA). The model spans 4 ODE equations which represent 18 parameters. Model parameterisation was performed *via* fitting to several western blot data.

Table 5.2. Table summarising known published HIF mathematical models and analyses of the models

Chapter 6: Sub-cellular structures and HIF

6.1 Introduction & Aims

6.1.1 Observed and distinct intracellular localisation of HIF-2α

Throughout the previous chapters, the majority of focus has been on the temporal profiling of the HIF signalling pathway. Alongside this, the use of high-resolution time-lapse imaging has also afforded us insights into the spatial characteristics of the pathway with regards to the cellular distribution pattern. A focus on intracellular localisation was spurred on when imaging HIF-2α, as the localisation was found to be non-homogenous, occurring as speckles mainly localised to the nucleus and excluded from the nucleolus (**Fig 6.1**). Despite the many reported functional similarities between HIF-1α and HIF-2α, HIF-1α was found to be homogenously localised to the cell nucleus. A large body of work is focused upon the difference between these two similar isoforms, dissecting their individual gene expression profiles, occurrences in pathology or unique crosstalk events (Raval, Lau et al. 2005; Bracken, Fedele et al. 2006; Elvidge, Glenny et al. 2006). To date, the subcellular localisation pattern of these two transcription factors has not been overtly addressed, although HIF-2α speckles were observed by Hara *et al.* as early as 1999 (Hara, Kobayashi et al. 1999). The aim for this chapter was to explore further the localisation pattern of HIF-2α. Towards the end of the project time-line, HIF-1β and PHD3 were also seen to show sub-cellular aggregates/speckles (**Fig 6.1**) and so additionally these were investigated in relation to the observed HIF-2α localisation pattern, though this avenue of work remains preliminary.

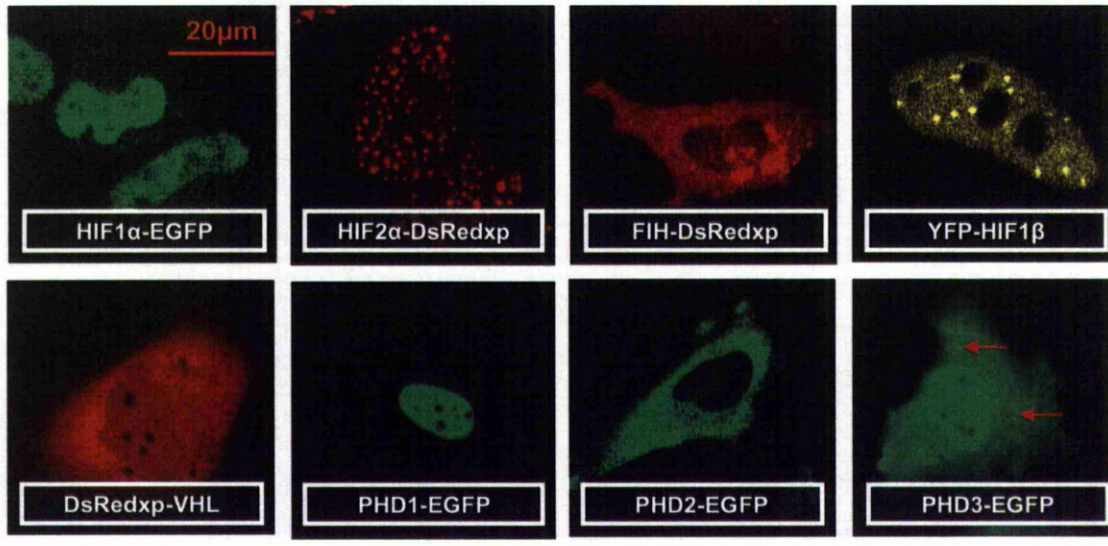

Fig 6.1. Live-cell confocal microscopy of HeLa cells ectopically expressing fluorescent fusion proteins of the canonical HIF pathway. Non-homogenous punctate fluorescent structures were observed for HIF-2α, HIF-1β and PHD3 (PHD3 aggregates are subtle at this magnification; red arrows have been used as a visual aid though a more zoomed image is shown in figure 6.16). Large aggregates of protein were seen when imaging FIH-DsRedxp.

6.1.2 Sub-cellular structures of the eukaryotic cell

The intracellular localisation of components, such as proteins, is often a functional and defining feature. Transcription factors elicit their effect on gene expression when localised to the cell nucleus, receptor proteins of the outer membrane are necessary to communicate extracellular information to the intracellular environment and mitochondrial proteins are required in the mitochondrial space and disruption to this can commit the cell to apoptosis etc. (Tafani, Karpinich et al. 2002; Rubenstein, Zauhar et al. 2006; Farnham 2009). Understanding the intracellular localisation of a protein is therefore often a part of understanding the function. To further complicate the issue, the eukaryotic cell is often portrayed as homogenous compartments separated into organelles *via* lipid membranes. It is through this mechanism that cellular organisation and spatial regulation are understood to be achieved. However, over the last few decades a very complex picture of the spatial regulation of mammalian cells has emerged (**Fig 6.2**) (Swift 1959; Beck 1961). It is becoming widely recognised that many non-lipid bound sub-cellular organisations exist and that these structures are integral to an assortment of physiological and pathological processes, ranging from autophagy, resistance to viral infection, mRNA splicing, ribosome biogenesis, spatially regulated transcription and the misfolded protein response (Kopito 2000; Lamond and Spector 2003; Jackson 2005; Sirri, Urcuqui-Inchima et al. 2008; Nakamura, Kimple et al. 2009; Geoffroy and Chelbi-Alix). These are often self-assembling structures composed of a rich variety of proteins, characterised with varying defining traits (listed at the end of the chapter in **Table 6.1**) (Spector 2001; Lamond and Spector 2003). In spite of representing membrane-free organisations, the known speckling phenomenon are often characterised by the cellular compartment they are found in, whether nuclear or cytoplasmic (Spector 2006). The nucleus is known to contain a rich assortment of sub-nuclear and punctate structures, including nuclear speckles, PML nuclear bodies, paraspeckles, cajal bodies, clastosomes, polycomb bodies, transcription factories as well as the nucleolus(Spector 2001; Lamond and Spector 2003). Cytoplasmic entities are less well described and not grouped as a coherent research field, possibly owing to the greater diversity of function and make-up. Focal adhesions are speckle-like (somewhat elongated) structures visible in the cytoplasm of the cell, forming part of the machinery needed for traction in cellular locomotion and as signalling hubs propagating

information from the extracellular environment (Fraley, Feng et al. 2010). Additionally, inclusion bodies and their sub-type aggresomes appear as speckle-like structures and these are known to exist in either (or both) the cytoplasm or the nucleus (Kopito 2000). Stress granules are irregular shaped entities, appearing in the cytoplasm as a result of stalled mRNA translation; additionally the stalled mRNA can shuttle between another subcellular body known as processing bodies (Yang, Yu et al. 2006).

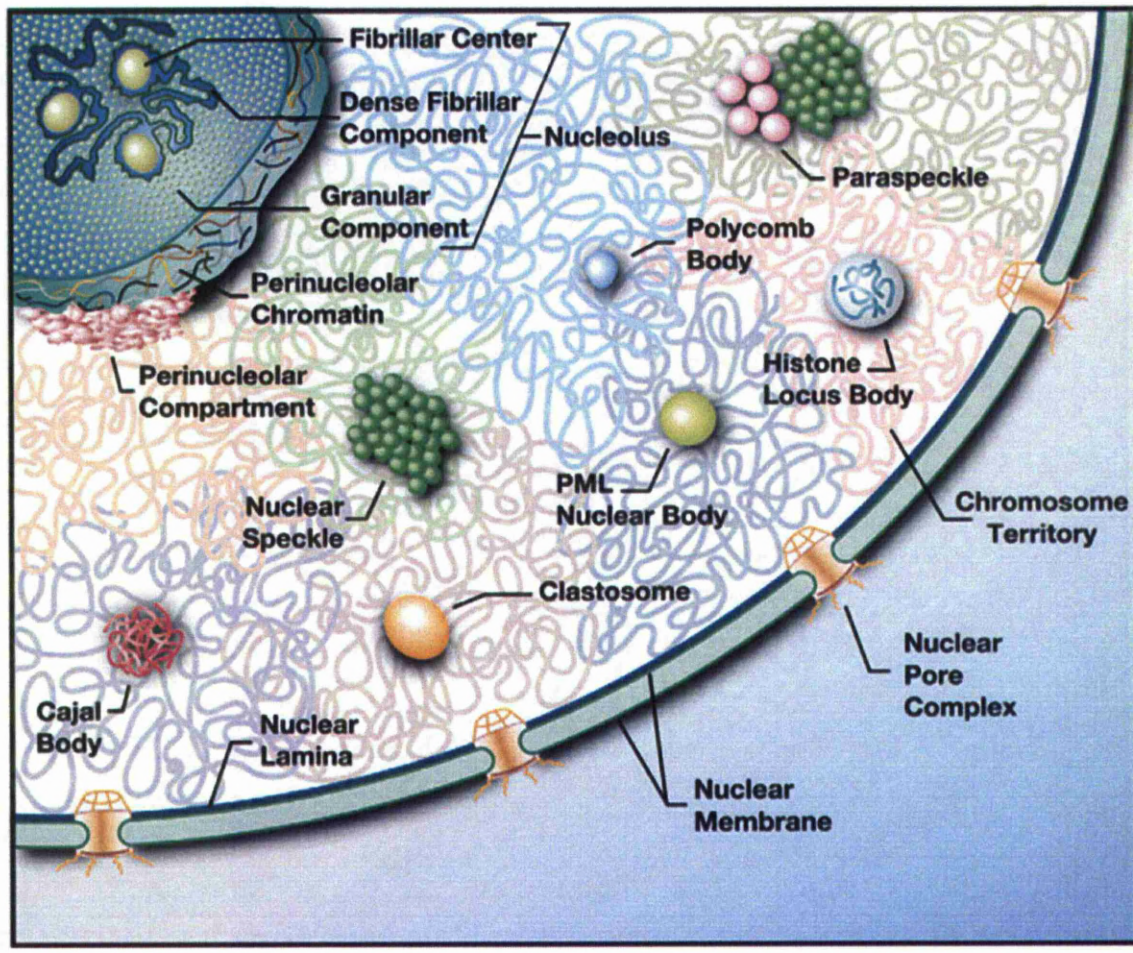

Fig 6.2. Figure taken from Mao *et al.* 2011 (Mao, Zhang et al. 2011). The picture is representative of a mammalian cell during interphase. Known nuclear cellular bodies are shown. For a detailed description of each entity see table 6.1.

6.2 Results

The non-homogenous spatial distribution of HIF-2α has not been addressed and there are very little clues in the literature to suggest to which speckling phenomenon HIF-2α belongs. We sought to systematically address key features of the various known speckling instances in relationship to the observed HIF-2α phenomenon.

6.2.1 Variance in localisation pattern of EGFP-HIF2α

An often fundamental and identifying feature of protein speckling is the cellular localisation. The localisation of EGFP-HIF2α expressed in HeLa cells was investigated. HeLa cells were plated and then transfected with pG-EGFP-HIF2α 24-hours prior to confocal imaging. Five by five tile scan images were then taken using a 63x objective in order to build a broad high-resolution mosaic image. Locations to image were selected at random. Fluorescence levels of both the nuclear and cytoplasmic compartment were then determined using the Cell Tracker software and nuclear to cytoplasmic ratio (N:C) calculated. The N:C ratio was used a determinant for the classification of the localisation pattern (**Fig 6.3**). Of the 74 cells imaged, 81% were found to have a N:C ratio greater than 5 appearing *very* nuclear, 11% were considered ubiquitous with N:C values between 1 to 4.99 and finally 8% were found to be preferentially cytoplasmic having N:C values below 1. In comparison, HIF-1α is found to be nuclear in 100% of instances (data not shown).

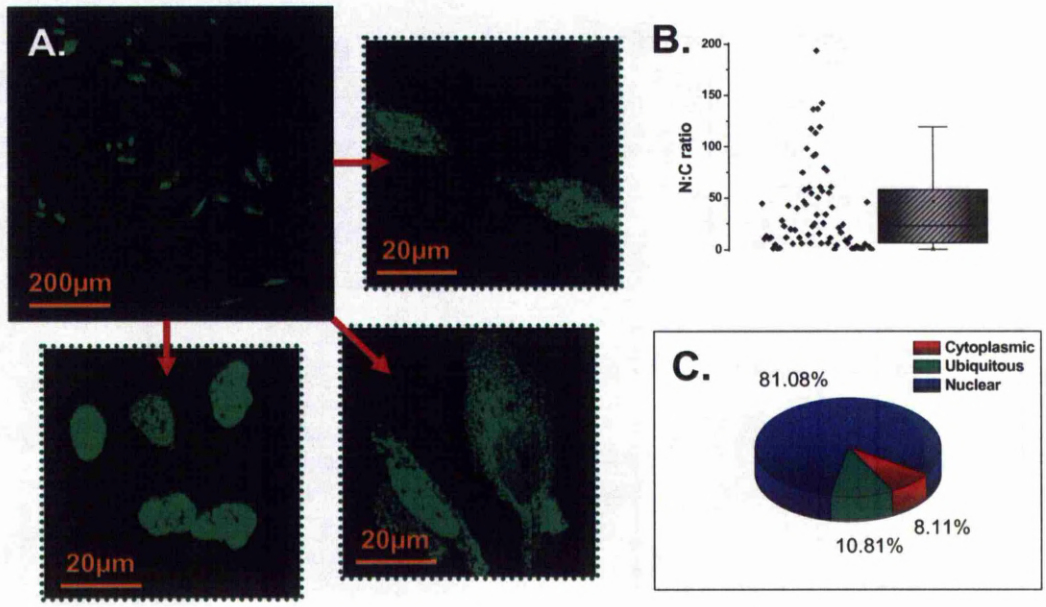

Fig 6.3. Live-cell confocal microscopy of HeLa cells (**A**) 5x5 Tile scan image of HeLa cells ectopically expressing EGFP-HIF2α. Three groups of cells are highlighted from the original image showing varied localisation patterns. (**B**) Calculated N:C ratio of all cells imaged. (**C**) Categorisation of localisation as determined using the N:C ratio data.

6.2.2 Are the speckles artefacts of fluorescent fusion?

The fusion of a fluorescent protein has been previously reported to lead to aggregates due to steric hindrance of the native protein (Thomas and Maule 2000). To investigate this possibility, HeLa cells were plated and then transfected with either fused or IRES expression vectors encoding fluorescent HIF-1α/-2α; noting the presence of an IRES sequence leads to the separate translation of EGFP from the protein of interest (Pelletier and Sonenberg 1988). After 24-hours cells were fixed (methodology in **section 2.6.4**.) and probed with anti-HIF-1α or anti-HIF2α primary antibodies, then prepared for imaging by labelling with red conjugate secondary antibodies. Confocal microscopy of the samples showed antibody detection of HIF-1α to be nuclear and uniform for both expression from the IRES and fused vectors (**Fig 6.4**). However, imaging of antibody detected HIF-2α once again showed a predominantly nuclear speckle-like localisation pattern, including for the unfused form. There was a good degree of correlation between the localisation of the fluorescent fusion speckles and the antibody detected proteins. Any discrepancy was argued by the fact that not all fluorescent fused EGFP may have fully matured (Harper, Finkenstadt et al. 2011).

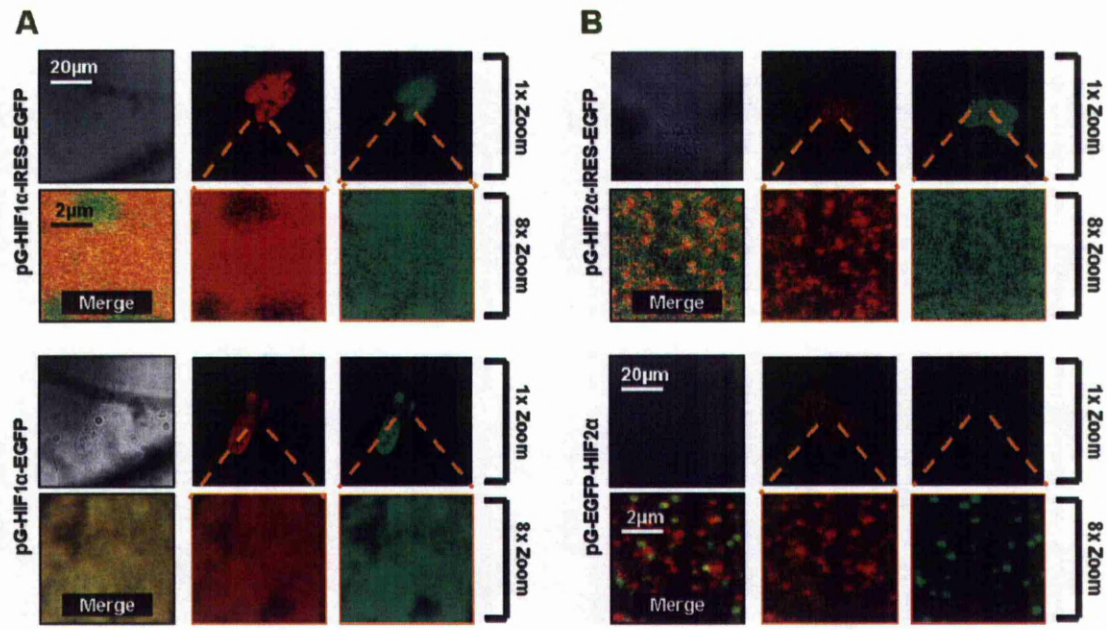

Fig 6.4. HeLa cells transiently transfected to express unfused EGFP, or HIF-α expression plasmids. 24-hours after transfection cells were fixed by paraformaldehyde and antibody labelled (red staining), probing for (**A**) HIF-1α or (**B**) HIF-2α.

6.2.3 Are the speckles the result of overexpression?

Most sub-cellular protein organisations are characterized as being either nuclear or cytoplasmic (Spector 2006). Our previous results indicate that EGFP-HIF2α speckles can exist in either the cell nucleus, cytoplasm or both. A possible explanation is that the over-expression of HIF-2α results in protein aggregates able to form in both cytoplasm and nucleus, but with a higher propensity for the nucleus due to the higher concentration of HIF-2α (Mayer and Buchner 2004). This would furthermore suggest the speckles to be an experimental artefact and likely to have reduced relevance for the endogenous level protein. To address this, non-transfected HeLa cells were analysed by immunocytochemistry probing for endogenous HIF-1α and HIF-2α protein. HeLa cells were plated and incubated for 24 hours, then either remained unstimulated or were treated with 0.5mM DMOG for 6 hours. After this period cells were then paraformaldehyde fixed. Samples were then antibody stained as for the previous experiment then imaged by confocal microscopy. HIF-1α levels were undetectable in the unstimulated sample, though strongly evident in the DMOG treated condition (**Fig 6.5**). The antibody labelling of HIF-1α in this condition were found again to be nuclear and homogenous DMOG stimulated. HIF-2α was detected in both unstimulated and stimulated conditions, at levels equivalent to one another, thereby mimicking the trend observed from earlier efforts of western blotting in chapter 3 and chapter 4. Once again, the fluorescent profile was found to be non-homogenous and speckle-like, mostly found in the cell nucleus with some observations of cytoplasmic speckling. These results strongly suggest that HIF-2α speckles to occur at the endogenous level and are not an artefact of over-expression.

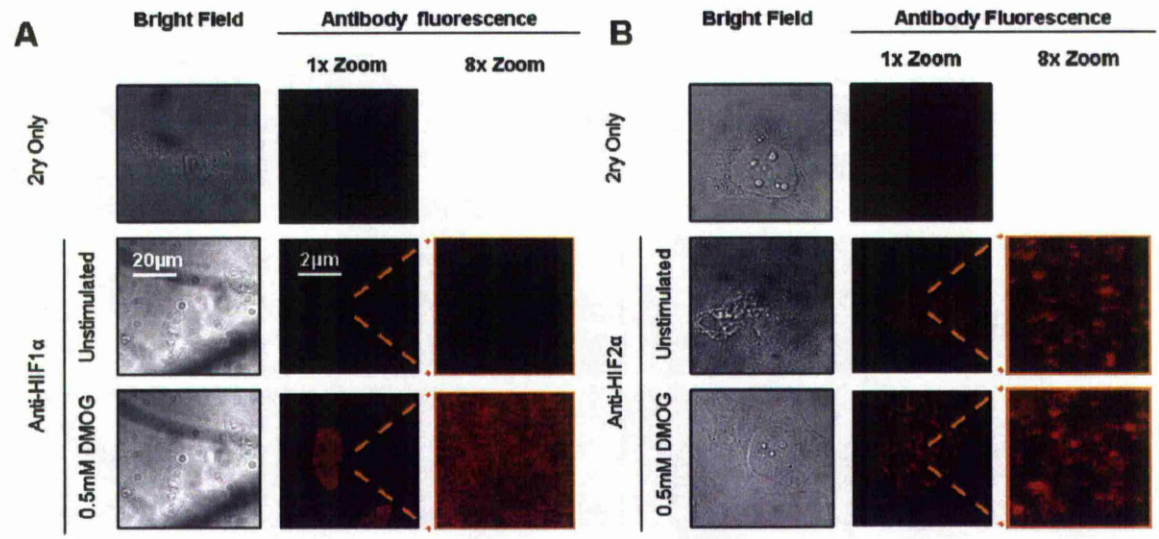

Fig 6.5. Untransfected HeLa cells either remained unstimulated or were treated with 0.5mM DMOG for 6-hours. Cells were then paraformaldehyde fixed and antibody labelled (red staining), probing for (**A**) HIF-1α or (**B**)HIF-2α.

6.2.4 Is EGFP-HIF2α speckling unique to HeLa cells?

An additional possibility was that speckling of HIF-2α was unique to our chosen cell line of HeLa. Previous reports of cell line discrepancy emerged for the investigation of gemini of cajal bodies in HeLa cells, originally investigated by Liu and Dreyfuss 1996. A marker protein exclusive to the gemini of cajal bodies in HeLa cells was found to have a much more general role in cell speckling in other cell lines (Nizami, Deryusheva et al. 2010). Several cell lines were therefore used to investigate whether HIF-2α speckling occurs in cell-type dependent manner. The cell lines to be used were, the neuroblastomas SK-N-AS cell line, the medulloblastoma cell lines D283 and Med8 and a mouse primary neuronal cell line. All cells were transiently transfected with pG-EGFP-HIF2α using FuGene 6. After 24-48 hours transfection cells were imaged by confocal microscopy. Speckling was observed in all instances, obeying a similar profile to the images of HeLa HIF-2α speckles (**Fig 6.6**).

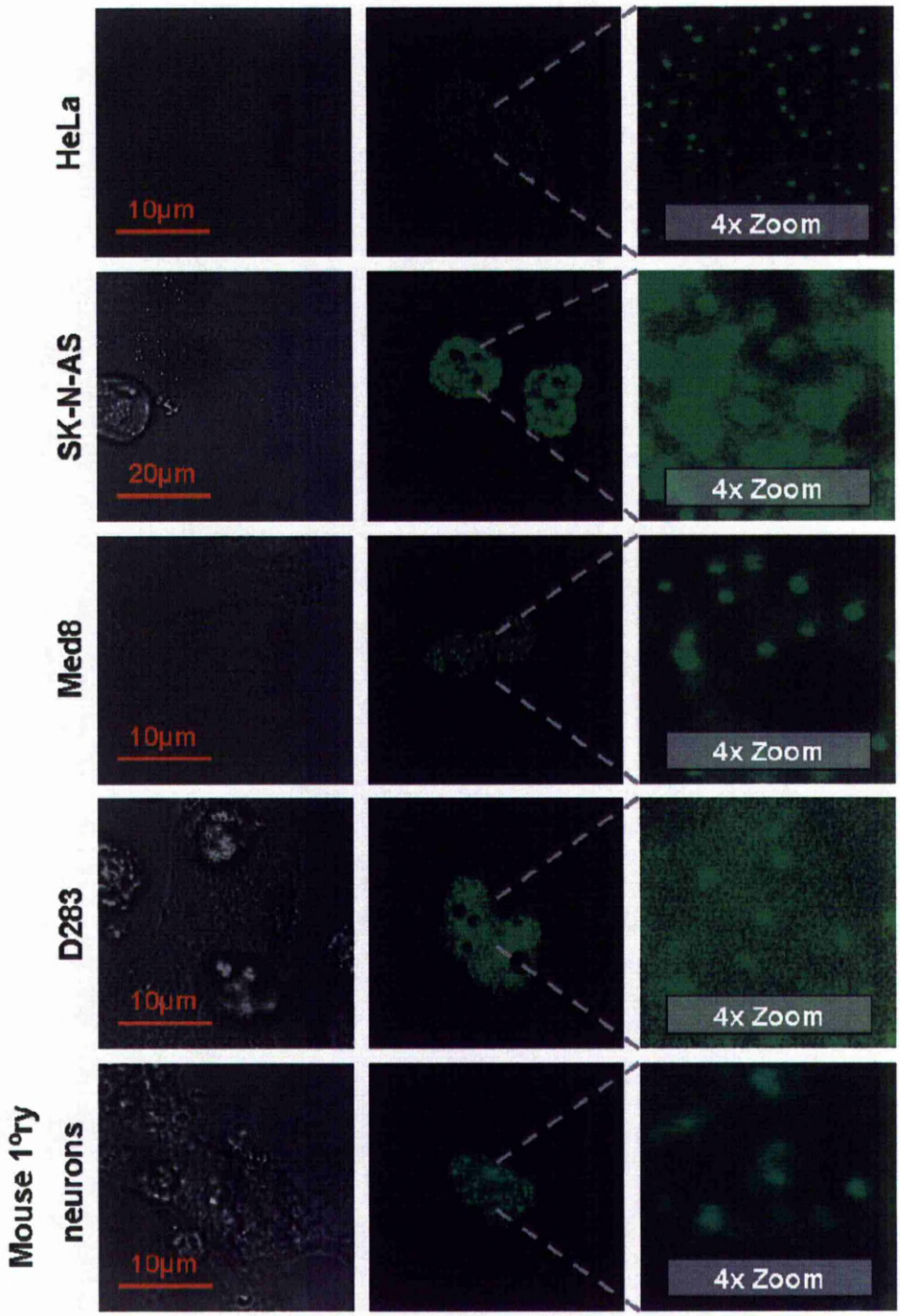

Fig 6.6. Live-cell confocal microscopy of five cell lines ectopically expressing EGFP-HIF2α.

6.2.5 Characteristics of speckles; size, count and velocity

A defining feature of many different speckling types is the size, morphology and number present in a cell. Inclusion bodies are cited to occur at a frequency of 1-3 per cell whereas up to 50 interchromatin granule clusters have been counted in a single-cell (Spector 2006). Revisiting our previous imaging data, the speckle occurrence was investigated. Images pertaining to the live-cell imaging of HeLa cells expressing were analysed by AQM kinetic tracker as the program

is able to automatically detect individual speckles after manually setting several detection parameters (**Fig 6.7**). Of the 15 cells analysed, the average number of speckles was found to be 105±39; a value exceeding records for most speckling phenomenon (Spector 2006). Next we quantified the number of HIF-2α speckles occurring in the non-transfected immunocytochemistry data described previously. Here we found a value of 64±32, measuring only 3 cells. Additionally the sizes of the speckles were calculated through these analysis procedures. From the EGFPHIF2α data set the average speckle size per cell was found to be 3.3μm with a standard error of the mean of 0.35. 96.3% (n=1522 of 1580 speckles) were found to be below 10μms. Only a weak correlation (R^2 = 0.03) was found between speckle size and number of speckles per cell. Finally, the ability to image speckles by time-lapse microscopy affords us the chance to measure the movement velocity of the speckles. From this we aimed to assay whether the speckles move faster or slower than Brownian motion, as similarly investigated by Chang *et al.* examining herpes viral replication compartments and nuclear speckles (Chang, Godinez et al. 2011). HeLa cells expressing EGFP-HIF2α were imaged every 0.5 seconds for 60 seconds by live-cell confocal microscopy, imaging a total of 16 cells. AQM kinetic tracker was used to detect and analyse speckle movements. The average speckle velocity was found to be 0.29μm/second with a standard error of the mean of 0.01. The majority of speckles, 68.2% (n= 175 of 255) were found to move under a distance of 0.3μm per second. Similar values were reported by Rino *et al.* 2007 in a study using fluorescence recovery after photobleaching to assess spliceosome movements. In this study, brownian motion was used to later computationally model the movements of the spliceosome speckles (Rino, Carvalho et al. 2007). Variance in speckle movement has been attributed to the density and compactness of the nucleus (Shav-Tal, Darzacq et al. 2006). So though we haven't implicitly tested our data against brownian motion models, it would appear that the movements of the HIF-2α speckles are within these limits.

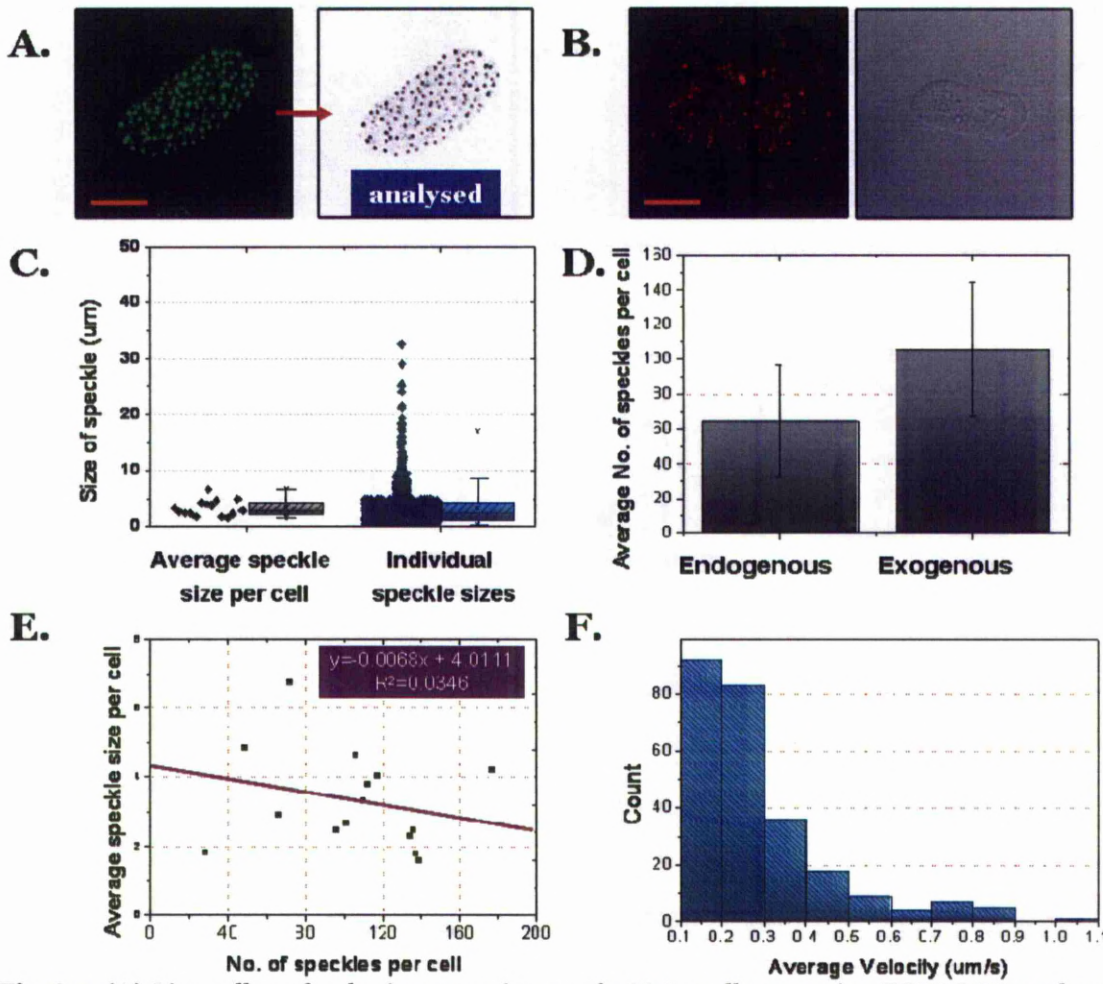

Fig 6.7. (**A**) Live-cell confocal microscopy image of a HeLa cell expressing EGFP-HIF2α, then the automatic detection of speckles using AQM kinetic tracker. Red crosses indicate detected speckle. (**B**) Immunocytochemistry preparation of non-transfected HeLa cell staining with an anti-HIF2α antibody and imaged by confocal microscopy, showing both fluorescence and brightfield channels. Scale bars for all images denote 10μms. (**C**) Box-and-whisker plot showing the average speckle size and individual speckle size calculated from HeLa cells expressing EGFP-HIF2α. (**D**) Comparison bar chart for the detected number of speckles between immunocytochemistry images of anti-HIF2α non-transfected cells and exogenous speckles detected in EGFP-HIF2α expressing cells. (**E**) A scatter plot of the correlation between speckle size and number, determined using EGFP-HIF2α expressing HeLa cells. (**F**) The velocity of the movement of speckles was determined after imaging EGFP-HIF2α for 60-seconds, imaging every 0.5 seconds.

6.2.6 FRAP analysis of speckles

Many speckling phenomenon have been shown to be dynamic, with regards to the flux of protein in and out and the movement of the speckle itself (Handwerger, Murphy et al. 2003; Chang, Godinez et al. 2011). Fluorescence recovery after photobleaching provides a powerful tool to assay protein dynamics and several speckling phenomenon have been evaluated using this methodology (Rantanen, Pursiheimo et al. 2008; van Royen, Farla et al. 2009). They have the capacity to provide highly quantitative data and with sufficient analysis can be used to determine diffusion coefficients, mobile and immobile

fractions present and the rate of exchange between immobile and mobile fractions (van Royen, Farla et al. 2009). Using this approach, we were interested to determine whether the speckles were static aggregates or dynamic entities. HeLa cells were transfected with pG-EGFP-HIF2α, after 24-48 hours cells were imaged by confocal microscopy and several cells selected ready for photobleaching. Photobleaching was carried, bleaching a circle of a diameter 6μms briefly and repetitively for 10 seconds using high intensities from a 488 nm argon ion laser. This process resulted in the immediate loss of speckle fluorescence in the bleached area. The fluorescence was found significantly recover within a minute of bleaching. Importantly, the fluorescence recovered at the same speckle locations strongly suggesting these to be dynamic entities with a continuous flux of protein in and out (**Fig 6.8**). Additional bleaching experiments were performed, single circular regions of 1μm (corresponding to a single-speckle) were bleached. From the 8 cells bleached in this instance, 7 were found to recover within 60-seconds. These data allude to the possibility of different HIF-2α speckling phenomenon within the cell.

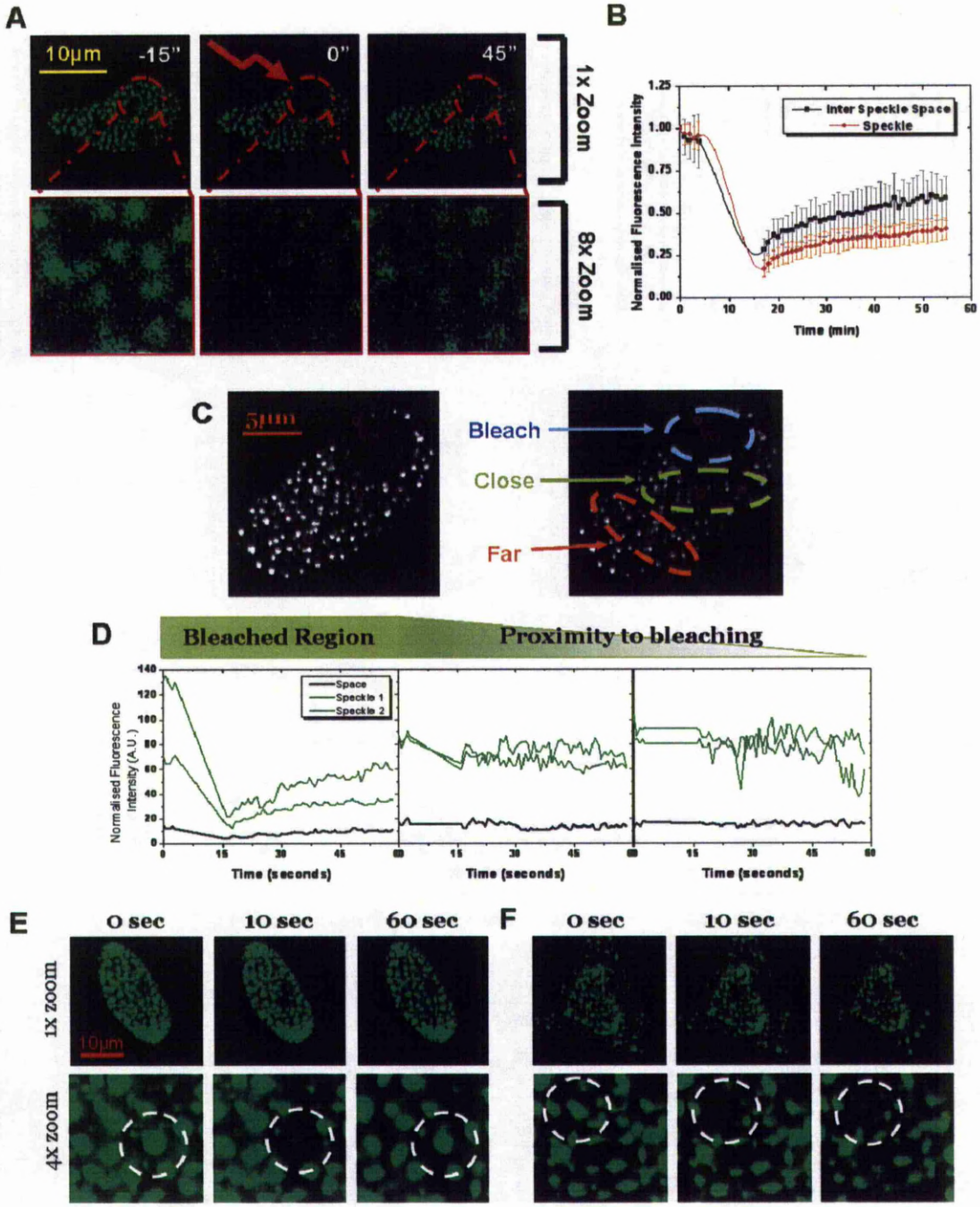

Fig 6.8. Fluorescence recovery after photobleaching of EGFP-HIF2α (**A**) Confocal imaging of HeLa cells transfected with EGFP-HIF2α. A circular of region of 6µms was bleached for 10secs following 75 iterations of high intensity excitation by a 488 argon ion laser. (**B**) The fluorescence levels of the bleached speckles and inter speckle space were quantified and plotted as an average. (**C**) Single-speckles fluorescence was measured at different proximities to the bleached region using Cell Tracker. (D) Representative plots of single speckle fluorescence recovery. (**E** & **F**) Confocal imaging of HeLa cells in which single speckles have been photobleached. (**E**) shows a representative cell seen to recover (**F**) shows a representative cell failing to recover fluorescence.

6.2.7 FRET analysis on HIF-2α self binding

Förster resonance energy transfer (FRET) is a technique used to investigate protein interactions in single living cells. The technique takes advantage of

overlapping excitation and emission spectra of a pair of fluorophores, in which the emission of one of the pair excites the fluorescence of the other when in close enough proximity of one another (Periasamy 2001). The photobleaching of one of an interacting pair has repercussions to the fluorescent output of the other, thereby providing quantifiable information on the interaction. Classically CFP and YFP are the FRET pair of choice, though a publication by Erickson *et al.* 2003 demonstrated the functioning of EGFP and DsRed as a FRET pairing. We aimed to examine if there was evidence of intermolecular FRET between HIF-2α, using the EGFP and DsRedxp fused forms cloned in chapter 3. HeLa cells were co-transfected with these expression vectors for 24-48 hours. Once again, single-speckle bleaching was performed, bleaching regions of 1μm (**Fig 6.9**). However, this time red fluorescence was bleached using high intensity emission from a helium/neon 543nm laser. Remarkably, not only was there no evidence of FRET but no evidence of fluorescence recovery for the experiment.

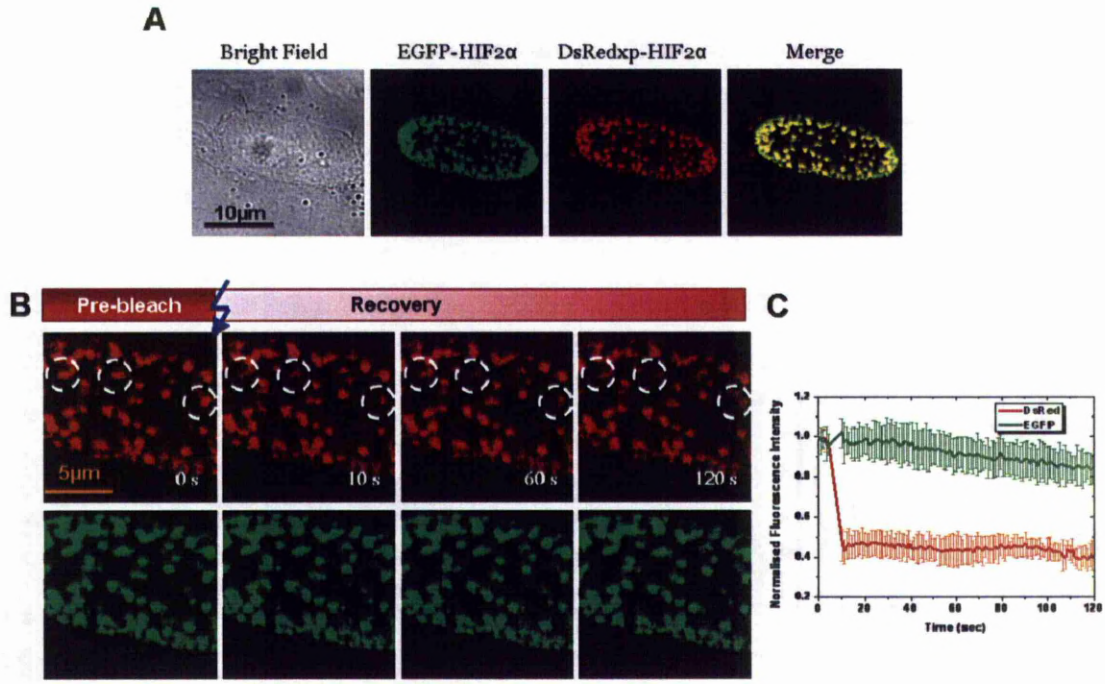

Fig 6.9. FRET analysis of intermolecular HIF-2α interactions. (**A**) Live cell microscopy of HeLa cells co-expressing EGFP-HIF2α and DsRedxp-HIF2α. (**B**) DsRedxp fluorescence was photobleached using high intensity 543nm laser excitation. (**C**) Quantified fluorescence of bleached speckles, showing EGFP and DsRedxp average cell traces and standard deviation. Fluorescence levels were normalised to to.

6.2.8 Negative correlation of speckle-localisation and RNApol2

Speckling can occur when transcription factors associate in high density with discrete nuclear structures responsible for gene expression termed transcription factories (Jackson 2005; Mitchell and Fraser 2008). Transcription factories add

a spatial element to our understanding of gene expression. An often defining feature of these factories is the presence of RNA pol II, the enzyme tasked with the transcription of DNA to RNA, including mRNA and microRNA. We sought to investigate the relationship of the nuclear localised speckles with RNA polII. HeLa cells were again transfected to express EGFP-HIF2α over a period of 24-hours. Cells were then fixed and prepared for immunocytochemistry staining, using a primary antibody against RNA pol II. The co-localisation of antibody detected RNA pol II fluorescence was compared to EGFP-HIF2α fluorescence. In contrast to expectations, RNA polII was found to negatively correlate with the localisation of HIF-2α (**Fig 6.10**). This may suggest a speckling phenomenon such as polycomb bodies, known as gene silencing cellular bodies that correlate to the absence of RNA pol II (Sexton, Schober et al. 2007).

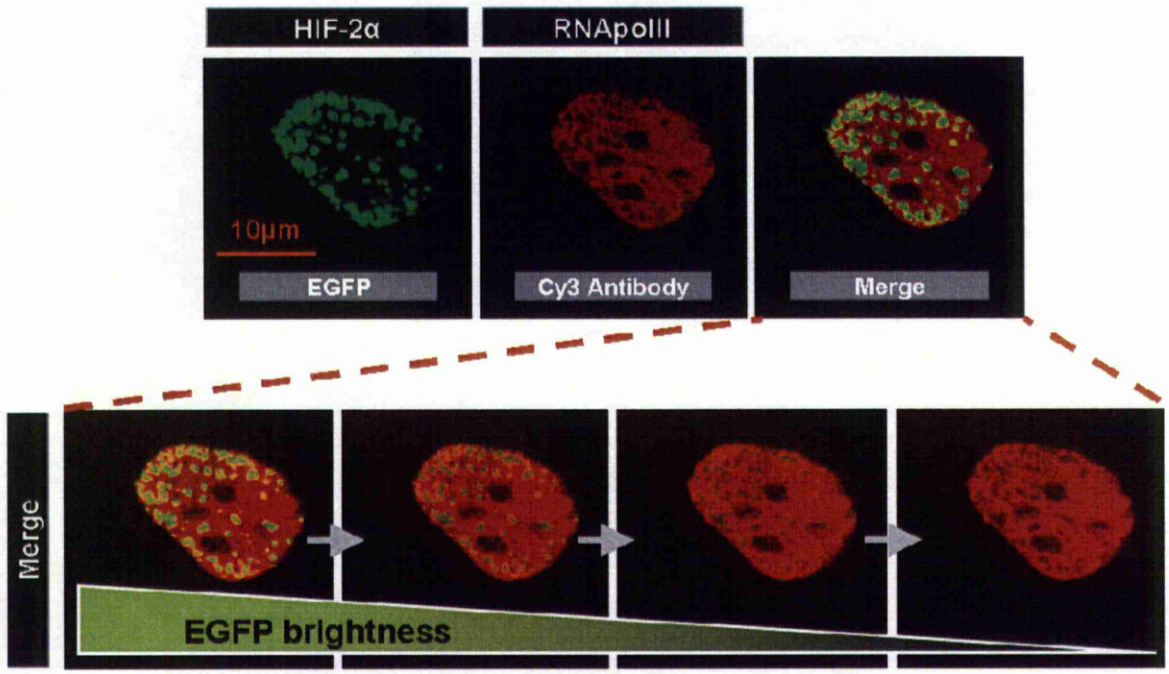

Fig 6.10. Immunocytochemistry of HeLa cells expressing EGFP-HIF2α and antibody probed for RNApol II. The negative correlation of localisation is highlighted by decreasing EGFP brightness.

6.2.9 Speckles are evident during mitosis (metaphase)

Several cellular bodies are sensitive to cell cycle progression, including OPT (Oct1/PTF/transcription) domains and mitotic interchromatin granules (MIG), in which the later is reported to become entirely diffuse during metaphase through to anaphase (Lamond and Spector 2003; Nizami, Deryusheva et al. 2010). To better characterise the HIF-2α speckles attention was given to dividing cells, and the status of the speckles investigated. Samples prepared earlier were imaged by confocal microscopy, using HeLa cells labelled for

endogenous HIF-2α (antibody). Cells showing distinct chromosome alignment, concordant with formation of the metaphase plate, were searched for and selected to image (Jaqaman, King et al. 2010) (**Fig 6.10**). During metaphase the cell morphology changes and depth increases, affecting the amount of cytoplasm present within the focal plane. To account for this, metaphase cells were imaged through a z-stack. From these images, the speckle like localisation of HIF-2α was once again observed. Thereby suggesting these are not MIGs or OPT domains.

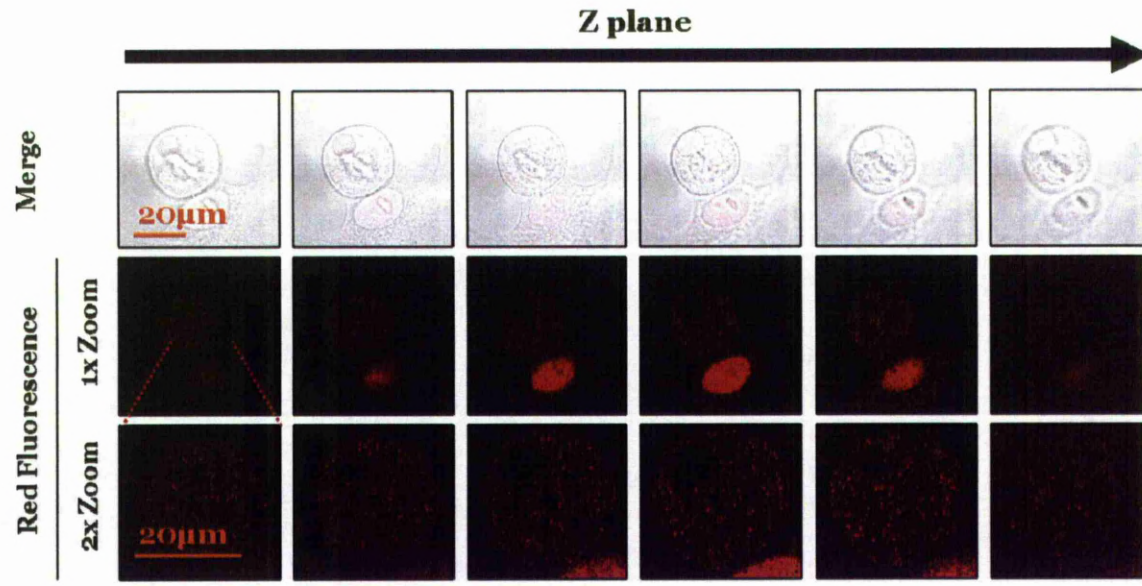

Fig 6.11. HeLa cells were fixed and prepared for immunocytochemistry using an anti-HIF2α antibody. A cell undergoing mitosis was imaged through the z-plane.

6.2.10 Sensitivity of HIF-2α speckles to microtubule disruption by Nocodazole

The active microtubule network is associated with aggresomes, stress granule formation, PML bodies and is indirectly associated with several more via the relationship of microtubules dynamics with cell cycle progression (Ivanov, Chudinova et al. 2003; Daniels, Marson et al. 2004; Bauer and Richter-Landsberg 2006; Cardinale, Cisterna et al. 2007). We were interested to determine whether HIF-2α speckles may belong to this subset of microtubule sensitive cellular bodies. To investigate this possibility, cells were transfected with EGFP-HIF2α then imaged by live-cell microscopy, remaining either unstimulated or treated with 1µM Nocodazole, a drug commonly employed to rapidly depolymerise microtubules (Vasquez, Howell et al. 1997). A degree of dynamism was seen when imaging HIF-2α speckles in the control condition, in which fluorescence levels increased or decreased and the morphology of the

speckles was also seen to change. This is in accordance with our earlier imaging of HIF-2α transiency and dynamics in chapter 4 (highlighted in **Fig 4.8**). Nocodazole treatment was found to acutely and dramatically affect the morphology and presentation of the speckles, often seen to lead to their increased size and irregularity. Though a range of responses was observed, also including the opposite situation in which some cells lost entirely the speckles. A high degree of cell death prevented a very accurate quantification of the response patterns. The data suggests that the HIF-2α speckles do have a relationship with the microtubule network, but the relationship appears to be complex and does not manifest as a single phenotypic response. Nevertheless, the data suggests the HIF-2α speckles to have a relationship with the subset of cellular bodies associated with the microtubule network. The resulting irregular aggregates after nocodazole treatment appears indicative of aggresomes.(Latonen 2011)

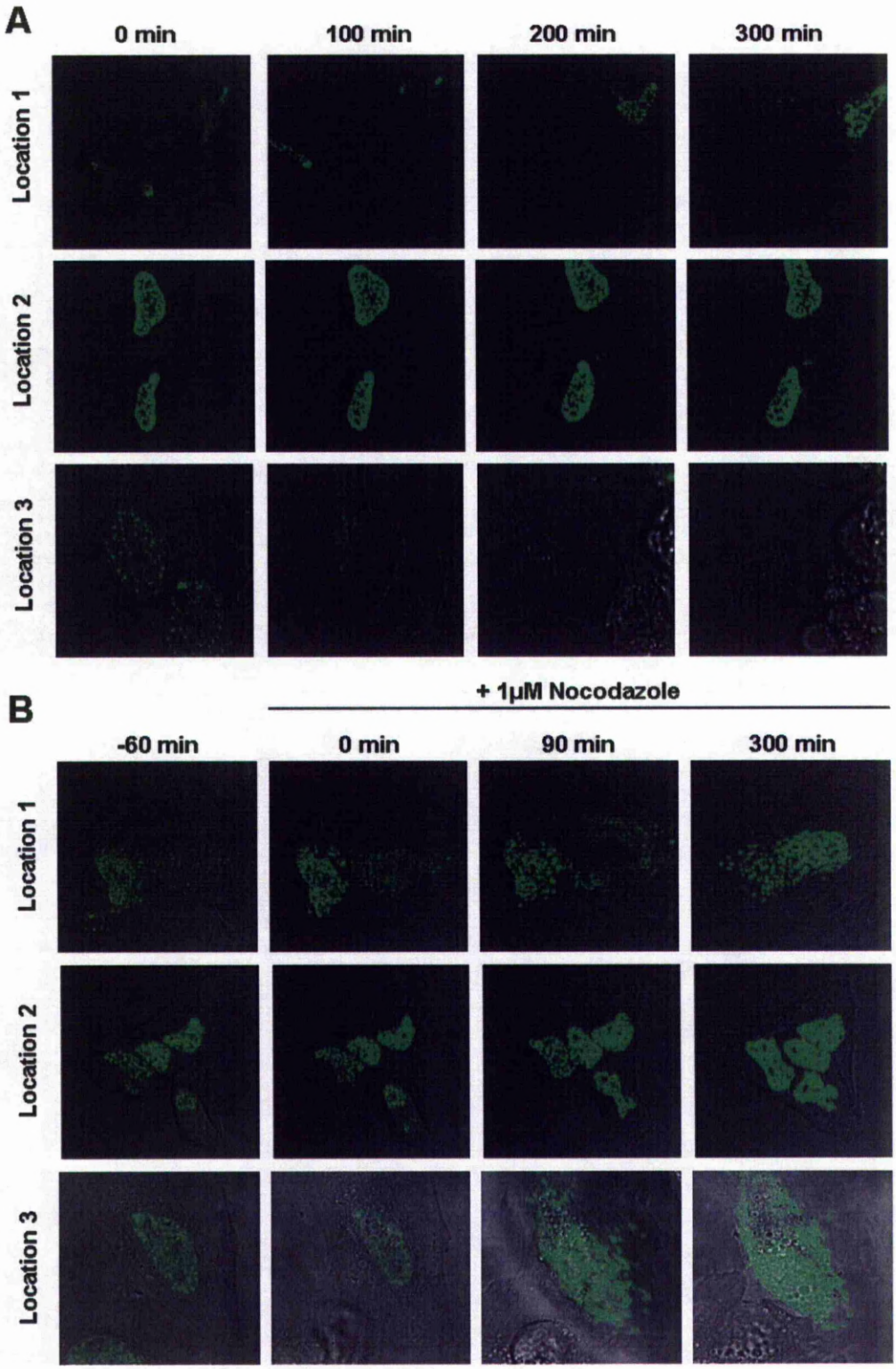

Fig 6.12. Live-cell confocal imaging of HeLa cells ectopically expressing EGFP-HIF2α. (**A**) Cells imaged for 300 minutes without stimulation. (B) Cells imaged for 60 minutes without stimulation, then imaged for a further 300 minutes following the addition of 1μM Nocodazole.

6.2.11 Co-localisation of HIF-2α with other speckling transcription factors

Many widely known transcription factors have been found to exist in the various cellular bodies; ongoing work within our own laboratory investigating separately p53 and NRF2, showed that both of these proteins form a type of cellular body. Review of both p53 and NRF2 attributes the localisation to the PML bodies (Fogal, Gostissa et al. 2000; Ben-Dor, Steiner et al. 2005). We were interested to see whether co-expression of fluorescent HIF-2α alongside p53 and NRF2 resulted in co-localisation of fluorescence, thereby implicating HIF-2α speckles with PML bodies. HeLa cells were co-transfected with expression vectors for DsRedxp-p53 and EGFP-HIF2α or with NRF2-venus and DsRedxp-HIF2α (p53 and NRF2 expression vectors were kindly supplied by Dr. R. Nelson and Miss K. Dunne, respectively). Expressing cells were imaged by confocal microscopy. A high degree of correlation was seen between the localisation patterns of all co-transfections, lending credence to the hypothesis that HIF-2α speckles are also related to PML bodies (**Fig 6.13**). A further observation was the reduced number and increased size of the HIF-2α speckles, though this data remains unquantified.

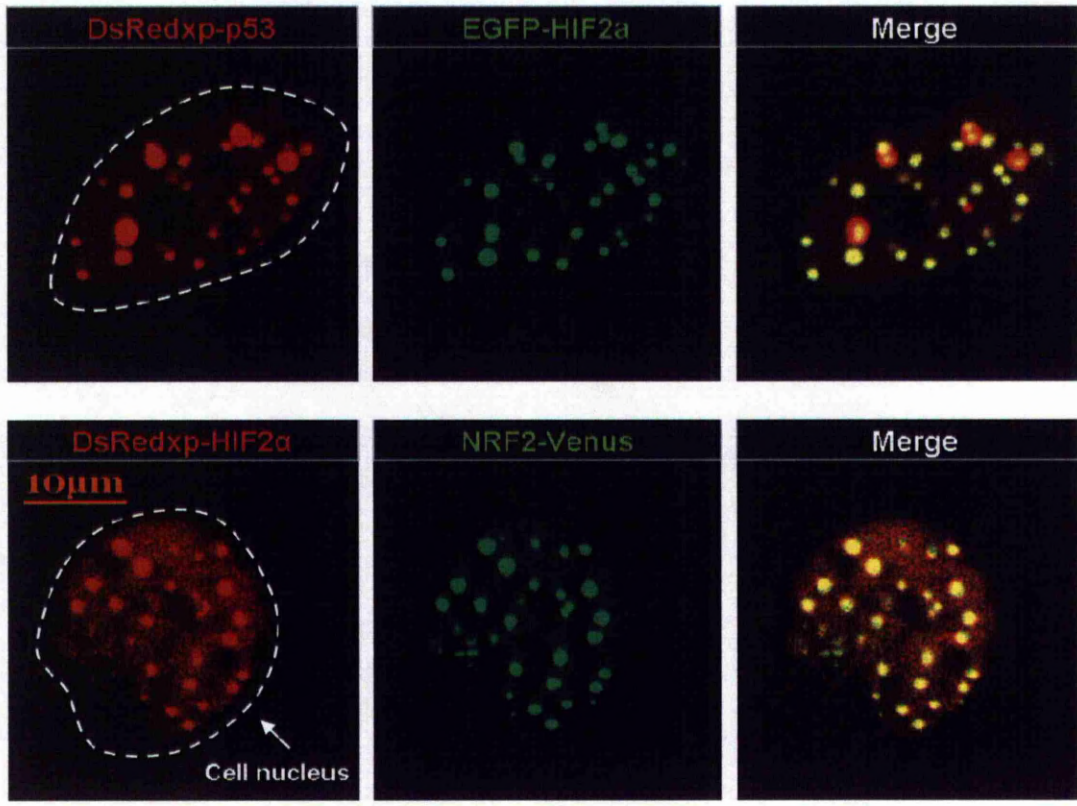

Fig 6.13. HeLa cells were co-transfected with HIF-2a and either NRF2 or p53 fluorescent fusion expression vectors then imaged by live-cell confocal microscopy.

6.2.12 Possible Fusion of speckles

A link between aggresomes and PML bodies has been reported, in which the fusion of PML bodies or PML-related aggregates is part of the maturation process of the nuclear aggresomes (Fu, Gao et al. 2005). This has also been shown to occur for Cajal bodies, which are able to associate and dissociate in the regulation of speckle size (Platani, Goldberg et al. 2000). Previous time-lapse imaging data of HIF-2aEGFP cells was reviewed and examined for fusion events (using images from the FRAP experiments of **Fig 6.8**). Several instances of possible fusion were observed, further suggesting the characteristics of the speckles to be dynamic and showing the HIF-2a speckles to exhibit a degree of plasticity (**Fig 6.14**). However, we cannot be truly certain that the speckles have fused and not just occupied a similar location in the x-y plane. A more detailed analysis method would be needed.

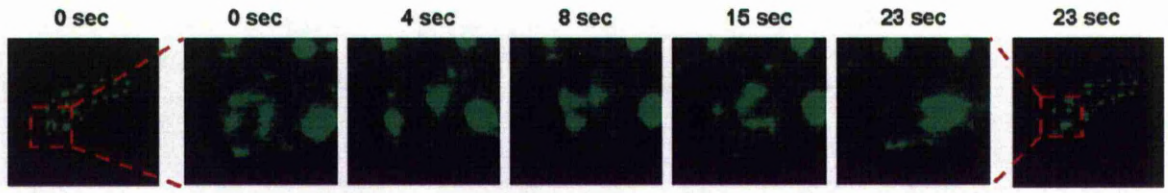

Fig 6.14. Live-cell confocal microscopy of a HeLa cell ectopically expressing EGFP-HIF2a. Magnified images are shown to highlight the possible fusion of speckles.

6.2.13 Evidence of dynamic morphology

Our current working hypothesis is that HIF-2α relates to several cellular bodies, including the aforementioned PML and aggresome structures. This would suggest a degree of dynamics in the morphology of the speckles to be presented. Control time-lapse images of unstimulated HeLa cells expressing exogenous EGFP-HIF-2α were reviewed in this light. From the time-lapse imaging data of ~50 cells, there were various instances in which the morphology of the speckles could be seen to change, often varying between aggregates and punctate speckles as well as re-localising to the perinuclear region or cytoplasm(**Fig 6.15**). These results may further suggest interplay between cellular bodies as proposed by Fu *et al.* (2005) between PML bodies and aggresomes.

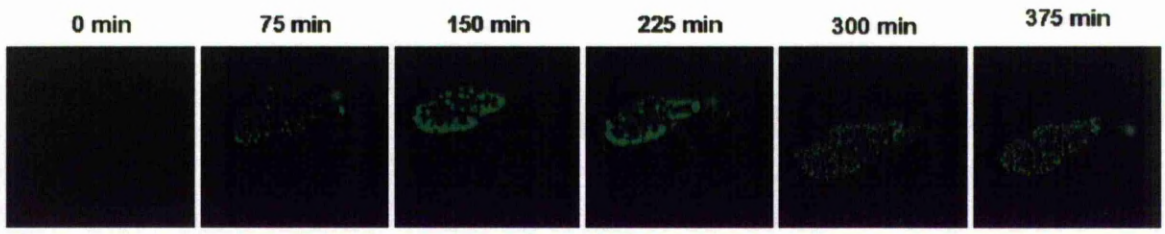

Fig 6.15. Live-cell confocal microscopy of a HeLa cell ectopically expressing EGFP-HIF2a. Cells were imaged in an unstimulated condition, though dynamics in the morphology of the HIF-2α cellular bodies was seen in some instances.

6.2.14 Speckles of other HIF signalling proteins

6.2.14.1 The relationship between HIF-2α and PHD3 aggresomes

From the canonical HIF signalling proteins, only PHD3 has been characterised as existing in cellular bodies, specifically found to reside in cytoplasmic aggresomes (Rantanen, Pursiheimo et al. 2008). Aggresomes have been primarily cited to be microtubule-dependent structures, suggested to have a role in the managing the cytotoxicity of misfolded proteins through the regulated aggregation of protein (Kopito 2000). Review of our previous confocal imaging of PHD3-EGFP showed punctate entities of cellular fluorescence, in accordance with the reported profile for PHD3 aggresomes (**Fig 6.16**). Aggresomes structures are sensitive to proteasomal inhibition, having been shown to relocalise PHD3-EGFP protein when in the presence of the proteasome inhibitor MG132. To further confirm the appearance of PHD3 aggresomes in our own experimental system, HeLa cells expressing PHD3-EGFP were imaged by live-cell confocal microscopy and stimulated using 10μM MG132 (**Fig 6.16**). Additionally, PHD1-EGFP and PHD2-EGFP were imaged to reinforce the data that suggests aggresomes to be a defining feature of PHD3 protein. From these data, a dramatic effect was observed on PHD3 localisation which appeared to gather in the cell nucleus simultaneously while more cellular bodies gathered and grew (**Fig 6.16**). Interestingly cellular bodies were found to accumulate in PHD2-EGFP expressing cells, though at a much reduced number and finally resulting in irregular large aggregates surrounding the cell nucleus. No such response was seen when imaging PHD1-EGFP expressing cells. Similarly we were interested to assess whether HIF-2α speckles were also sensitive to proteasome inhibition, thereby implicating them further with the subcellular proteolytic machinery. HeLa cells were transfected to express EGFP-HIF2α, 24 hours post transfection cells were treated with 10μM MG132 and imaged by time-lapse confocal microscopy. The characteristics and morphology of the

speckles was also seen to change dramatically, becoming more irregular and cytoplasmic.

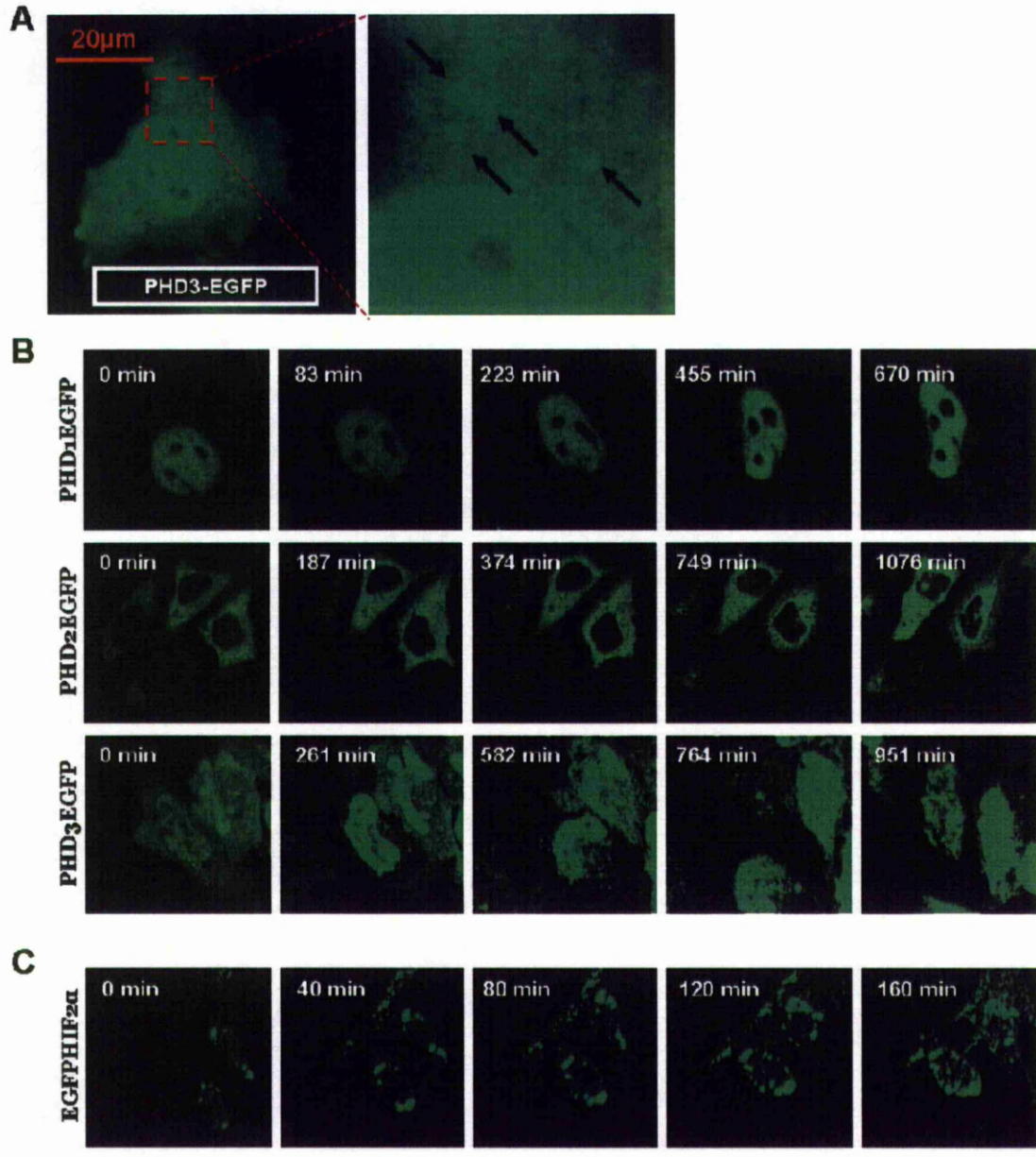

Fig 6.16. Live-cell confocal microscopy of HeLa cells. (**A**) Shows a single-cell expressing PHD3-EGFP highlighting the punctate cellular bodies detected. (**B**) Cells were transfected to express a fluorescent fusion PHD isoform (PHD1, PHD2 and PHD3). After 24-48 hours transfection cells were stimulated with 10μM MG132 and imaged. (**C**) MG132 treatment was also performed on cells ectopically expressing EGFP-HIF2α and the response imaged by live-cell confocal microscopy.

6.2.14.2 Preliminary investigation of HIF-1β speckles

Two publications from Prof. J. Fandrey's group have attempted FRET measurements for the interactions of HIF-1α and -2α with HIF-1β (Wotzlaw, Otto et al. 2007; Konietzny, Konig et al. 2009). In both papers, speckling was present for HIF-1α and HIF-1β, a result in contrast to our imaging of HIF-1α localisation. However, as we had not yet imaged HIF-1β we we're interested to

determine whether or not ectopic expression of HIF-1β demonstrated cellular bodies. Towards the end of my project a fluorescent fusion plasmid vector encoding YFP linked to HIF-1β was kindly donated (pG-YFP-HIF1β) by Prof. J. Fandrey. This plasmid was ectopically expressed in HeLa cells and imaged by live-cell confocal microscopy. HIF-1β fluorescence was found to be localised to the nucleus and furthermore found to be present as cellular bodies, in accordance with both Wotzlaw *et al.* (2007) and Koneitzny (2009) (shown earlier in **Fig 6.1**). We we're interested to further adapt from the work by Prof. J. Fandrey's group and co-express the HIF-α and –β isoforms alongside one another. However, to enable multiplexing of HIF-1αEGFP with YFP-HIF-1β it would be necessary to replace the present fluorescent protein as YFP and GFP have overlapping spectra (Harpur, Wouters et al. 2001). The pG-YFP-HIF-1β expression vectors was cloned using the gateway methodology and so contained sequences akin (but not exact) to the primers used in the production of gateway entry vectors, hampering future efforts to use gateway primers. To account for this, HIF-1β was cloned using a standard restriction digest approach to remove the YFP before ligating in a DsRedxp coding sequence (details in appendix). The new plasmid termed pG-DsRedxp-HIF1β was transfected into HeLa cells and subsequently imaged. Fluorescence expression from this new plasmid was also found to localise to cellular bodies. All images were processed using AQM kinetic tracker to measure the size and amount of HIF-1β speckles per cell. An average of 87.8 speckles was present per cell at an average size of 7.3μm with a SEM of 3.3; both values were found to overlap with the previous measurements for EGFP-HIF2α (**Fig 6.17**). In spite of the similarity in characteristics, one distinct difference was present; the HIF-1β speckles co-localised with structures visible on the bright field images.

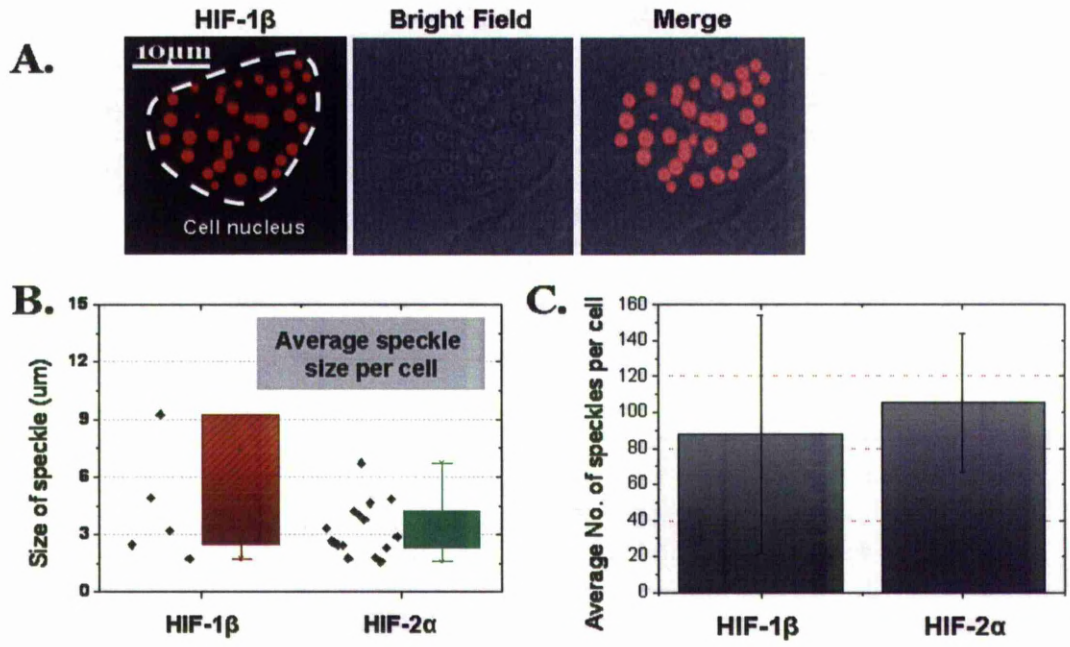

Fig 6.17. (**A**) HeLa cells were transfected with DsRedxp-HIF1β for 24-hours before live-cell confocal imaging expression. AQM kinetic tracker was used to analyse the speckle size and number per cell. (**B**) Box-and-whisker plot to show the comparative size of HIF-1β speckles compared to EGFP-HIF2α speckle. (**C**) Comparative numbers of HIF-1β and HIF-2α speckles. All data pertaining to EGFP-HIF2α was gathered and imaged previously in **Figure 6.7**.

6.2.14.3 Co-localisation of HIF-2α with HIF-1α and HIF-1β

Following the visualisation of HIF-1β cellular bodies and reports of HIF-1α speckles, we were interested in imaging the co-localisation of these proteins using when ectopically expressed (Wotzlaw, Otto et al. 2007; Konietzny, Konig et al. 2009). HeLa cells were co-transfected to express DsRedxp-HIF2α with either an unfused EGFP control, YFP-HIF1β or HIF-1αEGFP. Imaging of the expressing cells showed HIF-1β and HIF-2α fluorescence to co-localise. These speckles were again found to co-localise with contrast regions in the bright field image, as found when expressing HIF-1β alone (**Fig 6.18**). Remarkably and unexpectedly, co-expression of HIF-2α was found to alter the homogenous localisation of HIF-1α, which then co-localised to HIF-2α speckles; the speckles appeared to have an altered morphology and decreased frequency of occurrence, though this relationship remains currently unquantified.

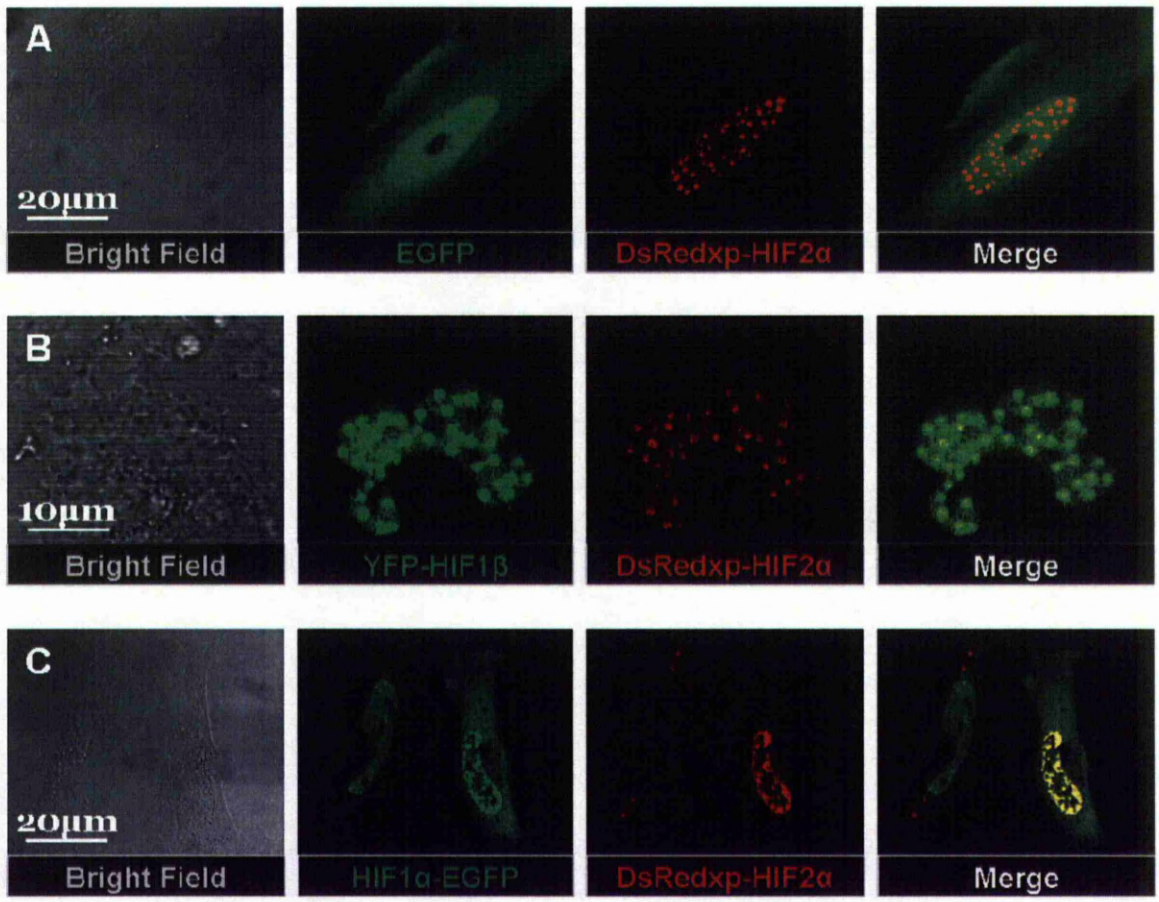

Fig 6.18. Live-cell confocal microscopy of transiently transfected HeLa cells expressing DsREDxp-HIF2α alongside (**A**) an unfused EGFP (**B**) YFP-HIF1β and (**C**) HIF-1αEGFP.

6.3 Discussion

In this chapter, we have begun to characterise the complex subcellular spatial patterning of HIF-2α. This has been achieved through the use of confocal microscopy, a technique which affords us the ability to look at single living-cells and their behaviour, not only with a high degree of temporal resolution as seen through chapters 4 and 5, but with a high-degree of spatial resolution; discerning and resolving structures/organelles to within a 200nm (Toprak, Kural et al. 2010). Initially experiments focused on the explanation of HIF-2α speckles, though over the course of the project the focus became broader identifying cellular bodies for PHD3 and HIF-1β. Of these, PHD3 has been previously and most assuredly identified existing as aggresomes which may confer hydroxylase sensitive apoptosis to cells, linking the HIF hypoxic response with another facet of cell fate. We observed PHD3 aggresomes in our own experimental system, though found no obvious link between the occurrence of aggresomes and hypoxia or any relationship to apoptosis (investigated in the course of chapter 5 experiments, data not shown). This work heavily implicates the involvement of the subcellular landscape in the HIF hypoxic signalling, suggesting HIF-2α levels to modulate the localisation of HIF-1α. This is the first study to implicitly address this possibility.

Name	Identifying characteristics	References
Aggresome (cytoplasmic)	Microtubule-dependent inclusion body, usually existing as only **a few per cell.** Are formed from the result of aggregated protein and are often rich in molecular chaperones.	(Kopito 2000)
Cajal Body	A nuclear entity, found to be present in all studied eukaryotes, containing newly synthesised involved in pre-messenger RNA splicing. Typically identified by the presence of coilin.	(Nizami, Deryusheva et al. 2010)
Clastosome	A **sub-type of PML bodies**, enriched for ubiquitin conjugates, proteasome and proteasome substrates. Found in numbers of **1-3** bodies per cell nucleus.	(Lafarga, Berciano et al. 2002)
Cleavage Body	An entity often accompanying and adjacent to Cajal bodies. They exist as **1-4** nuclear localised structures with a diameter ranging from **0.3-1.0 µms**. Characterised by the presence of CPSF-100* and CstF-64* and known to be more prominent at S and G2 phases of the **cell cycle.**	(Li, Roy et al. 2006)
Gems	Gemini of cajal bodies are found adjacent to cajal bodies. Defined by the presence of SMN protein, this definition has been subsequently contested as being cell type dependent. Several reports are unable to distinguish gems from Cajal bodies and so significant overlap in function and morphology is expected.	(Sleeman, Trinkle-Mulcahy et al. 2003; Nizami, Deryusheva et al. 2010)
Inclusion Body	A general term used to describe aggregated or wantonly polymerised protein, as occurs in several disease states or when expressing non-native protein or insoluble protein. Usually seeded at a single site and grow with addition of more protein.	(Kopito 2000)
Interchromatin Granules Clusters	See Nuclear Speckles.	
Mitotic Interchromatin Granules	Nuclear Speckles are freed from the nucleus during the course of nuclear breakdown and cell division. Speckling is lost during metaphase to anaphase.	(Lamond and Spector 2003)
Nuclear Aggresome	A class of aggresome, in which the proteolytic machinery is often hampered or overwhelmed leading to the translocation of nuclear aggresome to within the nucleolus. Nuclear Aggresomes are rich in a variety of proteins and RNA, but are distinct entities from their surrounding nucleolar environment.	(Latonen 2011)
Nuclear Bodies	See PML bodies.	
Nuclear Speckles	Nuclear speckles are enriched in splicing speckles, found to exist in the cell nucleus in sizes of **one to several µms**. Cited to contain transcription factors and machinery but be relatively inactive.	(Lamond and Spector 2003)
Nucleolus	A sub-nuclear region clearly apparent by light microscopy, known as the site of ribosome biogenesis. Size varies from **0.5 – 5.0 µms**.	(Raska, Shaw et al. 2006)
Nucleolar Caps	Nuclear entities that form adjacent to the nucleolus, known to contain markers of Cajal bodies and PML bodies. The morphology of nucleolar caps is sensitive to transcriptional arrest by Actinomycin D.	(Shav-Tal, Blechman et al. 2005)
OPT domain	A **cell cycle** sensitive nuclear body, appearing in G1 and disappearing in S-phase. Contains nascent transcripts and transcription factors, existing at sizes from **1.0-1.5 µms**.	(Spector 2001)
P62 Aggregates	Sometimes referred to as sequestosomes, these are cytoplasmic aggregates of p62 protein. Linked to autophagy and the organisation of upstream NF-κB signalling.	(Nakamura, Kimple et al. 2009)
Paraspeckle	Interchromatin speckles distinct from nuclear speckles. **5-20** entities are found in the nucleus. The speckles are characterised by the presence of paraspeckle protein 1 (pspc1).	(Fox and Lamond 2010)
PML bodies	Are a well established nuclear speckling phenomenon. Suggested to function as nuclear stores of inactive protein and viral infection resistance. Occurring as **1-30** per nucleus, at sizes ranging from **0.2-1.0 µms**. Distinctly characterised by the presence of PML protein.	(Maul 1998; Geoffroy and Chelbi-Alix)
Polycomb body	Polycomb bodies are a part of a gene silencing organisation, often correlating to the absence of RNA pol II. They exist as dynamic structures in the cell nucleus found in numbers of **12-16** per cell at sizes of **0.3-1.0µms**.	(Spector 2006; Sexton, Schober et al. 2007)

Table 6.1. A list of commonly referred to cellular bodies. A very well produced and similar table (with corresponding images of speckles) can be found in a publication from Spector (2006)

6.3.1 Identification of HIF-2α subcellular entities

The variety and complexity of subcellular organisation is vast. Ongoing research within this field is still discovering new phenomenon and redefining the characteristics of cellular bodies previously elucidated (Fox, Lam et al. 2002). This is evident with the PML bodies, in which the proposed function has become broader and broader over the last two decades. They we're originally discovered by electron microscopy from the separate works of Swift *et al.* (1959) and Beck *et al.* (1961) and then re-discovered in 1992 with the advent of antibody staining against key components (Brasch and Ochs 1992). As of now, they have been ascribed functions from antiviral defence, protein depots, transcriptional regulators as well as an arm of the misfolded protein degradation pathway (Tashiro, Muto et al. 2004; Fu, Gao et al. 2005; Geoffroy and Chelbi-Alix 2011). PML bodies are only one example from the list of many cellular bodies. Amongst the rich backdrop of known cellular bodies we have attempted to identify whether HIF-2α belongs to any known example. Originally, HIF-2α speckles were identified in bovine arterial endothelial cells in 1999 using the ectopic expression of fluorescent linked HIF-2α. The localisation pattern was stated but not explained and has remained largely unqueried in subsequent papers (Hara, Kobayashi et al. 1999; Konietzny, Konig et al. 2009). Although a paper published from the group of Prof. J. Fandrey reported in 2004 a possible link between PML protein distribution and HIF-1 localisation (Berchner-Pfannschmidt, Wotzlaw et al. 2004). However, our own work to concretely identify the HIF-2α speckles will undoubtedly be ongoing beyond this thesis. From the data gathered so far we can begin to hypothesise and discuss the identification of the HIF-2α cellular bodies. Firstly, from the frequency of HIF-2α speckles, there is no recorded cellular body known to exist in similar numbers. Transcription factories occur in high numbers in HeLa cells to the order of the thousands (Razin, Gavrilov et al. 2011). Paraspeckles occur in numbers of 10-20, nuclear speckles 25-50 and PML bodies occur at numbers ranging from 10-30 (Spector 2006). HIF-1α has been additionally been linked to PML protein in work published by Bernardi *et al.* (2006), who found PML protein to inhibit expression of HIF-1α mRNA during hypoxia via a physical interaction with mTOR; a facilitator of HIF-1α translation (Bernardi, Guernah et al. 2006; Knaup, Jozefowski et al. 2009). Our observed co-localisation of HIF-2α with p53 and NRF2 suggest that in spite of the frequency of occurrence,

HIF-2α and PML bodies are related. However, the sheer variety of HIF-2α speckle characteristics suggests this to not be the only explanation. HIF-2α cellular bodies were found to be cytoplasmic or nuclear, as dynamic and static structures, to be partially sensitive to nocodazole, to respond to proteasome inhibition and to fuse and aggregate. Several of these data collected suggested HIF-2α speckles to share a relationship with the aggresome phenomenon. Also of the measured size, HIF-2α fits the defined characteristic of stress granules, aggresomes and nuclear stress bodies (Spector 2006). This observed relationship is further reinforced as HIF-2α speckles often manifested as irregular aggregates, not just as neat nuclear punctate structures (Markossian and Kurganov 2004). Many citations for aggresomes focus on them as cytoplasmic entities, though aggresomes can exist in a nuclear form as thoroughly discussed by Latonen 2011 (Latonen 2011). A publication from Fu *et al.* (2005) suggests that the co-existence and relationship of HIF-2α PML bodies and aggresomes is plausible; reporting that the fusion of PML bodies is a route for aggresome formation. Although, if HIF-2α is indeed a part of the aggresomal system, it reinforces the hypothesis from Bedaouin *et al* that aggresomes function beyond simple aggregates of misfolded protein (Beaudoin, Goggin et al. 2008). For certain our HIF-2α construct was fluorescent in bodies and therefore the GFP protein at least intact to some degree. Also, analysis of HIF-2α expression plasmids on HRE-luciferase carried out in chapter 3 shows the fluorescent fusion forms to be transcriptionally active. To further account for the diversity in HIF-2α speckle characteristics, PML bodies have been shown to have a relationship with Cajal bodies; structures commonly found in low number in highly transcriptionally active cells (Sun, Xu et al. 2005). The interplay of these subcellular entities may therefore explain the atypical manifestation of the HIF-2α speckles, which may occur as an amalgamation of several phenomena (Platani, Goldberg et al. 2000; Markossian and Kurganov 2004; Fu, Gao et al. 2005; Latonen 2011). Together these form an axis of cellular bodies involved in the proteolytic response to protein and it is therefore not surprising that proteins extensively degraded such as HIF-2α and PHD3 may associate with these structures (Tian, McKnight et al. 1997; Nakayama, Qi et al. 2009; Latonen). Though it remains unexplained and an interesting question, what role HIF-2α plays in the recruitment of HIF-1α to these foci and how the aggregation of various protein components of the HIF signalling

network affects hypoxic signalling (with special regards to the HIF-PHD feedback loop).

In summary of the chapter, we have (further) identified the novel subcellular localisation of the HIF-2α isoform and provided evidence to suggest that HIF-2α enters into several speckling phenomenon with different dynamic properties. However, the mechanisms' regulating the interplay of these speckles remains unknown, as does the possible interjection of the HIF-2α speckles with the canonical hypoxic signalling network.

Chapter 7: Nuclear membrane instability results in unstimulated asynchronous translocations

7.1 Introduction

This project has made extensive use of live-cell confocal microscopy in order to explore the spatial and temporal dynamics of the HIF-signalling network. This work is part of a drive towards a greater appreciation of dynamic events and the power of live-cell imaging in elucidating these (Haraguchi 2002). However, as the approach is still relatively new there are undiscussed issues that may compromise the study of translocation dynamics. There are numerous signalling systems that are currently being researched and evaluated for dynamism, in terms of synthesis/degradation cycles and/or nuclear-cytoplasmic translocations, including ERK, NRF2, NF-κB, STAT, GR, p53, glucocorticoid receptor signalling as well as our own work with the HIF signalling system (Pariante, Pearce et al. 1997; Lahav, Rosenfeld et al. 2004; Nelson, Ihekwaba et al. 2004; Yoshiura, Ohtsuka et al. 2007; Shankaran, Ippolito et al. 2009; Zhang, Pi et al.). Often when a dynamic translocation event of a specific protein is discovered, a large amount of work can go into the understanding and dissection of this event with little regard to non-specificity or artefact. During the course of these experiments and primarily through the imaging of a variety of different fluorescent proteins, asynchronous and unstimulated nuclear-cytoplasmic translocations were often found to be present. This chapter describes the determination and characterisation of these spontaneous translocations.

7.2 Results

7.2.1.1 Analysis of PHD2EGFP spontaneous cytoplasmic:nuclear translocations

Throughout chapter 5, the various PHD proteins were imaged by live-cell confocal microscopy and this data strongly alluded to the presence of nuclear-cytoplasmic translocations. This was particularly visible when imaging fluorescent-tagged PHD2, a cytoplasmic protein that was observed to spontaneously flood into the nucleus. Here we re-examined this data in the light of these translocation events.

HeLa cells were transiently transfected using the CMV containing plasmid, pPHD2-EGFP. After 24-48 hours of transfection, cells visibly expressing PHD2 were imaged every ~5-minutes for up to ~25-hours. Images of cells showing spontaneous translocations were processed using the small-circle cell-tracking

analysis method, used to measure both cytoplasmic and nuclear fluorescence and thereby determine the nuclear:cytoplasmic ratio (N:C ratio). The translocation profile is seemingly subtle and at times difficult to detect with a degree of certainty. This is partly due to the low amplitude change from a resting N:C of ~0.4 to a peak max of ~1.0 (**Fig 7.1**). Also multiple peaks were apparent. The presence of multiple-peaks means that some peaks occur in such close proximity as to obscure whether one or multiple events transpired. These difficulties prompted the development of a more systematic analysis method.

7.2.1.2 Systematic identification of PHD2 translocation peaks

Using the translocation data imaging data, a series of processing steps were developed (**Fig 7.1.**). The raw data produced by Cell Tracker image processing was smoothed by averaging every three data points along the time-series. This reduced the noise apparent in the data, which made the data suitable to apply a peak detection threshold to.

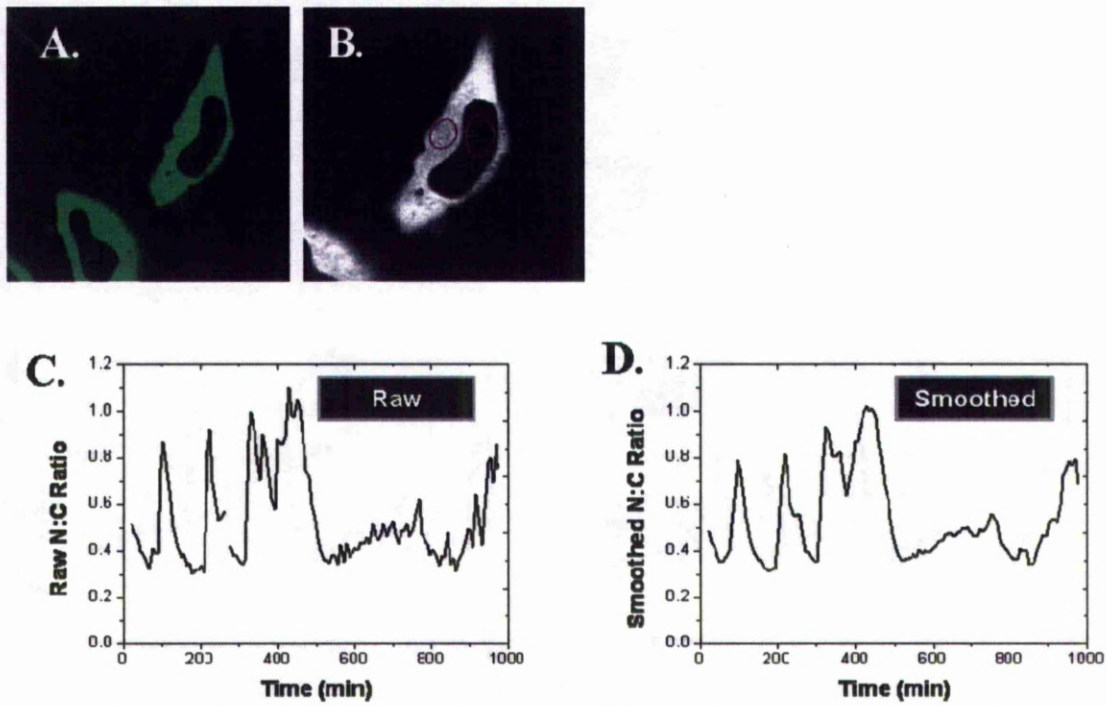

Fig 7.1. Process of fluorescence quantification and data preparation. (**A**) shows a PHD2EGFP transfected and expressing HeLa cell. (**B**) shows the tracking method used to measure the nuclear/cytoplasmic ratio of the translocations. (**C**) Is the raw data from the tracking measurement and (**D**) the smoothed data, performed by averaging every 3-data points.

The desire for the rapid and unbiased identification of the PHD2-EGFP translocations led us to consider several thresholding mechanisms to be used for the identification of translocation peaks within the cell traces of fluorescence. In work published by Turner *et al.* (2010) a similar thresholding system was employed in the identification of p65 nuclear-cytoplasmic

oscillations. In their work, a pre-stimulus threshold was applied which was determined as the average fluorescence levels of the pre-stimulus period plus two standard deviations. The PHD2 translocations are asynchronous and spontaneous, preventing us from adapting this threshold. This led us to develop and considered four alternative methods, termed; (1) Jumping threshold (2) Local minima (3) Modal threshold and (4) Cell mean threshold (**Fig 7.2.**). The jumping threshold functions by calculating if the current fluorescence value is more than 0.3 of the value 5-time points previously; the value of 0.3 was empirically determined after investigating the amplitude of the translocations and assessing the noise in measurements (from several tracked cells). The jumping threshold was therefore designed to capitalise on the sharp rise of the peak. However, this methodology suffered when peaks occurred close together and of varied amplitudes. A second methodology was attempted, the local minima threshold. Here, the minimum value within 100 minutes at any given time point was calculated and this served as the basis for the threshold (100 minutes either way was determined as an appropriate width for a peak). Next we adapted the pre-stimulus threshold from Turner *et al.* (2010), this time using the entire cell fluorescence to calculate the average plus one standard deviation. Alongside this methodology, we also used a modal threshold which rounds all cell fluorescence values up to the nearest 0.1, and then calculates the mode from all these values plus one standard deviation. The ability of the four threshold methods to detect the translocation peaks were validated against by eye scoring. Each threshold was asked to find 53 human identified peaks, of this number, the jump method found 54.7% (29 peaks), the local minima found 66.0% (35 peaks), the modal found 94.3% (50 peaks) and the cell mean 96.2% (51 peaks). For all further work, all peak translocations were automatically detected and scored by the cell mean threshold.

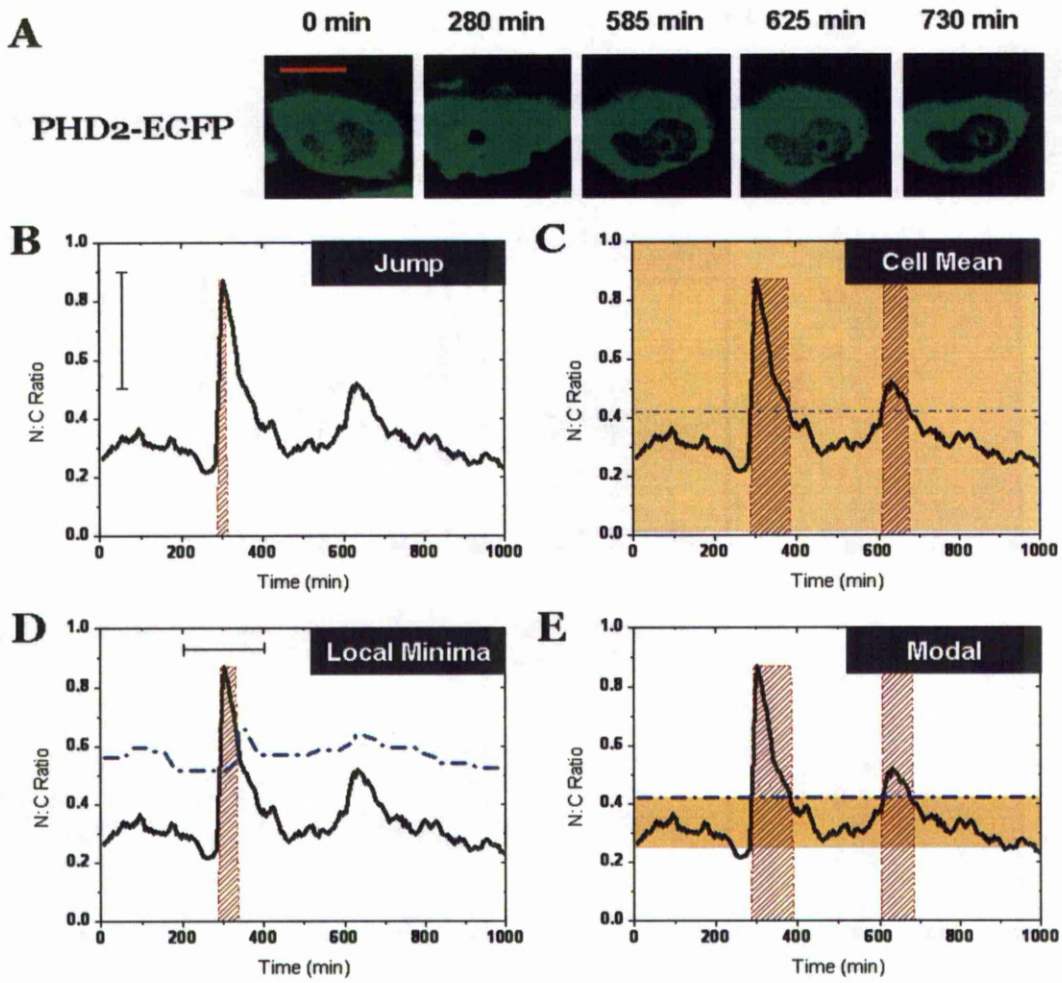

Fig 7.2. (**A**) Live-cell confocal microscopy of a HeLa cell expressing PHD2-EGFP undergoing spontaneous cytoplasmic-nuclear translocations. This cell was one of many used in the validation of a threshold method for the detection of the translocations. Four threshold methods were developed and applied to the data. The threshold line, where applicable, is shown in blue and the peaks detected shown as a red box. (**B**) The jump method determines whether the fluorescence data is ≥0.3 than levels 5-time points ago. The jump scale is indicated. (**C**) The cell mean method sets the threshold as an average of all fluorescence over the time course plus one standard deviation. (**D**) The local minima set the threshold as the lowest fluorescence level within 100-minutes of each time point plus 0.3. The width of the local minimum is shown. (**E**) The modal threshold works by rounding up every fluorescent value to the nearest 0.1, then calculating the modal average of these values plus one standard deviation.

7.2.2 Characterisation of PHD2-EGFP translocations; timing, frequency and profile

Using the analysis approach outlined, the N:C traces for 88 translocating cells were analysed. Of the 88 translocating cells, 78 were found to show a 2nd peak, 62 a 3rd peak and 34 cells a 4th peak. The time to first observed translocation spanned the experiment time-course, though 42 cells were found to translocate within 200 minutes (**Fig 7.3**). Subsequent peaks displayed a similar timing, in which the majority (>50%) of repeat translocations occurred within 200 minutes of the previous translocation. Despite the asynchrony in onset and

frequency there was a strong synchrony in the normalised translocation profile. The peaks are easily superimposable; the import rate shows the greatest homogeneity and the export rate a relatively higher degree of variability (**Fig 7.3**). The average peak was found to have a duration of ~120 minutes, counting from the initial rise of fluorescence to the re-establishment of a steady-state.

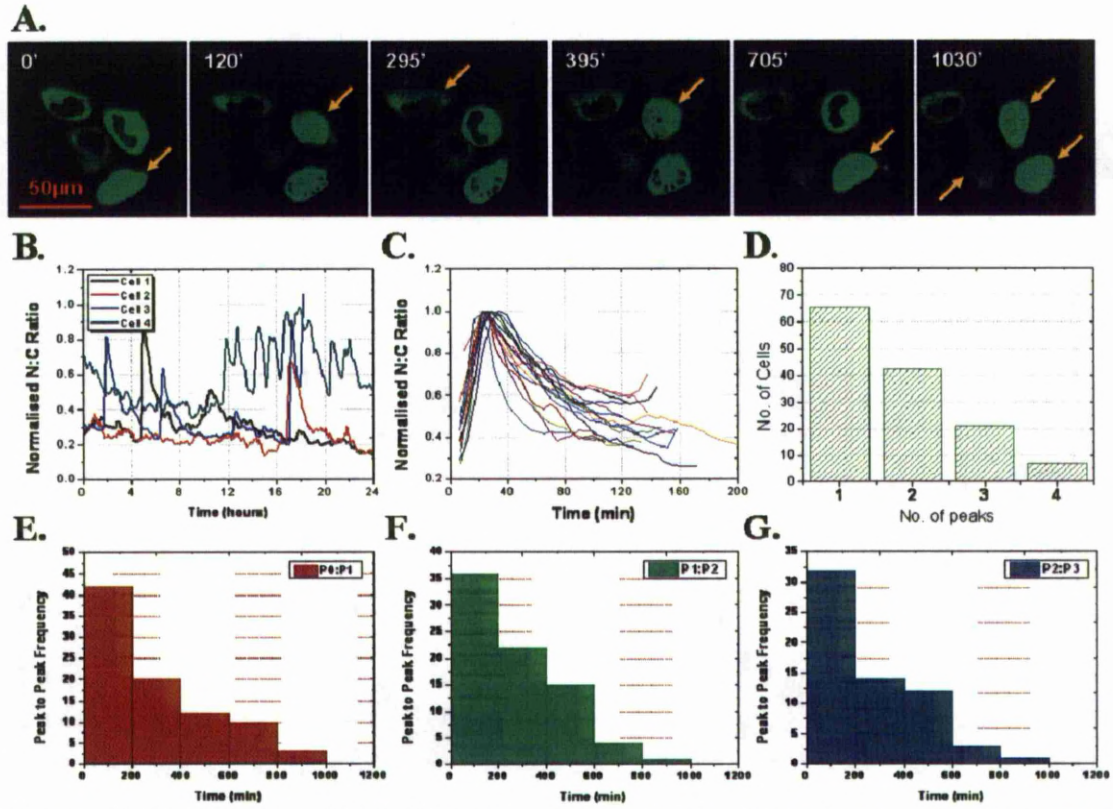

Fig 7.3. Characterisation of PHD2EGFP spontaneous cytoplasmic:nuclear translocations using HeLa cells ectopically expressing PHD2EGFP. (**A**) shows time-lapse imaging of PHD2EGFP with translocations indicated and (**B**) is the corresponding quantified N:C profile of the shown cells. (**C**) Shows all peak profiles isolated and superimposed and (**D**) a histogram of no. of translocations observed per cell. (**E-G**) Show histogram of the timing of translocations for the (**E**) experimental start point to initial peak, (**F**) the first peak to second peak and (**G**) the second peak to third peak.

7.2.3 Inheritability of nuclear membrane instability

From our data set of PHD2-EGFP time-lapse confocal imaging, we isolated several dividing cells and quantified the N:C ratio of fluorescence for both daughters in order to examine the inheritability of the translocations. Of the 11 pairs analysed, 10 were found to both show a single translocation, 6 were found to both show two translocations and 2 were found to both show three translocations. Analysis of the synchrony of daughter cell 1st peak translocations (after division) showed that 2 pairs translocated within 30-minutes of each other, 4 pairs within 60-minutes and 6 pairs within 90-minutes (**Fig 7.4**).

Taken together, the data indicates that the propensity for translocations is to some degree inheritable or the process predetermined before division.

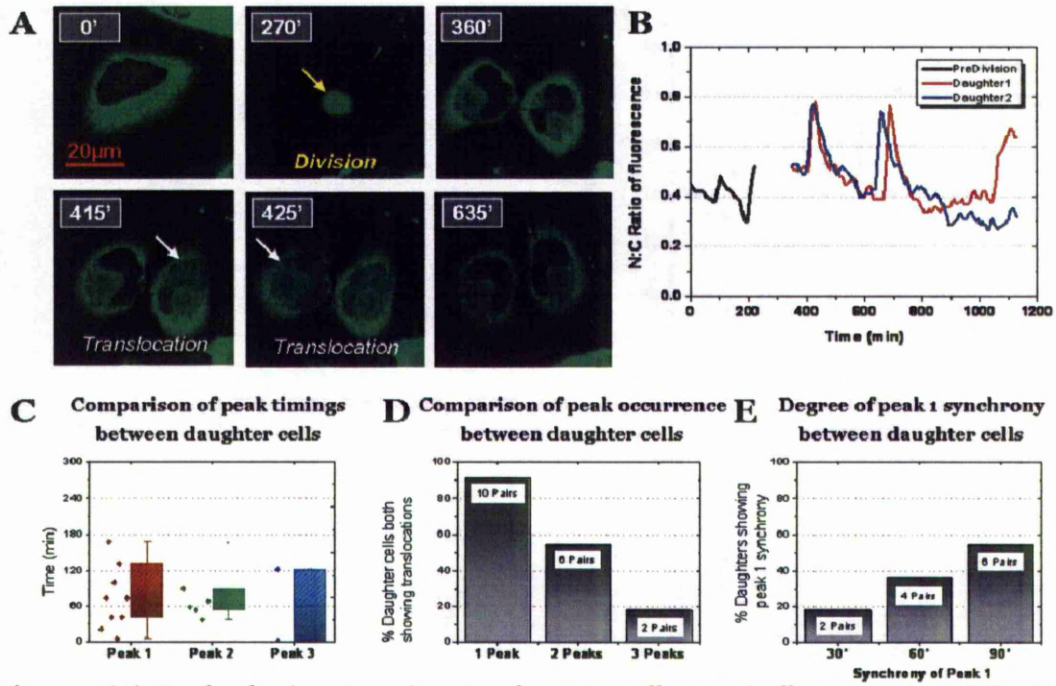

Fig 7.4. (**A**) Confocal microscopy images of a HeLa cells ectopically expressing PHD2-EGFP. The cell is followed through cell division. (**B**) The N:C ratio for fluorescence was followed from the parent cell to the daughters. A representative plot is shown corresponding to the images shown in (**A**). (**C**) A box-and-whisker plot showing the timing difference between daughter translocations for the three successive peaks. (**D**) Comparison of the occurrence of translocations in daughter cells, shown as % of daughter pairs both translocating for a number of peaks. (**E**) The synchrony of daughter cells is plotted as the % of daughter in which the 1st peak occurs within 30, 60 or 90-minutes of one another.

7.2.4 Are PHD2EGFP translocations sensitive to expression level of PHD2EGFP?

Under the hypothesis that the PHD2 translocations are facilitated through protein-protein interactions (such as may occur for the regulated transport into the nucleus) we could expect that this mechanism may be sensitive to different levels of PHD2 (Steinhoff, Pientka et al. 2009). The use of transient transfection affords us the chance to investigate the effect of different expression levels of PHD2 on the characteristics of the translocations. Previously attained imaging data were segregated into three categories of overall fluorescence intensity, namely, high, medium and low fluorescence intensity. The fluorescence intensity correlates with the expression-level and is therefore a readout of cellular PHD2 expression (Yen, Xu et al. 2008). The translocation profile between these three groups was compared (**Fig 7.5**). There was little evidence that varying degrees of PHD2 expression affected the translocation of PHD2. All

response curves remained superimposable, and the frequency of translocations failed to show a strong correlation with fluorescence intensity.

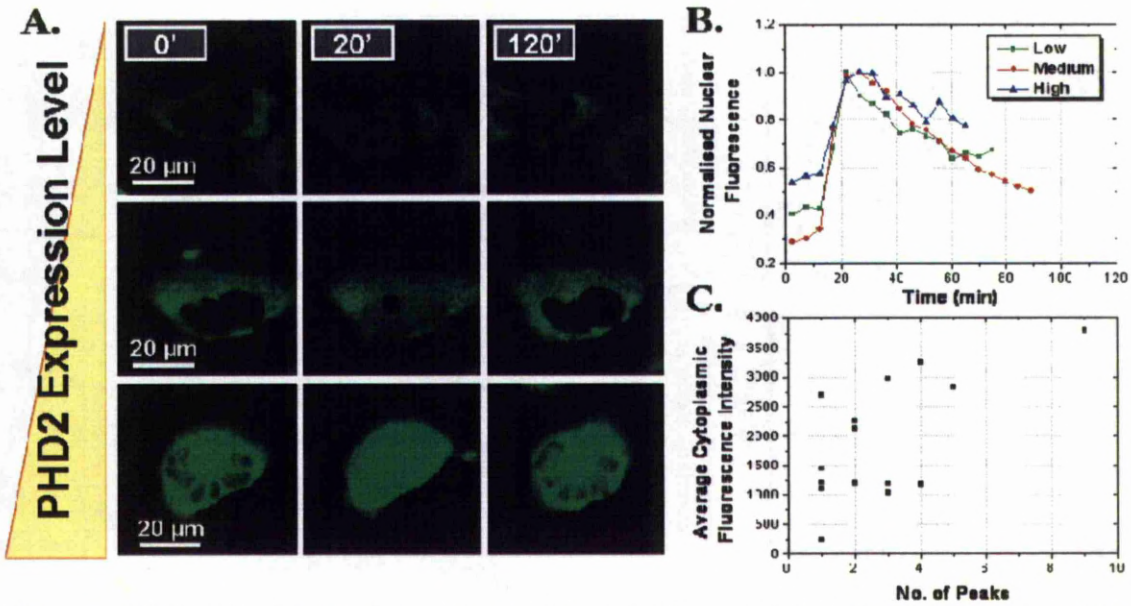

Fig 7.5. (**A**) Confocal microscopy images of transiently transfected HeLa cells expressing PHD2-EGFP. Images have been artificially synchronised to compare translocation, arbitrarily setting to as to just before translocation point. Cells of different fluorescence levels are shown. (**B**) Cell traces of nuclear fluorescence levels, showing three cells with different expression levels, separated into low, medium and high expression determined from their cytoplasmic fluorescence (**C**) Scatter plot comparing average cytoplasmic fluorescence with the occurrence of translocations.

7.2.5 Are PHD2EGFP translocations cell-type specific?

So far these translocation events have only been investigated in HeLa cells which leaves open an important question as to whether the phenomenon is a general or cell type specific feature. Previously SK-N-AS cells were optimised for use with live-cell confocal microscopy and further validated for work with hypoxia and the HIF system. We therefore used SK-N-AS cells transiently transfecting them with the pPHD2-EGFP plasmid vector for 24-48 hours. Cells were imaged by confocal microscopy for a time-course over 20-hours. Whereas for HeLa cells translocations were observed in 24% of all cells (n= 19 of 79 total cells), no translocations were observed in SK-N-AS cells. This prompted us to investigate another available cell line, the medulloblastoma DAOY cell line (Jacobsen, Jenkyn et al. 1985). DAOY cells were transiently transfected with the pPHD2-EGFP expression vector in the same manner as for the HeLa cells. After 24-48 hours cells were imaged by confocal microscopy for up to 24 hours. In this instance, 21% (n=11 of 52 cells) of imaged DAOY cells were seen to translocate (**Fig 7.6**). The translocation profile remained similar to HeLa cells,

comparing Cell Tracker quantified normalised N:C fluorescence traces (data not shown).

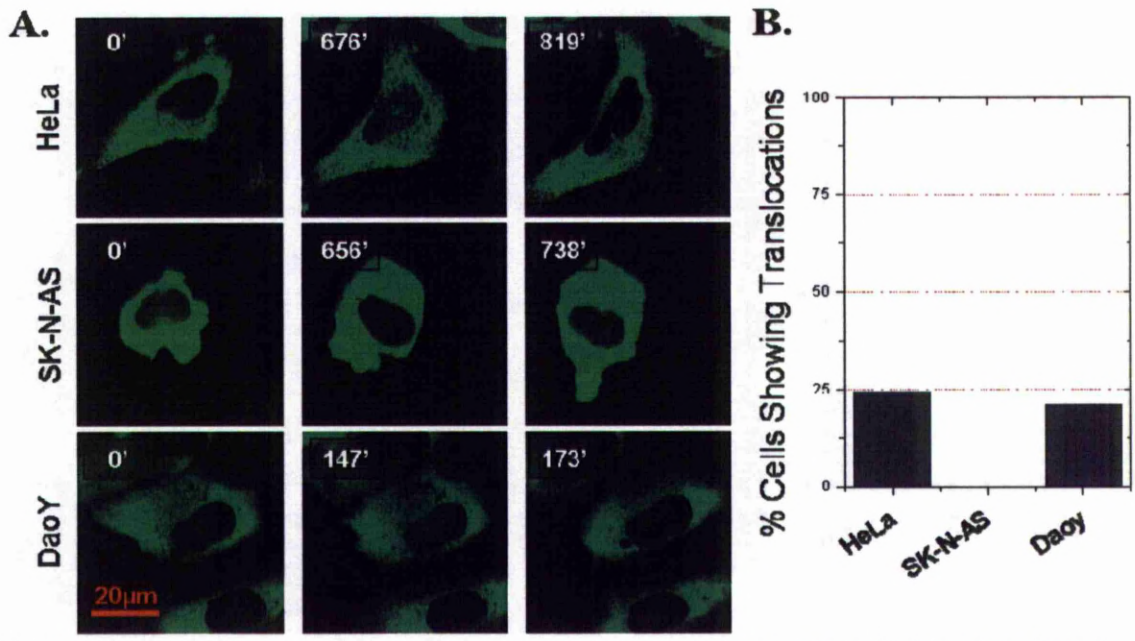

Fig 7.6. (**A**) Time-lapse confocal microscopy of three cell lines transiently transfected with PHD2EGFP and the (**B**) % of imaged cells showing a visible translocation event over a period of ~20-hours.

7.2.6 The affect of mutating PHD2 on PHD2EGFP localisation dynamics

Next we examined whether any sequences or motifs within the PHD2 protein are necessary for the translocations to occur. To this end several fluorescent tagged PHD2 mutants were used, kind donations from Prof. R. Depping, Lüebeck. The mutants available were; Δ1-100, Δ101-200, Δ180-220, Δ201-300 and Δ301-426. The amino acid residues between 6 and20 have been shown to contain the function nuclear export sequence for PHD2 (Yasumoto, Kowata et al. 2009). We hypothesised that one these domains may have a role in the spontaneous translocations of the PHD2 protein. Initially, all mutant PHD2 forms were examined for their resting localisation in both HeLa and SK-N-AS cells using single time-point imaging. Cells were each transfected with either an unfused EGFP, wild-type PHD2-EGFP or one of the mutant PHD2 expression vectors. Cells were then imaged by confocal microscopy for up to 20 hours. For the first images, the N:C ratio of all cells was determined using Cell Tracker to quantify fluorescence levels (**Fig 7.7**). All mutants were found to be predominantly cytoplasmic, except for Δ1-100 which was found to be near

ubiquitous in HeLa and SK-N-AS cells with an average N:C ratio of ~1.4 and ~1.0 correspondingly, in line with the findings from Yasumoto et al. (2009).

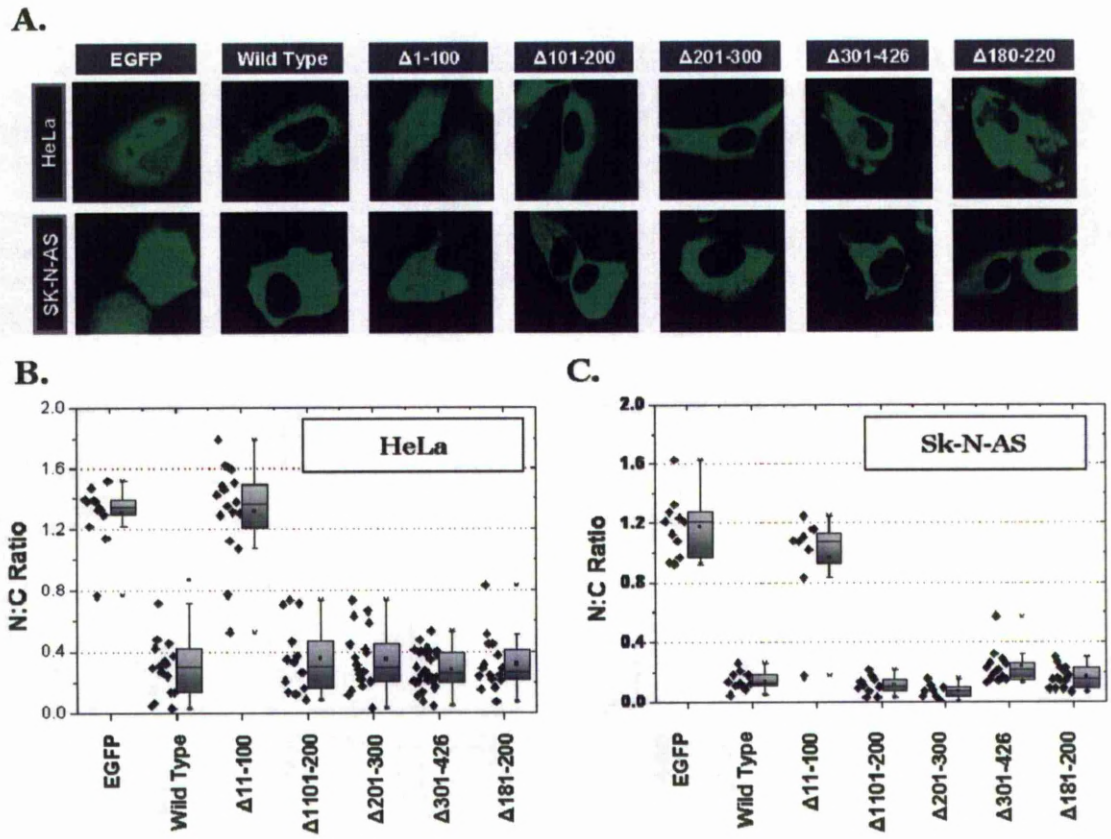

Fig 7.7. (**A**) Imaging of HeLa and SK-N-AS cells ectopically expressing either an unfused EGFP vector, wild-type PHD2-EGFP or a mutant PHD2EGFP. (**B**) Cell Tracker was used to quantify the N:C ratios of fluorescence for a number of cells, the values are plotted in a box-and-whisker format.

From the same experiment, the translocation potential of the cytoplasmic mutants was investigated (in the HeLa cells). Time-lapse imaging showed all cytoplasmic mutants were able to undergo translocations in a manner akin to the wild-type protein (**Fig 7.8**). This data strongly suggested that either the critical regulatory sequence is contained within the first 100 amino acids of the PHD2 protein, or that the domain structure of the PHD2 protein is unimportant for the generation of the spontaneous translocations.

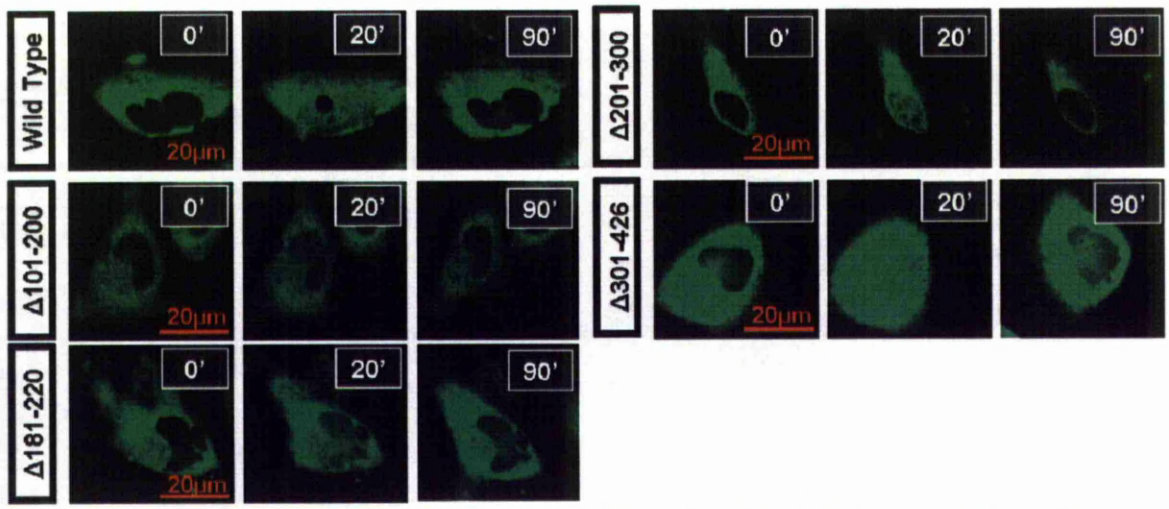

Fig 7.8. HeLa cells were transfected with various fluorescent fusion PHD2 expression vectors, encoding either wild-type PHD2 or a mutant form. All images are shown from the initiation of a spontaneous translocation event.

7.2.7 Evidence of spontaneous nuclear-cytoplasmic translocations of other proteins

Throughout the live-cell imaging of various proteins in this project there has been multiple suggestions of translocation-style events. Re-evaluation of the data has indicated this for HIF-1β, PHD1 as well as HIF-2α (**Fig 7.9**). These proteins are localised to the nucleus in basal conditions and so the translocations involve the movement of nuclear protein to the cytoplasm, the reverse of the PHD2 scenario. The presence of translocation events within other protein members of the HIF pathway prompted the further examination as to whether these events were connected.

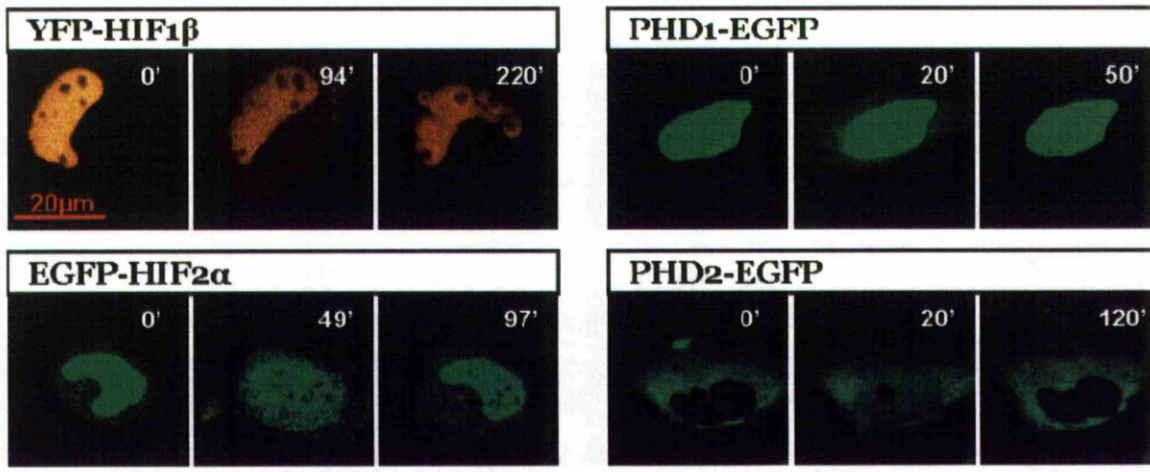

Fig 7.9. Live-cell confocal microscopy of HeLa cells expressing various fluorescent fusion plasmids related to the HIF signalling network. All images are shown from the initiation of a spontaneous translocation event.

7.2.8 Are the translocations specific to complexes of the HIF system or a general feature?

To assess the specificity of the translocations to the HIF system, HeLa cells were co-transfected with two unrelated proteins. The proteins selected were HIF-1β and Rel-B of the NF-κB pathway. The proteins were considered unrelated after confirmation by literature review (retrieving no papers in a pubmed search together). Once transfected cells were then imaged by confocal microscopy and then fluorescence levels quantified using Cell Tracker. Confirmation by eye and quantification of nuclear intensity profile indicated that both proteins translocated (nucleus to cytoplasm) simultaneously in all instances and with the same export rate (**Fig 7.10**). This further conforms to the hypothesis that the translocation events are a general cell-type specific event, while non-specific for the proteins involved. This would therefore imply that the nuclear-cytoplasmic translocations may occur simultaneously alongside cytoplasmic-nuclear translocations.

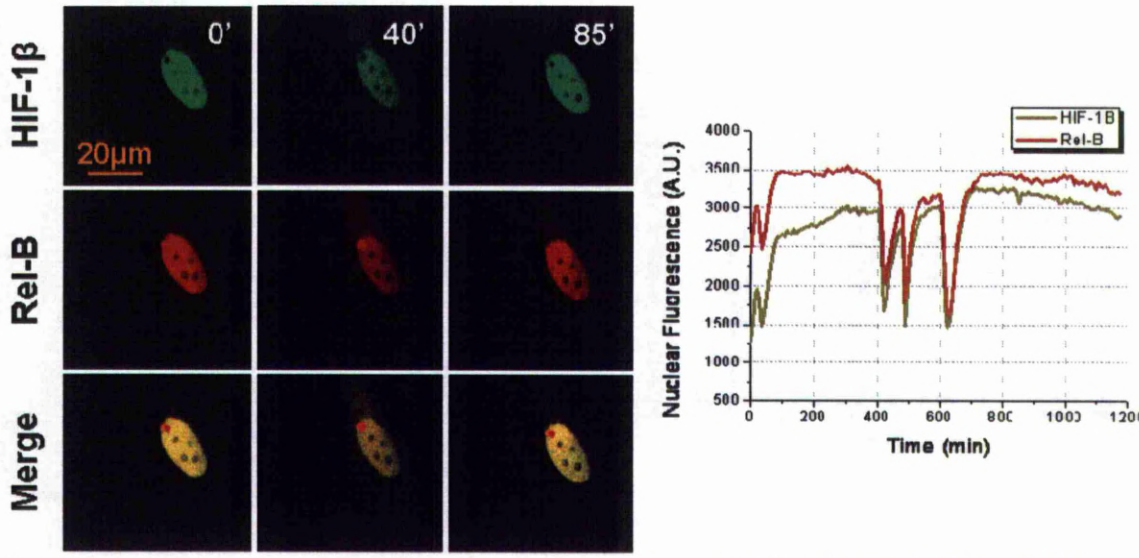

Fig 7.10. Time-lapse imaging of HeLa cells transiently transfected with YFP-HIF1β and RelB-DsRedxp. Images are of a single translocation event. Plotted data shows the nuclear fluorescence trace for the cell for the experiment duration.

7.2.9 Vesicle formation as a source of disruption to nuclear envelope integrity

The evidence gathered supports nuclear envelope disruption as a source of the translocations. The previous images were then carefully scrutinised for visual clues pertaining towards this hypothesised nuclear envelope disruption. Several of the translocating cells were found to have distinct vesicle-like formations that

grow in size, before seemingly bursting and disappearing and then reforming again. The bursting of these vesicles coincides with the translocation of the observed protein (**Fig 7.11**). We conclude that this process is responsible for the disruption of nuclear envelope integrity which leads to the re-localisation of all the observed proteins so far.

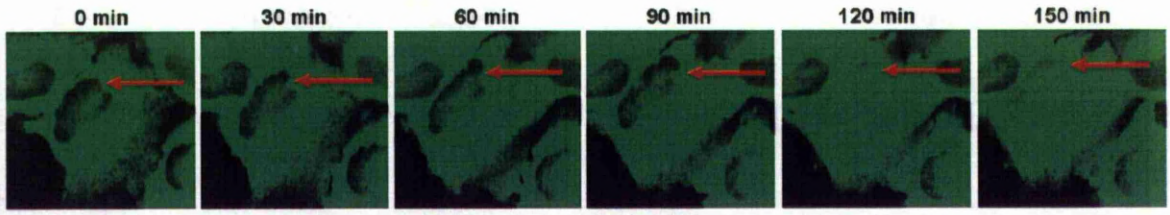

Fig 7.11. Time-lapse imaging of HeLa cells transiently transfected with PHD2EGFP. Red arrow indicates nuclear vesicle-like formation, which grows and ruptures, coinciding with the translocation of fluorescent PHD2 at 120 minutes.

7.3 Discussion

Throughout the live-cell imaging of the HIF system we have been able to observe a seemingly novel biological phenomenon that gives rise to dysregulated cellular localisation patterns in several transformed cell lines. Evidence suggests that these events occur due to disruption in the nuclear envelope mediated *via* nuclear vesicle formation and subsequent bursting. This process is dynamic and asynchronous throughout a population of cells and thereby difficult to detect with standard bulk-cell assays (Levsky and Singer 2003). These nuclear envelope disruption events effect the general cell architecture and thus can be expected to affect a large amount of cellular components allowing nuclear proteins untimely exposure to the cytoplasm and vice versa; perhaps even organelles such as mitochondria may gain access to the nucleus due to these events (Bakeeva, Skulachev et al. 2001). The potential scope of detrimental affects is vastly diverse. For certain it refocuses a cautionary approach to research grade cell lines as both HeLa and Daoy are extensively used as models in cell biology (Jacobsen, Jenkyn et al. 1985; Chilov, Camenisch et al. 1999; Taylor, Furuta et al. 2000; Hofer, Desbaillets et al. 2002; Peyrl, Krapfenbauer et al. 2003; Meley, Spiller et al. 2010).

7.3.1 Nuclear membrane instability resembles Vpr-induced herniations

At the onset of this work describing nuclear membrane instability we were unaware of any such publication detailing this phenomenon. Since the significant completion of this body of data we have since found a publication

which most likely describes what was witnessed here. The paper was published in Science by de Norohna *et al.* (2001), titled 'Dynamic Disruptions in Nuclear Envelope Architecture and Integrity Induced by HIV-1 Vpr'. The paper reports that the presence of viral protein R, a HIV gene product, affects the lamin structures and induces nuclear herniations in HeLa cells that occasionally rupture and disrupt nuclear membrane integrity. The loss of nuclear membrane integrity is then shown to affect the regulated localisation of components of the cell cycle machinery, including wee1, cdc25 and cyclin B1. The dysregulated localisation of these components has consequences on the cells ability to proliferate (de Noronha, Sherman et al. 2001). Rupturing nuclear herniations were also identified in a study by Hoyt *et al.* (2004) using mouse L929 cells. In this case, reovirus infection and subsequent expression of σ1s viral protein were found to be responsible for inducing herniations (Hoyt, Bouchard et al. 2004). In opposition to these publications, we have not purposely instigated viral infection and have still managed to detect nuclear herniation events in two cell lines, namely the HeLa cervical carcinoma cells and DaoY medulloblastoma cells (Gey GO 1952; Jacobsen, Jenkyn et al. 1985). This contradiction is made more important as the de Norohna *et al.* (2001) study also used HeLa cells in their investigation into nuclear herniations. One explanation for these differences between the same cell line is HeLa cells across different labs and at differing times may have differing genetic statuses, owing to the genomic instability of the cell line (Irelan, Wu et al. 2011). However, this would also imply that the virally induced nuclear herniations can be mimicked through accumulations of mutations. Both de Noronha *et al.* and Hoyt *et al.* found the underlying mechanism to be the disruption of the nuclear lamins and nuclear pore complexes. The nuclear lamins constitute a structural element to the nucleus, providing shape and mechanical stability as well as effecting the genomic organization (Dechat, Adam et al. 2010). Their position in the nuclear integrity would suggest that the nuclear lamins would be a likely candidate in explaining the underlying molecular causes of the nuclear herniations in our system.

7.3.2 Consequence of nuclear herniations

Regardless, the un-stimulated occurrence of herniations in two unrelated cell lines may suggest the mechanism to be present in other transformed cells. In spite of this speculation, de Noronha *et al.* 2001 showed that the herniations

actually induced cell cycle arrest, a feature that would not expectantly be favourable or selected for. Analysis of our own cells showed no compromising effect to cell cycle (data not shown). Currently, there is limited work regarding nuclear herniations and therefore it is difficult to speculate the consequences. The compromising of nuclear integrity may aid in the transfection of certain cell lines. Typically cationic lipid transfection requires the nuclear envelope breakdown and reformation in order for the plasmid to reach the nucleus and to be expressed (Zabner, Fasbender et al. 1995). Cells lines undergoing nuclear herniations would not be dependent on this step and transfections may occur in a cell-division independent manner. This may explain a portion of the heterogeneity observed when imaging fluorescent HIF-α and the HRE-luciferase in Chapter 4. Beyond research methodology, the occurrence of disrupted nuclear membrane integrity is likely to have other repercussions. It is known that the nuclear lamina is disrupted in many diseases, though the exact relationship of dysfunctional lamina to the pathology of the disease often remains unknown (Dechat, Adam et al. 2010). If these dysfunctions lead to herniations, it may be that the mislocalisation of a diverse set of cellular make-up contributes to these pathologies. The involvement of mislocalisation of protein in the etiology of disease was thoroughly addressed by Park *et al.* 2011, who reported a direct correlation of protein localisation and disease association (Park, Yang et al. 2011). Broadly speaking, many processes, proteins, RNA and cellular components are influenced by the regulated separation of the cell nucleus from the cytoplasm. It could thereby be expected that the untimely mislocalisation of cellular components could have a broad range of effects beyond the documented cell cycle arrest; including the disturbance of inhibitory cytoplasmic sequestration of NRF2, activation of Rho via loss of Net1 nuclear sequestration and the expression of migration stimulating factor by nuclear sequestered precursor mRNA to name but a few (**Table 7.1**) (Graef, Chen et al. 2001; Zipper and Mulcahy 2002; Kay, Ellis et al. 2005). The presence of asynchronous translocations also introduces heterogeneity into the population of cells. Work published by Paszek *et al.* suggested that heterogeneity to be protective for tissues, some of this concept may carry across to populations of cells experiencing spontaneous herniations (Paszek, Ryan et al. 2010). In our own work it is possible these nuclear herniations contributed to the cytoplasmic localization patterns of HIF-2α (**Chapter 6**). Within available literature on the

HIF system, several localisation sensitive mechanisms have been reported, including work by Jokilehto *et al.* (2010) who reported that the mislocalisation of PHD2 to the cell nucleus promotes anchorage-independent carcinoma cell growth, promoting malignancy (Jokilehto, Hogel et al. 2010). Additionally the regulation of HIF-PHD binding is facilitated by the localization of the OS-9 protein (Baek, Mahon et al. 2005; Brockmeier, Platzek et al. 2011). Lastly, SIAH2 specificity for targeting PHD3 over PHD2 for degradation is also cited to be localisation dependent (Nakayama, Qi et al. 2009). All these reasons alone warrant caution when investigating cellular processes in cell lines that are known or suspected to undergo spontaneous nuclear herniations.

Known processes using: **Cytoplasmic sequestration**		
NF-κB	Cytoplasmic sequestration of p65 by IκBα prior to receiving an inducing stimulus, allowing p65 to move to the nucleus	(Nelson, Ihekwaba et al. 2004)
NRF2	The redox-sensitive transcription factor is sequestered by KEAP-1 until an activating stimuli allows NRF2 to translocate to the nucleus.	(Zipper and Mulcahy 2002)
NFAT	The dephosphorylation of the NFAT transcription factor complex unmasks a nuclear localisation domain, resulting in translocation.	(Graef, Chen et al. 2001)
ERK	ERK is sequestered in the cytoplasm by MEK. Upon stimulation ERK translocates to the nucleus. Under continuous stimulation ERK oscillates.	(Shankaran, Ippolito et al. 2009)
GR	GR is sequestered in an unliganded state in the cytoplasm. When bound to cortisol the GR NLS become exposed, stimulating nuclear translocation	(Biddie and Hager 2009)
NFAT	Cytoplasmic localisation of NFAT is promoted via basal hyperphosphorylation. Dephosphorylation of NFAT following calcium influx allows NFAT to travel to the nucleus.	(Mancini and Toker 2009)
Cell Cycle	The regulated compartmentalisation of several components such as cyclin B is part of the series of events controlling cell cycle progression.	(Kong, Barnes et al. 2000)

Known processes using: **Nuclear sequestration**		
Net1	Net1 is a nuclear sequestered guanine nucleotide exchange factor, relocation of Net1 to the cytoplasm leads to the activation of Rho.	(Schmidt and Hall 2002)
p53	Typically p53 is localised and functional as a transcription factor in the cell nucleus. The localisation of p53 to the cytoplasm is cited to have diverse implications. One such is the promotion of apoptosis.	(Liu and Xirodimas 2010)

Table 7.1. A non-exhaustive list of known examples in which the regulated nuclear or cytoplasmic sequestration of a protein is important to function.

Chapter 8: Discussion

8.1 General Discussion

This project has used a combination of single-cell imaging and mathematical modelling alongside traditional molecular biology techniques to investigate the oxygen-sensitive hypoxia-inducible factor (HIF) signalling system.

8.1.1 Reflection on thesis aims

The project initially set out to confirm and characterise the existence of intracellular dynamics of the HIF-α transcription factor in response to perturbed oxygen levels. Such dynamics were previously hypothesised with reference to the presence of a delayed negative feedback within the HIF system (Marxsen, Stengel et al. 2004; Stiehl, Wirthner et al. 2006). To this end, several subsidiary aims were established; (1) To assess the suitability of both fluorescent proteins and bioluminescence for use in low oxygen conditions; (2) To clone and then validate the use of plasmid constructs to enable the single-cell visualisation of this system; (3) To image the HIF system using the generated molecular tools, investigating both the protein and transcriptional response to hypoxia.

During the course of addressing these aims, several further questions became apparent. The single-cell data provided evidence for previously unreported distinctive patterns of HIF-2α subcellular localisation, whilst also showing the nuclear-cytoplasmic translocations of several canonical members of the HIF pathway. These phenomena were investigated in Chapters 6 and 7 respectively. Additionally, the quantitative nature of the HIF-α imaging experimentation, and the emerging complexity of the HIF system provided strong arguments for the use of mathematical modelling to further investigate feedback dynamics (Sung and McNally 2010). To this end, a collaboration was successfully built with the University of Liverpool Department of Mathematics following extensive training in mathematical modelling by (our now collaborator) Dr. Rachel Bearon.

During the course of the project some further undiscussed goals and aims were briefly investigated only to be subsequently found impractical or largely unparsed. Nevertheless, I believe the main aims of this thesis were met.

8.2 HIF-signalling: Current Relevance and Future Perspective

The work carried out spanned three broad themes: the use of molecular reporters in hypoxia, the kinetics of HIF-α and the subcellular localisation pattern of HIF-2α. The project was mainly focussed on the dynamic properties of the system and their characterisation using single-cell imaging and mathematical modelling.

8.2.1 The Dynamics of HIF signalling

Dynamics is a broad term encapsulating the continuous changes that perpetuate through signalling systems (nicely reviewed by Kholodennko 2006) (Kholodenko 2006). We characterised some of the spatial and temporal dynamics present in the HIF system, finding them to be influenced by both intrinsic and extrinsic perturbations.

To our knowledge, this is the first study to attempt an in-depth analysis of the dynamics of the hypoxia response system (as governed by HIF). For future work, it will no doubt be interesting to investigate these dynamics away from the potential pit falls of HIF-α overexpression. The use of the ODD-EGFP in chapter 4 presented one such possibility and currently our laboratory is also preparing a lentiviral system in which to achieve stable expression of full length fluorescent HIF-1α and HIF-2α. This approach will be used to further validate the cell cycle-related modulation of HIF, whilst also providing more assured information on the occurrence of normoxic stabilisation.

In the context of the HIF-2α system, the cellular speckles (observed in chapter 6) could be explored across a population of cells without varied expression levels possibly contributing to heterogeneity. This may represent an interesting avenue of research, as the consequence of the speckles on HIF signalling remains an entirely open question.

The dynamics of pVHL have been left relatively unexplored. In light of the citations suggesting the shuttling of pVHL to be important to HIF (as well as the proposed cell cycle regulation of pVHL), it may be interesting to characterise these events with respect to HIF dynamics (Lee, Neumann et al. 1999; Liu, Xin et al. 2010).

8.2.2 Modelling HIF signalling

Unlike many signalling systems there have been relatively few mathematical models developed for HIF signalling. The most established being the model proposed by Kohn *et al.* which was further developed through the works of Dayan *et al.*, Yu *et al.* and Heiner *et al.* We would propose that the 4C-model may offer additional insights, appraising the signalling network from a bottom-up approach as opposed to the top-down approaches taken by other HIF-models to date. For the 4C-model to truly achieve this, the mathematical model (and the predictive power) will need to be further developed and become more relative to data from other groups. Here we discuss the future perspectives for the further development of the model in light of current and emerging technologies.

8.2.2.1 Beyond the 4C-model

There is significant potential for further development of the current 4C-model and therefore every development should be qualified with a specific question. For example, should future data be unexplainable using the current model, an effort would be made to adjust the model accordingly. Despite the very broad and near limitless possibility for further model elaboration, it is possible to suggest several directions for progress (**Fig 8.1**).

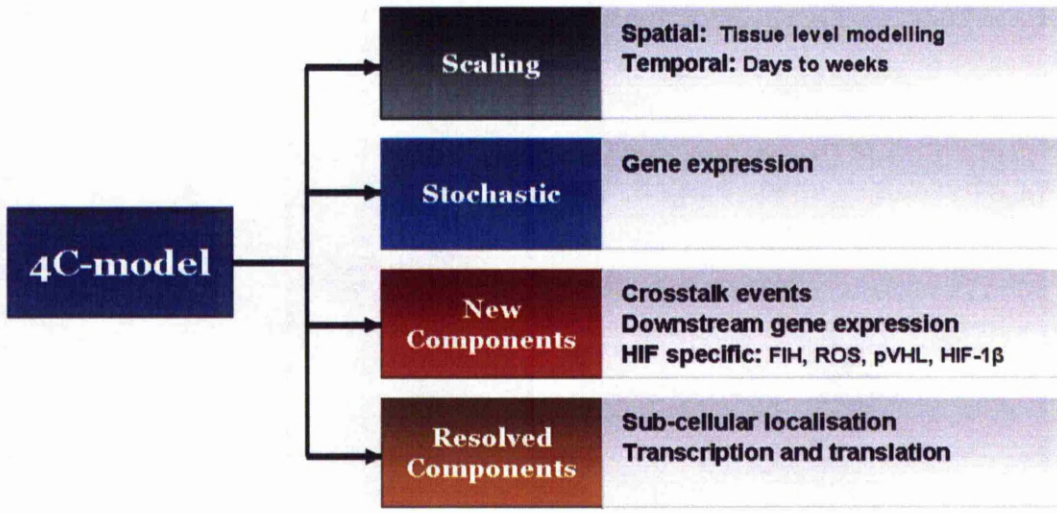

Fig 8.1. Outline of future development routes for the 4C-model

Firstly the model details a single isolated cell and lacks the additional complexity of scaling to tissue levels. Many remaining questions concerning HIF are questions targeted to multicellular arrangements in which blood supply, cell division, apoptosis, cytokine production, O_2-consumption and diffusion are all

implicit. The tumour environment is one such example of a multicellular arrangement and muscles under exercise another. Work from Dr. A Popel's group has attempted to model the unity of features such as VEGF, HIF expression with muscle during exercise (Mac Gabhann, Ji et al. 2007; Schnell 2007; Lai, Zhou et al. 2009). A perhaps interesting aspect to this scale model would be the inclusion of tissue level feedback motifs occurring in the forms of VEGF and EPO, controlling vasculature and erythropoiesis respectively. Although this task is far from trivial, a model of HIF transcriptional activity and downstream gene expression would need the regulating intracellular feedbacks. Bringing these ideas to our 4C-model might involve the resolution of gene expression profiles of important HIF genes such as VEGF, EPO, BNIP3 or one of the hundreds of others possible relevant to tissue level function (perhaps even going as far to include stochasticity) (Althaus, Bernaudin et al. 2006). Microarray data makes this more realistic when working within a mathematical model framework (Wolkenhauer 2002). As the 4C-model already describes gene expression of PHD2 and PHD3, these parameters can be used to normalise expression to other genes.

A further possible route of model-development is to expand the model architecture to include new components. Our data suggests the involvement of cell cycle in HIF-signalling. From further investigation into cell cycle, the responsiveness of HIF at different phases at varying oxygen conditions could be assessed, particularly as G1/S arrest is purported to occur in hypoxia (Alarcon, Byrne et al. 2004; Hubbi, Luo et al.). This would constitute an inter-system feedback mechanism by which HIF regulates cell cycle and cell cycle regulates HIF-α abundance, something that may be important in highly proliferating cancer cells (Hubbi, Luo et al. 2011). The expansion of model components can also be envisaged for other members of the pathway, such as pVHL, FIH, HIF-3α or HIF-1β and perhaps even the SIAH proteins. This would be in line with work from Heiner *et al.* (2010) whose analysis of the core components of the HIF-model included pVHL. The addition of new components may allow us to consider model simulations over longer time-scales, moving from hours to days to weeks (Bruning, Cerone et al. 2011). Similarly, it may be of interest to model HIF-2α, which is cited to accumulate at later time points (or possibly with different dynamics) and investigate the impact on downstream gene transcription Bracken, 2006 #310}.

Alternatively, the core model components could be further resolved. There has been much speculation and discussion regarding the compartmentalisation of the PHD proteins. From our own 4c-model framework the spatial characteristics could be explored by introducing nuclear import and export rates of the HIF-α and the PHD proteins which may now be quantifiable using single-cell imaging experiments such as FRAP and FCS(Wu, Corbett et al. 2009; Pfeifer, Kaschek et al.). Such spatial consideration may allow the effect of the localisation on hydroxylation to be further explored. It may also be relevant to resolve the synthesis terms of the 4C-model into separate mRNA and translation rates. In support for this, a recent global study on protein expression by Yen *et al.* found translational rates to be the defining point for protein abundance, a finding in contrast to our use of mRNA abundance (Yen, Xu et al. 2008).

Finally, the 4C-model was built on data using arbitrary units of fluorescence. A desirable goal for future model fitting would be to have the units of the model more reflective of those encountered in the cellular environment and for the model to work with absolute quantification. This would help us to understand the exact ratio of HIF to PHD protein, address the relevance of stochasticity and to investigate the saturation potential of the system. A recent technology developed by Beynon *et al.* 2005 enables the absolute measurement of protein in a technique termed QconCAT (Beynon, Doherty et al. 2005). This technology may allow us to adopt absolute protein abundance into our current 4C-model, a level of detail which has not been truly achieved by any HIF model to date.

8.3 General principles

Our work investigating HIF signalling dynamics has relevance beyond the immediate hypoxia field of research, raising several general points for discussion.

8.3.1 Delayed Negative Feedback motifs

Our work has highlighted that non-overtly dynamic signalling systems can still be regulated by more subtle, dynamic mechanisms. We believe other signalling systems could well be approached in a similar manner and these endeavours may enrich our understanding. It is common practice to measure the average amplitude of response, sometimes with little consideration to possible shifts in kinetics or asynchrony between cells. This is partially due to the practicalities of population-wide techniques such as western blot, RTq-PCR, microarrays etc.

Here we have implemented the live-cell imaging of the HIF system to enable the development of a mathematical model, both of which are useful tools to understand regulatory events at high spatial and/or temporal resolution. Such regulatory features are emerging to be important in managing the phenotype of response. The encoding of information is of importance to our understanding of cell signalling and thereby our ability to manage and manipulate intra-cellular signalling systems with therapeutics, which is a principal goal for our field of biological research (Patel, Heyward et al. 2011). We have investigated to some extent how the HIF system may encode information: from memory of stimulus, to amplitude, duration and steady-state levels. Underlying this notion is the delayed negative feedback loop supplied by the relationship between HIF and PHD.

Negative feedback loops exist on many levels of biological signalling networks: from transcriptional cycles (Harper, Finkenstadt et al. 2011), to subcellular protein feedbacks (Ihekwaba, Broomhead et al. 2004; Nelson, Ihekwaba et al. 2004), to tissue-level feedbacks (Forsythe, Jiang et al. 1996), to behavioural (Worland 1976; Turrigiano 2007). Typically, a negative feedback loop requires an inducing species and repressing species. From this architecture alone a steady-state solution is reached or homeostasis maintained. This can be considered to be the case in many biochemical reactions which are fast acting and sensitive to changes in product or substrate. Homeostasis can also be a much more complicated situation, in which the maintenance of a set state in face of extrinsic perturbations is necessary for function. Such a situation has

been shown for the maintenance of neuronal function in spite of changes in cell size and condition (Turrigiano 2007). In considering the HIF negative feedback loops, we have explored the addition of a further feature: an intrinsic delay. The inclusion of a delay opens the possibility of transitional-state dynamics (dynamic instability), manifesting as either simple transiency or complex oscillatory profiles. Although dynamic instability may be an unstimulated feature of certain biological events, such as transcription, in cell signalling dynamic instability is often in response to an external cue. The resulting transitional dynamics offer the potential to encode contextual information. The most dynamic and striking example of this is found in the various intracellular oscillators that have been discovered, including ERK (Shankaran, Ippolito et al. 2009), p53 (Lahav, Rosenfeld et al. 2004), NF-κB (Nelson, Ihekwaba et al. 2004) and calcium (Dolmetsch, Xu et al. 1998). The transitional-state dynamics of the latter two have both been shown to alter the downstream gene expression profile.

Oscillatory systems also require a sufficient degree of non-linearity. If such non-linearity is absent, the potential for complex dynamics is markedly reduced (or impossible). Many signalling systems may not have such vivid oscillatory outputs but still have meaningful dynamic properties (Plachta, Bollenbach et al. 2011). Our own model has highlighted the flexibility of a simple delayed negative feedback loop. We would hypothesise that the plasticity of this motif encourages context-specific response patterns which oscillatory systems would be more robust against. Our work with a simpler system should highlight that other signalling networks could perhaps be assessed for the way these feedbacks encode information and whether this has phenotypic consequences.

Dynamics can be quantified and appraised in various ways ranging from amplitude, period, peak-duration, steady-state levels and reset periods all changing over the course of different stimuli and cell type (Kholodenko 2006). Many of these features have been shown to have an impact on the phenotype of response in other signalling systems, including the dose-to-duration response of yeast *Saccharomyces cerevisiae* after exposure to mating pheromone, in which growth or mating is selected for based on duration of the intracellular signalling components(Behar, Hao et al. 2008). The amplitude of calcium entry into developing B-cells affects the sensitivity to ligand induced cell death (Limnander, Depeille et al. 2011). Both duration and amplitude are thought to

be important for sonic hedgehog ligand induced differentiation of cells in development, as the temporal profile of signalling translates to the formation of different cell types (Ribes, Balaskas et al. 2010). The steady-state protein levels (albeit a fluctuating stochastic steady-state) of Bcl-xl determine the propensity of the cell to commit to apoptosis.

In a goal beyond the scope of this thesis, an improved appreciation and knowledge of encoding could lead to therapeutics which may act to edit the message of transcription factors rather than simply activating or repressing, or allow a better appraisal of a disease and therefore the course of treatment. Also as hypoxia plays a role in stem cell maintenance and proliferation, it may be possible that the kinetics of oxygen and hypoxia are also important to this field (Barnhart and Simon 2007; Seton-Rogers).

8.3.2 Live-cell imaging; versatility and applicability

Live-cell imaging allows for the unparalled measurement and observation of many of the processes of life. Developments in technology and methodology in this field are therefore very important for the scope of biological questions that we can answer. Of the current technologies, confocal microscopy and the imaging of fluorescence is the most popular, owing to the comparative resolution, relevant fluorescent probes and versatile speed of image acquisition. Nevertheless, other technologies have their own merits, including bright field imaging and wide-field luminescence (Stephens and Allan 2003; Troy, Jekic-McMullen et al. 2004; Selinummi, Ruusuvuori et al. 2009).

The application of confocal microscopy to cell biology is generally limited to our ability to fluorescently label cellular components. The list of labelling methods and targets is extensive, easily covering the components of the central dogma, DNA, RNA and protein and additional elements such as lipids (Lindhout, Fransz et al. 2007; Mac Gabhann, Ji et al. 2007; Bao, Rhee et al. 2009; Spandl, White et al. 2009). The use of fluorescent proteins and genetic manipulation make it almost possible to label any protein-of-interest (Wiedenmann, Oswald et al. 2009). Additionally, many probes exist that are reactive with the biochemical status and changes of the cellular environment, sensitive to redox-state, concentration of dissolved oxygen, metabolites etc (O'Riordan, Fitzgerald et al. 2007; Hilderbrand ; van Lith, Tiwari et al. 2011). A recent and very well cited paper by Wang *et al.* 2008 has also managed to measure superoxide flashes in single-mitochondria when exposed to anoxia, hypoxia and re-

oxygenation, imaging a dramatic increase in superoxide production following re-oxygenation (Wang, Fang et al. 2008). The possible probes and proteins alone offer a huge scope of relating oxygen consumption dynamics, redox state and mitochondrial status with HIF protein dynamics. Improvements to labelling are typically made by reducing the toxicity, invasiveness and non-specificity as well as improving the spectral characteristics of the labels available. Furthermore, the advent of superresolution has circumvented the issue of the diffraction limit and we're thereby able to resolve structures smaller ~200nm while still gaining all the benefits associated with confocal microscopy (Toprak, Kural et al. 2010). Super-resolution imaging may prove useful in the characterisation of the various cellular bodies of the HIF signalling system, providing quantitative data on the amount of protein present via the single-molecule level imaging. Beyond this, many other techniques may also prove to be of worth for this avenue of work such as FRAP, FRET and fluorescence cross correlation spectroscopy (FCCS), which are able to provide a rich variety of quantitative data regarding diffusion and binding affinities, enabling us to further calculate the percentage of HIF-2α localised to the possible protein stores and evaluating the visible complexes. From such data we can begin to hypothesise the likely impact of the subcellular localisation of HIF components on overall HIF signalling (alongside other experiments). During the course of the project, we attempted the live-cell measurement of protein turnover. New technologies can permit us to revisit this. The live-cell measurement of protein stability is possible using plasmid expression vectors encoding a fusion protein of interest and an IRES separated unfused DsRedxp, thereby green and red fluorescence are from the same mRNA. The relative ratio of green fluorescence to red fluorescence can be used in the quantification of protein turnover, as originally reported by Yen *et al.* (2008) and known as global protein stability analysis. Separately to this knowledge we have begun to clone expression vectors in line with this thinking for HIF-1α and HIF-2α. This approach has the additional benefit when coupled with transient transfection to relate expression level of the reference red fluorescent protein to the fused protein of interest, relating either HIF-1α accumulation profile or HIF-2α speckle morphology to expression.

Live-cell confocal microscopy is therefore able to generate data greater than the initial specific research questions. The live imaging of single-cells almost

automatically provides information on cell morphology, migratory response, viability, cell division rates and cell-to-cell variance. Some of these principals were demonstrated during our investigation into intracellular signalling dynamics with the HIF system. Cell death rates were calculated after imaging cells transfected with HIF-α, division rates were explored to calculate whether overexpression of HIF-1α induced cell-cycle arrest and also cell-to-cell variance was ardently assessed.

The major limitation encountered with taking into account the total available information was with the analysis software and the quantification of the visual data. Several image analysis tools were used, Cell Tracker, AQM kinetic analysis and LSM image browser and many more exist that were largely untried including Cell Profiler, Image J and Carnegie web based Cell Tracking Software. With the development of suitable software our imaging data could be revisited, further analysed and intracellular dynamics correlated with other visual data. This would make the investigation more systematic and less biased towards specific outcomes. The power of the available software is far from ideal; the tracking of a single-cell by fluorescence for a 20-hour time-course can take up to several hours due to the very semi-automatic processing. This is cause for concern for two reasons; firstly there may be discrepancies between the way the two independent researchers analyse and track the cell and secondly the inefficiency of the tracking process limits the number of cells that can effectively be analysed. The statistical power of the data is subject to the number of cells analysed and some patterns may only be truly evident with more cells. In current opinion, the considerable versatility and applicability of live-cell imaging to the study of signalling systems such as HIF, is limited by the ability to systematically and computationally quantify the visual data.

8.3.3 The purpose and practice of mathematical modelling

Mathematical modelling is often employed alongside biology, improving the analytical capacity and insight biologists are able to gain from data. This relationship has been in development over the course of centuries, though has now considerably expanded with the advent of new technology and biological measurements, into the current field of systems biology (Hester, Iliescu et al. 2011). A conventional role for the mathematical modelling used by systems biology is to investigate emergent properties not predicted by the component make-up and to computationally address information too complex for intuition

alone to process, while also allowing the real-time predicted measurement of all model features (Bhalla and Iyengar 1999; Sung and McNally 2010). Almost every biological event discussed throughout this thesis has been mathematically modelled, whether it is the motion and formation of cellular bodies, the biochemical networks underlying energy production, single-cell and tissue-level modelling of inflammation, mitochondrial bioenergetics, the process of apoptosis and cell cycle, gene transcription, tumour growth, vascular biology or intracellular dynamics of HIF signalling (Kohn, Riss et al. 2004; Nelson, Ihekwaba et al. 2004; Goel, Chou et al. 2006; Vodovotz, Chow et al. 2006; von Stosch, Peres et al. 2010).

There are numerous examples of successful predictions arising from mathematical models of cell signalling systems. Oscillations of p53 were predicted before they were measured. In actin dynamics, the transition rate of asters to stars was successfully predicted to be scaled to the ratio of available fascin protein to total actin. The centralisation of the *C. elegans* nucleus was predicted to arise from a pulling mechanism, as opposed to the equally favoured pushing hypothesis of the time (Bhalla and Iyengar 1999; Mogilner, Wollman et al. 2006). Many of these models have also begun to inform clinical and practical applications. Mathematical models of cardiac electrophysiology have been used to predict the ideal tissue contact points for electro-stimulation and fibrillation regime to prevent damage (Trayanova 2006; Vigmond, Vadakkumpadan et al. 2009). As well as the predictive power of modelling, a further advantage is in the recording of a functional description of our understanding of the signalling events. Commonly still, a *model* is often a pictorial representation of the components involved and these picture networks have become increasingly complex with the integration of –omic data. In contrast to this, a mathematical model is functional, testable and is able to readily integrate more information – potentially to the point in which it would be too complex for intuition to process. In essence, a single mathematical model could embody a large degree of literature, an important concept due to the rate of information gain in biological science.

8.4 Final Comments

At the outset of my PhD my knowledge basis and viewpoint of cell signalling was very much fixed from textbook static diagrams of signalling pathways. The backdrop of my own and adjacent projects has helped me develop an appreciation and awareness of the complexity and fluidity inherent in cellular signalling networks. This awareness naturally leads to the question of how to best facilitate our understanding of such complexity and this has led to my personal involvement and interest in the field of systems biology. I now appreciate that there has been a slow and continuous movement to integrate complex biological information and this movement has recently and rapidly expanded in the post genomic era, giving rise to the current incarnation of systems biology. Systems biology is known in many guises and the exact definition is still somewhat variable between practitioners, although the use of computational power and mathematics is a commonly employed tool within this field. Mathematics provides a very natural framework to address cell signalling as models and equations are not only descriptive but functional. From this functionality models are able to provide biologists with predictions and testable hypotheses. For these models to be meaningful, they require the sensible abstraction of signalling networks and constraint against biological measurements. These series of realisations have led to my understanding of the continued importance of an interdisciplinary approach; how development in the physics of microscopy enhances our ability to measure biological events and how engineering is required in the building of complex apparatus for use in these measurements; how software developers enhance our ability to analyse, present, record, retrieve and exchange data. These contributions occur before a biologist and mathematician are able to collaborate over information and to advance the understanding over a particular problem. I believe we have shown that this process was worthwhile for the investigation of the HIF system and this approach has advanced the insight into the spatiotemporal dynamics of this pathway as well as the plausibility that the kinetics of HIF-α accumulation encode context.

Finally, I look forward to witnessing and being apart of the continued progression of systems biology, applying and developing my knowledge accordingly.

Chapter 9: Bibliography

Abel, J. and T. Haarmann-Stemmann (2010). "An introduction to the molecular basics of aryl hydrocarbon receptor biology." Biol Chem **391**(11): 1235-1248.

Adibhatla, R. M. and J. F. Hatcher (2010). "Lipid oxidation and peroxidation in CNS health and disease: from molecular mechanisms to therapeutic opportunities." Antioxid Redox Signal **12**(1): 125-169.

Agbor, T. A. and C. T. Taylor (2008). "SUMO, hypoxia and the regulation of metabolism." Biochem Soc Trans **36**(Pt 3): 445-448.

Alarcon, T., H. M. Byrne, et al. (2004). "A mathematical model of the effects of hypoxia on the cell-cycle of normal and cancer cells." J Theor Biol **229**(3): 395-411.

Alarcon, T. and K. M. Page (2007). "Mathematical models of the VEGF receptor and its role in cancer therapy." J R Soc Interface **4**(13): 283-304.

Althaus, J., M. Bernaudin, et al. (2006). "Expression of the gene encoding the pro-apoptotic BNIP3 protein and stimulation of hypoxia-inducible factor-1alpha (HIF-1alpha) protein following focal cerebral ischemia in rats." Neurochem Int **48**(8): 687-695.

Appelhoff, R. J., Y. M. Tian, et al. (2004). "Differential function of the prolyl hydroxylases PHD1, PHD2, and PHD3 in the regulation of hypoxia-inducible factor." J Biol Chem **279**(37): 38458-38465.

Aprelikova, O., G. V. Chandramouli, et al. (2004). "Regulation of HIF prolyl hydroxylases by hypoxia-inducible factors." J Cell Biochem **92**(3): 491-501.

Ashall, L., C. A. Horton, et al. (2009). "Pulsatile stimulation determines timing and specificity of NF-kappaB-dependent transcription." Science **324**(5924): 242-246.

Avni, R., B. Cohen, et al. (2011). "Hypoxic stress and cancer: imaging the axis of evil in tumor metastasis." NMR Biomed **24**(6): 569-581.

Baba, M., S. Hirai, et al. (2001). "Tumor suppressor protein VHL is induced at high cell density and mediates contact inhibition of cell growth." Oncogene **20**(22): 2727-2736.

Baek, J. H., P. C. Mahon, et al. (2005). "OS-9 interacts with hypoxia-inducible factor 1alpha and prolyl hydroxylases to promote oxygen-dependent degradation of HIF-1alpha." Mol Cell **17**(4): 503-512.

Bailey, D. M., I. S. Young, et al. (2004). "Regulation of free radical outflow from an isolated muscle bed in exercising humans." Am J Physiol Heart Circ Physiol **287**(4): H1689-1699.

Bakeeva, L. E., V. P. Skulachev, et al. (2001). "Mitochondria enter the nucleus (one further problem in chronic alcoholism)." Biochemistry (Mosc) **66**(12): 1335-1341.

Banerjee, D. and F. J. Slack (2005). "Temporal and spatial patterning of an organ by a single transcription factor." Genome Biol **6**(2): 205.

Bao, G., W. J. Rhee, et al. (2009). "Fluorescent probes for live-cell RNA detection." Annu Rev Biomed Eng **11**: 25-47.

Barnhart, B. C. and M. C. Simon (2007). "Metastasis and stem cell pathways." Cancer Metastasis Rev **26**(2): 261-271.

Barontini, M. and P. L. Dahia (2010). "VHL disease." Best Pract Res Clin Endocrinol Metab **24**(3): 401-413.

Barrick, D., D. U. Ferreiro, et al. (2008). "Folding landscapes of ankyrin repeat proteins: experiments meet theory." Curr Opin Struct Biol **18**(1): 27-34.

Bartfeld, S., S. Hess, et al. (2010). "High-throughput and single-cell imaging of NF-kappaB oscillations using monoclonal cell lines." BMC Cell Biol **11**: 21.

Barth, S., J. Nesper, et al. (2007). "The peptidyl prolyl cis/trans isomerase FKBP38 determines hypoxia-inducible transcription factor prolyl-4-hydroxylase PHD2 protein stability." Mol Cell Biol **27**(10): 3758-3768.

Basu, S., R. Mehreja, et al. (2004). "Spatiotemporal control of gene expression with pulse-generating networks." Proc Natl Acad Sci U S A **101**(17): 6355-6360.

Batchelor, E., A. Loewer, et al. (2011). "Stimulus-dependent dynamics of p53 in single cells." Mol Syst Biol **7**: 488.

Bauer, N. G. and C. Richter-Landsberg (2006). "The dynamic instability of microtubules is required for aggresome formation in oligodendroglial cells after proteolytic stress." J Mol Neurosci **29**(2): 153-168.

Beaudoin, S., K. Goggin, et al. (2008). "Aggresomes do not represent a general cellular response to protein misfolding in mammalian cells." BMC Cell Biol **9**: 59.

Beck, J. S. (1961). "Variations in the morphological patterns of "autoimmune" nuclear fluorescence." Lancet **1**(7188): 1203-1205.

Behar, M., N. Hao, et al. (2008). "Dose-to-duration encoding and signaling beyond saturation in intracellular signaling networks." PLoS Comput Biol **4**(10): e1000197.

Belaiba, R. S., S. Bonello, et al. (2007). "Hypoxia up-regulates hypoxia-inducible factor-1alpha transcription by involving phosphatidylinositol 3-kinase and nuclear factor kappaB in pulmonary artery smooth muscle cells." Mol Biol Cell **18**(12): 4691-4697.

Belaidi, E., M. Joyeux-Faure, et al. (2009). "Major role for hypoxia inducible factor-1 and the endothelin system in promoting myocardial infarction and hypertension in an animal model of obstructive sleep apnea." J Am Coll Cardiol **53**(15): 1309-1317.

Bellot, G., R. Garcia-Medina, et al. (2009). "Hypoxia-induced autophagy is mediated through hypoxia-inducible factor induction of BNIP3 and BNIP3L via their BH3 domains." Mol Cell Biol **29**(10): 2570-2581.

Ben-Dor, A., M. Steiner, et al. (2005). "Carotenoids activate the antioxidant response element transcription system." Mol Cancer Ther **4**(1): 177-186.

Berchner-Pfannschmidt, U., C. Wotzlaw, et al. (2004). "Visualization of the three-dimensional organization of hypoxia-inducible factor-1 alpha and interacting cofactors in subnuclear structures." Biol Chem **385**(3-4): 231-237.

Bernardi, R., I. Guernah, et al. (2006). "PML inhibits HIF-1alpha translation and neoangiogenesis through repression of mTOR." Nature **442**(7104): 779-785.

Berner, R. A., J. M. Vandenbrooks, et al. (2007). "Evolution. Oxygen and evolution." Science **316**(5824): 557-558.

Berra, E., E. Benizri, et al. (2003). "HIF prolyl-hydroxylase 2 is the key oxygen sensor setting low steady-state levels of HIF-1alpha in normoxia." Embo J **22**(16): 4082-4090.

Berra, E., D. Roux, et al. (2001). "Hypoxia-inducible factor-1 alpha (HIF-1 alpha) escapes O(2)-driven proteasomal degradation irrespective of its subcellular localization: nucleus or cytoplasm." EMBO Rep **2**(7): 615-620.

Beynon, R. J., M. K. Doherty, et al. (2005). "Multiplexed absolute quantification in proteomics using artificial QCAT proteins of concatenated signature peptides." Nat Methods **2**(8): 587-589.

Bhalla, U. S. and R. Iyengar (1999). "Emergent properties of networks of biological signaling pathways." Science **283**(5400): 381-387.

Biddie, S. C. and G. L. Hager (2009). "Glucocorticoid receptor dynamics and gene regulation." Stress **12**(3): 193-205.

Birol, G., S. Wang, et al. (2007). "Oxygen distribution and consumption in the macaque retina." Am J Physiol Heart Circ Physiol **293**(3): H1696-1704.

Boellmann, F., L. Zhang, et al. (2010). "Genome-wide analysis of DNA methylation and gene expression changes in the mouse lung following subchronic arsenate exposure." Toxicol Sci **117**(2): 404-417.

Bowie, A. and L. A. O'Neill (2000). "Oxidative stress and nuclear factor-kappaB activation: a reassessment of the evidence in the light of recent discoveries." Biochem Pharmacol **59**(1): 13-23.

Bracken, C. P., A. O. Fedele, et al. (2006). "Cell-specific regulation of hypoxia-inducible factor (HIF)-1alpha and HIF-2alpha stabilization and transactivation in a graded oxygen environment." J Biol Chem **281**(32): 22575-22585.

Brahimi-Horn, C., N. Mazure, et al. (2005). "Signalling via the hypoxia-inducible factor-1alpha requires multiple posttranslational modifications." Cell Signal **17**(1): 1-9.

Brasch, K. and R. L. Ochs (1992). "Nuclear bodies (NBs): a newly "rediscovered" organelle." Exp Cell Res **202**(2): 211-223.
Brigati, C., B. Banelli, et al. (2010). "Inflammation, HIF-1, and the epigenetics that follows." Mediators Inflamm **2010**: 263914.
Brockmeier, U., C. Platzek, et al. (2011). "The function of hypoxia-inducible factor (HIF) is independent of the endoplasmic reticulum protein OS-9." PLoS One **6**(4): e19151.
Broughton, B. R., D. C. Reutens, et al. (2009). "Apoptotic mechanisms after cerebral ischemia." Stroke **40**(5): e331-339.
Bruning, U., L. Cerone, et al. (2011). "MicroRNA-155 Promotes Resolution of Hypoxia-Inducible Factor-1 {alpha} Activity During Prolonged Hypoxia." Mol Cell Biol.
Buonocore, G., S. Perrone, et al. (2010). "Oxygen toxicity: chemistry and biology of reactive oxygen species." Semin Fetal Neonatal Med **15**(4): 186-190.
Burrill, D. R. and P. A. Silver (2011). "Synthetic circuit identifies subpopulations with sustained memory of DNA damage." Genes Dev **25**(5): 434-439.
Cai, H., D. Liu, et al. (2008). "CaM Kinase II-dependent pathophysiological signalling in endothelial cells." Cardiovasc Res **77**(1): 30-34.
Cai, L., N. Friedman, et al. (2006). "Stochastic protein expression in individual cells at the single molecule level." Nature **440**(7082): 358-362.
Cai, Q. and E. S. Robertson (2010). "Ubiquitin/SUMO modification regulates VHL protein stability and nucleocytoplasmic localization." PLoS One **5**(9).
Cai, Q., S. C. Verma, et al. (2010). "Hypoxia inactivates the VHL tumor suppressor through PIASy-mediated SUMO modification." PLoS One **5**(3): e9720.
Callus, B. A., D. M. Moujallad, et al. (2008). "Triggering of apoptosis by Puma is determined by the threshold set by prosurvival Bcl-2 family proteins." J Mol Biol **384**(2): 313-323.
Calzado, M. A., L. de la Vega, et al. (2009). "An inducible autoregulatory loop between HIPK2 and Siah2 at the apex of the hypoxic response." Nat Cell Biol **11**(1): 85-91.
Carbia-Nagashima, A., J. Gerez, et al. (2007). "RSUME, a small RWD-containing protein, enhances SUMO conjugation and stabilizes HIF-1alpha during hypoxia." Cell **131**(2): 309-323.
Cardinale, S., B. Cisterna, et al. (2007). "Subnuclear localization and dynamics of the Pre-mRNA 3' end processing factor mammalian cleavage factor I 68-kDa subunit." Mol Biol Cell **18**(4): 1282-1292.
Carmeliet, P., Y. Dor, et al. (1998). "Role of HIF-1alpha in hypoxia-mediated apoptosis, cell proliferation and tumour angiogenesis." Nature **394**(6692): 485-490.
Carreau, A., B. El Hafny-Rahbi, et al. (2011). "Why is the partial oxygen pressure of human tissues a crucial parameter?: Small molecules and hypoxia." J Cell Mol Med.
Cassavaugh, J. and K. M. Lounsbury (2011). "Hypoxia-mediated biological control." J Cell Biochem **112**(3): 735-744.
Cha, S. T., P. S. Chen, et al. (2010). "MicroRNA-519c suppresses hypoxia-inducible factor-1alpha expression and tumor angiogenesis." Cancer Res **70**(7): 2675-2685.
Chachami, G., E. Paraskeva, et al. (2009). "Transport of hypoxia-inducible factor HIF-1alpha into the nucleus involves importins 4 and 7." Biochem Biophys Res Commun **390**(2): 235-240.
Chan, D. A., P. D. Sutphin, et al. (2005). "Coordinate regulation of the oxygen-dependent degradation domains of hypoxia-inducible factor 1 alpha." Mol Cell Biol **25**(15): 6415-6426.
Chang, L., W. J. Godinez, et al. (2011). "Herpesviral replication compartments move and coalesce at nuclear speckles to enhance export of viral late mRNA." Proc Natl Acad Sci U S A **108**(21): E136-144.
Chen, W. W., M. Niepel, et al. (2010). "Classic and contemporary approaches to modeling biochemical reactions." Genes Dev **24**(17): 1861-1875.

Chilov, D., G. Camenisch, et al. (1999). "Induction and nuclear translocation of hypoxia-inducible factor-1 (HIF-1): heterodimerization with ARNT is not necessary for nuclear accumulation of HIF-1alpha." J Cell Sci **112 (Pt 8)**: 1203-1212.

Chimploy, K., M. L. Tassotto, et al. (2000). "Ribonucleotide reductase, a possible agent in deoxyribonucleotide pool asymmetries induced by hypoxia." J Biol Chem **275**(50): 39267-39271.

Choi, C. Y., D. A. Chan, et al. (2008). "Molecular imaging of hypoxia-inducible factor 1 alpha and von Hippel-Lindau interaction in mice." Mol Imaging **7**(3): 139-146.

Chrast, R., H. S. Scott, et al. (1997). "Cloning of two human homologs of the Drosophila single-minded gene SIM1 on chromosome 6q and SIM2 on 21q within the Down syndrome chromosomal region." Genome Res **7**(6): 615-624.

Chudakov, D. M., M. V. Matz, et al. (2010). "Fluorescent proteins and their applications in imaging living cells and tissues." Physiol Rev **90**(3): 1103-1163.

Clifford, S. C., D. Astuti, et al. (2001). "The pVHL-associated SCF ubiquitin ligase complex: molecular genetic analysis of elongin B and C, Rbx1 and HIF-1alpha in renal cell carcinoma." Oncogene **20**(36): 5067-5074.

Cockman, M. E., J. D. Webb, et al. (2009). "Proteomics-based identification of novel factor inhibiting hypoxia-inducible factor (FIH) substrates indicates widespread asparaginyl hydroxylation of ankyrin repeat domain-containing proteins." Mol Cell Proteomics **8**(3): 535-546.

Cockman, M. E., J. D. Webb, et al. (2009). "FIH-dependent asparaginyl hydroxylation of ankyrin repeat domain-containing proteins." Ann N Y Acad Sci **1177**: 9-18.

Cohen, A. A., T. Kalisky, et al. (2009). "Protein dynamics in individual human cells: experiment and theory." PLoS One **4**(4): e4901.

Comerford, K. M., T. J. Wallace, et al. (2002). "Hypoxia-inducible factor-1-dependent regulation of the multidrug resistance (MDR1) gene." Cancer Res **62**(12): 3387-3394.

Cory, A. H., T. C. Owen, et al. (1991). "Use of an aqueous soluble tetrazolium/formazan assay for cell growth assays in culture." Cancer Commun **3**(7): 207-212.

Covello, K. L., J. Kehler, et al. (2006). "HIF-2alpha regulates Oct-4: effects of hypoxia on stem cell function, embryonic development, and tumor growth." Genes Dev **20**(5): 557-570.

Cowden, K. D. and M. C. Simon (2002). "The bHLH/PAS factor MOP3 does not participate in hypoxia responses." Biochem Biophys Res Commun **290**(4): 1228-1236.

Culver, C., A. Sundqvist, et al. (2010). "Mechanism of hypoxia-induced NF-kappaB." Mol Cell Biol **30**(20): 4901-4921.

Cummins, E. P., E. Berra, et al. (2006). "Prolyl hydroxylase-1 negatively regulates IkappaB kinase-beta, giving insight into hypoxia-induced NFkappaB activity." Proc Natl Acad Sci U S A **103**(48): 18154-18159.

D'Angelo, G., E. Duplan, et al. (2003). "Cyclosporin A prevents the hypoxic adaptation by activating hypoxia-inducible factor-1alpha Pro-564 hydroxylation." J Biol Chem **278**(17): 15406-15411.

Daniels, M. J., A. Marson, et al. (2004). "PML bodies control the nuclear dynamics and function of the CHFR mitotic checkpoint protein." Nat Struct Mol Biol **11**(11): 1114-1121.

Dayan, F., M. Monticelli, et al. (2009). "Gene regulation in response to graded hypoxia: the non-redundant roles of the oxygen sensors PHD and FIH in the HIF pathway." J Theor Biol **259**(2): 304-316.

Dayan, F., D. Roux, et al. (2006). "The oxygen sensor factor-inhibiting hypoxia-inducible factor-1 controls expression of distinct genes through the bifunctional transcriptional character of hypoxia-inducible factor-1alpha." Cancer Res **66**(7): 3688-3698.

de Noronha, C. M., M. P. Sherman, et al. (2001). "Dynamic disruptions in nuclear envelope architecture and integrity induced by HIV-1 Vpr." Science **294**(5544): 1105-1108.

Dechat, T., S. A. Adam, et al. (2010). "Nuclear lamins." Cold Spring Harb Perspect Biol **2**(11): a000547.

Depping, R., A. Steinhoff, et al. (2008). "Nuclear translocation of hypoxia-inducible factors (HIFs): involvement of the classical importin alpha/beta pathway." Biochim Biophys Acta **1783**(3): 394-404.
Dequeant, M. L., E. Glynn, et al. (2006). "A complex oscillating network of signaling genes underlies the mouse segmentation clock." Science **314**(5805): 1595-1598.
Dery, M. A., M. D. Michaud, et al. (2005). "Hypoxia-inducible factor 1: regulation by hypoxic and non-hypoxic activators." Int J Biochem Cell Biol **37**(3): 535-540.
DiGregorio, P. J., J. A. Ubersax, et al. (2001). "Hypoxia and nitric oxide induce a rapid, reversible cell cycle arrest of the Drosophila syncytial divisions." J Biol Chem **276**(3): 1930-1937.
Ding, H., Q. Liu, et al. (2011). "Polymorphisms of hypoxia-related genes in subjects susceptible to acute mountain sickness." Respiration **81**(3): 236-241.
Dioum, E. M., R. Chen, et al. (2009). "Regulation of hypoxia-inducible factor 2alpha signaling by the stress-responsive deacetylase sirtuin 1." Science **324**(5932): 1289-1293.
Dixit, R. and R. Cyr (2003). "Cell damage and reactive oxygen species production induced by fluorescence microscopy: effect on mitosis and guidelines for non-invasive fluorescence microscopy." Plant J **36**(2): 280-290.
Doherty, M. K., D. E. Hammond, et al. (2009). "Turnover of the human proteome: determination of protein intracellular stability by dynamic SILAC." J Proteome Res **8**(1): 104-112.
Dolmetsch, R. E., K. Xu, et al. (1998). "Calcium oscillations increase the efficiency and specificity of gene expression." Nature **392**(6679): 933-936.
Doran, D. M., K. Kulkarni-Datar, et al. (2010). "Hypoxia activates constitutive luciferase reporter constructs." Biochimie **93**(2): 361-368.
Dupont, G., L. Combettes, et al. (2011). "Calcium oscillations." Cold Spring Harb Perspect Biol **3**(3).
Eliasson, P. and J. I. Jonsson (2010). "The hematopoietic stem cell niche: low in oxygen but a nice place to be." J Cell Physiol **222**(1): 17-22.
Eltzschig, H. K., P. Abdulla, et al. (2005). "HIF-1-dependent repression of equilibrative nucleoside transporter (ENT) in hypoxia." J Exp Med **202**(11): 1493-1505.
Elvidge, G. P., L. Glenny, et al. (2006). "Concordant regulation of gene expression by hypoxia and 2-oxoglutarate-dependent dioxygenase inhibition: the role of HIF-1alpha, HIF-2alpha, and other pathways." J Biol Chem **281**(22): 15215-15226.
Ema, M., S. Taya, et al. (1997). "A novel bHLH-PAS factor with close sequence similarity to hypoxia-inducible factor 1alpha regulates the VEGF expression and is potentially involved in lung and vascular development." Proc Natl Acad Sci U S A **94**(9): 4273-4278.
Epstein, A. C., J. M. Gleadle, et al. (2001). "C. elegans EGL-9 and mammalian homologs define a family of dioxygenases that regulate HIF by prolyl hydroxylation." Cell **107**(1): 43-54.
Erez, N., P. Stambolsky, et al. (2004). "Hypoxia-dependent regulation of PHD1: cloning and characterization of the human PHD1/EGLN2 gene promoter." FEBS Lett **567**(2-3): 311-315.
Espenshade, P. J. and A. L. Hughes (2007). "Regulation of sterol synthesis in eukaryotes." Annu Rev Genet **41**: 401-427.
Esser, C. (2009). "The immune phenotype of AhR null mouse mutants: not a simple mirror of xenobiotic receptor over-activation." Biochem Pharmacol **77**(4): 597-607.
Eungdamrong, N. J. and R. Iyengar (2004). "Computational approaches for modeling regulatory cellular networks." Trends Cell Biol **14**(12): 661-669.
Eungdamrong, N. J. and R. Iyengar (2004). "Modeling cell signaling networks." Biol Cell **96**(5): 355-362.
Evans, R. G., B. S. Gardiner, et al. (2008). "Intrarenal oxygenation: unique challenges and the biophysical basis of homeostasis." Am J Physiol Renal Physiol **295**(5): F1259-1270.
Falkowski, P. G. (2006). "Evolution. Tracing oxygen's imprint on earth's metabolic evolution." Science **311**(5768): 1724-1725.

Fandrey, J., T. A. Gorr, et al. (2006). "Regulating cellular oxygen sensing by hydroxylation." Cardiovasc Res **71**(4): 642-651.
Farnham, P. J. (2009). "Insights from genomic profiling of transcription factors." Nat Rev Genet **10**(9): 605-616.
Fogal, V., M. Gostissa, et al. (2000). "Regulation of p53 activity in nuclear bodies by a specific PML isoform." Embo J **19**(22): 6185-6195.
Fong, G. H. and K. Takeda (2008). "Role and regulation of prolyl hydroxylase domain proteins." Cell Death Differ **15**(4): 635-641.
Forsythe, J. A., B. H. Jiang, et al. (1996). "Activation of vascular endothelial growth factor gene transcription by hypoxia-inducible factor 1." Mol Cell Biol **16**(9): 4604-4613.
Fox, A. H., Y. W. Lam, et al. (2002). "Paraspeckles: a novel nuclear domain." Curr Biol **12**(1): 13-25.
Fox, A. H. and A. I. Lamond (2010). "Paraspeckles." Cold Spring Harb Perspect Biol **2**(7): a000687.
Fraley, S. I., Y. Feng, et al. (2010). "A distinctive role for focal adhesion proteins in three-dimensional cell motility." Nat Cell Biol **12**(6): 598-604.
Fu, L., Y. S. Gao, et al. (2005). "Nuclear aggresomes form by fusion of PML-associated aggregates." Mol Biol Cell **16**(10): 4905-4917.
Gainer, J. L. (1987). "Hypoxia and atherosclerosis: re-evaluation of an old hypothesis." Atherosclerosis **68**(3): 263-266.
Galban, S., Y. Kuwano, et al. (2008). "RNA-binding proteins HuR and PTB promote the translation of hypoxia-inducible factor 1alpha." Mol Cell Biol **28**(1): 93-107.
Gale, D. P. and P. H. Maxwell (2010). "The role of HIF in immunity." Int J Biochem Cell Biol **42**(4): 486-494.
Galea, A. M. and A. J. Brown (2009). "Special relationship between sterols and oxygen: were sterols an adaptation to aerobic life?" Free Radic Biol Med **47**(6): 880-889.
Gardner, L. B., Q. Li, et al. (2001). "Hypoxia inhibits G1/S transition through regulation of p27 expression." J Biol Chem **276**(11): 7919-7926.
Geoffroy, M. C. and M. K. Chelbi-Alix (2011). "Role of promyelocytic leukemia protein in host antiviral defense." J Interferon Cytokine Res **31**(1): 145-158.
Gerald, D., E. Berra, et al. (2004). "JunD reduces tumor angiogenesis by protecting cells from oxidative stress." Cell **118**(6): 781-794.
Geva-Zatorsky, N., N. Rosenfeld, et al. (2006). "Oscillations and variability in the p53 system." Mol Syst Biol **2**: 2006 0033.
Gey GO, C. W., Kubicek MT (1952). "Tissue culture studies of the proliferative capacity of cervical carcinoma and normal epithelium." Cancer Res **12**: 264-265.
Ghorbel, M. T., J. M. Coulson, et al. (2003). "Cross-talk between hypoxic and circadian pathways: cooperative roles for hypoxia-inducible factor 1alpha and CLOCK in transcriptional activation of the vasopressin gene." Mol Cell Neurosci **22**(3): 396-404.
Giaccia, A. J., M. C. Simon, et al. (2004). "The biology of hypoxia: the role of oxygen sensing in development, normal function, and disease." Genes Dev **18**(18): 2183-2194.
Ginouves, A., K. Ilc, et al. (2008). "PHDs overactivation during chronic hypoxia "desensitizes" HIFalpha and protects cells from necrosis." Proc Natl Acad Sci U S A **105**(12): 4745-4750.
Goel, G., I. C. Chou, et al. (2006). "Biological systems modeling and analysis: a biomolecular technique of the twenty-first century." J Biomol Tech **17**(4): 252-269.
Gordan, J. D., J. A. Bertout, et al. (2007). "HIF-2alpha promotes hypoxic cell proliferation by enhancing c-myc transcriptional activity." Cancer Cell **11**(4): 335-347.
Gorres, K. L. and R. T. Raines (2010). "Prolyl 4-hydroxylase." Crit Rev Biochem Mol Biol **45**(2): 106-124.
Gradin, K., J. McGuire, et al. (1996). "Functional interference between hypoxia and dioxin signal transduction pathways: competition for recruitment of the Arnt transcription factor." Mol Cell Biol **16**(10): 5221-5231.

Graef, I. A., F. Chen, et al. (2001). "NFAT signaling in vertebrate development." Curr Opin Genet Dev **11**(5): 505-512.
Grosfeld, A., I. P. Stolze, et al. (2007). "Interaction of hydroxylated collagen IV with the von hippel-lindau tumor suppressor." J Biol Chem **282**(18): 13264-13269.
Gross, L. A., G. S. Baird, et al. (2000). "The structure of the chromophore within DsRed, a red fluorescent protein from coral." Proc Natl Acad Sci U S A **97**(22): 11990-11995.
Groulx, I. and S. Lee (2002). "Oxygen-dependent ubiquitination and degradation of hypoxia-inducible factor requires nuclear-cytoplasmic trafficking of the von Hippel-Lindau tumor suppressor protein." Mol Cell Biol **22**(15): 5319-5336.
Gustafsson, M. V., X. Zheng, et al. (2005). "Hypoxia requires notch signaling to maintain the undifferentiated cell state." Dev Cell **9**(5): 617-628.
Guzy, R. D., B. Hoyos, et al. (2005). "Mitochondrial complex III is required for hypoxia-induced ROS production and cellular oxygen sensing." Cell Metab **1**(6): 401-408.
Hackenbeck, T., K. X. Knaup, et al. (2009). "HIF-1 or HIF-2 induction is sufficient to achieve cell cycle arrest in NIH3T3 mouse fibroblasts independent from hypoxia." Cell Cycle **8**(9): 1386-1395.
Hahn, J. S. (2009). "The Hsp90 chaperone machinery: from structure to drug development." BMB Rep **42**(10): 623-630.
Hamanaka, R. B. and N. S. Chandel (2009). "Mitochondrial reactive oxygen species regulate hypoxic signaling." Curr Opin Cell Biol **21**(6): 894-899.
Handwerger, K. E., C. Murphy, et al. (2003). "Steady-state dynamics of Cajal body components in the Xenopus germinal vesicle." J Cell Biol **160**(4): 495-504.
Hara, K. Y. (2009). "Permeable cell assay: a method for high-throughput measurement of cellular ATP synthetic activity." Methods Mol Biol **577**: 251-258.
Hara, S., C. Kobayashi, et al. (1999). "Nuclear localization of hypoxia-inducible factor-2alpha in bovine arterial endothelial cells." Mol Cell Biol Res Commun **2**(2): 119-123.
Harada, H., S. Itasaka, et al. (2009). "The Akt/mTOR pathway assures the synthesis of HIF-1alpha protein in a glucose- and reoxygenation-dependent manner in irradiated tumors." J Biol Chem **284**(8): 5332-5342.
Haraguchi, T. (2002). "Live cell imaging: approaches for studying protein dynamics in living cells." Cell Struct Funct **27**(5): 333-334.
Harper, C. V., B. Finkenstadt, et al. (2011). "Dynamic analysis of stochastic transcription cycles." PLoS Biol **9**(4): e1000607.
Harpur, A. G., F. S. Wouters, et al. (2001). "Imaging FRET between spectrally similar GFP molecules in single cells." Nat Biotechnol **19**(2): 167-169.
Hawes, J. J. and K. M. Reilly (2010). "Bioluminescent approaches for measuring tumor growth in a mouse model of neurofibromatosis." Toxicol Pathol **38**(1): 123-130.
Heiner, M. and K. Sriram (2010). "Structural analysis to determine the core of hypoxia response network." PLoS One **5**(1): e8600.
Hellen, C. U. and P. Sarnow (2001). "Internal ribosome entry sites in eukaryotic mRNA molecules." Genes Dev **15**(13): 1593-1612.
Helton, R., J. Cui, et al. (2005). "Brain-specific knock-out of hypoxia-inducible factor-1alpha reduces rather than increases hypoxic-ischemic damage." J Neurosci **25**(16): 4099-4107.
Hendriksen, I. J. and T. Meeuwsen (2003). "The effect of intermittent training in hypobaric hypoxia on sea-level exercise: a cross-over study in humans." Eur J Appl Physiol **88**(4-5): 396-403.
Henry, J. R. and J. F. Harrison (2004). "Plastic and evolved responses of larval tracheae and mass to varying atmospheric oxygen content in Drosophila melanogaster." J Exp Biol **207**(Pt 20): 3559-3567.
Henze, A. T., J. Riedel, et al. (2010). "Prolyl hydroxylases 2 and 3 act in gliomas as protective negative feedback regulators of hypoxia-inducible factors." Cancer Res **70**(1): 357-366.
Hester, R. L., R. Iliescu, et al. (2011). "Systems biology and integrative physiological modelling." J Physiol **589**(Pt 5): 1053-1060.

Hetz, S. K. and T. J. Bradley (2005). "Insects breathe discontinuously to avoid oxygen toxicity." Nature **433**(7025): 516-519.
Hilderbrand, S. A. (2010). "Labels and probes for live cell imaging: overview and selection guide." Methods Mol Biol **591**: 17-45.
Hindryckx, P., M. De Vos, et al. (2010). "Hydroxylase inhibition abrogates TNF-alpha-induced intestinal epithelial damage by hypoxia-inducible factor-1-dependent repression of FADD." J Immunol **185**(10): 6306-6316.
Hirose, K., M. Morita, et al. (1996). "cDNA cloning and tissue-specific expression of a novel basic helix-loop-helix/PAS factor (Arnt2) with close sequence similarity to the aryl hydrocarbon receptor nuclear translocator (Arnt)." Mol Cell Biol **16**(4): 1706-1713.
Hirsila, M., P. Koivunen, et al. (2003). "Characterization of the human prolyl 4-hydroxylases that modify the hypoxia-inducible factor." J Biol Chem **278**(33): 30772-30780.
Hofer, T., I. Desbaillets, et al. (2002). "Characterization of HIF-1 alpha overexpressing HeLa cells and implications for gene therapy." Comp Biochem Physiol C Toxicol Pharmacol **133**(4): 475-481.
Hoffman, R. (2002). "Green fluorescent protein imaging of tumour growth, metastasis, and angiogenesis in mouse models." Lancet Oncol **3**(9): 546-556.
Hoffman, R. M. (2004). "Imaging tumor angiogenesis with fluorescent proteins." Apmis **112**(7-8): 441-449.
Hoffman, R. M. (2005). "The multiple uses of fluorescent proteins to visualize cancer in vivo." Nat Rev Cancer **5**(10): 796-806.
Holmquist-Mengelbier, L., E. Fredlund, et al. (2006). "Recruitment of HIF-1alpha and HIF-2alpha to common target genes is differentially regulated in neuroblastoma: HIF-2alpha promotes an aggressive phenotype." Cancer Cell **10**(5): 413-423.
Horak, P., A. R. Crawford, et al. (2010). "Negative feedback control of HIF-1 through REDD1-regulated ROS suppresses tumorigenesis." Proc Natl Acad Sci U S A **107**(10): 4675-4680.
House, C. M., A. Moller, et al. (2009). "Siah proteins: novel drug targets in the Ras and hypoxia pathways." Cancer Res **69**(23): 8835-8838.
Hoyt, C. C., R. J. Bouchard, et al. (2004). "Novel nuclear herniations induced by nuclear localization of a viral protein." J Virol **78**(12): 6360-6369.
Huang, C., Y. Han, et al. (2009). "SENP3 is responsible for HIF-1 transactivation under mild oxidative stress via p300 de-SUMOylation." Embo J **28**(18): 2748-2762.
Huang, X., Q. T. Le, et al. (2010). "MiR-210--micromanager of the hypoxia pathway." Trends Mol Med **16**(5): 230-237.
Hubbi, M. E., W. Luo, et al. (2011). "MCM proteins are negative regulators of hypoxia-inducible factor 1." Mol Cell **42**(5): 700-712.
Hughey, J. J., T. K. Lee, et al. (2010). "Computational modeling of mammalian signaling networks." Wiley Interdiscip Rev Syst Biol Med **2**(2): 194-209.
Hyland, P. L., A. L. Keegan, et al. (2000). "Effect of a dCTP:dTTP pool imbalance on DNA replication fidelity in Friend murine erythroleukemia cells." Environ Mol Mutagen **36**(2): 87-96.
Ihekwaba, A. E., D. S. Broomhead, et al. (2004). "Sensitivity analysis of parameters controlling oscillatory signalling in the NF-kappaB pathway: the roles of IKK and IkappaBalpha." Syst Biol (Stevenage) **1**(1): 93-103.
Ilangovan, G., A. Bratasz, et al. (2005). "Non-invasive measurement of tumor oxygenation using embedded microparticulate EPR spin probe." Adv Exp Med Biol **566**: 67-73.
Imamura, H., K. P. Nhat, et al. (2009). "Visualization of ATP levels inside single living cells with fluorescence resonance energy transfer-based genetically encoded indicators." Proc Natl Acad Sci U S A **106**(37): 15651-15656.
Imamura, T., H. Kikuchi, et al. (2009). "HIF-1alpha and HIF-2alpha have divergent roles in colon cancer." Int J Cancer **124**(4): 763-771.

Imbert, V., R. A. Rupec, et al. (1996). "Tyrosine phosphorylation of I kappa B-alpha activates NF-kappa B without proteolytic degradation of I kappa B-alpha." Cell **86**(5): 787-798.
Irelan, J. T., M. J. Wu, et al. (2011). "Rapid and quantitative assessment of cell quality, identity, and functionality for cell-based assays using real-time cellular analysis." J Biomol Screen **16**(3): 313-322.
Irisarri, M., S. Lavista-Llanos, et al. (2009). "Central role of the oxygen-dependent degradation domain of Drosophila HIFalpha/Sima in oxygen-dependent nuclear export." Mol Biol Cell **20**(17): 3878-3887.
Ivanov, P. A., E. M. Chudinova, et al. (2003). "Disruption of microtubules inhibits cytoplasmic ribonucleoprotein stress granule formation." Exp Cell Res **290**(2): 227-233.
Iyer, N. V., S. W. Leung, et al. (1998). "The human hypoxia-inducible factor 1alpha gene: HIF1A structure and evolutionary conservation." Genomics **52**(2): 159-165.
Jackson, D. A. (2005). "The amazing complexity of transcription factories." Brief Funct Genomic Proteomic **4**(2): 143-157.
Jacobsen, P. F., D. J. Jenkyn, et al. (1985). "Establishment of a human medulloblastoma cell line and its heterotransplantation into nude mice." J Neuropathol Exp Neurol **44**(5): 472-485.
Janssens, S. and J. Tschopp (2006). "Signals from within: the DNA-damage-induced NF-kappaB response." Cell Death Differ **13**(5): 773-784.
Jaqaman, K., E. M. King, et al. (2010). "Kinetochore alignment within the metaphase plate is regulated by centromere stiffness and microtubule depolymerases." J Cell Biol **188**(5): 665-679.
Jiang, B. H., G. L. Semenza, et al. (1996). "Hypoxia-inducible factor 1 levels vary exponentially over a physiologically relevant range of O2 tension." Am J Physiol **271**(4 Pt 1): C1172-1180.
Johnson, A. B. and M. C. Barton (2007). "Hypoxia-induced and stress-specific changes in chromatin structure and function." Mutat Res **618**(1-2): 149-162.
Jokilehto, T., H. Hogel, et al. (2010). "Retention of prolyl hydroxylase PHD2 in the cytoplasm prevents PHD2-induced anchorage-independent carcinoma cell growth." Exp Cell Res **316**(7): 1169-1178.
Jokilehto, T. and P. M. Jaakkola (2010). "The role of HIF prolyl hydroxylases in tumour growth." J Cell Mol Med **14**(4): 758-770.
Joseph, V. and J. M. Pequignot (2009). "Breathing at high altitude." Cell Mol Life Sci **66**(22): 3565-3573.
Jost, S. C., L. Collins, et al. (2009). "Measuring brain tumor growth: combined bioluminescence imaging-magnetic resonance imaging strategy." Mol Imaging **8**(5): 245-253.
Kallio, P. J., K. Okamoto, et al. (1998). "Signal transduction in hypoxic cells: inducible nuclear translocation and recruitment of the CBP/p300 coactivator by the hypoxia-inducible factor-1alpha." Embo J **17**(22): 6573-6586.
Kang, X., J. Li, et al. (2010). "PIASy stimulates HIF1alpha SUMOylation and negatively regulates HIF1alpha activity in response to hypoxia." Oncogene **29**(41): 5568-5578.
Katschinski, D. M. (2006). "Is there a molecular connection between hypoxia and aging?" Exp Gerontol **41**(5): 482-484.
Kaur, B., F. W. Khwaja, et al. (2005). "Hypoxia and the hypoxia-inducible-factor pathway in glioma growth and angiogenesis." Neuro Oncol 7(2): 134-153.
Kay, R. A., I. R. Ellis, et al. (2005). "The expression of migration stimulating factor, a potent oncofetal cytokine, is uniquely controlled by 3'-untranslated region-dependent nuclear sequestration of its precursor messenger RNA." Cancer Res **65**(23): 10742-10749.
Kenneth, N. S. and S. Rocha (2008). "Regulation of gene expression by hypoxia." Biochem J **414**(1): 19-29.
Kholodenko, B. N. (2006). "Cell-signalling dynamics in time and space." Nat Rev Mol Cell Biol 7(3): 165-176.

Khurana, A., K. Nakayama, et al. (2006). "Regulation of the ring finger E3 ligase Siah2 by p38 MAPK." J Biol Chem **281**(46): 35316-35326.
Kim, P. M. and B. Tidor (2003). "Limitations of quantitative gene regulation models: a case study." Genome Res **13**(11): 2391-2395.
King, A., M. A. Selak, et al. (2006). "Succinate dehydrogenase and fumarate hydratase: linking mitochondrial dysfunction and cancer." Oncogene **25**(34): 4675-4682.
Kinoshita, K., Y. Kikuchi, et al. (2004). "Altered DNA binding specificity of Arnt by selection of partner bHLH-PAS proteins." Nucleic Acids Res **32**(10): 3169-3179.
Knaup, K. X., K. Jozefowski, et al. (2009). "Mutual regulation of hypoxia-inducible factor and mammalian target of rapamycin as a function of oxygen availability." Mol Cancer Res **7**(1): 88-98.
Kohn, K. W., J. Riss, et al. (2004). "Properties of switch-like bioregulatory networks studied by simulation of the hypoxia response control system." Mol Biol Cell **15**(7): 3042-3052.
Koivunen, P., M. Hirsila, et al. (2007). "Inhibition of hypoxia-inducible factor (HIF) hydroxylases by citric acid cycle intermediates: possible links between cell metabolism and stabilization of HIF." J Biol Chem **282**(7): 4524-4532.
Kong, M., E. A. Barnes, et al. (2000). "Cyclin F regulates the nuclear localization of cyclin B1 through a cyclin-cyclin interaction." Embo J **19**(6): 1378-1388.
Konietzny, R., A. Konig, et al. (2009). "Molecular imaging: into in vivo interaction of HIF-1alpha and HIF-2alpha with ARNT." Ann N Y Acad Sci **1177**: 74-81.
Kopito, R. R. (2000). "Aggresomes, inclusion bodies and protein aggregation." Trends Cell Biol **10**(12): 524-530.
Koumenis, C., C. Naczki, et al. (2002). "Regulation of protein synthesis by hypoxia via activation of the endoplasmic reticulum kinase PERK and phosphorylation of the translation initiation factor eIF2alpha." Mol Cell Biol **22**(21): 7405-7416.
Krijnen, P. A., R. Nijmeijer, et al. (2002). "Apoptosis in myocardial ischaemia and infarction." J Clin Pathol **55**(11): 801-811.
Krishnan, J., P. Ahuja, et al. (2008). "Essential role of developmentally activated hypoxia-inducible factor 1alpha for cardiac morphogenesis and function." Circ Res **103**(10): 1139-1146.
Krohn, K. A., J. M. Link, et al. (2008). "Molecular imaging of hypoxia." J Nucl Med **49 Suppl 2**: 129S-148S.
Kuchimaru, T., T. Kadonosono, et al. (2010). "In vivo imaging of HIF-active tumors by an oxygen-dependent degradation protein probe with an interchangeable labeling system." PLoS One **5**(12): e15736.
Kulshreshtha, R., R. V. Davuluri, et al. (2008). "A microRNA component of the hypoxic response." Cell Death Differ **15**(4): 667-671.
Kulshreshtha, R., M. Ferracin, et al. (2007). "A microRNA signature of hypoxia." Mol Cell Biol **27**(5): 1859-1867.
Lafarga, M., M. T. Berciano, et al. (2002). "Clastosome: a subtype of nuclear body enriched in 19S and 20S proteasomes, ubiquitin, and protein substrates of proteasome." Mol Biol Cell **13**(8): 2771-2782.
Lahav, G., N. Rosenfeld, et al. (2004). "Dynamics of the p53-Mdm2 feedback loop in individual cells." Nat Genet **36**(2): 147-150.
Lai, N., H. Zhou, et al. (2009). "Modeling oxygenation in venous blood and skeletal muscle in response to exercise using near-infrared spectroscopy." J Appl Physiol **106**(6): 1858-1874.
Lamond, A. I. and D. L. Spector (2003). "Nuclear speckles: a model for nuclear organelles." Nat Rev Mol Cell Biol **4**(8): 605-612.
Lando, D., D. J. Peet, et al. (2002). "Asparagine hydroxylation of the HIF transactivation domain a hypoxic switch." Science **295**(5556): 858-861.
Lang, K. J., A. Kappel, et al. (2002). "Hypoxia-inducible factor-1alpha mRNA contains an internal ribosome entry site that allows efficient translation during normoxia and hypoxia." Mol Biol Cell **13**(5): 1792-1801.

Latonen, L. (2011). "Nucleolar aggresomes as counterparts of cytoplasmic aggresomes in proteotoxic stress. Proteasome inhibitors induce nuclear ribonucleoprotein inclusions that accumulate several key factors of neurodegenerative diseases and cancer." Bioessays **33**(5): 386-395.

Lau, J., J. Henriksnas, et al. (2009). "Oxygenation of islets and its role in transplantation." Curr Opin Organ Transplant **14**(6): 688-693.

Lebedeva, S., M. Jens, et al. (2011). "Transcriptome-wide Analysis of Regulatory Interactions of the RNA-Binding Protein HuR." Mol Cell.

Lee, J. W., S. H. Bae, et al. (2004). "Hypoxia-inducible factor (HIF-1)alpha: its protein stability and biological functions." Exp Mol Med **36**(1): 1-12.

Lee, R. C., R. L. Feinbaum, et al. (1993). "The C. elegans heterochronic gene lin-4 encodes small RNAs with antisense complementarity to lin-14." Cell **75**(5): 843-854.

Lee, S., M. Neumann, et al. (1999). "Transcription-dependent nuclear-cytoplasmic trafficking is required for the function of the von Hippel-Lindau tumor suppressor protein." Mol Cell Biol **19**(2): 1486-1497.

Lee, S. G., H. Lee, et al. (2001). "Transcriptional repression of the human p53 gene by cobalt chloride mimicking hypoxia." FEBS Lett **507**(3): 259-263.

Lei, Z., B. Li, et al. (2009). "Regulation of HIF-1alpha and VEGF by miR-20b tunes tumor cells to adapt to the alteration of oxygen concentration." PLoS One **4**(10): e7629.

Levsky, J. M. and R. H. Singer (2003). "Gene expression and the myth of the average cell." Trends Cell Biol **13**(1): 4-6.

Li, L., Y. Qu, et al. (2007). "Relationship between HIF-1alpha expression and neuronal apoptosis in neonatal rats with hypoxia-ischemia brain injury." Brain Res **1180**: 133-139.

Li, L., K. Roy, et al. (2006). "Dynamic nature of cleavage bodies and their spatial relationship to DDX1 bodies, Cajal bodies, and gems." Mol Biol Cell **17**(3): 1126-1140.

Li, Z., X. Na, et al. (2002). "Ubiquitination of a novel deubiquitinating enzyme requires direct binding to von Hippel-Lindau tumor suppressor protein." J Biol Chem **277**(7): 4656-4662.

Li, Z., D. Wang, et al. (2005). "VHL protein-interacting deubiquitinating enzyme 2 deubiquitinates and stabilizes HIF-1alpha." EMBO Rep **6**(4): 373-378.

Li, Z., D. Wang, et al. (2002). "Identification of a deubiquitinating enzyme subfamily as substrates of the von Hippel-Lindau tumor suppressor." Biochem Biophys Res Commun **294**(3): 700-709.

Limnander, A., P. Depeille, et al. (2011). "STIM1, PKC-delta and RasGRP set a threshold for proapoptotic Erk signaling during B cell development." Nat Immunol **12**(5): 425-433.

Lin, Q., Y. J. Lee, et al. (2006). "Differentiation arrest by hypoxia." J Biol Chem **281**(41): 30678-30683.

Lindholm, P. and C. E. Lundgren (2009). "The physiology and pathophysiology of human breath-hold diving." J Appl Physiol **106**(1): 284-292.

Lindhout, B. I., P. Fransz, et al. (2007). "Live cell imaging of repetitive DNA sequences via GFP-tagged polydactyl zinc finger proteins." Nucleic Acids Res **35**(16): e107.

Lipniacki, T., K. Puszynski, et al. (2007). "Single TNFalpha trimers mediating NF-kappaB activation: stochastic robustness of NF-kappaB signaling." BMC Bioinformatics **8**: 376.

Lisy, K. and D. J. Peet (2008). "Turn me on: regulating HIF transcriptional activity." Cell Death Differ **15**(4): 642-649.

Liu, G. and D. P. Xirodimas (2010). "NUB1 promotes cytoplasmic localization of p53 through cooperation of the NEDD8 and ubiquitin pathways." Oncogene **29**(15): 2252-2261.

Liu, J., R. Qu, et al. (2005). "Real-time imaging of hypoxia-inducible factor-1 activity in tumor xenografts." J Radiat Res (Tokyo) **46**(1): 93-102.

Liu, L., X. Ning, et al. (2008). "Hypoxia-inducible factor-1 alpha contributes to hypoxia-induced chemoresistance in gastric cancer." Cancer Sci **99**(1): 121-128.

Liu, W., H. Xin, et al. (2010). "Hypoxia and cell cycle regulation of the von Hippel-Lindau tumor suppressor." Oncogene **30**(1): 21-31.

Liu, Y., Z. Huo, et al. (2010). "Prolyl hydroxylase 3 interacts with Bcl-2 to regulate doxorubicin-induced apoptosis in H9c2 cells." Biochem Biophys Res Commun **401**(2): 231-237.
Liu, Y. V., J. H. Baek, et al. (2007). "RACK1 competes with HSP90 for binding to HIF-1alpha and is required for O(2)-independent and HSP90 inhibitor-induced degradation of HIF-1alpha." Mol Cell **25**(2): 207-217.
Loboda, A., A. Jozkowicz, et al. (2010). "HIF-1 and HIF-2 transcription factors--similar but not identical." Mol Cells **29**(5): 435-442.
Loboda, A., A. Stachurska, et al. (2009). "HIF-1 induction attenuates Nrf2-dependent IL-8 expression in human endothelial cells." Antioxid Redox Signal **11**(7): 1501-1517.
Locasale, J. W. (2007). "Computational investigations into the origins of short-term biochemical memory in T cell activation." PLoS One **2**(7): e627.
Lomb, D. J., L. A. Desouza, et al. (2009). "Prolyl hydroxylase inhibitors depend on extracellular glucose and hypoxia-inducible factor (HIF)-2alpha to inhibit cell death caused by nerve growth factor (NGF) deprivation: evidence that HIF-2alpha has a role in NGF-promoted survival of sympathetic neurons." Mol Pharmacol **75**(5): 1198-1209.
Loor, G. and P. T. Schumacker (2008). "Role of hypoxia-inducible factor in cell survival during myocardial ischemia-reperfusion." Cell Death Differ **15**(4): 686-690.
Lopez-Barneo, J., P. Ortega-Saenz, et al. (2009). "Oxygen sensing in the carotid body." Ann N Y Acad Sci **1177**: 119-131.
Loser, P., G. S. Jennings, et al. (1998). "Reactivation of the previously silenced cytomegalovirus major immediate-early promoter in the mouse liver: involvement of NFkappaB." J Virol **72**(1): 180-190.
Lu, H., Y. Li, et al. (2009). "Hypoxia-inducible factor-1alpha blocks differentiation of malignant gliomas." Febs J **276**(24): 7291-7304.
Lu, X. and Y. Kang (2010). "Hypoxia and hypoxia-inducible factors: master regulators of metastasis." Clin Cancer Res **16**(24): 5928-5935.
Ma, R., A. Taruttis, et al. (2009). "Multispectral optoacoustic tomography (MSOT) scanner for whole-body small animal imaging." Opt Express **17**(24): 21414-21426.
Mac Gabhann, F., J. W. Ji, et al. (2007). "VEGF gradients, receptor activation, and sprout guidance in resting and exercising skeletal muscle." J Appl Physiol **102**(2): 722-734.
Mahon, P. C., K. Hirota, et al. (2001). "FIH-1: a novel protein that interacts with HIF-1alpha and VHL to mediate repression of HIF-1 transcriptional activity." Genes Dev **15**(20): 2675-2686.
Majmundar, A. J., W. J. Wong, et al. (2010). "Hypoxia-inducible factors and the response to hypoxic stress." Mol Cell **40**(2): 294-309.
Makarov, P. R., I. Wiswedel, et al. (2002). "Hypoxia/reoxygenation-induced damage to mitochondrial activity is determined by glutathione threshold in astroglia-rich cell cultures." Brain Res **933**(2): 91-97.
Malec, V., O. R. Gottschald, et al. (2010). "HIF-1 alpha signaling is augmented during intermittent hypoxia by induction of the Nrf2 pathway in NOX1-expressing adenocarcinoma A549 cells." Free Radic Biol Med **48**(12): 1626-1635.
Malhotra, R., D. W. Tyson, et al. (2008). "Hypoxia-inducible factor-1alpha is a critical mediator of hypoxia induced apoptosis in cardiac H9c2 and kidney epithelial HK-2 cells." BMC Cardiovasc Disord **8**: 9.
Maltepe, E., B. Keith, et al. (2000). "The role of ARNT2 in tumor angiogenesis and the neural response to hypoxia." Biochem Biophys Res Commun **273**(1): 231-238.
Malthankar-Phatak, G. H., A. B. Patel, et al. (2008). "Effects of continuous hypoxia on energy metabolism in cultured cerebro-cortical neurons." Brain Res **1229**: 147-154.
Mancini, M. and A. Toker (2009). "NFAT proteins: emerging roles in cancer progression." Nat Rev Cancer **9**(11): 810-820.
Manning, G., D. B. Whyte, et al. (2002). "The protein kinase complement of the human genome." Science **298**(5600): 1912-1934.

Mao, Y. S., B. Zhang, et al. (2011). "Biogenesis and function of nuclear bodies." Trends Genet **27**(8): 295-306.
Markossian, K. A. and B. I. Kurganov (2004). "Protein folding, misfolding, and aggregation. Formation of inclusion bodies and aggresomes." Biochemistry (Mosc) **69**(9): 971-984.
Marxsen, J. H., P. Stengel, et al. (2004). "Hypoxia-inducible factor-1 (HIF-1) promotes its degradation by induction of HIF-alpha-prolyl-4-hydroxylases." Biochem J **381**(Pt 3): 761-767.
Masson, N., R. J. Appelhoff, et al. (2004). "The HIF prolyl hydroxylase PHD3 is a potential substrate of the TRiC chaperonin." FEBS Lett **570**(1-3): 166-170.
Masuda, K., K. Abdelmohsen, et al. (2009). "RNA-binding proteins implicated in the hypoxic response." J Cell Mol Med **13**(9A): 2759-2769.
Masuda, N. and B. Doiron (2007). "Gamma oscillations of spiking neural populations enhance signal discrimination." PLoS Comput Biol **3**(11): e236.
Matsuzawa, S., S. Takayama, et al. (1998). "p53-inducible human homologue of Drosophila seven in absentia (Siah) inhibits cell growth: suppression by BAG-1." Embo J **17**(10): 2736-2747.
Matsuzawa, S. I. and J. C. Reed (2001). "Siah-1, SIP, and Ebi collaborate in a novel pathway for beta-catenin degradation linked to p53 responses." Mol Cell **7**(5): 915-926.
Matveev, S. V., L. M. Vinokurov, et al. (1996). "Effect of the ATP level on the overall protein biosynthesis rate in a wheat germ cell-free system." Biochim Biophys Acta **1293**(2): 207-212.
Maul, G. G. (1998). "Nuclear domain 10, the site of DNA virus transcription and replication." Bioessays **20**(8): 660-667.
Maxwell, P. H., C. W. Pugh, et al. (2001). "Activation of the HIF pathway in cancer." Curr Opin Genet Dev **11**(3): 293-299.
Maxwell, P. H., M. S. Wiesener, et al. (1999). "The tumour suppressor protein VHL targets hypoxia-inducible factors for oxygen-dependent proteolysis." Nature **399**(6733): 271-275.
Mayer, M. and J. Buchner (2004). "Refolding of inclusion body proteins." Methods Mol Med **94**: 239-254.
Maynard, M. A., A. J. Evans, et al. (2005). "Human HIF-3alpha4 is a dominant-negative regulator of HIF-1 and is down-regulated in renal cell carcinoma." Faseb J **19**(11): 1396-1406.
McCahill, A., J. Warwicker, et al. (2002). "The RACK1 scaffold protein: a dynamic cog in cell response mechanisms." Mol Pharmacol **62**(6): 1261-1273.
Mekhail, K., L. Gunaratnam, et al. (2004). "HIF activation by pH-dependent nucleolar sequestration of VHL." Nat Cell Biol **6**(7): 642-647.
Meley, D., D. G. Spiller, et al. (2010). "p53-mediated delayed NF-kappaB activity enhances etoposide-induced cell death in medulloblastoma." Cell Death Dis **1**: e41.
Mengel, B., A. Hunziker, et al. (2010). "Modeling oscillatory control in NF-kappaB, p53 and Wnt signaling." Curr Opin Genet Dev **20**(6): 656-664.
Metzen, E., U. Berchner-Pfannschmidt, et al. (2003). "Intracellular localisation of human HIF-1 alpha hydroxylases: implications for oxygen sensing." J Cell Sci **116**(Pt 7): 1319-1326.
Metzen, E., D. P. Stiehl, et al. (2005). "Regulation of the prolyl hydroxylase domain protein 2 (phd2/egln-1) gene: identification of a functional hypoxia-responsive element." Biochem J **387**(Pt 3): 711-717.
Mitchell, J. A. and P. Fraser (2008). "Transcription factories are nuclear subcompartments that remain in the absence of transcription." Genes Dev **22**(1): 20-25.
Mogilner, A., R. Wollman, et al. (2006). "Quantitative modeling in cell biology: what is it good for?" Dev Cell **11**(3): 279-287.
Mojsilovic-Petrovic, J., D. Callaghan, et al. (2007). "Hypoxia-inducible factor-1 (HIF-1) is involved in the regulation of hypoxia-stimulated expression of monocyte chemoattractant protein-1 (MCP-1/CCL2) and MCP-5 (Ccl12) in astrocytes." J Neuroinflammation **4**: 12.

Mole, D. R., C. Blancher, et al. (2009). "Genome-wide association of hypoxia-inducible factor (HIF)-1alpha and HIF-2alpha DNA binding with expression profiling of hypoxia-inducible transcripts." J Biol Chem **284**(25): 16767-16775.

Morita-Fujimura, Y., M. Fujimura, et al. (2001). "Superoxide during reperfusion contributes to caspase-8 expression and apoptosis after transient focal stroke." Stroke **32**(10): 2356-2361.

Moriyama, E. H., M. J. Niedre, et al. (2008). "The influence of hypoxia on bioluminescence in luciferase-transfected gliosarcoma tumor cells in vitro." Photochem Photobiol Sci **7**(6): 675-680.

Moroz, E., S. Carlin, et al. (2009). "Real-time imaging of HIF-1alpha stabilization and degradation." PLoS One **4**(4): e5077.

Moslehi, J., Y. A. Minamishima, et al. (2010). "Loss of hypoxia-inducible factor prolyl hydroxylase activity in cardiomyocytes phenocopies ischemic cardiomyopathy." Circulation **122**(10): 1004-1016.

Mukherjee, T., W. S. Kim, et al. (2011). "Interaction between Notch and Hif-alpha in development and survival of Drosophila blood cells." Science **332**(6034): 1210-1213.

Murdoch, C., M. Muthana, et al. (2005). "Hypoxia regulates macrophage functions in inflammation." J Immunol **175**(10): 6257-6263.

Murphy, M. P. (2009). "How mitochondria produce reactive oxygen species." Biochem J **417**(1): 1-13.

Mylonis, I., G. Chachami, et al. (2006). "Identification of MAPK phosphorylation sites and their role in the localization and activity of hypoxia-inducible factor-1alpha." J Biol Chem **281**(44): 33095-33106.

Nakamura, K., A. J. Kimple, et al. (2009). "PB1 domain interaction of p62/sequestosome 1 and MEKK3 regulates NF-kappaB activation." J Biol Chem **285**(3): 2077-2089.

Nakayama, K., I. J. Frew, et al. (2004). "Siah2 regulates stability of prolyl-hydroxylases, controls HIF1alpha abundance, and modulates physiological responses to hypoxia." Cell **117**(7): 941-952.

Nakayama, K., J. Qi, et al. (2009). "The ubiquitin ligase Siah2 and the hypoxia response." Mol Cancer Res **7**(4): 443-451.

Nangaku, M., I. Kojima, et al. (2006). "Novel drugs and the response to hypoxia: HIF stabilizers and prolyl hydroxylase." Recent Pat Cardiovasc Drug Discov **1**(2): 129-139.

Nardinocchi, L., R. Puca, et al. (2009). "Inhibition of HIF-1alpha activity by homeodomain-interacting protein kinase-2 correlates with sensitization of chemoresistant cells to undergo apoptosis." Mol Cancer **8**: 1.

Nashat, A. H. and R. Langer (2003). "Temporal characteristics of activation, deactivation, and restimulation of signal transduction following depolarization in the pheochromocytoma cell line PC12." Mol Cell Biol **23**(14): 4788-4795.

Natarajan, R., F. N. Salloum, et al. (2006). "Hypoxia inducible factor-1 activation by prolyl 4-hydroxylase-2 gene silencing attenuates myocardial ischemia reperfusion injury." Circ Res **98**(1): 133-140.

Nelson, D. E., A. E. Ihekwaba, et al. (2004). "Oscillations in NF-kappaB signaling control the dynamics of gene expression." Science **306**(5696): 704-708.

Ni, L., C. Bruce, et al. (2009). "Dynamic and complex transcription factor binding during an inducible response in yeast." Genes Dev **23**(11): 1351-1363.

Niatsetskaya, Z., M. Basso, et al. (2010). "HIF prolyl hydroxylase inhibitors prevent neuronal death induced by mitochondrial toxins: therapeutic implications for Huntington's disease and Alzheimer's disease." Antioxid Redox Signal **12**(4): 435-443.

Nilsson, G. (1996). "Brain and body oxygen requirements of Gnathonemus petersii, a fish with an exceptionally large brain." J Exp Biol **199**(Pt 3): 603-607.

Nizami, Z., S. Deryusheva, et al. (2010). "The Cajal body and histone locus body." Cold Spring Harb Perspect Biol **2**(7): a000653.

Novak, B. and J. J. Tyson (2008). "Design principles of biochemical oscillators." Nat Rev Mol Cell Biol **9**(12): 981-991.
Nys, K., A. Van Laethem, et al. (2010). "A p38(MAPK)/HIF-1 pathway initiated by UVB irradiation is required to induce Noxa and apoptosis of human keratinocytes." J Invest Dermatol **130**(9): 2269-2276.
Nytko, K. J., N. Maeda, et al. (2011). "Vitamin C is dispensable for oxygen sensing in vivo." Blood.
O'Riordan, T. C., K. Fitzgerald, et al. (2007). "Sensing intracellular oxygen using near-infrared phosphorescent probes and live-cell fluorescence imaging." Am J Physiol Regul Integr Comp Physiol **292**(4): R1613-1620.
Ohh, M. (2006). "Ubiquitin pathway in VHL cancer syndrome." Neoplasia **8**(8): 623-629.
Ohh, M., R. L. Yauch, et al. (1998). "The von Hippel-Lindau tumor suppressor protein is required for proper assembly of an extracellular fibronectin matrix." Mol Cell **1**(7): 959-968.
Okuda, H., K. Saitoh, et al. (2001). "The von Hippel-Lindau tumor suppressor protein mediates ubiquitination of activated atypical protein kinase C." J Biol Chem **276**(47): 43611-43617.
Pahl, H. L. (1999). "Activators and target genes of Rel/NF-kappaB transcription factors." Oncogene **18**(49): 6853-6866.
Pan, Y., K. D. Mansfield, et al. (2007). "Multiple factors affecting cellular redox status and energy metabolism modulate hypoxia-inducible factor prolyl hydroxylase activity in vivo and in vitro." Mol Cell Biol **27**(3): 912-925.
Pariante, C. M., B. D. Pearce, et al. (1997). "Steroid-independent translocation of the glucocorticoid receptor by the antidepressant desipramine." Mol Pharmacol **52**(4): 571-581.
Park, S., J. S. Yang, et al. (2011). "Protein localization as a principal feature of the etiology and comorbidity of genetic diseases." Mol Syst Biol **7**: 494.
Pasanen, A., M. Heikkila, et al. (2010). "Hypoxia-inducible factor (HIF)-3alpha is subject to extensive alternative splicing in human tissues and cancer cells and is regulated by HIF-1 but not HIF-2." Int J Biochem Cell Biol **42**(7): 1189-1200.
Paszek, P., S. Ryan, et al. (2010). "Population robustness arising from cellular heterogeneity." Proc Natl Acad Sci U S A **107**(25): 11644-11649.
Patel, Y., C. A. Heyward, et al. (2011). "Predicting the points of interaction of small molecules in the NF-kappaB pathway." BMC Syst Biol **5**: 32.
Patten, D. A., V. N. Lafleur, et al. (2010). "Hypoxia-inducible factor-1 activation in nonhypoxic conditions: the essential role of mitochondrial-derived reactive oxygen species." Mol Biol Cell **21**(18): 3247-3257.
Patterson, A. J. and L. Zhang (2010). "Hypoxia and fetal heart development." Curr Mol Med **10**(7): 653-666.
Pelletier, J. and N. Sonenberg (1988). "Internal initiation of translation of eukaryotic mRNA directed by a sequence derived from poliovirus RNA." Nature **334**(6180): 320-325.
Peng, Y., Z. Yang, et al. (2010). "Genetic variations in Tibetan populations and high-altitude adaptation at the Himalayas." Mol Biol Evol **28**(2): 1075-1081.
Perez-Perri, J. I., J. M. Acevedo, et al. (2011). "Epigenetics: new questions on the response to hypoxia." Int J Mol Sci **12**(7): 4705-4721.
Periasamy, A. (2001). "Fluorescence resonance energy transfer microscopy: a mini review." J Biomed Opt **6**(3): 287-291.
Pescador, N., Y. Cuevas, et al. (2005). "Identification of a functional hypoxia-responsive element that regulates the expression of the egl nine homologue 3 (egln3/phd3) gene." Biochem J **390**(Pt 1): 189-197.
Peyrl, A., K. Krapfenbauer, et al. (2003). "Protein profiles of medulloblastoma cell lines DAOY and D283: identification of tumor-related proteins and principles." Proteomics **3**(9): 1781-1800.
Pfaffl, M. W., G. W. Horgan, et al. (2002). "Relative expression software tool (REST) for group-wise comparison and statistical analysis of relative expression results in real-time PCR." Nucleic Acids Res **30**(9): e36.

Pfeifer, A. C., D. Kaschek, et al. (2010). "Model-based extension of high-throughput to high-content data." BMC Syst Biol **4**: 106.
Pietenpol, J. A. and Z. A. Stewart (2002). "Cell cycle checkpoint signaling: cell cycle arrest versus apoptosis." Toxicology **181-182**: 475-481.
Piret, J. P., D. Mottet, et al. (2002). "Is HIF-1alpha a pro- or an anti-apoptotic protein?" Biochem Pharmacol **64**(5-6): 889-892.
Plachta, N., T. Bollenbach, et al. (2011). "Oct4 kinetics predict cell lineage patterning in the early mammalian embryo." Nat Cell Biol **13**(2): 117-123.
Platani, M., I. Goldberg, et al. (2000). "In vivo analysis of Cajal body movement, separation, and joining in live human cells." J Cell Biol **151**(7): 1561-1574.
Poellinger, L. and U. Lendahl (2008). "Modulating Notch signaling by pathway-intrinsic and pathway-extrinsic mechanisms." Curr Opin Genet Dev **18**(5): 449-454.
Puga, A., Y. Xia, et al. (2002). "Role of the aryl hydrocarbon receptor in cell cycle regulation." Chem Biol Interact **141**(1-2): 117-130.
Purvis, J. E., R. Radhakrishnan, et al. (2009). "Steady-state kinetic modeling constrains cellular resting states and dynamic behavior." PLoS Comput Biol **5**(3): e1000298.
Qin, J. Y., L. Zhang, et al. (2010). "Systematic comparison of constitutive promoters and the doxycycline-inducible promoter." PLoS One **5**(5): e10611.
Qutub, A. A. and A. S. Popel (2007). "Three autocrine feedback loops determine HIF1 alpha expression in chronic hypoxia." Biochim Biophys Acta **1773**(10): 1511-1525.
Ramanathan, M., G. Hasko, et al. (2005). "Analysis of signal transduction pathways in macrophages using expression vectors with CMV promoters: a cautionary tale." Inflammation **29**(2-3): 94-102.
Rane, S., M. He, et al. (2009). "Downregulation of miR-199a derepresses hypoxia-inducible factor-1alpha and Sirtuin 1 and recapitulates hypoxia preconditioning in cardiac myocytes." Circ Res **104**(7): 879-886.
Rantanen, K., J. Pursiheimo, et al. (2008). "Prolyl hydroxylase PHD3 activates oxygen-dependent protein aggregation." Mol Biol Cell **19**(5): 2231-2240.
Raska, I., P. J. Shaw, et al. (2006). "New insights into nucleolar architecture and activity." Int Rev Cytol **255**: 177-235.
Rausenberger, J., C. Fleck, et al. (2009). "Signatures of gene expression noise in cellular systems." Prog Biophys Mol Biol **100**(1-3): 57-66.
Raval, R. R., K. W. Lau, et al. (2005). "Contrasting properties of hypoxia-inducible factor 1 (HIF-1) and HIF-2 in von Hippel-Lindau-associated renal cell carcinoma." Mol Cell Biol **25**(13): 5675-5686.
Raymond, J. and D. Segre (2006). "The effect of oxygen on biochemical networks and the evolution of complex life." Science **311**(5768): 1764-1767.
Razin, S. V., A. A. Gavrilov, et al. (2011). "Transcription factories in the context of the nuclear and genome organization." Nucleic Acids Res.
Rey, S. and G. L. Semenza (2010). "Hypoxia-inducible factor-1-dependent mechanisms of vascularization and vascular remodelling." Cardiovasc Res **86**(2): 236-242.
Ribes, V., N. Balaskas, et al. (2010). "Distinct Sonic Hedgehog signaling dynamics specify floor plate and ventral neuronal progenitors in the vertebrate neural tube." Genes Dev **24**(11): 1186-1200.
Rino, J., T. Carvalho, et al. (2007). "A stochastic view of spliceosome assembly and recycling in the nucleus." PLoS Comput Biol **3**(10): 2019-2031.
Rius, J., M. Guma, et al. (2008). "NF-kappaB links innate immunity to the hypoxic response through transcriptional regulation of HIF-1alpha." Nature **453**(7196): 807-811.
Roach, S. K., S. B. Lee, et al. (2005). "Differential activation of the transcription factor cyclic AMP response element binding protein (CREB) in macrophages following infection with pathogenic and nonpathogenic mycobacteria and role for CREB in tumor necrosis factor alpha production." Infect Immun **73**(1): 514-522.

Robinson, V. L. (2009). "Rethinking the central dogma: noncoding RNAs are biologically relevant." Urol Oncol **27**(3): 304-306.
Roe, J. S., H. Kim, et al. (2006). "p53 stabilization and transactivation by a von Hippel-Lindau protein." Mol Cell **22**(3): 395-405.
Rubenstein, L. A., R. J. Zauhar, et al. (2006). "Molecular dynamics of a biophysical model for beta2-adrenergic and G protein-coupled receptor activation." J Mol Graph Model **25**(4): 396-409.
Ryan, S., C. T. Taylor, et al. (2005). "Selective activation of inflammatory pathways by intermittent hypoxia in obstructive sleep apnea syndrome." Circulation **112**(17): 2660-2667.
Rytkonen, K. T. and J. F. Storz (2010). "Evolutionary origins of oxygen sensing in animals." EMBO Rep **12**(1): 3-4.
Rytkonen, K. T., T. A. Williams, et al. (2011). "Molecular evolution of the metazoan PHD-HIF oxygen-sensing system." Mol Biol Evol **28**(6): 1913-1926.
Sahlin, K., I. G. Shabalina, et al. (2010). "Ultraendurance exercise increases the production of reactive oxygen species in isolated mitochondria from human skeletal muscle." J Appl Physiol **108**(4): 780-787.
Sainson, R. C. and A. L. Harris (2006). "Hypoxia-regulated differentiation: let's step it up a Notch." Trends Mol Med **12**(4): 141-143.
Sakaue-Sawano, A., H. Kurokawa, et al. (2008). "Visualizing spatiotemporal dynamics of multicellular cell-cycle progression." Cell **132**(3): 487-498.
Saker, M., C. Moreira, et al. (2009). "DNA profiling of complex bacterial populations: toxic cyanobacterial blooms." Appl Microbiol Biotechnol **85**(2): 237-252.
Sang, N., D. P. Stiehl, et al. (2003). "MAPK signaling up-regulates the activity of hypoxia-inducible factors by its effects on p300." J Biol Chem **278**(16): 14013-14019.
Schmidt, A. and A. Hall (2002). "The Rho exchange factor Net1 is regulated by nuclear sequestration." J Biol Chem **277**(17): 14581-14588.
Schmierer, B., B. Novak, et al. (2010). "Hypoxia-dependent sequestration of an oxygen sensor by a widespread structural motif can shape the hypoxic response--a predictive kinetic model." BMC Syst Biol **4**: 139.
Schneider-Poetsch, T., J. Ju, et al. (2010). "Inhibition of eukaryotic translation elongation by cycloheximide and lactimidomycin." Nat Chem Biol **6**(3): 209-217.
Schnell, S., Grima, R., Maini, PK. (2007). "Multiscale modeling in Biology." American Scientist **95**: 10.
Schodel, J., S. Oikonomopoulos, et al. (2011). "High-resolution genome-wide mapping of HIF-binding sites by ChIP-seq." Blood **117**(23): e207-217.
Schwanhausser, B., D. Busse, et al. (2011). "Global quantification of mammalian gene expression control." Nature **473**(7347): 337-342.
Schwartz, J. R., P. J. Sarvaiya, et al. (2010). "Glucocorticoid receptor knock down reveals a similar apoptotic threshold but differing gene regulation patterns in T-cell and pre-B-cell acute lymphoblastic leukemia." Mol Cell Endocrinol **320**(1-2): 76-86.
Selinummi, J., P. Ruusuvuori, et al. (2009). "Bright field microscopy as an alternative to whole cell fluorescence in automated analysis of macrophage images." PLoS One **4**(10): e7497.
Semenza, G. L. (2003). "Targeting HIF-1 for cancer therapy." Nat Rev Cancer **3**(10): 721-732.
Semenza, G. L. (2011). "Crosstalk Between Oxygen Sensing and the Cell Cycle Machinery." Am J Physiol Cell Physiol.
Semenza, G. L. and G. L. Wang (1992). "A nuclear factor induced by hypoxia via de novo protein synthesis binds to the human erythropoietin gene enhancer at a site required for transcriptional activation." Mol Cell Biol **12**(12): 5447-5454.
Serebrovskaya, E. O., E. F. Edelweiss, et al. (2009). "Targeting cancer cells by using an antireceptor antibody-photosensitizer fusion protein." Proc Natl Acad Sci U S A **106**(23): 9221-9225.

Serganova, I., M. Doubrovin, et al. (2004). "Molecular imaging of temporal dynamics and spatial heterogeneity of hypoxia-inducible factor-1 signal transduction activity in tumors in living mice." Cancer Res **64**(17): 6101-6108.
Sermeus, A. and C. Michiels (2011). "Reciprocal influence of the p53 and the hypoxic pathways." Cell Death Dis **2**: e164.
Seton-Rogers, S. (2011). "Hypoxia: HIF switch." Nat Rev Cancer **11**(6): 391.
Sexton, T., H. Schober, et al. (2007). "Gene regulation through nuclear organization." Nat Struct Mol Biol **14**(11): 1049-1055.
Shankaran, H., D. L. Ippolito, et al. (2009). "Rapid and sustained nuclear-cytoplasmic ERK oscillations induced by epidermal growth factor." Mol Syst Biol **5**: 332.
Shav-Tal, Y., J. Blechman, et al. (2005). "Dynamic sorting of nuclear components into distinct nucleolar caps during transcriptional inhibition." Mol Biol Cell **16**(5): 2395-2413.
Shav-Tal, Y., X. Darzacq, et al. (2006). "Gene expression within a dynamic nuclear landscape." Embo J **25**(15): 3469-3479.
Sheflin, L. G., A. P. Zou, et al. (2004). "Androgens regulate the binding of endogenous HuR to the AU-rich 3'UTRs of HIF-1alpha and EGF mRNA." Biochem Biophys Res Commun **322**(2): 644-651.
Shen, H., G. Nelson, et al. (2006). "Automated tracking of gene expression in individual cells and cell compartments." J R Soc Interface **3**(11): 787-794.
Shi, H. (2009). "Hypoxia inducible factor 1 as a therapeutic target in ischemic stroke." Curr Med Chem **16**(34): 4593-4600.
Shimba, S., T. Wada, et al. (2004). "EPAS1 promotes adipose differentiation in 3T3-L1 cells." J Biol Chem **279**(39): 40946-40953.
Shimba, S., T. Wada, et al. (2001). "Arylhydrocarbon receptor (AhR) is involved in negative regulation of adipose differentiation in 3T3-L1 cells: AhR inhibits adipose differentiation independently of dioxin." J Cell Sci **114**(Pt 15): 2809-2817.
Shinae Kizaka-Kondoh, S. T. a. M. H. (2009). "Imaging and Targeting of the Hypoxia-inducible Factor 1-active Microenvironment." Imaging and Targeting of the Hypoxia-inducible Factor 1-active Microenvironment **22**(2).
Siegel, M. R. and H. D. Sisler (1963). "Inhibition of Protein Synthesis in Vitro by Cycloheximide." Nature **200**: 675-676.
Sigal, A., R. Milo, et al. (2006). "Variability and memory of protein levels in human cells." Nature **444**(7119): 643-646.
Sirri, V., S. Urcuqui-Inchima, et al. (2008). "Nucleolus: the fascinating nuclear body." Histochem Cell Biol **129**(1): 13-31.
Sleeman, J. E., L. Trinkle-Mulcahy, et al. (2003). "Cajal body proteins SMN and Coilin show differential dynamic behaviour in vivo." J Cell Sci **116**(Pt 10): 2039-2050.
Smith, T. G. and N. P. Talbot (2010). "Prolyl hydroxylases and therapeutics." Antioxid Redox Signal **12**(4): 431-433.
Spandl, J., D. J. White, et al. (2009). "Live cell multicolor imaging of lipid droplets with a new dye, LD540." Traffic **10**(11): 1579-1584.
Spector, D. L. (2001). "Nuclear domains." J Cell Sci **114**(Pt 16): 2891-2893.
Spector, D. L. (2006). "SnapShot: Cellular bodies." Cell **127**(5): 1071.
Sreedhar, A. S., E. Kalmar, et al. (2004). "Hsp90 isoforms: functions, expression and clinical importance." FEBS Lett **562**(1-3): 11-15.
Stadtman, E. R. (2006). "Protein oxidation and aging." Free Radic Res **40**(12): 1250-1258.
Steinhoff, A., F. K. Pientka, et al. (2009). "Cellular oxygen sensing: Importins and exportins are mediators of intracellular localisation of prolyl-4-hydroxylases PHD1 and PHD2." Biochem Biophys Res Commun **387**(4): 705-711.
Stephens, D. J. and V. J. Allan (2003). "Light microscopy techniques for live cell imaging." Science **300**(5616): 82-86.

Stiehl, D. P., R. Wirthner, et al. (2006). "Increased prolyl 4-hydroxylase domain proteins compensate for decreased oxygen levels. Evidence for an autoregulatory oxygen-sensing system." J Biol Chem **281**(33): 23482-23491.

Stolze, I., U. Berchner-Pfannschmidt, et al. (2002). "Hypoxia-inducible erythropoietin gene expression in human neuroblastoma cells." Blood **100**(7): 2623-2628.

Stolze, I. P., Y. M. Tian, et al. (2004). "Genetic analysis of the role of the asparaginyl hydroxylase factor inhibiting hypoxia-inducible factor (FIH) in regulating hypoxia-inducible factor (HIF) transcriptional target genes [corrected]." J Biol Chem **279**(41): 42719-42725.

Strack, R. L., D. E. Strongin, et al. (2010). "Chromophore formation in DsRed occurs by a branched pathway." J Am Chem Soc **132**(24): 8496-8505.

Sugimoto, T., E. Tatsumi, et al. (1984). "Determination of cell surface membrane antigens common to both human neuroblastoma and leukemia-lymphoma cell lines by a panel of 38 monoclonal antibodies." J Natl Cancer Inst **73**(1): 51-57.

Sun, J., H. Xu, et al. (2005). "Interactions between coilin and PIASy partially link Cajal bodies to PML bodies." J Cell Sci **118**(Pt 21): 4995-5003.

Sun, S., X. Ning, et al. (2009). "Hypoxia-inducible factor-1alpha induces Twist expression in tubular epithelial cells subjected to hypoxia, leading to epithelial-to-mesenchymal transition." Kidney Int **75**(12): 1278-1287.

Sun, X., G. Niu, et al. (2010). "Tumor hypoxia imaging." Mol Imaging Biol **13**(3): 399-410.

Sung, M. H. and J. G. McNally (2010). "Live cell imaging and systems biology." Wiley Interdiscip Rev Syst Biol Med **3**(2): 167-182.

Swift, H. (1959). "Studies on nuclear fine structure." Brookhaven Symp Biol **12**: 134-152.

Tafani, M., N. O. Karpinich, et al. (2002). "Cytochrome c release upon Fas receptor activation depends on translocation of full-length bid and the induction of the mitochondrial permeability transition." J Biol Chem **277**(12): 10073-10082.

Taguchi, A., K. Yanagisawa, et al. (2008). "Identification of hypoxia-inducible factor-1 alpha as a novel target for miR-17-92 microRNA cluster." Cancer Res **68**(14): 5540-5545.

Tamama, K., H. Kawasaki, et al. (2011). "Differential roles of hypoxia inducible factor subunits in multipotential stromal cells under hypoxic condition." J Cell Biochem **112**(3): 804-817.

Tashiro, S., A. Muto, et al. (2004). "Repression of PML nuclear body-associated transcription by oxidative stress-activated Bach2." Mol Cell Biol **24**(8): 3473-3484.

Taylor, C. T. (2008). "Mitochondria and cellular oxygen sensing in the HIF pathway." Biochem J **409**(1): 19-26.

Taylor, C. T., G. T. Furuta, et al. (2000). "Phosphorylation-dependent targeting of cAMP response element binding protein to the ubiquitin/proteasome pathway in hypoxia." Proc Natl Acad Sci U S A **97**(22): 12091-12096.

Taylor, C. T. and J. C. McElwain (2010). "Ancient atmospheres and the evolution of oxygen sensing via the hypoxia-inducible factor in metazoans." Physiology (Bethesda) **25**(5): 272-279.

Taylor, C. T. and J. Pouyssegur (2007). "Oxygen, hypoxia, and stress." Ann N Y Acad Sci **1113**: 87-94.

Taylor, M. S. (2001). "Characterization and comparative analysis of the EGLN gene family." Gene **275**(1): 125-132.

Tennant, D. A. and E. Gottlieb (2010). "HIF prolyl hydroxylase-3 mediates alpha-ketoglutarate-induced apoptosis and tumor suppression." J Mol Med **88**(8): 839-849.

Thannickal, V. J. (2009). "Oxygen in the evolution of complex life and the price we pay." Am J Respir Cell Mol Biol **40**(5): 507-510.

Thannickal, V. J. and B. L. Fanburg (2000). "Reactive oxygen species in cell signaling." Am J Physiol Lung Cell Mol Physiol **279**(6): L1005-1028.

Thirstrup, K., S. Christensen, et al. (2011). "Endogenous 2-oxoglutarate levels impact potencies of competitive HIF prolyl hydroxylase inhibitors." Pharmacol Res **64**(3): 268-273.

Thomas, C. L. and A. J. Maule (2000). "Limitations on the use of fused green fluorescent protein to investigate structure-function relationships for the cauliflower mosaic virus movement protein." J Gen Virol **81**(Pt 7): 1851-1855.
Thorwarth, D. and M. Alber (2010). "Implementation of hypoxia imaging into treatment planning and delivery." Radiother Oncol **97**(2): 172-175.
Tian, H., S. L. McKnight, et al. (1997). "Endothelial PAS domain protein 1 (EPAS1), a transcription factor selectively expressed in endothelial cells." Genes Dev **11**(1): 72-82.
Tian, Y. M., D. R. Mole, et al. (2006). "Characterization of different isoforms of the HIF prolyl hydroxylase PHD1 generated by alternative initiation." Biochem J **397**(1): 179-186.
To, K. K., O. A. Sedelnikova, et al. (2006). "The phosphorylation status of PAS-B distinguishes HIF-1alpha from HIF-2alpha in NBS1 repression." Embo J **25**(20): 4784-4794.
Toffoli, S. and C. Michiels (2008). "Intermittent hypoxia is a key regulator of cancer cell and endothelial cell interplay in tumours." Febs J **275**(12): 2991-3002.
Toprak, E., C. Kural, et al. (2010). "Super-accuracy and super-resolution getting around the diffraction limit." Methods Enzymol **475**: 1-26.
Trayanova, N. (2006). "Defibrillation of the heart: insights into mechanisms from modelling studies." Exp Physiol **91**(2): 323-337.
Treins, C., S. Giorgetti-Peraldi, et al. (2005). "Regulation of hypoxia-inducible factor (HIF)-1 activity and expression of HIF hydroxylases in response to insulin-like growth factor I." Mol Endocrinol **19**(5): 1304-1317.
Troy, T., D. Jekic-McMullen, et al. (2004). "Quantitative comparison of the sensitivity of detection of fluorescent and bioluminescent reporters in animal models." Mol Imaging **3**(1): 9-23.
Tsien, R. Y. (1998). "The green fluorescent protein." Annu Rev Biochem **67**: 509-544.
Tsujimoto, Y. (1997). "Apoptosis and necrosis: intracellular ATP level as a determinant for cell death modes." Cell Death Differ **4**(6): 429-434.
Tuckerman, J. R., Y. Zhao, et al. (2004). "Determination and comparison of specific activity of the HIF-prolyl hydroxylases." FEBS Lett **576**(1-2): 145-150.
Tunster, S. J., M. Van De Pette, et al. (2010). "BACs as tools for the study of genomic imprinting." J Biomed Biotechnol **2011**: 283013.
Turner, D. A., P. Paszek, et al. (2010). "Physiological levels of TNFalpha stimulation induce stochastic dynamics of NF-kappaB responses in single living cells." J Cell Sci **123**(Pt 16): 2834-2843.
Turrens, J. F. (2003). "Mitochondrial formation of reactive oxygen species." J Physiol **552**(Pt 2): 335-344.
Turrigiano, G. (2007). "Homeostatic signaling: the positive side of negative feedback." Curr Opin Neurobiol **17**(3): 318-324.
Uchida, T., F. Rossignol, et al. (2004). "Prolonged hypoxia differentially regulates hypoxia-inducible factor (HIF)-1alpha and HIF-2alpha expression in lung epithelial cells: implication of natural antisense HIF-1alpha." J Biol Chem **279**(15): 14871-14878.
van Hagen, M., R. M. Overmeer, et al. (2010). "RNF4 and VHL regulate the proteasomal degradation of SUMO-conjugated Hypoxia-Inducible Factor-2alpha." Nucleic Acids Res **38**(6): 1922-1931.
Van Hoecke, M., A. S. Prigent-Tessier, et al. (2007). "Evidence of HIF-1 functional binding activity to caspase-3 promoter after photothrombotic cerebral ischemia." Mol Cell Neurosci **34**(1): 40-47.
van Lith, M., S. Tiwari, et al. (2011). "Real-time monitoring of redox changes in the mammalian endoplasmic reticulum." J Cell Sci **124**(Pt 14): 2349-2356.
van Riel, N. A. (2006). "Dynamic modelling and analysis of biochemical networks: mechanism-based models and model-based experiments." Brief Bioinform **7**(4): 364-374.
van Royen, M. E., P. Farla, et al. (2009). "Fluorescence recovery after photobleaching (FRAP) to study nuclear protein dynamics in living cells." Methods Mol Biol **464**: 363-385.

Vasquez, R. J., B. Howell, et al. (1997). "Nanomolar concentrations of nocodazole alter microtubule dynamic instability in vivo and in vitro." Mol Biol Cell **8**(6): 973-985.
Vigmond, E., F. Vadakkumpadan, et al. (2009). "Towards predictive modelling of the electrophysiology of the heart." Exp Physiol **94**(5): 563-577.
Vodovotz, Y., C. C. Chow, et al. (2006). "In silico models of acute inflammation in animals." Shock **26**(3): 235-244.
Volm, M. and R. Koomagi (2000). "Hypoxia-inducible factor (HIF-1) and its relationship to apoptosis and proliferation in lung cancer." Anticancer Res **20**(3A): 1527-1533.
von Stosch, M., J. Peres, et al. (2010). "Modelling biochemical networks with intrinsic time delays: a hybrid semi-parametric approach." BMC Syst Biol **4**: 131.
Vousden, K. H. (2006). "Outcomes of p53 activation--spoilt for choice." J Cell Sci **119**(Pt 24): 5015-5020.
Wall, M. A., M. Socolich, et al. (2000). "The structural basis for red fluorescence in the tetrameric GFP homolog DsRed." Nat Struct Biol **7**(12): 1133-1138.
Walmsley, S. R., E. R. Chilvers, et al. (2011). "Prolyl hydroxylase 3 (PHD3) is essential for hypoxic regulation of neutrophilic inflammation in humans and mice." J Clin Invest **121**(3): 1053-1063.
Walmsley, S. R., C. Print, et al. (2005). "Hypoxia-induced neutrophil survival is mediated by HIF-1alpha-dependent NF-kappaB activity." J Exp Med **201**(1): 105-115.
Wang, G. L., B. H. Jiang, et al. (1995). "Hypoxia-inducible factor 1 is a basic-helix-loop-helix-PAS heterodimer regulated by cellular O2 tension." Proc Natl Acad Sci U S A **92**(12): 5510-5514.
Wang, W., H. Fang, et al. (2008). "Superoxide flashes in single mitochondria." Cell **134**(2): 279-290.
Wangsa-Wirawan, N. D. and R. A. Linsenmeier (2003). "Retinal oxygen: fundamental and clinical aspects." Arch Ophthalmol **121**(4): 547-557.
Webb, J. D., M. L. Coleman, et al. (2009). "Hypoxia, hypoxia-inducible factors (HIF), HIF hydroxylases and oxygen sensing." Cell Mol Life Sci **66**(22): 3539-3554.
Wen, W., J. Ding, et al. (2010). "Suppression of cyclin D1 by hypoxia-inducible factor-1 via direct mechanism inhibits the proliferation and 5-fluorouracil-induced apoptosis of A549 cells." Cancer Res **70**(5): 2010-2019.
Wenger, R. H. and D. M. Katschinski (2005). "The hypoxic testis and post-meiotic expression of PAS domain proteins." Semin Cell Dev Biol **16**(4-5): 547-553.
Whitfield, M. L., L. X. Zheng, et al. (2000). "Stem-loop binding protein, the protein that binds the 3' end of histone mRNA, is cell cycle regulated by both translational and posttranslational mechanisms." Mol Cell Biol **20**(12): 4188-4198.
Wiedenmann, J., F. Oswald, et al. (2009). "Fluorescent proteins for live cell imaging: opportunities, limitations, and challenges." IUBMB Life **61**(11): 1029-1042.
Wiener, L., M. Feola, et al. (1976). "Monitoring tissue oxygenation of the heart after myocardial revascularization." Am J Cardiol **38**(1): 38-45.
Wiesener, M. S., J. S. Jurgensen, et al. (2003). "Widespread hypoxia-inducible expression of HIF-2alpha in distinct cell populations of different organs." Faseb J **17**(2): 271-273.
Wiseman, H. and B. Halliwell (1996). "Damage to DNA by reactive oxygen and nitrogen species: role in inflammatory disease and progression to cancer." Biochem J **313 (Pt 1)**: 17-29.
Wolkenhauer, O. (2002). "Mathematical modelling in the post-genome era: understanding genome expression and regulation--a system theoretic approach." Biosystems **65**(1): 1-18.
Woods, S., A. Farrall, et al. (2008). "The bHLH/Per-Arnt-Sim transcription factor SIM2 regulates muscle transcript myomesin2 via a novel, non-canonical E-box sequence." Nucleic Acids Res **36**(11): 3716-3727.
Woods, S. L. and M. L. Whitelaw (2002). "Differential activities of murine single minded 1 (SIM1) and SIM2 on a hypoxic response element. Cross-talk between basic helix-loop-helix/per-Arnt-Sim homology transcription factors." J Biol Chem **277**(12): 10236-10243.

Worland, J. (1976). "Effects of positive and negative feedback on behavior control in hyperactive and normal boys." J Abnorm Child Psychol **4**(4): 315-326.
Wotzlaw, C., T. Otto, et al. (2007). "Optical analysis of the HIF-1 complex in living cells by FRET and FRAP." Faseb J **21**(3): 700-707.
Wu, J., A. H. Corbett, et al. (2009). "The intracellular mobility of nuclear import receptors and NLS cargoes." Biophys J **96**(9): 3840-3849.
Xie, Z. R., H. T. Yang, et al. (2007). "The role of microRNA in the delayed negative feedback regulation of gene expression." Biochem Biophys Res Commun **358**(3): 722-726.
Xu, Y., Y. Zuo, et al. (2010). "Induction of SENP1 in endothelial cells contributes to hypoxia-driven VEGF expression and angiogenesis." J Biol Chem **285**(47): 36682-36688.
Xue, J., X. Li, et al. (2010). "Prolyl hydroxylase-3 is down-regulated in colorectal cancer cells and inhibits IKKbeta independent of hydroxylase activity." Gastroenterology **138**(2): 606-615.
Yamada, K. and N. Inagaki (2002). "ATP-sensitive K(+) channels in the brain: sensors of hypoxic conditions." News Physiol Sci **17**: 127-130.
Yang, H., Y. A. Minamishima, et al. (2007). "pVHL acts as an adaptor to promote the inhibitory phosphorylation of the NF-kappaB agonist Card9 by CK2." Mol Cell **28**(1): 15-27.
Yang, W. H., J. H. Yu, et al. (2006). "RNA-associated protein 55 (RAP55) localizes to mRNA processing bodies and stress granules." Rna **12**(4): 547-554.
Yang, X. M., Y. S. Wang, et al. (2009). "Role of PI3K/Akt and MEK/ERK in mediating hypoxia-induced expression of HIF-1alpha and VEGF in laser-induced rat choroidal neovascularization." Invest Ophthalmol Vis Sci **50**(4): 1873-1879.
Yasumoto, K., Y. Kowata, et al. (2009). "Role of the intracellular localization of HIF-prolyl hydroxylases." Biochim Biophys Acta **1793**(5): 792-797.
Yeger-Lotem, E., S. Sattath, et al. (2004). "Network motifs in integrated cellular networks of transcription-regulation and protein-protein interaction." Proc Natl Acad Sci U S A **101**(16): 5934-5939.
Yen, H. C., Q. Xu, et al. (2008). "Global protein stability profiling in mammalian cells." Science **322**(5903): 918-923.
Yewdell, J. W., J. R. Lacsina, et al. (2011). "Out with the old, in with the new? Comparing methods for measuring protein degradation." Cell Biol Int **35**(5): 457-462.
Yoshiura, S., T. Ohtsuka, et al. (2007). "Ultradian oscillations of Stat, Smad, and Hes1 expression in response to serum." Proc Natl Acad Sci U S A **104**(27): 11292-11297.
Young, R. M., S. J. Wang, et al. (2008). "Hypoxia-mediated selective mRNA translation by an internal ribosome entry site-independent mechanism." J Biol Chem **283**(24): 16309-16319.
Yu, Y. A., T. Timiryasova, et al. (2003). "Optical imaging: bacteria, viruses, and mammalian cells encoding light-emitting proteins reveal the locations of primary tumors and metastases in animals." Anal Bioanal Chem **377**(6): 964-972.
Yun, Z., H. L. Maecker, et al. (2002). "Inhibition of PPAR gamma 2 gene expression by the HIF-1-regulated gene DEC1/Stra13: a mechanism for regulation of adipogenesis by hypoxia." Dev Cell **2**(3): 331-341.
Zabner, J., A. J. Fasbender, et al. (1995). "Cellular and molecular barriers to gene transfer by a cationic lipid." J Biol Chem **270**(32): 18997-19007.
Zhang, Q., J. Pi, et al. (2010). "A systems biology perspective on Nrf2-mediated antioxidant response." Toxicol Appl Pharmacol **244**(1): 84-97.
Zhang, Y., Z. Shao, et al. (2009). "The HIF-1 hypoxia-inducible factor modulates lifespan in C. elegans." PLoS One **4**(7): e6348.
Zhao, H. W., D. Zhou, et al. (2010). "Experimental selection for Drosophila survival in extremely high O2 environments." PLoS One **5**(7): e11701.
Zhou, J., T. Schmid, et al. (2006). "Tumor hypoxia and cancer progression." Cancer Lett **237**(1): 10-21.
Zimmer, M. (2002). "Green fluorescent protein (GFP): applications, structure, and related photophysical behavior." Chem Rev **102**(3): 759-781.

Zipper, L. M. and R. T. Mulcahy (2002). "The Keap1 BTB/POZ dimerization function is required to sequester Nrf2 in cytoplasm." J Biol Chem **277**(39): 36544-36552.

Appendix

1.1 Plasmid Expression Vectors and Reporters used and produced

All confocal images are of living HeLa cells transiently transfected shown at various magnifications.

1. pG-HIF1α-IRES-EGFP

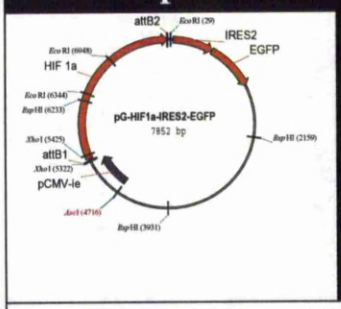

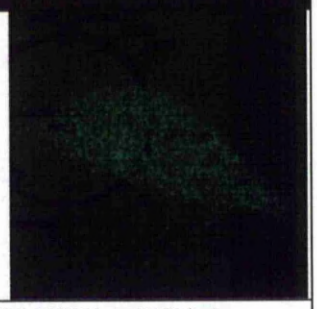

Diagnostic Digest: AflII (4913bp, 2939bp)

History

Parent Plasmid: pHIF-1α (donated by Prof S. Edwards)
Cloned using Gateway® Invitrogen Recombination
5' primer:
gggacaagtttgtacaaaaaagcaggcttcaccatggagggcgccggcggc
3' primer: ggggaccactttgtacaagaaagctgggtcgttaacttgatccaaagc

2. pG-HIF1α-EGFP

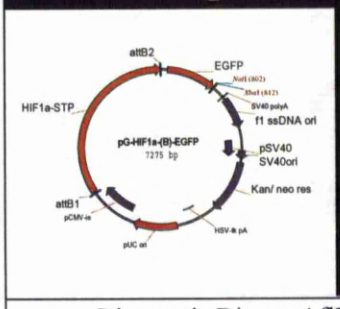

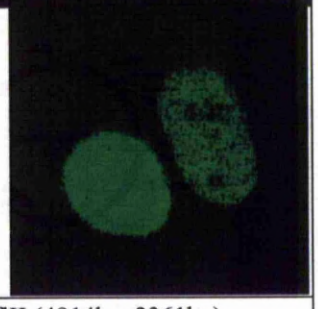

Diagnostic Digest: AflII (4914bp, 2361bp)

History

Parent Plasmid: pHIF-1α (donated by Prof S. Edwards
Cloned using Gateway® Invitrogen Recombination
5' primer:
gggacaagtttgtacaaaaaagcaggcttcaccatggagggcgccggcggc
3' primer: ggggaccactttgtacaagaaagctgggtcgttaacttgatccaaagc

3. pG-EGFP-HIF1α

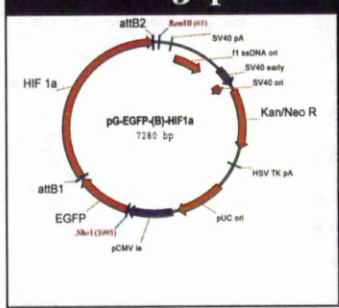

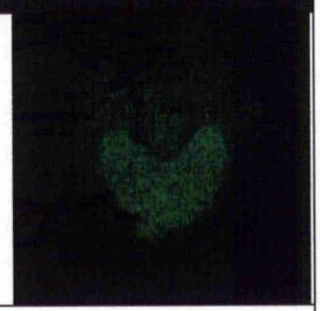

Diagnostic Digest: AgeI (5408bp, 1872bp)

History

Parent Plasmid: pHIF-1α (donated by Prof S. Edwards)
Cloned using Gateway® Invitrogen Recombination
5' primer:
gggacaagtttgtacaaaaaagcaggcttcaccatggagggcgccggcggc
3' primer: ggggaccactttgtacaagaaagctgggtctcagttaacttgatccaa

4. pG-proHIF1α-EGFP

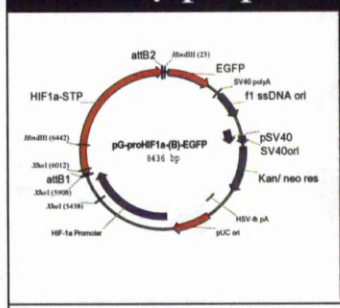

Diagnostic Digest: HindIII (6419bp, 2017bp)

History

Replaced CMV promoter from pG-HIF1αEGFP with a 1.7kb cloned human HIF1α promoter using a digest-ligation protocol [**Very Weak Expression**]
5' primer (KpnI): gcgtgggtaccttctcttcaggcatttcccatggttc
3' primer: (NheI): agagagctagcggtgaatcggtccccgccat

5. YFP-HIF1β

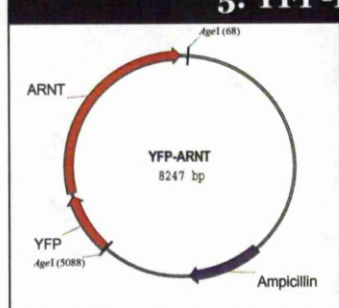

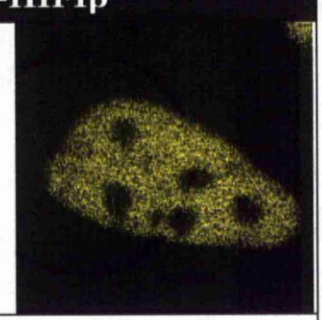

Diagnostic Digest: Kpn1 (7056bp, 1191bp)

History

Donated by Prof. J. Fandrey, University of Duisburg
Ref: Eur Respir J 2008; 32: 210–217

6. pG-DsRedxp-HIF1β

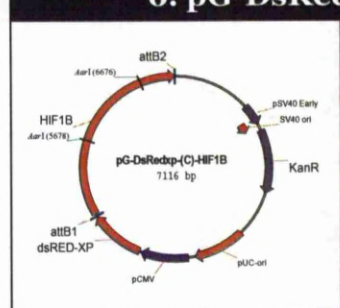

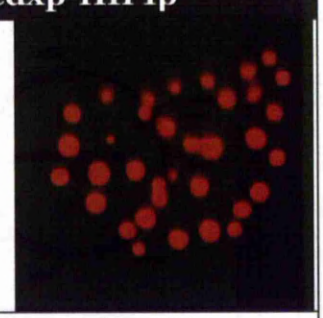

Diagnostic Digest: Aar1 (6118bp, 998bp)

History

Replaced fluorophore from YFP-HIF1β by restriction digest (using bmt1 and xho1) and subsequent ligation. DsRedxp was removed from pG-DsRedxp-HIF2α.

7. pcDNA3-hEPAS

No Map **Not Fluorescent**

Diagnostic Digest: N/A

History

Donated by Dr. S. McKnight, UT Southwestern Medical Center
Ref: Oncogene (2007) 26, 7480–7489

8. pG-DsRedxp-HIF2α

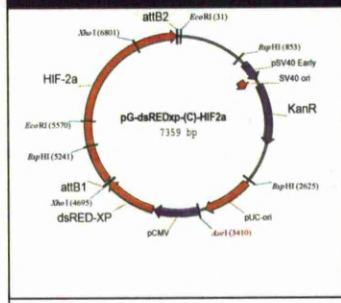

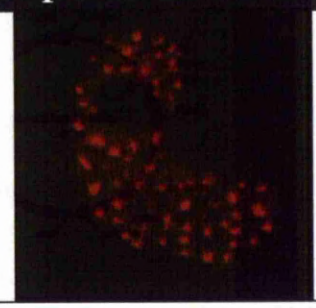

Diagnostic Digest: XhoI (5253bp, 2106bp)

History

Parent Plasmid: hEPAS myc-pcDNA3
Cloned using Gateway® Invitrogen Recombination
5' primer: ggggacaagtttgtacaaaaaagcaggcttcaccatgacagctgacaaggag
3' primer: ggggaccactttgtacaagaaagctgggtctcaggtggcctcgtccag

9. pG-HIF2α-IRES-EGFP

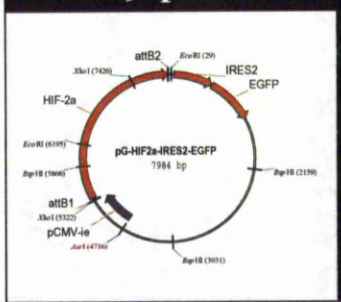

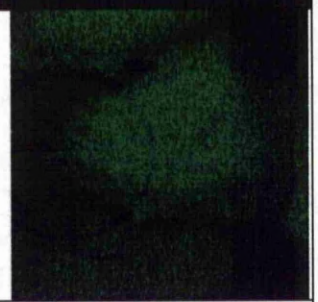

Diagnostic Digest: EcoRI (6166bp, 1818bp)

History

Parent Plasmid: hEPAS myc-pcDNA3
Cloned using Gateway® Invitrogen Recombination
5' primer:
ggggacaagtttgtacaaaaaagcaggcttcaccatgacagctgacaaggag
3' primer: ggggaccactttgtacaagaaagctgggtctcaggtggcctcgtccag

10. pG-EGFP-HIF2α

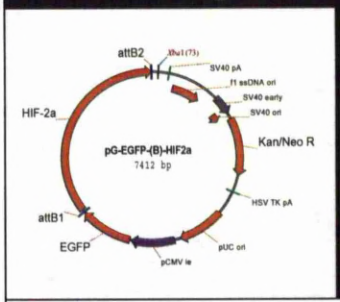

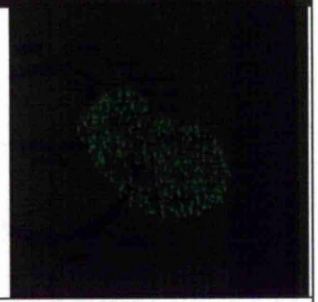

Diagnostic Digest: EcoRI (5593bp, 1819bp)

History

Parent Plasmid: hEPAS myc-pcDNA3
Cloned using Gateway® Invitrogen Recombination
5' primer:
ggggacaagtttgtacaaaaaagcaggcttcaccatgacagctgacaaggag
3' primer: ggggaccactttgtacaagaaagctgggtctcaggtggcctcgtccag

11. pRC-CMV-HA-VHL

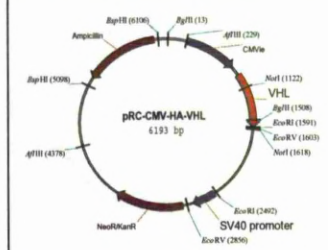

Not Fluorescent

Diagnostic Digest: AflIII (4149bp, 2044bp)

History

Donated by Dr. Michael Ohh (MD. William G. Kaelin)
Ref: Nat Med. 1995 Aug . 1(8):822-6

12. pG-VHL-IRES-DsRedxp

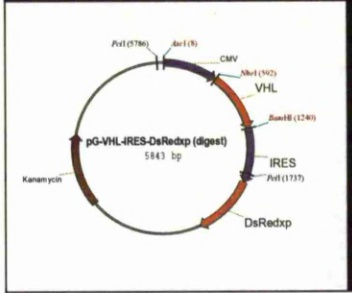

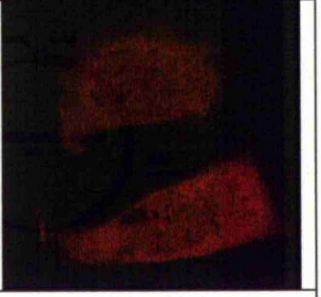

Diagnostic Digest: NotI (4100bp, 1743bp)

History

Parent Plasmid: hEPAS myc-pcDNA3
Cloned by digest-ligation into pIRES2-DsRedxp (Clontech)
5' primer (NheI): attcagctagcatgccccggagggcggag

3' primer(BamHI): gtcatggatcctcaatctcccatccgttg

13. pG-VHL-DsRedxp

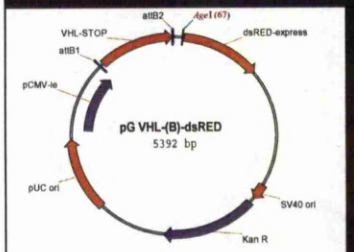

Diagnostic Digest: NotI (4156bp, 1236bp)

History

Parent Plasmid: hEPAS myc-pcDNA3
Cloned using Gateway® Invitrogen Recombination
5' primer:
ggggacaagtttgtacaaaaaagcaggcttcaccatgccccggagggcggagaa
3' primer: ggggaccactttgtacaagaaagctgggtcatctcccatccgttgatcac

14. pG-DsRedxp-VHL

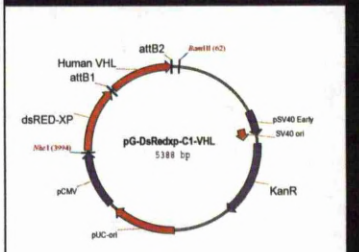

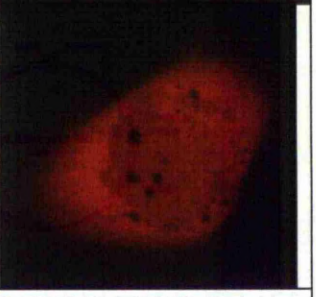

Diagnostic Digest: BspHI (3616bp, 1772bp)

History

Parent Plasmid: hEPAS myc-pcDNA3
Cloned using Gateway® Invitrogen Recombination
5' primer:
ggggacaagtttgtacaaaaaagcaggcttcaccatgccccggagggcggagaa
3' primer: ggggaccactttgtacaagaaagctgggtctcaatctcccatccgttgat

15. pEGFP-N1-FIH

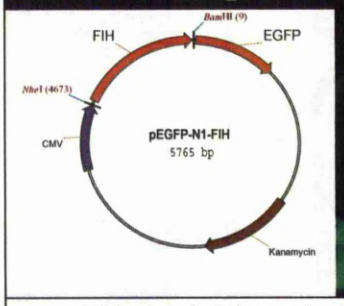

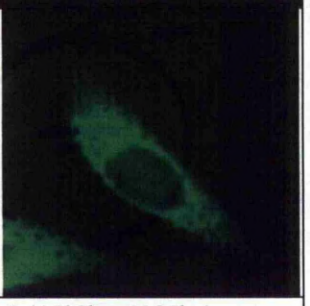

Diagnostic Digest: AseI (4630bp, 1135bp)

History

Donated by PhD Dr. Med. Eric Metzen
Reference: J Cell Sci. 2003 Apr 1. 116(Pt 7):1319-26.
Image taken from reference publication.

16. pG-FIH-IRES-DsRedxp

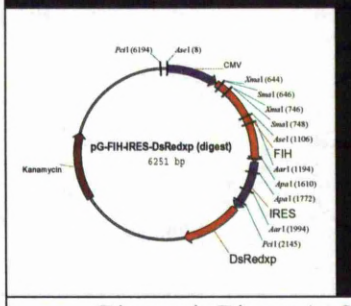

Diagnostic Digest: AseI (5153bp, 1098bp)

History

Parent Plasmid: pEGFP-N1-FIH
Cloned by digest-ligation into pIRES2-DsRedxp (Clontech)
5' primer (NheI): attcagctagcatggcggcgacagcggcg
3' primer (BamHI): gtcatggatccctagttgtatcggcccttgat

17. pG-FIH-DsRedxp

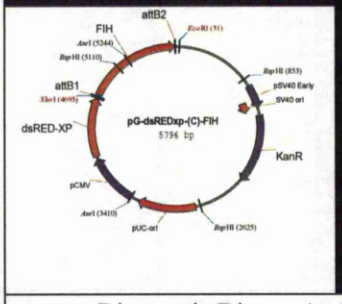

Diagnostic Digest: AseI (3962bp, 1834bp)

History

Parent Plasmid: pEGFP-N1-FIH
Cloned using Gateway® Invitrogen Recombination
5' primer:
gggacaagtttgtacaaaaaagcaggcttcaccatggcggcgacagcggcg

18. pEGFP-N1-PHD2

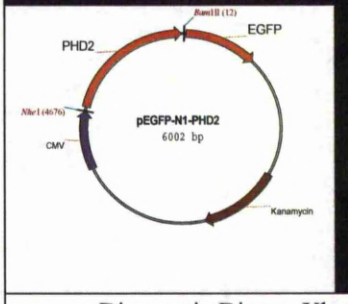

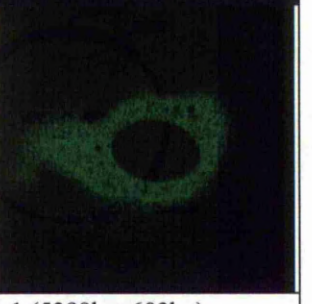

Diagnostic Digest: XhoI (5399bp, 603bp)

History

Donated by PhD Dr. Med. Eric Metzen
Reference: J Cell Sci. 2003 Apr 1. 116(Pt 7):1319-26.

3' primer: ggggaccactttgtacaagaaagctgggtcctagttgtatcggccctt

19. pEGFP-PHD2 Δ6-20

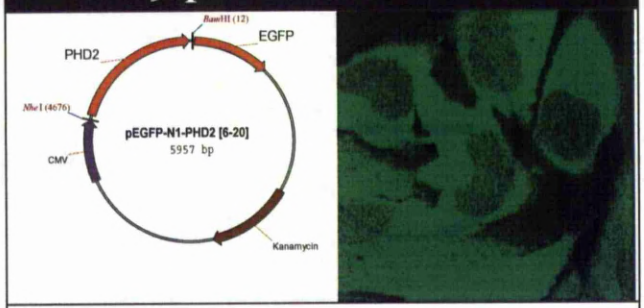

Diagnostic Digest: Xho1 (5399bp, 558bp)

History

Donated by Prof. R. Depping, University of Lüebeck
Ref: Biochem Biophys Res Commun. 2009. 387(4): 705-711

20. pEGFP-N1-PHD2 Δ181-220

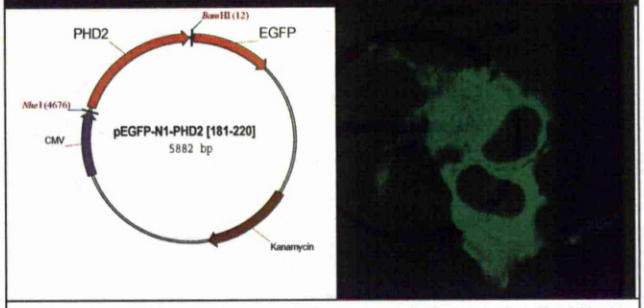

Diagnostic Digest: Xho1 (5882bp) or AflIII (4338bp, 1544bp)

History

Donated by Prof. R. Depping, University of Lüebeck
Ref: Biochem Biophys Res Commun. 2009. 387(4): 705-711

21. pEGFP-PHD2 Δ1-100

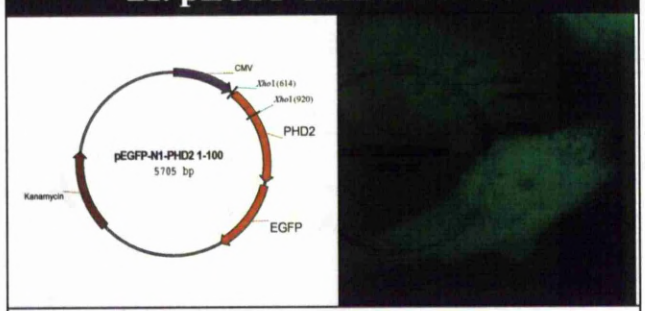

Diagnostic Digest: Xho1 (5399bp, 306bp)

History

Donated by Prof. R. Depping, University of Lüebeck
Ref: Biochem Biophys Res Commun. 2009. 387(4): 705-711

22. pEGFP-N1-PHD2 Δ101-200

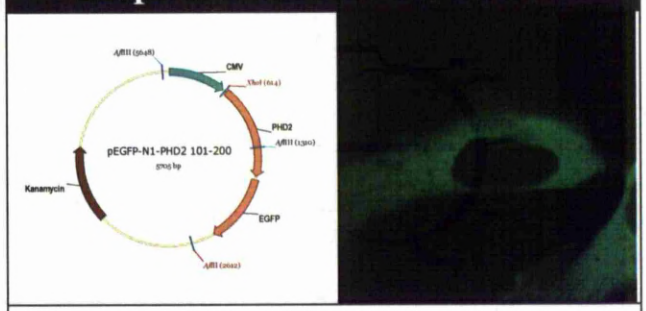

Diagnostic Digest: AflIII (4388bp, 1367bp)

History

Donated by Prof. R. Depping, University of Lüebeck
Ref: Biochem Biophys Res Commun. 2009. 387(4): 705-711

23. pEGFP-PHD2 Δ201-300

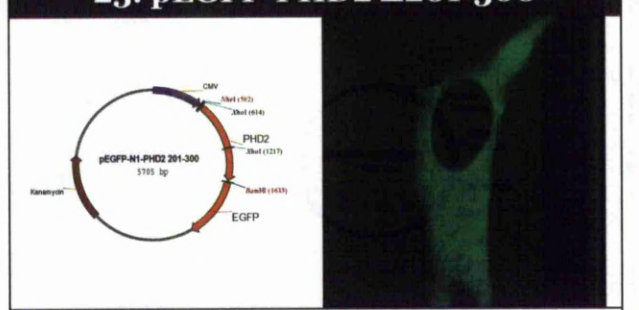

Diagnostic Digest: Xho1 (5102bp, 603bp)

History

Donated by Prof. R. Depping, University of Lüebeck
Ref: Biochem Biophys Res Commun. 2009. 387(4): 705-711

24. pEGFP-N1-PHD2 Δ301-426

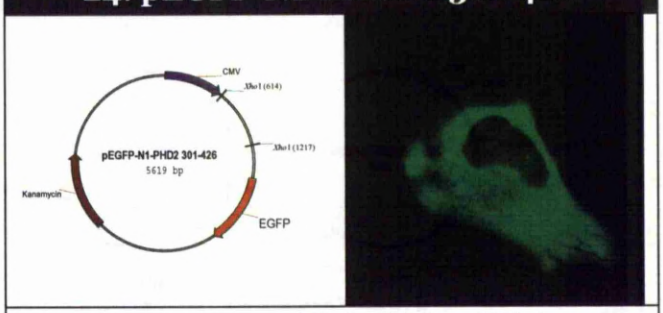

Diagnostic Digest: Xho1 (5016bp, 603bp)

History

Donated by Prof. R.Depping, University of Lüebeck
Ref: Biochem Biophys Res Commun. 2009. 387(4): 705-711

25. pEGFP-PHD1

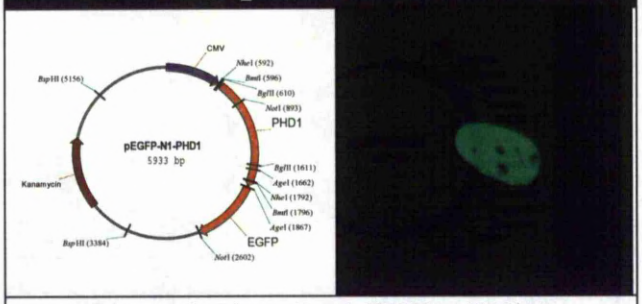

Diagnostic Digest: Bmt1 (4733bp, 1200bp)

History

Retrieved from the Addgene plasmid database under reference number 21400. Originally deposited by Dr. E. Metzen , University of Duisburg

26. pEGFP-N1-PHD3

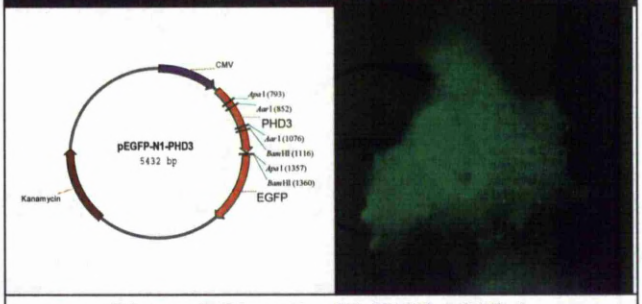

Diagnostic Digest:BamH1 (5188bp, 244bp)

History

Retrieved from the Addgene plasmid database under reference number 21402. Originally deposited by Dr. E. Metzen , University of Duisburg

27. pG-proPHD2EGFP

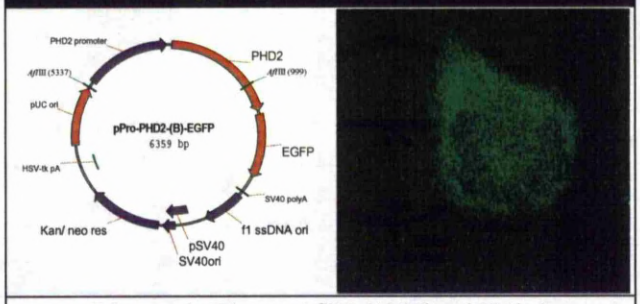

Diagnostic Digest: AflIII (4338bp, 2021bp)

History

Replaced CMV promoter from pPHD2-EGFP with a 1kb cloned human PHD2 promoter using a digest-ligation protocol.

27. pG-ODD-EGFP

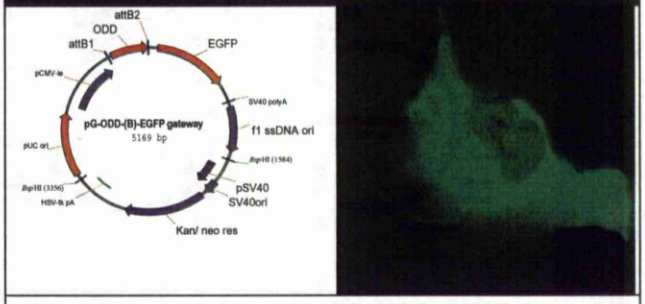

Diagnostic Digest: BspH1 (3397bp, 1772bp)

History

Parent Plasmid: pG-HIF1αEGFP
Cloned Oxygen-Dependent Degradation domain of HIF-1α using Gateway® Invitrogen Recombination
5' primer:
ggggacaagtttgtacaaaaaagcaggcttcaccatggaattcaagttggaa
3' primer: ggggaccactttgtacaagaaagctgggtcagtagtttctttatgtat

28. pG-frODD-EGFP

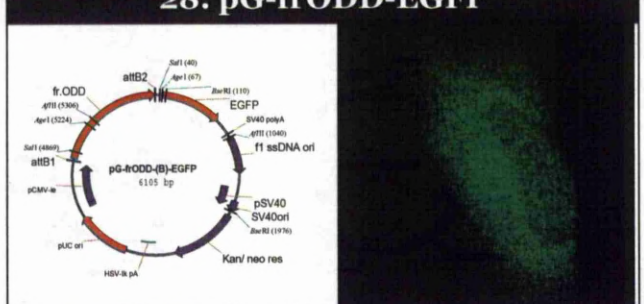

Diagnostic Digest: AflII (4226bp, 1839bp)

History

Parent Plasmid: pG-HIF1αEGFP
Cloned Oxygen-Dependent Degradation domain of HIF-1α using Gateway® Invitrogen Recombination.
5' primer:
ggggacaagtttgtacaaaaaagcaggcttcaccatggaattcaagttggaa
3' primer:

29. pG-nucODD-EGFP

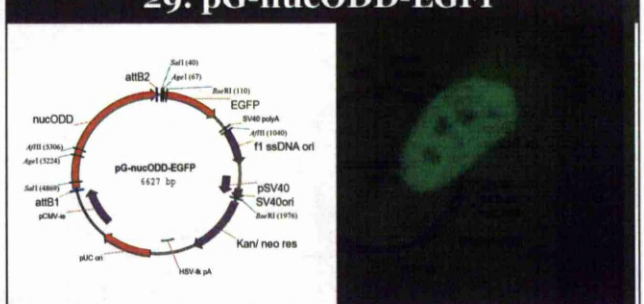

Diagnostic Digest: SalI (4829bp, 1798bp)

History

Parent Plasmid: pG-HIF1αEGFP
Cloned Oxygen-Dependent Degradation domain of HIF-1α using Gateway® Invitrogen Recombination
5' primer:
ggggacaagtttgtacaaaaaagcaggcttcaccatggaattcaagttggaa
3' primer: ggggaccactttgtacaagaaagctgggtcgttaacttgatccaaagc

ggggacaagtttgtacaaaaaagcaggcttcaccatgacctgcttggtgctg

30. EGLN1 PROM_01

Luciferase reporter

History
Purchased from SwitchGear Genomics. Contains a 1000bp PHD2 promoter sequence upstream of the transcriptional start site. Information available on the website.

31. EGLN3 PROM_01

Luciferase reporter

History
Purchased from SwitchGear Genomics. Contains a 1000bp PHD3 promoter sequence upstream of the transcriptional start site. Information available on the website.

32. PGL2.HRE-luc

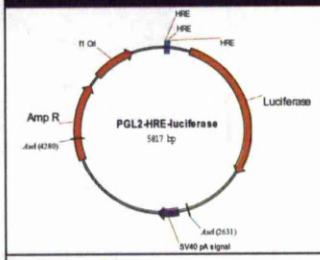

Luciferase reporter

Diagnostic Digest: Ase1 (4168bp, 1649bp)

History
Donated by Dr. Giovanni Mellilo
Ref: Oncogene 2007 (26) 3920-3929

33. PGL416.HIF1α-luc

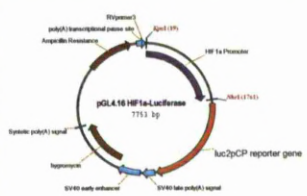

Luciferase reporter

History
1.7kb promoter removed by restriction digest from pG-proHIF-1α-EGFP and ligated into pGL4.16 promega luciferase vector.

All Cell Tracker Analysed Cells

1.2 Nuclear Fluorescence levels of HIF-1αEGFP in 1% O2; Experiment described in Chapter 4.2.2

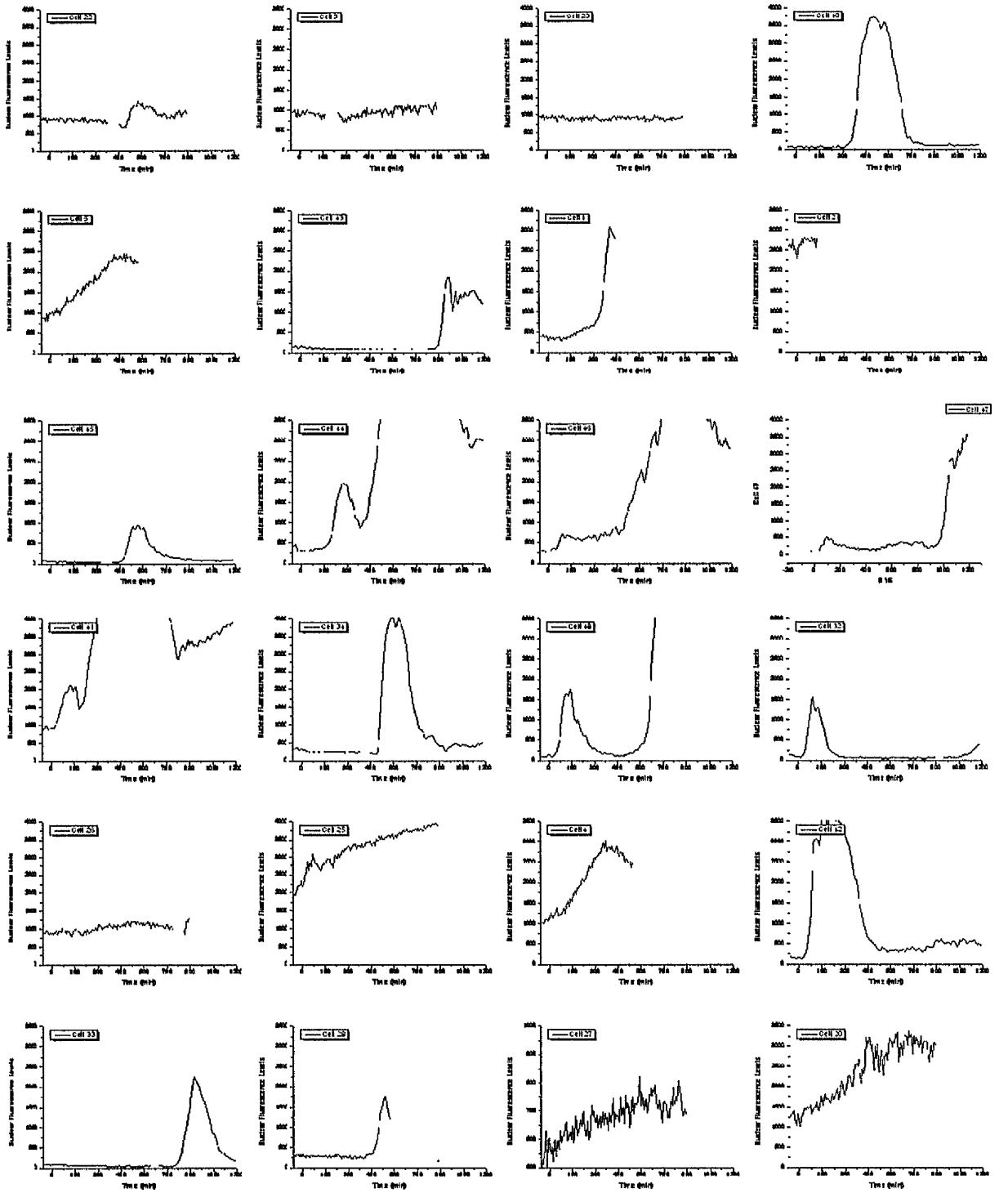

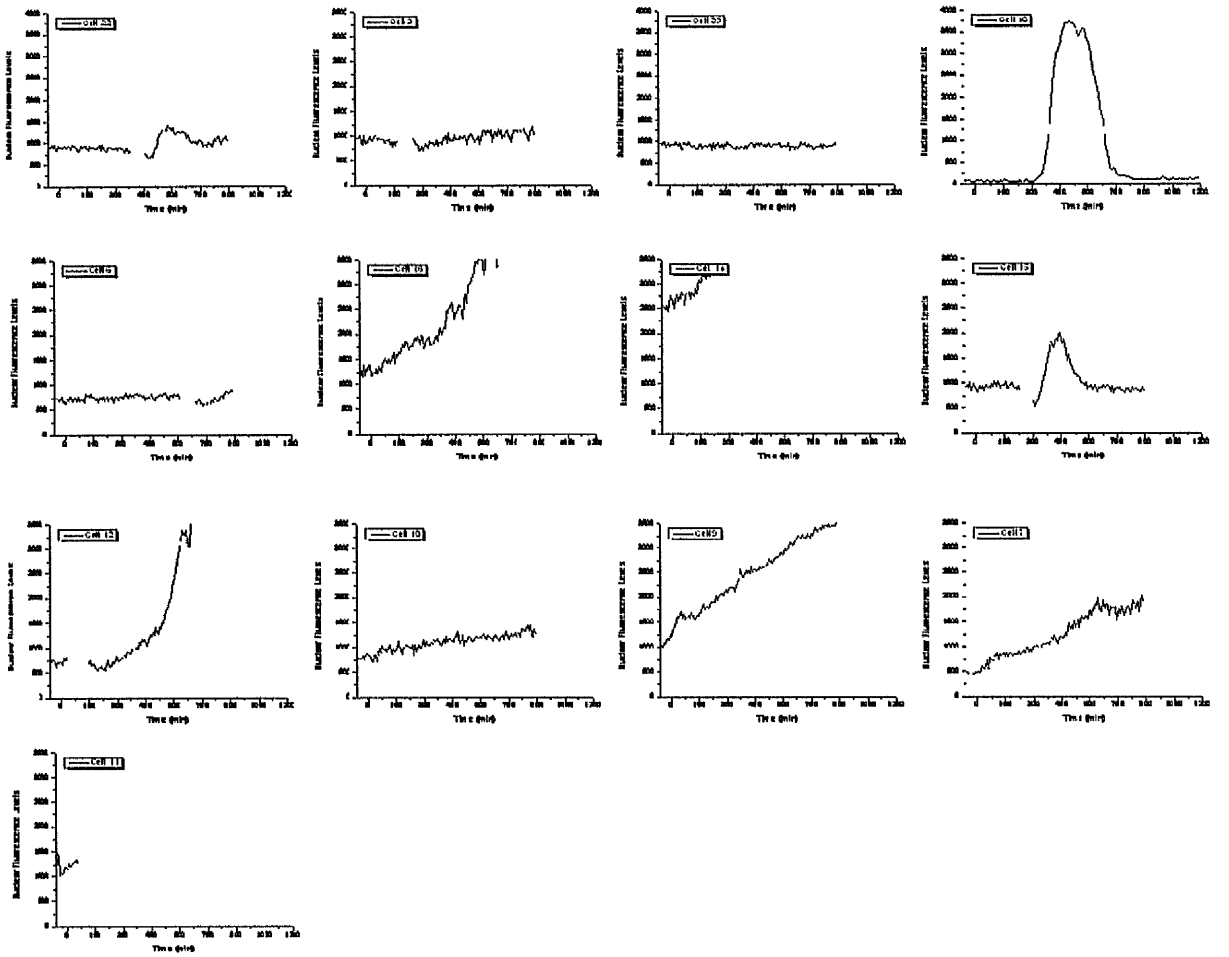

1.3 Nuclear Fluorescence levels of EGFPHIF-2α in 1% O2; Experiment described in Chapter 4.2.3

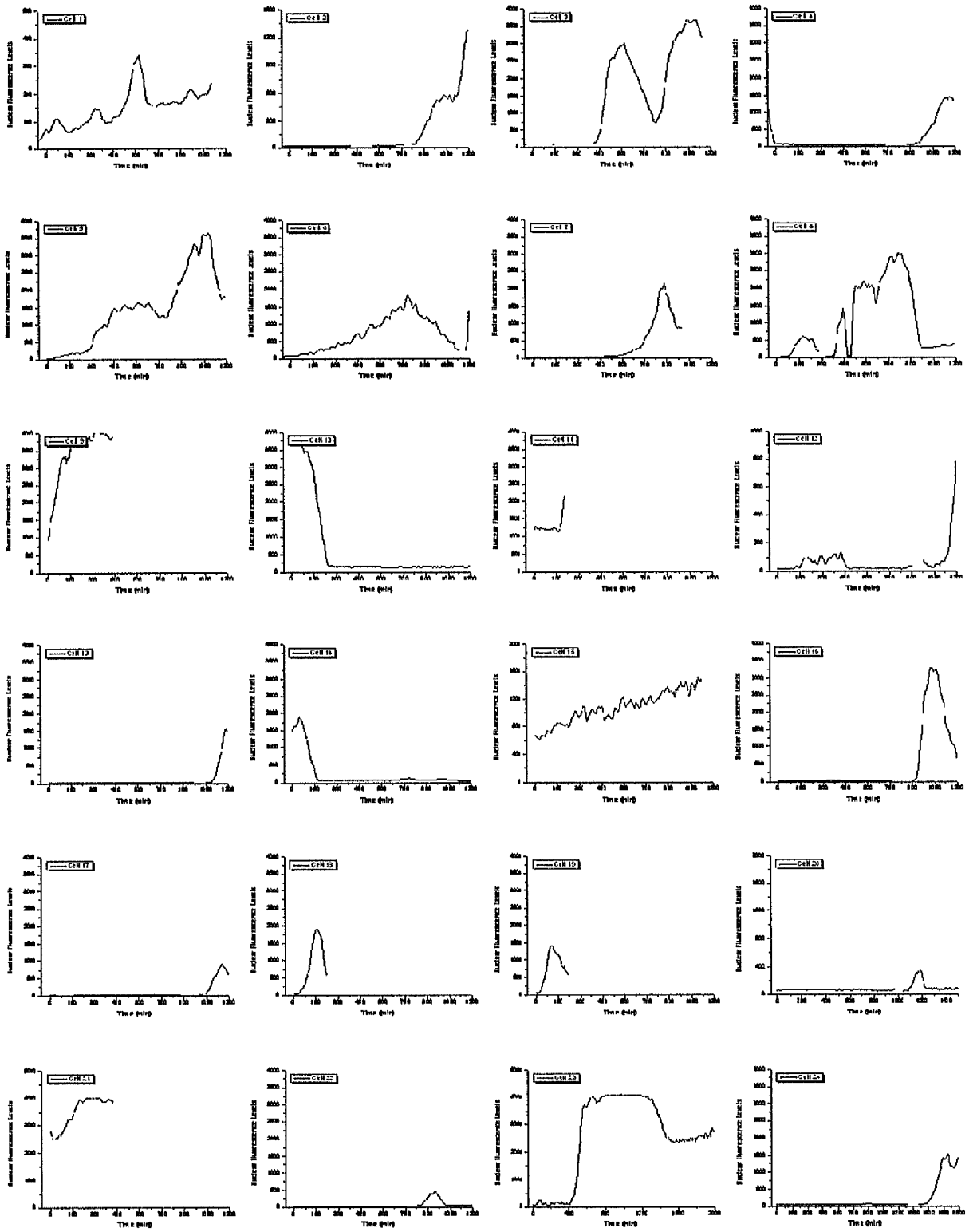

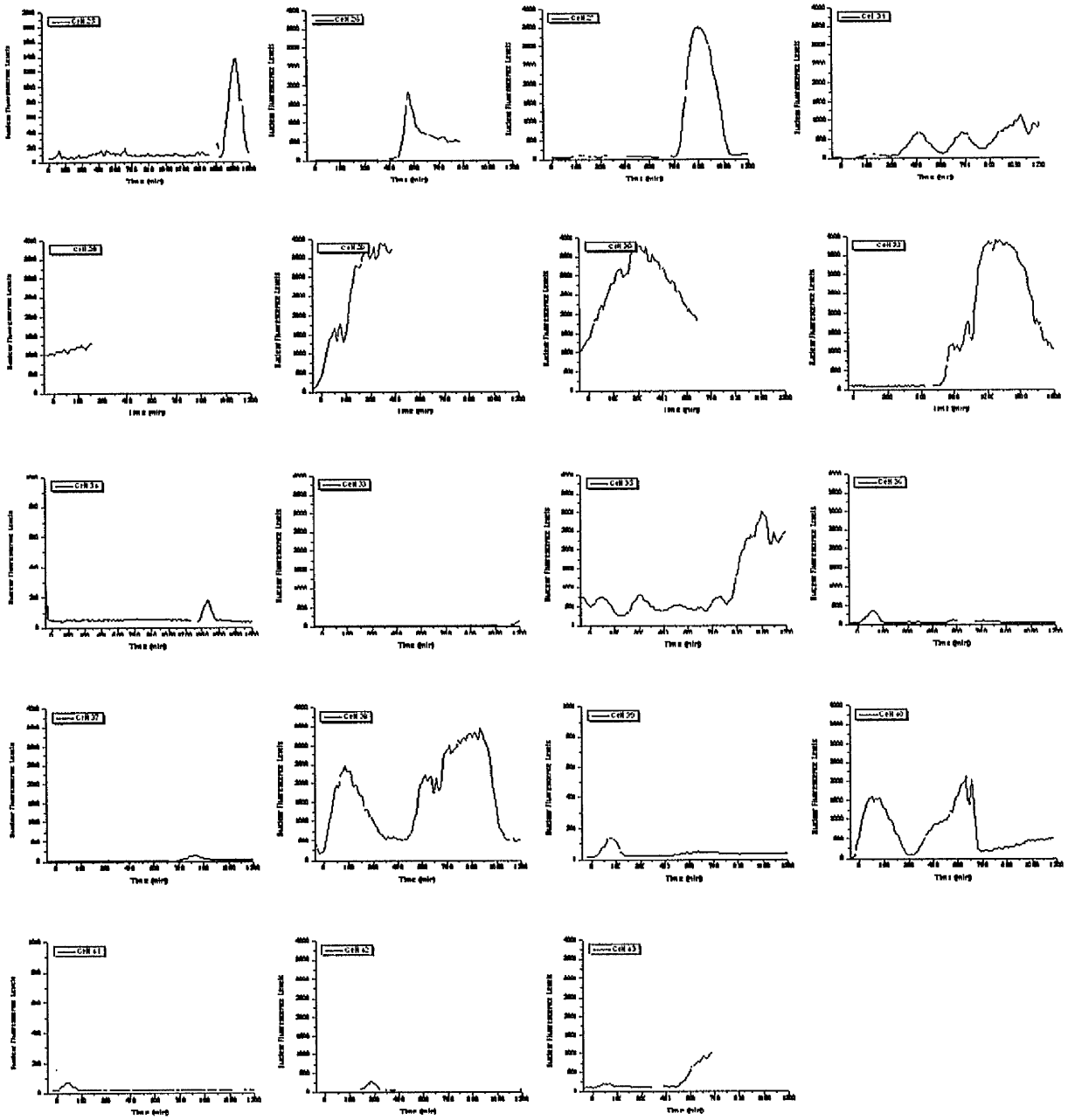

1.4 Nuclear Fluorescence levels of HIF-1α in 1% O2 for SHPHD2 cells; Experiment described in Chapter 5.2.5.3

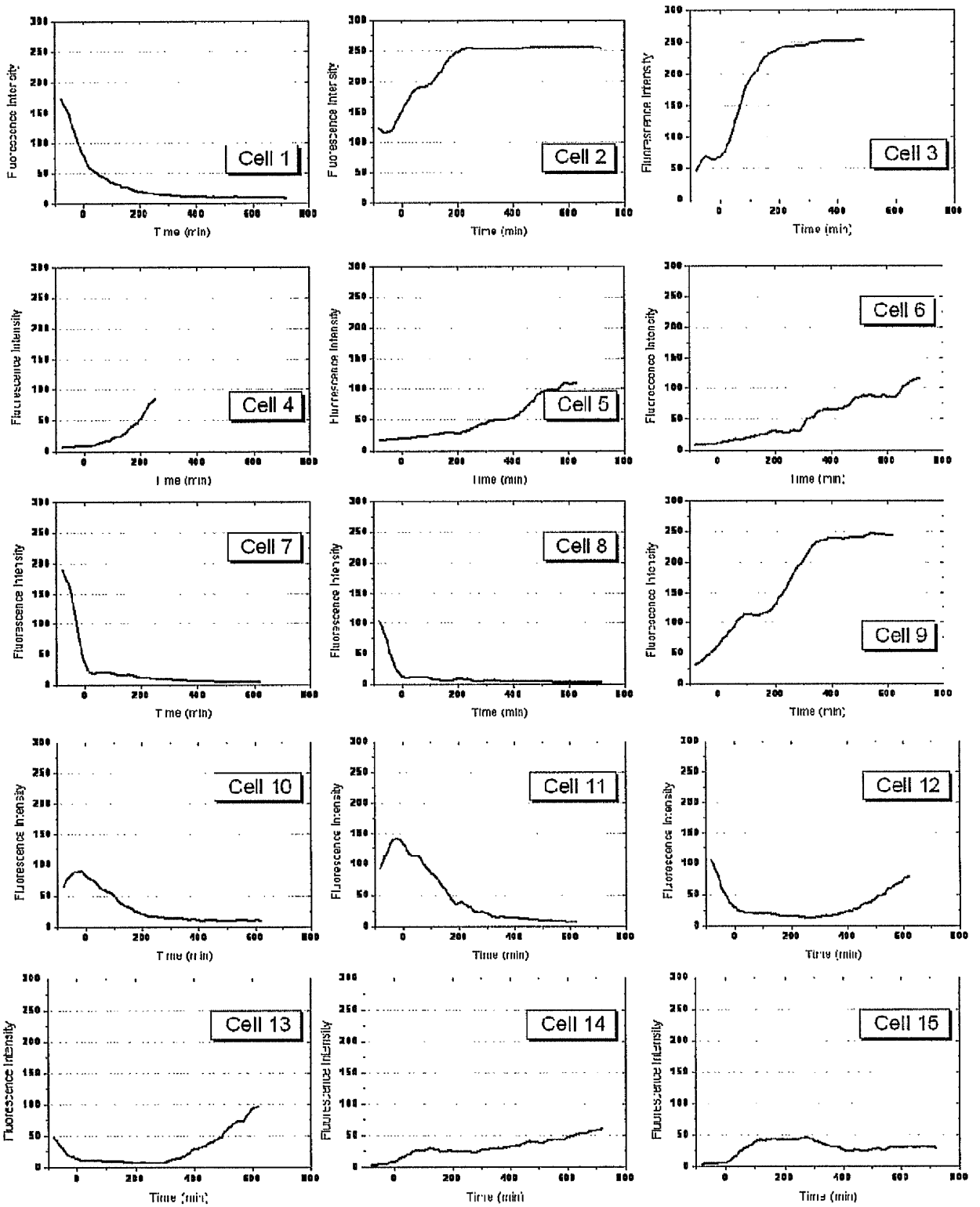

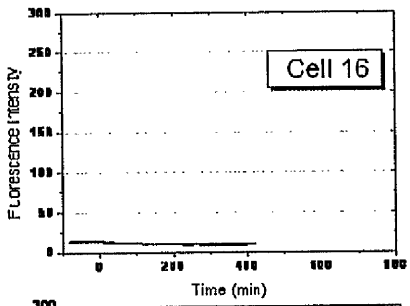
Cell 16
Fluorescence Intensity
Time (min)

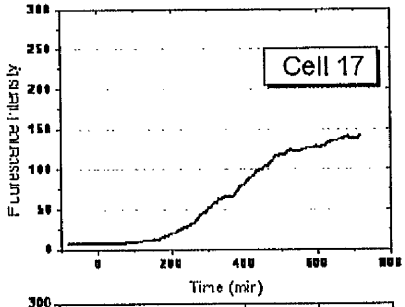
Cell 17
Fluorescence Intensity
Time (min)

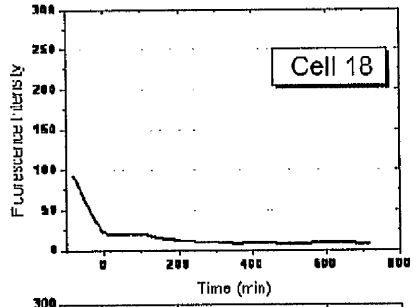
Cell 18
Fluorescence Intensity
Time (min)

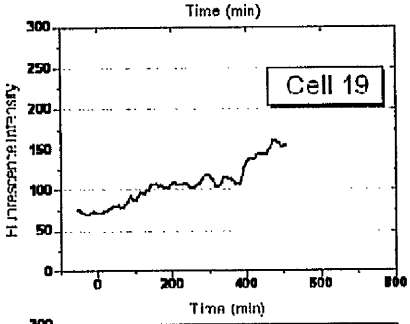
Cell 19
Fluorescence Intensity
Time (min)

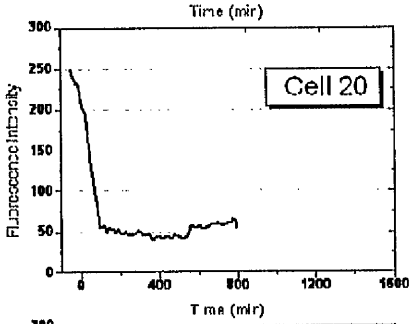
Cell 20
Fluorescence Intensity
Time (min)

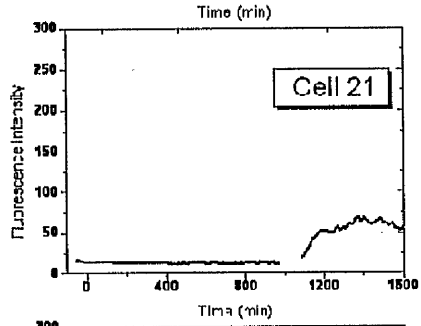
Cell 21
Fluorescence Intensity
Time (min)

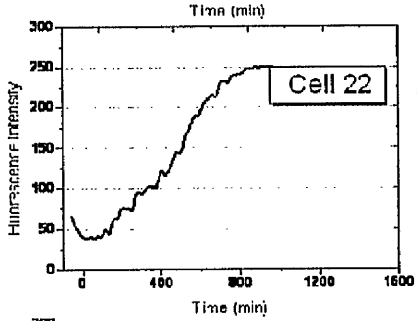
Cell 22
Fluorescence Intensity
Time (min)

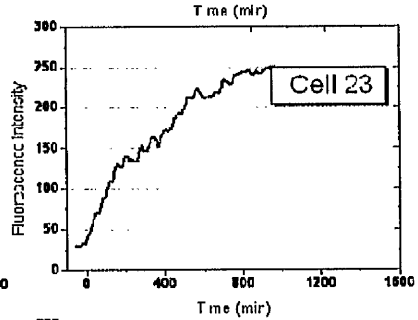
Cell 23
Fluorescence Intensity
Time (min)

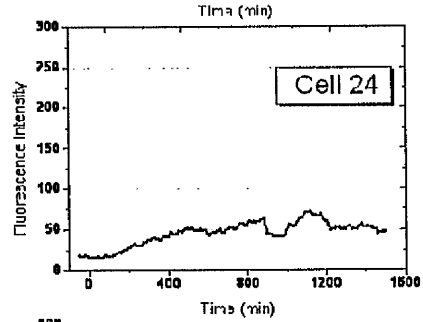
Cell 24
Fluorescence Intensity
Time (min)

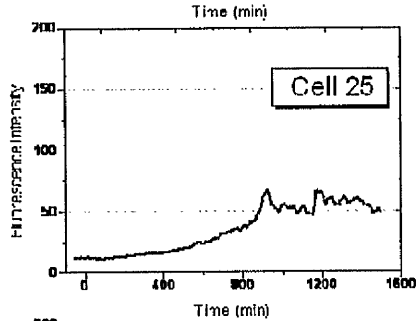
Cell 25
Fluorescence Intensity
Time (min)

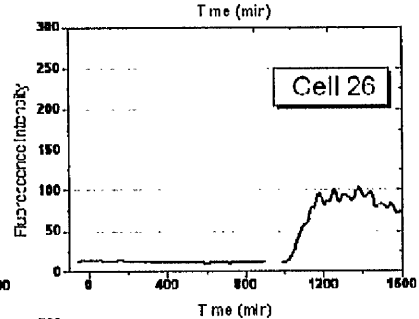
Cell 26
Fluorescence Intensity
Time (min)

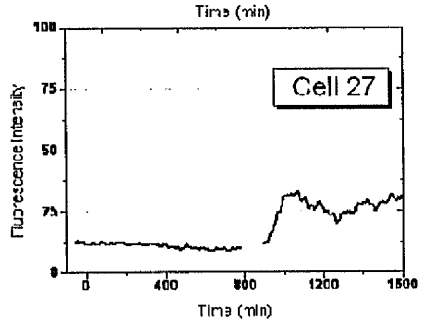
Cell 27
Fluorescence Intensity
Time (min)

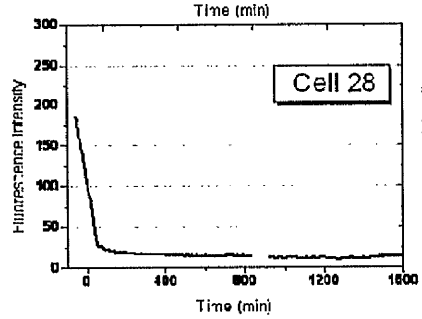
Cell 28
Fluorescence Intensity
Time (min)

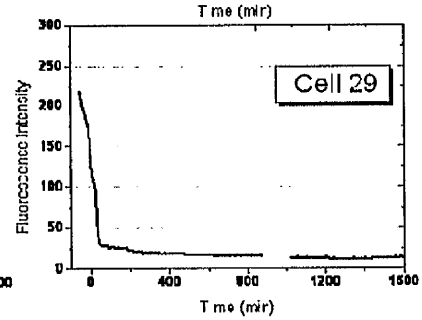
Cell 29
Fluorescence Intensity
Time (min)